Simulating the effects of Anterior Cruciate Ligament Injury and Treatment on Cartilage Loading during Walking

By

Colin R. Smith

A dissertation submitted in partial fulfillment of

the requirements for the degree of

Doctor of Philosophy

(Mechanical Engineering)

at the

UNIVERSITY OF WISCONSIN-MADISON

2017

Date of final oral examination: 11/1/2017

The dissertation is approved by the following members of the Final Oral Committee:

Darryl Thelen, Professor, Mechanical Engineering
Bryan Heiderscheit, Professor, Orthopedics and Rehabilitation
Heidi Ploeg, Associate Professor, Mechanical Engineering
Ilse Jonkers, Associate Professor, Movement and Rehabilitation Sciences
Corrine Henak, Assistant Professor, Mechanical Engineering
Peter Adamczyk, Assistant Professor, Mechanical Engineering

Acknowledgements

I am extremely grateful to the mentors, colleagues, friends, and family who have supported me throughout my PhD. I would like to acknowledge the United States National Institutes of Health, the National Center for Simulation in Rehabilitation Research, and the Whitaker International Foundation for funding my graduate research.

I would like to thank Darryl Thelen for his mentorship. Your expertise, guidance, and friendship were integral to my success and experience as a graduate student. I also want to thank the other members of the UW Neuromuscular Biomechanics lab for creating a positive and encouraging work environment. I will miss the morning KNEEMOS meetings, despite their unfortunate timing. I especially want to thank Rachel Lenhart, Mike Vignos, Scott Brandon, Josh Roth, Jarred Kaiser, and Moria Bittmann for their contributions and collaboration.

Thank you to each of the members of my thesis committee, Bryan Heiderscheit, Heidi Ploeg, Ilse Jonkers, Corrine Henak, and Peter Adamczyk, for your suggestions and advice. I especially appreciated the clinical input from Bryan and Geoff Baer. Thanks to Lauren Michael, Christina Koch, and the entire Center for High Throughput Computing team for your computing resources and technical advice. Thanks to Scott Delp and the Neuromuscular biomechanics lab at Stanford University and Ilse Jonkers and the Human Movement Biomechanics Research Group at KU Leuven for hosting me on summer visits.

Finally, I would like to thank all of my friends and family who continue to support my interests. Especially my parents and brother, you have been generous to accommodate my academic lifestyle.

Abstract

Current treatments for anterior cruciate ligament injury are largely successful at restoring stability to the knee and enabling patients to return to functional activities. However, the long-term outcomes are suboptimal, with high percentages of patients showing signs of early onset osteoarthritis (OA) 10 years post-injury regardless of treatment. *In vitro* and animal studies indicate that alterations in cartilage loading patterns following injury disrupt tissue homeostasis and are likely a key factor in the initiation of OA. Dynamic imaging studies indicate altered kinematics, and thus loading patterns, are present in ACL deficient and reconstructed knees during functional movements. Thus, improvements in both conservative rehabilitation and surgical reconstruction treatments for ACL injury are necessary to restore cartilage loading and preserve the long-term health of the knee.

Musculoskeletal computer simulation provides opportunity to gain insight into the how modification in treatments effect knee mechanics during movement. However, existing simulation frameworks either focus on resolving detailed knee mechanics with finite element models, or the muscle forces necessary to generate a measured movement using musculoskeletal models. Few simulation frameworks are capable of simultaneously resolving whole-body and joint scale dynamics. Traditionally, despite the substantial uncertainty in model parameters and the objective used to resolved muscle redundancy, musculoskeletal simulations have been performed in a deterministic manner. This dissertation introduces the Concurrent Optimization of Muscle Activations and Kinematics (COMAK) framework to predict muscle forces and knee joint mechanics during movement in a probabilistic manner.

The COMAK framework was then applied to investigate conservative and surgical treatments for ACL injury. The framework predictions indicate that wear patterns in ACL and menisci deficient

knees correspond with regions that experience increased contact pressure during walking. To better inform surgical practices, the framework was used to assess the influence of controllable factors (graft stiffness, reference strain, and tunnel locations) on predicted knee mechanics during walking. For conservative treatment, model predictions indicate that cartilage loading patterns during walking cannot be restored solely through altered muscle coordination strategies.

Table of Contents

Introduction

A Background on Osteoarthritis following ACL Injury and Computational Simulation of Knee Mechanics

Colin R. Smith, Scott C.E. Brandon, Darryl Thelen

Osteoarthritis

Osteoarthritis (OA) is a common and debilitating joint disease characterized by articular cartilage degradation. OA affects 10% of men and 13% of women over age 60[1], most commonly in the knee joint[2]. The predominate symptoms of OA are joint pain and stiffness, which result in reduced physical activity and often lead to obesity and cardiovascular complications[3]. In 2003, lost earnings and health care costs due to OA in the US exceeded $128 billion[4]. Unfortunately, the molecular etiology of OA is not well understood, which has limited the development of medications and tissue engineering treatments. While conservative treatment can delay the progression of OA, late stage OA can only be treated by total joint replacement. Thus, improved treatments to mitigate the pathogenesis of OA are important to improve the quality of life for current generations.

OA is not isolated to the elderly population. Injury to the knee can initiate the development of post-traumatic osteoarthritis (PTOA) in healthy young adults. One of the leading causes of PTOA is an injury to the anterior cruciate ligament (ACL)[5]. While both conservative and surgical treatments to ACL rupture effectively restore stability to the knee and return patients to pre-injury activity levels, up to 50% of patients develop OA within 10 years regardless of the treatment[6]. OA in patients with ACL injury occurs 15 to 20 years earlier than primary OA, which results in extended periods of pain and disability before a total knee replacement (TKR) becomes a feasible option[7].

There is significant variability in both conservative rehabilitation and surgical reconstruction treatments for ACL injury. In the United States, nearly 95% of patients undergo reconstruction, however, in Europe as low as 50% of patients select the surgical treatment[8]. Conservative treatments typically involve rehabilitative exercises, proprioceptive training and more recently, neuromuscular retraining[9]. The objectives of neuromuscular retraining are to induce compensatory changes in muscle activation patterns and facilitate dynamic joint stability in patients with ACL injury[10]. Surgical reconstruction of the ACL requires arthroscopic replacement of the torn ACL with a graft, which is most commonly a section of the patellar or hamstrings tendon. To place the graft, two bone tunnels are drilled, one in the femur and one in the tibia. The ACL graft is then pulled through both tunnels and fixed. The surgeon has a number of choices in performing the surgery, including graft type, drilling technique/location, graft pretension, and fixation method. The connection between these controllable factors in conservative and surgical treatments and the resulting knee mechanics is not well understood, however it is likely to have significant influence on the treatment outcomes.

Although the cause of PTOA has not been established, it is theorized that altered cartilage loading during functional movement following the injury is a key factor[11]. In animal studies of ACL transection, it has been shown that changes in cartilage contact pressures coincide with the development of OA[12]. Altered cartilage loading is known to occur in humans as well, as dynamic imaging studies have shown that ACL reconstructed[13,14] and deficient[15,16] patients exhibit tibiofemoral kinematic differences compared to healthy controls during locomotor movements. In light of these findings, recent orthopedic research has focused on improving surgical procedures to restore healthy cartilage loading patterns. However, it is not clear how each surgical parameter such as graft placement, stiffness and pretension can be altered to achieve this goal. Interestingly, despite similar incidence of PTOA, cartilage loading patterns are not typically addressed by conservative treatments.

The considerable number of factors involved in both treatments for ACL injury and the complexity of the biomechanical interactions that determine functional knee loading make computer simulation an important tool to provide insight into reducing the development of PTOA. Further, the difficulty of obtaining *in vivo* measures of soft tissue loading necessitates computer simulation to quantify the sensitivity of functional knee loading to treatment interventions. The following section provides a background on the existing techniques to quantify knee loading during functional movement through simulation.

Computational Simulation of Knee Mechanics

(Adapted from "Simulation of Soft Tissue Loading from Observed Movement Dynamics" a chapter in the Handbook of Human Movement)

In the musculoskeletal system, soft tissues both mobilize and constrain skeletal motion. Muscles generate forces that are transmitted to the skeleton by tendons that can elastically deform. Ligaments, connective tissues, and articular cartilage connect the bones, distribute loading, and guide joint motion. Although the relative motion of bones can be measured and analyzed with increasing precision [17,18], soft tissue loading is not easily measured *in vivo*. Therefore, simulations are often required to investigate the mechanical loading and behavior of soft tissues during movement, and the resulting effects on other structures within the musculoskeletal system (Fig. 1). One of the earliest musculoskeletal models assessed the contributions of muscle loading to joint injury and bone fractures [19]. Since then, increasingly complex models have been introduced to characterize musculoskeletal tissue mechanics at various scales, including lower-extremity models to assess the contributions of muscles to hip, knee and ankle joint loads during walking [20–23] and multiscale models to assess cartilage tissue and cellular deformations under functional loads [24,25].

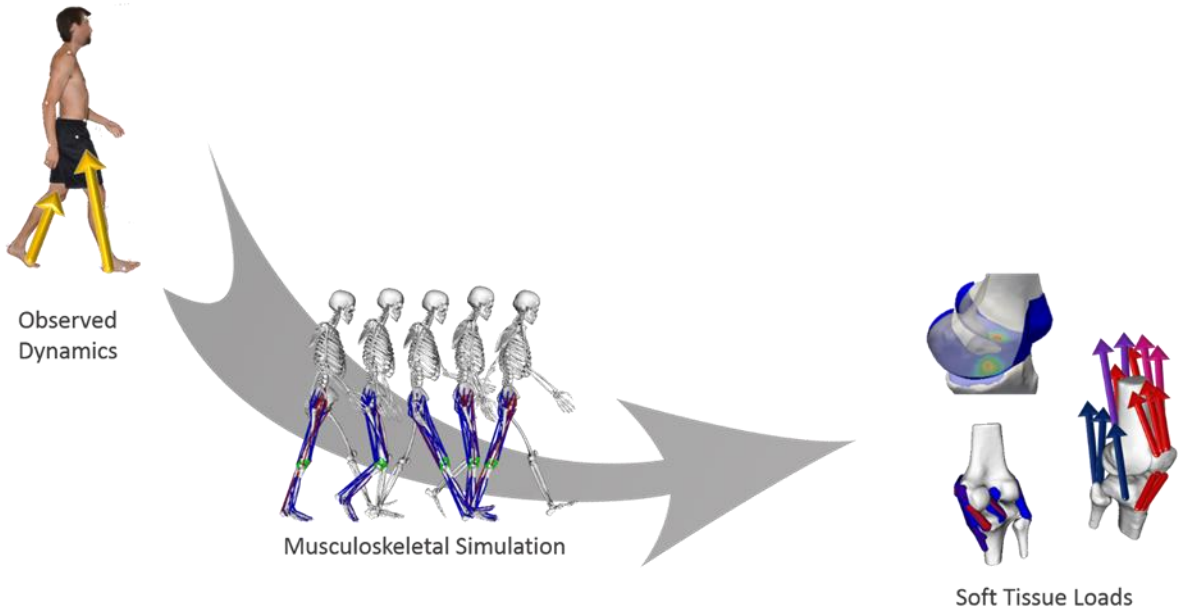

Figure 1 Simulation of soft tissue loading from observed dynamics. Experimental measurements of whole-body motion and external forces are supplied as inputs to a musculoskeletal simulation, which yields estimates of the internal soft tissue (i.e. muscle, ligament, and articular cartilage) loads.

In biomechanical models of human movement, passive soft tissues are often omitted and simplified joints (e.g. hinge, ball-and-socket) are assumed. These reduced degree-of-freedom (DOF) joints impose kinematic constraints to account for the action of soft tissues at each joint. While simplified multibody musculoskeletal models are useful for investigating muscle coordination and resultant joint loading, they do not allow estimation of the soft tissue loads needed to constrain joint motion. To address this limitation, high resolution finite element (FE) models have been applied to elucidate the complex interactions of morphology, micro-motion, and soft tissue loading for many of the joints in the human body. However, due to their computational complexity, FE simulations are typically driven at the joint-level using a combination of prescribed kinematics and external loads. Therefore, they inherently cannot account for the interrelationship between whole-body dynamics, muscle forces, and joint-level mechanics. Improved algorithms and computational hardware will likely facilitate multi-scale and multi-domain simulations in the future. However, with current techniques it

remains exceedingly computationally demanding to incorporate detailed finite element joints into a muscle driven simulation framework. To overcome this limitation, concurrent body and joint level musculoskeletal simulation techniques have been introduced.

The concurrent approach ensures dynamic consistency between the simulated full body movement and joint-level mechanics, resulting in joint kinematics that evolve naturally from the soft tissue forces. Concurrent simulations avoid the complexity of the FE approaches without requiring the oversimplified joint representations of traditional musculoskeletal models. The ability to describe joint motion completely using soft tissue loads and contact between articulating joint surfaces is retained by using strand-based ligaments and elastic foundation contact models. This approach is approximately two orders of magnitude faster than a comparable FE simulation[26], enabling many more simulations to be performed with various individuals, activities, or sets of model parameters. While a FE approach may be used to analyze only a few discrete instants during a dynamic motion[27], a concurrent approach can be used to simulate the entire motion [28]. Hence, the computational efficiency of the concurrent approach enables stochastic (e.g. Monte Carlo) simulations to more fully probe the sensitivity of model predictions to inherent uncertainty in measurements and model parameters.

In the following sections, the traditional *sequential* simulation approaches where multibody movement dynamics are solved independently of joint mechanics will first be reviewed. Second, the state-of-the-art *concurrent* simulation approaches to simultaneously solve for muscle forces and internal joint mechanics that generate observed whole body movement will be reviewed (Fig. 2).

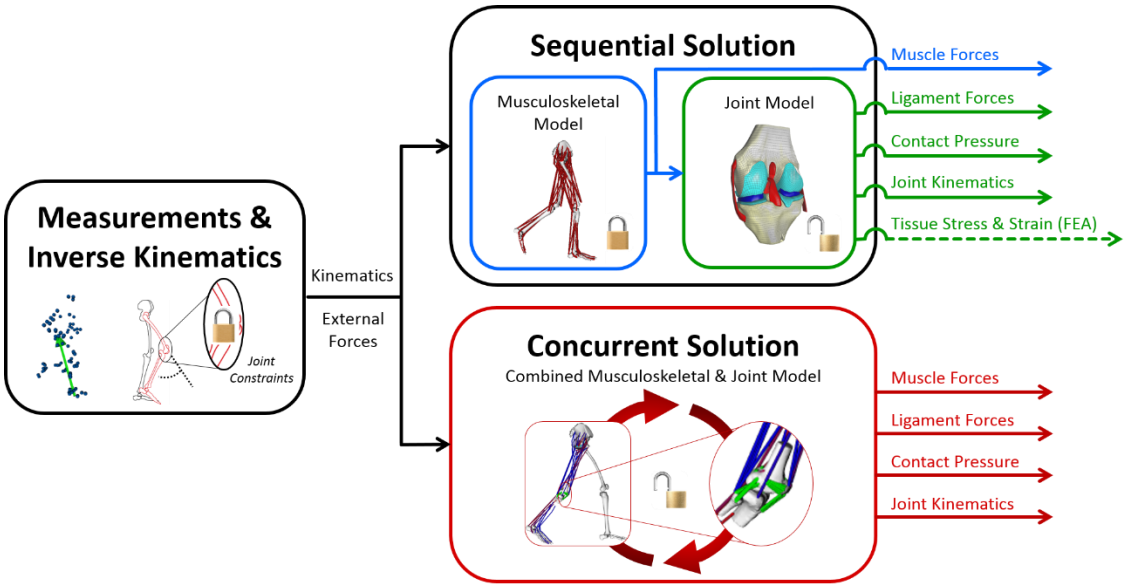

Figure 2 Sequential vs Concurrent modeling of soft tissue loading. The traditional "Sequential Solution" first resolves the muscle forces using a simplified multibody model, then applies these forces to a detailed joint model. While this approach enables the use of complex, high-fidelity joint-level models to assess ligament and cartilage loading, it de-couples the muscle forces from joint-level mechanics. An alternative "Concurrent Solution" approach has recently been proposed wherein the muscle forces and joint mechanics are solved simultaneously such that the joint kinematics, ligament forces, and cartilage pressures are directly coupled with the muscle forces. In each image, a padlock symbol is superimposed to indicate the presence or absence of kinematic joint constraints. In the "Sequential Solution", the musculoskeletal model is the OpenSim Gait 2392 model, and the joint model is the Open Knee finite element model [29,30]. The "Concurrent Solution" model is described by Lenhart et al. [31].

Sequential Simulation Techniques

Traditionally, soft tissue loads are obtained through the sequential solution of one or more models at differing physiological scales (Fig. 2). First, a whole-body musculoskeletal model is used to estimate the musculotendon forces and resulting net joint loads necessary to generate the observed motion. This whole-body model typically contains a simplified set of coordinates and constraints for each joint (e.g. ball and socket at the hip, hinge at knee and ankle). Then, a finer-resolution joint-level model uses musculotendon loads and joint pose as boundary conditions, and predicts the deformation and internal loading of ligaments, connective tissue, and articular cartilage. This joint-level model may include a rigid [32], elastic foundation [33], or finite element representation [34] of articular contact, and

varying degrees of kinematic and kinetic constraints. The challenges associated with both of these modeling stages are detailed in the following sections.

Perhaps the most difficult challenge in modeling the human musculoskeletal system during functional movement is the distribution of forces amongst agonist and antagonist muscles. Each joint of the human body is spanned by more muscles than required to control the joint motion, leading to the "muscle redundancy problem". Furthermore, antagonist muscles that act in opposite directions at a given joint are often simultaneously activated; thus, for each joint there is an infinite set of muscle forces that will generate an observed motion.

Early mathematical models resolved muscle redundancy through physiologically-informed simplification. Morrison[35] outlined a series of hypotheses about knee mechanics which formed the basis for his musculoskeletal model of soft tissue loading in the knee. For example, any anterior muscle or external force applied to the knee joint was solely resisted by the anterior cruciate ligament (ACL), torsional action about the proximal-distal axis of the joint was neglected, and redundancy of knee flexor muscles was resolved by comparing experimental muscle excitation (EMG) data to decide whether hamstrings or gastrocnemii muscles should be activated at a given instant. These simplifying assumptions captured salient features of knee mechanics, and resulted in a model that provided a unique solution for muscle, joint contact, and primary ligament loading during observed movements. However, the accuracy of soft tissue load estimates, and implications regarding relationships between soft tissue loading and joint kinematics, were limited.

Subsequent models attempted to include greater flexibility in muscle coordination, by optimizing the force distribution at discrete instants in time to minimize an *a priori* objective function[36–39]. This process is known as static optimization, where the muscle forces needed to generate the dynamic joint moments are estimated. Note that the "static" terminology refers to independent

solution of the optimization problem at each time step, as opposed to dynamic optimization which solves all time steps simultaneously. Motor control studies have shown that humans appear to exhibit varying degrees of optimality in motor planning and execution[40–42]; therefore, using optimization to emulate physiological distribution of muscle forces is not just mathematically convenient, but also desirable[37]. Unfortunately, it remains very challenging to establish a true "objective" of the human motor control system in performing functional movements. Many investigations have shown that the minimization of the sum of squares or cubes of muscles forces[38,39] sometimes weighted by muscle volume[43] can provide muscle force estimates that are temporally similar to experimental EMG data in healthy normal subjects. However, subtle changes to the objective function can lead to dramatic changes in estimated joint loads[44].

Many other approaches have been implemented to resolve the muscle force distribution problem for observed movements, including: EMG-driven modeling[45,46], synergy-based optimization[47], dynamic optimization[48–50], and various tracking algorithms including computed muscle control[51], neuromusculoskeletal tracking[52], and PID control of joints[53,54]. These approaches may provide advantages over static optimization if, for example, the subject of interest exhibits abnormal muscle activation (EMG-driven modeling) or is moving rapidly such that muscle contraction dynamics are significant (dynamic optimization). Any of these methods can be suitable for distributing muscle forces in a two-stage sequential modeling approach.

After the muscle forces are resolved in the first stage of the sequential modeling workflow, they are applied to a detailed joint model to calculate soft tissue loading. With advancements in algorithms and computational hardware, these joint level models have become increasingly sophisticated in the number of structures modeled and the fidelity of their representations.

The most rudimentary models of passive tissue loading employ rigid assumptions for articular contact, where the centers of joint rotation, points of contact, and moment arms of each muscle and soft tissue are geometrically defined[32,35]. Using these models, given a known set of joint kinematics, external loads, and muscle forces, it is possible to estimate a limited set of ligament and net contact forces. However, in order to formulate a mathematically-determinate system, such models include only a small subset of the passive structures crossing a joint, and typically fail to capture any elastic deformation of soft tissues. This approach is computationally efficient and may yield reasonable results for the overall magnitude of joint contact forces[55,56]. However, it fails to yield insight into the interaction of kinematics and soft tissue loads because kinematics are prescribed prior to the soft tissue analysis.

A more nuanced description of joint mechanics is enabled by the use of a rigid body, penetration-based "elastic foundation" model for articular contact[33,57] and strand based ligaments[58]. In the elastic foundation model, each articular surface is discretized into a surface mesh of small polygonal elements with independent springs acting normal to each face. When contact occurs, the interpenetration of rigid mesh surfaces is used to compute spring deflection, and thereby pressure, for each surface element. Strand based ligament models use bundles of nonlinear springs to represent the elastic contribution of ligaments to joint mechanics. Using these approaches, joint models where all six degrees of freedom are controlled by the combined action of muscle, ligament, and articular contact loads have been developed[59,60]. However, an elastic foundation model only provides surface contact pressures, and cannot resolve internal tissue-level stresses and strains.

Finite element (FE) analysis is a powerful method for quantifying the mechanics of ligament, capsule, and cartilage tissues[61,62]. The fundamental principal of FE analysis is to discretize complex tissue geometries into a set of small three-dimensional elements that can be analyzed using numerical

solution techniques. Finite element modeling enables studies such as the sensitivity of passive knee joint mechanics to ACL reconstruction graft parameters[63,64], the effect of a menisectomy on knee cartilage stress[65], the relationship between focal cartilage defects and osteoarthritis[66], or evaluations of the stability of the hip[67] or glenohumeral[68] joints. Finite element modeling can even be used to investigate the importance of depth-wise changes in mechanical structure within a thin layer of articular cartilage[69], or to simulate changes in cartilage stiffness and strength due to variation in nanoscale cross-link density between tropocollagen molecules[70]. The primary limitation on the use of FE models in biomechanical studies is computational cost. For example, a finite element representation of the knee, including poroviscoelastic properties for the cartilage, may take days or even weeks to solve under quasi-static conditions[61]. Thus, in the sequential modeling workflow, joint mechanics are often resolved only at specific instances in a movement.

While the sequential approach has yielded valuable insight into the magnitudes of soft tissue loading, and provides a straightforward methodology to simulate soft tissue loading across multiple scales, several limitations exist. In the sequential approach, muscle forces are often computed to equilibrate only a subset of the available degrees of freedom. However, a different solution will be obtained if additional degrees of freedom are considered[71,72]. Perhaps more importantly, the sequential modeling approach solves the full-body and joint-level dynamics separately, neglecting the interaction between scales and thereby failing to account for inherent coupling. As a result, it does not allow muscle forces to be affected by subtle changes in joint kinematics which arise via deformation of ligament, capsular, and cartilage tissues. The human neuromuscular system modulates muscle forces to control joint rotations and translations; muscle forces therefore arise in proportion with their capability to induce accelerations along each degree of freedom. But the contribution of a muscle to accelerating each degree of freedom is not static; it changes dynamically with the pose of a joint. Using the knee for example[73], quadriceps forces are directly affected by the position of the patella. However,

patellar position is influenced by translation of the tibiofemoral joint as well as strain in the patellar tendon, and these parameters vary with quadriceps force. Thus, to analyze soft tissue loading during dynamic motions, it is imperative to ensure that joint kinematics are coupled with soft tissue loads. The coupling between dynamic motion, muscles and soft tissue loads is likely amplified in cases where soft tissue injury or disease exists, and compromises the native function of the joint.

Concurrent Simulaton Techniques

To capture the interactions between body scale musculoskeletal behavior and joint scale soft tissue mechanics, the dynamics of each scale must be coupled. For example, coupled simulations are needed to investigate how one may alter neuromuscular coordination to adapt for ligament damage that compromises joint stability. However, concurrent solution of the neuromuscular control and joint behavior necessitates different modeling and simulation techniques than are required for sequential simulation approaches.

Ideally, a soft tissue FE representation of the joint mechanics would be solved within a multibody muscle-driven simulation, thereby allowing for characterization of the tissue deformation and stress patterns. However, the practical challenges and computational demands of simultaneously solving multibody dynamic and finite element models has generally precluded this approach[74]. To avoid the computational bottle neck, investigators have either used surrogate approaches to limit the number of FE model calls, or opted for simpler elastic foundation models and strand-based structures to represent articular cartilage contact and ligaments, respectively (see Table 1 for summary of 3D knee models that use such approaches).

Table 1 Summary of three-dimensional knee models in literature. Included models contained: all three bones (Tibia, Femur, Patella), both tibiofemoral (TF) and patellofemoral (PF) joint contact, a six-degree-of-freedom (DOF) tibiofemoral joint, both muscle and contact forces, and high-fidelity contact surfaces.

Year(s)	*Authors*	*Geometry*	*Meniscus*	*Contact Model*	*Solution Method*	*Muscle Control*	*Motions*
1989	Essinger et al.	TKA	n/a	Elastic Foundation	Sequential	Passive Springs	Flexion-Extension
1998a; 1998b	Kim	Native	-	Elastic Foundation (TF) / Rigid (PF)	Sequential	Constant Force	Flexion-Extension
1998a; 1998b	Pandy et al	Native[T,P]	-	Elastic Foundation (PF) / Rigid (PF)	Sequential	Passive; Constant Force	Flexion-Extension
2001	Piazza and Delp	TKA	n/a	Rigid Surfaces	Sequential	EMG-driven	Step-up
2004	Caruntu and Hefzy	Native[T]	-	Elastic Foundation	Sequential	Constant Force	Flexion-Extension
2004; 2005; 2006	Shelburne et al.	Native	Posterior Shear Force	Elastic Foundation	Sequential	Dynamic Optimization	Gait, Vertical Jump
2007; 2009; 2011	Shin et al.	Native	-	Elastic Foundation	Concurrent	Passive Springs	Single Leg Landing
2010	Dhaher et al.	Native	Finite Element	Finite Element	Sequential	Constant Force	Extension
2010; 2012; 2013	Guess et al.	Native	Multibody Deformable	Elastic Foundation	Concurrent	PD Controller	Squat, Gait
2013	Hast et al.	TKA	n/a	Elastic Foundation	Sequential	Dual Joint Optimization	Gait
2013; 2014	Stylianou et al., Guess et al.	TKA	n/a	Elastic Foundation	Concurrent	PID Controller	Squat, Toe-Rise, Gait
2014, 2014, 2016	Adouni et al., Marouane et al.	Native	Finite Element	Finite Element	Concurrent	Static Optimization	Gait (6 instants)
2014	Thelen et al.	TKA	-	Elastic Foundation	Concurrent	Computed Muscle Control	Gait
2015	Lenhart et al.	Native	-	Elastic Foundation	Concurrent	Computed Muscle Control	Flexion-Extension
2015, 2016	Marra et al., Chen et al.	TKA	n/a	Elastic Foundation	Concurrent	Force-Dependent Kinematics	Gait
2016	Halonen et al.	Native	Finite Element	Finite Element	Sequential	PID Controller	Gait
2016	Smith et al. (a,b)	Native/TKA	-	Elastic Foundation	Concurrent	COMAK	Gait
2016	Eskinazi et al.	TKA	n/a	Surrogate Finite Element	Concurrent	PD Controller	Flexion-Extension

[T]Geometry assumed planar tibia surface
[P]Geometry assumed planar patella surface

Surrogate approaches can be used to generate a numerical input-output relationship for a complex finite element model that, following calibration, can be queried efficiently within a dynamic simulation. For example, Lin et al. [92,93] was able to pre-compute a regression relationship between joint kinematics and contact loads for a finite element knee model over a large range of anatomically reasonable kinematic poses. In a subsequent multibody dynamic simulation, they showed that the regression equations could be queried in place of solving the FE model, with negligible computational cost and relatively close adherence to the FE solutions. An alternative "adaptive surrogate modeling", or "lazy-learning", scheme has also been proposed[94], wherein a FE model is still used to generate a surrogate regression model, but the FE model is only solved when the input states differ significantly from previously-encountered states within a dynamic simulation. For situations where the model

parameters are well-defined, surrogate modeling approaches can afford significant computational savings. However, any alteration in finite element model parameters or geometry would require re-calibration of the surrogate regression equations, which can make it computationally demanding to fully assess sensitivities of the model outcomes.

The alternative approach used to represent joint mechanics within a dynamic simulation uses strand-based ligaments and an elastic foundation articular contact model. As described above, the elastic foundation model solves for the contact pressure on each face in a surface mesh based on the local penetration depth. In doing so, the pressure on each face is solved independently, making the problem more computationally tractable within the context of a whole body dynamic simulation. Advanced algorithms have recently been introduced which use bounding volume hierarchy techniques developed by the computer graphics field to further improve the speed of elastic foundation implementations[95]. Strand-based ligaments also provide vastly improved speeds compared to FE models by representing ligaments as bundles of independent one-dimensional nonlinear springs.

Six degree of freedom, multi-body joint models can greatly enhance the information obtained in a musculoskeletal simulation of movement. Traditionally, movement simulation models use simplified joints (e.g. hinge or ball-and-socket) in which artificial mathematical constraints restrict secondary motion. In contrast, a six degree of freedom joint model directly includes representations of the soft tissues (ligaments, cartilage) that span a joint, and thus can provide estimates of the physiological loads needed to constrain motion. A number of investigators have demonstrated the viability of simulating dynamic six degree of freedom joint behavior during passive and simple movement conditions (Table 1, *concurrent* solution method). However, six DOF joints introduce significant complexity into calculation of the neuromuscular control needed to generate active, multi-joint movement. Conventional tracking control algorithms are predicated on linked-segment models

with constrained joints. With constrained joints, the capacity of individual muscles to transmit joint loads and induce whole body accelerations is readily calculated, and this information is then used to compute controls that generate a desired movement [51,52,96]. In a six degree of freedom joint with soft constraints, muscle loads are no longer instantaneously transmitted across a joint, complicating the calculation of a muscle's capacity to induce acceleration along a specific DOF. This makes it challenging to use static optimization approaches to resolve muscle redundancy at a discrete time step within a dynamic simulation. Dynamic optimization is a powerful alternative for determining a muscle activation patterns that generate a desired movement [48,50,97,98], but dynamic optimization is much more computationally expensive and as a result not widely used to simulate subject-specific movement.

Recently, two different research groups have introduced approaches for computing muscle coordination patterns and six degree of freedom joint mechanics that are dynamically consistent with observed movements[28,99,100]. These studies define a set of *primary* degrees of freedom (DOF) which can be readily and reliably measured using standard gait analysis techniques (e.g. pelvis translations and rotations, hip rotations, tibiofemoral flexion, ankle flexion). A set of *secondary* DOF is also defined, which consist of kinematics (e.g. tibiofemoral translations and non-sagittal rotations) that are poorly measured with conventional motion capture[101,102]. A multibody musculoskeletal simulation is then performed where the *primary* degrees of freedom track the observed movement, and the secondary DOF evolve naturally from the soft tissues acting within a six degree of freedom joint. Muscle force distribution within these algorithms[99,100] is resolved using numerical optimization at each time frame to minimize an assumed cost function, such as the sum of weighted muscle activations squared[39,43]. For relatively slow activities such as human gait, these approaches have been shown to yield patterns of muscle activation that are similar to experimental EMG, and yield reasonable predictions of *in vivo* knee contact forces[28,103]. Furthermore, these methods are not restricted to knee joint analysis. The

method of Andersen et al.[100], called force-dependent-kinematics (FDK), has been recently used to examine joint mechanics at the spine[104], shoulder[105], wrist[106], and hip[107] joints.

The following chapters of this dissertation present the Concurrent Optimization of Muscle Activations and Kinematics (COMAK) algorithm, which is capable of simulating full six degree of freedom tibiofemoral, patellofemoral, and meniscal mechanics during gait [28,108–110]. The COMAK algorithm is demonstrated using a multibody knee model with elastic foundation contact and strand based ligaments to study the effect of ACL injury and treatments on knee mechanics during walking.

References

1. Zhang, Y. & Jordan, J. Epidemiology of Osteoarthritis. *Clin. Geriatr. Med.* **26,** 355–369 (2010).

2. Oliveria, S. A., Felson, D. T., Reed, J. I., Cirillo, P. A. & Walker, A. M. Incidence of symptomatic hand, hip, and knee osteoarthritis among patients in a health maintenance organization. *Arthritis Rheum.* **38,** 1134–1141 (1995).

3. Ettinger, W., Davis, M., Neuhaus, J. & Mallon, K. "Long-term physical functioning in persons with knee osteoarthritis from NHANES I: effects of comorbid medical conditions. *J. Clin. Epidemiol.* **47,** 809–815 (1994).

4. Yelin, E. *et al.* Medical care expenditures and earnings losses among persons with arthritis and other rheumatic conditions in 2003, and comparisons with 1997. *Arthritis Rheum.* **56,** 1397–1407 (2007).

5. Anderson, D. D. *et al.* Post-traumatic osteoarthritis: Improved understanding and opportunities for early intervention. *J. Orthop. Res.* **29,** 802–809 (2011).

6. Oiestad, B. E., Engebretsen, L., Storheim, K. & Risberg, M. a. Knee Osteoarthritis After Anterior Cruciate Ligament Injury: A Systematic Review. *Am. J. Sports Med.* **37,** 1434–1443

(2009).

7. Roos, H., Adalberth, T., Dahlberg, L. & Lohmander, L. Osteoarthritis of the knee after injury to the anterior cruciate ligament or meniscus: influence of time and age. *Osteoarthr. Cartil.* **3,** 261–267 (1995).

8. Magnussen, R. A. *et al.* Cross-cultural Comparison of Patients Undergoing ACL Reconstruction in United States and Norway. *Knee Surg. Sport. Traumatol. Arthrosc.* **18,** 98–105 (2010).

9. Strehl, A. & Eggli, S. The value of conservative treatment in ruptures of the anterior cruciate ligament (ACL). *J. Trauma* **62,** 1159–1162 (2007).

10. Risberg, M. A., Mørk, M., Jenssen, H. K. & Holm, I. Design and implementation of a neuromuscular training program following anterior cruciate ligament reconstruction. *J. Orthop. Sports Phys. Ther.* **31,** 620–631 (2001).

11. Buckwalter, J. a, Anderson, D. D., Brown, T. D., Tochigi, Y. & Martin, J. a. The Roles of Mechanical Stresses in the Pathogenesis of Osteoarthritis: Implications for Treatment of Joint Injuries. *Cartilage* **4,** 286–294 (2013).

12. Herzog, W. *et al.* Material and functional properties of articular cartilage and patellofemoral contact mechanics in an experimental model of osteoarthritis. *J. Biomech.* **31,** 1137–1145 (1998).

13. Tashman, S., Collon, D., Anderson, K., Kolowich, P. & Anderst, W. Abnormal Rotational Knee Motion During Running After Anterior Cruciate Ligament Reconstruction. *Am. J. Sports Med.* **32,** 975–983 (2004).

14. Papannagari, R. *et al.* In vivo kinematics of the knee after anterior cruciate ligament reconstruction: a clinical and functional evaluation. *Am. J. Sports Med.* **34,** 2006–12 (2006).

15. Li, G. *et al.* Anterior cruciate ligament deficiency alters the in vivo motion of the tibiofemoral cartilage contact points in both the anteroposterior and mediolateral directions. *J. Bone Joint Surg. Am.* **88,** 1826–34 (2006).

16. Defrate, L. E. *et al.* The 6 degrees of freedom kinematics of the knee after anterior cruciate ligament deficiency: an in vivo imaging analysis. *Am. J. Sports Med.* **34,** 1240–6 (2006).

17. Miranda, D. L. *et al.* Knee biomechanics during a jump-cut maneuver: effects of sex and ACL surgery. *Med. Sci. Sports Exerc.* **45,** 942–51 (2013).

18. Farrokhi, S. *et al.* Altered tibiofemoral joint contact mechanics and kinematics in patients with knee osteoarthritis and episodic complaints of joint instability. *Clin. Biomech. (Bristol, Avon)* **29,** 629–35 (2014).

19. Pauwels, F. Der schenkelhalsbruch em mechanisches problem : Grundlagen des Heilungsvorganges Prognose und kausale Therapie. *Stuttgart Ferdinand Enke Verlag* (1935). doi:10.1590/1413

20. Kutzner, I. *et al.* Loading of the knee joint during activities of daily living measured in vivo in five subjects. *J. Biomech.* **43,** 2164–73 (2010).

21. Herzog, W. & Longino, D. The role of muscles in joint degeneration and osteoarthritis. *J. Biomech.* **40 Suppl 1,** S54-63 (2007).

22. D'Lima, D. D. *et al.* Tibial forces measured in vivo after total knee arthroplasty. *J.Arthroplasty* **21,** 255–262 (2006).

23. Heller, M. O. *et al.* Musculo-skeletal loading conditions at the hip during walking and stair climbing. *J. Biomech.* **34,** 883–93 (2001).

24. Halloran, J. P. *et al.* Multiscale mechanics of articular cartilage: potentials and challenges of coupling musculoskeletal, joint, and microscale computational models. *Ann. Biomed. Eng.* **40,** 2456–74 (2012).

25. Erdemir, A., McLean, S., Herzog, W. & van den Bogert, A. J. Model-based estimation of muscle forces exerted during movements. *Clin. Biomech.* **22,** 131–154 (2007).

26. Guess, T. M., Liu, H., Bhashyam, S. & Thiagarajan, G. A multibody knee model with discrete cartilage prediction of tibio-femoral contact mechanics. *Comput. Methods Biomech. Biomed. Engin.* **16,** 256–70 (2013).

27. Adouni, M. & Shirazi-Adl, A. Partitioning of knee joint internal forces in gait is dictated by the knee adduction angle and not by the knee adduction moment. *J. Biomech.* **47,** 1696–703 (2014).

28. Smith, C. R., Vignos, M. F., Lenhart, R. L., Kaiser, J. & Thelen, D. G. The Influence of Component Alignment and Ligament Properties on Tibiofemoral Contact Forces in Total Knee Replacement. *J. Biomech. Eng.* **138,** (2016).

29. Erdemir, A. Open Knee: Open Source Modeling & Simulation to Enable Scientific Discovery and Clinical Care in Knee Biomechanics. *J. Knee Surg.* **19,** 107–116 (2016).

30. Erdemir, A. Open Knee: A Pathway to Community Driven Modeling and Simulation in Joint Biomechanics. *J. Med. Device.* **7,** 40910 (2013).

31. Lenhart, R. L., Kaiser, J., Smith, C. R. & Thelen, D. G. Prediction and Validation of Load-Dependent Behavior of the Tibiofemoral and Patellofemoral Joints During Movement. *Ann. Biomed. Eng.* (2015). doi:10.1007/s10439-015-1326-3

32. Schipplein, O. D. & Andriacchi, T. P. Interaction between active and passive knee stabilizers during level walking. *J.Orthop.Res.* **9,** 113–119 (1991).

33. Blankevoort, L., Kuiper, J. H., Huiskes, R. & Grootenboer, H. J. ARTICULAR CONTACT IN A THREE-DIMENSIONAL MODEL OF THE KNEE. *J. Biomech.* **24,** 1019–1031 (1991).

34. Besier, T. F., Gold, G. E., Beaupr??, G. S. & Delp, S. L. A Modeling Framework to Estimate Patellofemoral Joint Cartilage Stress In Vivo. *Med. Sci. Sport. Exerc.* **37,** 1924–1930 (2005).

35. Morrison, J. B. The mechanics of the knee joint in relation to normal walking. *J. Biomech.* **3,** 51–61 (1970).

36. Seireg, A. & Arvikar, R. J. The Prediction of Musclular Load Sharing and Joint Forces in Lower Extremities during Walking. *JBiomech* **8,** 89–102 (1975).

37. Hardt, D. E. Determining muscle forces in the leg during normal human walking - An application and evaluation of optimization methods. *Journal of Biomechanical Engineering* **100,** 72–78 (1978).

38. Pedotti, A., Krishnan, V. V. & Stark, L. Optimization of muscle-force sequencing in human locomotion. *Math. Biosci.* **38,** 57–76 (1978).

39. Crowninshield, R. D. & Brand, R. a. A physiologically based criterion of muscle force prediction in locomotion. *J. Biomech.* **14,** 793–801 (1981).

40. Bertram, J. E. A. Constrained optimization in human walking: cost minimization and gait plasticity. *J. Exp. Biol.* **208,** 979–91 (2005).

41. Ota, K., Shinya, M. & Kudo, K. Sub-optimality in motor planning is retained throughout 9 days practice of 2250 trials. *Sci. Rep.* **6,** 37181 (2016).

42. Todorov, E. & Jordan, M. I. Optimal feedback control as a theory of motor coordination. *Nat. Neurosci.* **5,** 1226–35 (2002).

43. Happee, R. & Van der Helm, F. C. T. The control of shoulder muscles during goal directed movements, an inverse dynamic analysis. *J. Biomech.* **28,** 1179–1191 (1995).

44. DeMers, M. S., Pal, S. & Delp, S. L. Changes in tibiofemoral forces due to variations in muscle activity during walking. *J. Orthop. Res.* **32,** 769–776 (2014).

45. Buchanan, T. S., Lloyd, D. G., Manal, K. & Besier, T. F. Neuromusculoskeletal modeling: estimation of muscle forces and joint moments and movements from measurements of neural command. *J. Appl. Biomech.* **20,** 367–95 (2004).

46. Lloyd, D. G. & Besier, T. F. An EMG-driven musculoskeletal model to estimate muscle forces and knee joint moments in vivo. *J. Biomech.* **36,** 765–776 (2003).

47. Sartori, M., Gizzi, L., Lloyd, D. G. & Farina, D. A musculoskeletal model of human locomotion driven by a low dimensional set of impulsive excitation primitives. *Front. Comput. Neurosci.* **7,** 79 (2013).

48. Davy, D. T. & Audu, M. L. A dynamic optimization technique for predicting muscle forces in the swing phase of gait. *J. Biomech.* **20,** 187–201 (1987).

49. Yamaguchi, G. T. & Zajac, F. E. A planar model of the knee joint to characterize the knee extensor mechanism. *J. Biomech.* **22,** 1–10 (1989).

50. Anderson, F. C. & Pandy, M. G. Dynamic optimization of human walking. *J.Biomech.Eng* **123,** 381–390 (2001).

51. Thelen, D. G., Anderson, F. C. & Delp, S. L. Generating dynamic simulations of movement using computed muscle control. *J. Biomech.* **36,** 321–328 (2003).

52. Seth, A. & Pandy, M. G. A neuromusculoskeletal tracking method for estimating individual

muscle forces in human movement. *J. Biomech.* **40,** 356–66 (2007).

53. Guess, T. M., Stylianou, A. P. & Kia, M. Concurrent prediction of muscle and tibiofemoral contact forces during treadmill gait. *J. Biomech. Eng.* **136,** 21032 (2014).

54. Kłodowski, A. *et al.* Merge of motion analysis, multibody dynamics and finite element method for the subject-specific analysis of cartilage loading patterns during gait: differences between rotation and moment-driven models of human knee joint. *Multibody Syst. Dyn.* **37,** 271–290 (2016).

55. Winby, C. R., Lloyd, D. G., Besier, T. F. & Kirk, T. B. Muscle and external load contribution to knee joint contact loads during normal gait. *J. Biomech.* **42,** 2294–300 (2009).

56. Brandon, S. C. E., Miller, R. H., Thelen, D. G. & Deluzio, K. J. Selective lateral muscle activation in moderate medial knee osteoarthritis subjects does not unload medial knee condyle. *J. Biomech.* **47,** 1409–15 (2014).

57. Bei, Y. & Fregly, B. J. Multibody dynamic simulation of knee contact mechanics. *Med.Eng Phys.* **26,** 777–789 (2004).

58. Blankevoort, L. & Huiskes, R. Ligament-Bone Interaction in a Three-Dimensional Model of the Knee. *J. Biomech. Eng.* **113,** 263–269 (1991).

59. Essinger, J. R., Leyvraz, P. F., H, J. H. H. J. & Robertson, D. D. A mathematical model for the evaluation of the behavior during flexion of condylar-type knee prostheses. *J Biomech* **22,** 1229–12241 (1989).

60. Halloran, J. P., Easley, S. K., Petrella, A. J. & Rullkoetter, P. J. Comparison of deformable and elastic foundation finite element simulations for predicting knee replacement mechanics. *J. Biomech. Eng.* **127,** 813–8 (2005).

61. Kazemi, M., Dabiri, Y. & Li, L. P. Recent advances in computational mechanics of the human knee joint. *Comput. Math. Methods Med.* **2013,** 718423 (2013).

62. Zheng, M., Zou, Z., Bartolo, P. J. D. S., Peach, C. & Ren, L. Finite Element Models of the Human Shoulder Complex: A Review of Their Clinical Implications and Modelling Techniques. *Int. j. numer. method. biomed. eng.* **30,** 659–80 (2016).

63. Peña, E., Martínez, M. A., Calvo, B., Palanca, D. & Doblaré, M. A finite element simulation of the effect of graft stiffness and graft tensioning in ACL reconstruction. *Clin. Biomech.* **20,** 636–644 (2005).

64. Dhaher, Y. Y., Salehghaffari, S. & Adouni, M. Anterior laxity , graft-tunnel interaction and surgical design variations during anterior cruciate ligament reconstruction : A probabilistic simulation of the surgery. *J. Biomech.* **49,** 3009–3016 (2016).

65. Tanska, P., Mononen, M. E. & Korhonen, R. K. A multi-scale finite element model for investigation of chondrocyte mechanics in normal and medial meniscectomy human knee joint during walking. *J. Biomech.* **48,** 1397–1406 (2015).

66. Papaioannou, G., Demetropoulos, C. K. & King, Y. H. Predicting the effects of knee focal articular surface injury with a patient-specific finite element model. *Knee* **17,** 61–68 (2010).

67. Ferguson, S. J., Bryant, J. T., Ganz, R. & Ito, K. The influence of the acetabular labrum on hip joint cartilage consolidation: a poroelastic finite element model. *J. Biomech.* **33,** 953–60 (2000).

68. Ellis, B. J. *et al.* Finite element modelling of the glenohumeral capsule can help assess the tested region during a clinical exam. *Comput. Methods Biomech. Biomed. Engin.* **13,** 413–418 (2010).

69. Halonen, K. S., Mononen, M. E., Jurvelin, J. S., Töyräs, J. & Korhonen, R. K. Importance of depth-wise distribution of collagen and proteoglycans in articular cartilage-A 3D finite element

study of stresses and strains in human knee joint. *J. Biomech.* **46,** 1184–1192 (2013).

70. Adouni, M. & Dhaher, Y. Y. A multi-scale elasto-plastic model of articular cartilage. *J. Biomech.* **49,** 2891–2898 (2016).

71. Jinha, A., Ait-Haddou, R. & Herzog, W. Predictions of co-contraction depend critically on degrees-of-freedom in the musculoskeletal model. *J. Biomech.* **39,** 1145–52 (2006).

72. Marouane, H., Shirazi-Adl, A. & Adouni, M. 3D active-passive response of human knee joint in gait is markedly altered when simulated as a planar 2D joint. *Biomech. Model. Mechanobiol.* (2016). doi:10.1007/s10237-016-0846-6

73. Lin, Y.-C., Walter, J. P., Banks, S. a, Pandy, M. G. & Fregly, B. J. Simultaneous prediction of muscle and contact forces in the knee during gait. *J. Biomech.* **43,** 945–52 (2010).

74. Koolstra, J. H. & Van Eijden, T. M. G. J. Combined finite-element and rigid-body analysis of human jaw joint dynamics. *J. Biomech.* **38,** 2431–2439 (2005).

75. Kim, S. Muscle-ligament interactions at the human knee (I) - Maximum isometric leg exercises. *KSME Int. J.* **12,** 1079–1089 (1998).

76. Kim, S. Three-Dimensional Dynamic Model of the Knee. *KSME Int. J.* **12,** 1041–1063 (1998).

77. Pandy, M. G., Sasaki, K. & Kim, S. A Three-Dimensional Musculoskeletal Model of the Human Knee Joint. Part 1: Theoretical Construct. *Comput. Biomech.Biomed.Engin.* **1,** 87–108 (1998).

78. Pandy, M. G., Sasaki, K., Taylor, P., Pandy, M. G. & Sasaki, K. A Three-Dimensional Musculoskeletal Model of the Human Knee Joint. Part 2: Analysis of Ligament Function. *Comput Methods Biomech Biomed Engin* **1,** 265–283 (1998).

79. Piazza, S. J. & Delp, S. L. Three-Dimensional Dynamic Simulation of Total Knee Replacement

Motion During a Step-Up Task. **123,** 599–606 (2001).

80. Caruntu, D. I. & Hefzy, M. S. 3-D Anatomically Based Dynamic Modeling of the Human Knee to Include Tibio-Femoral and Patello-Femoral Joints. *J. Biomech. Eng.* **126,** 44 (2004).

81. Shelburne, K. B., Pandy, M. G., Anderson, F. C. & Torry, M. R. Pattern of anterior cruciate ligament force in normal walking. *J. Biomech.* **37,** 797–805 (2004).

82. Shelburne, K. B., Torry, M. R. & Pandy, M. G. Muscle, Ligament, and Joint-Contact Forces at the Knee during Walking. *Med. Sci. Sport. Exerc.* **37,** 1948–1956 (2005).

83. Shelburne, K. B., Torry, M. R. & Pandy, M. G. Contributions of muscles, ligaments, and the ground-reaction force to tibiofemoral joint loading during normal gait. *J.Orthop.Res.* **24,** 1983–1990 (2006).

84. Shin, C. S., Chaudhari, A. M. & Andriacchi, T. P. The effect of isolated valgus moments on ACL strain during single-leg landing: A simulation study. *J. Biomech.* **42,** 280–285 (2009).

85. Shin, C. S., Chaudhari, A. M. & Andriacchi, T. P. Valgus plus internal rotation moments increase anterior cruciate ligament strain more than either alone. *Med. Sci. Sports Exerc.* **43,** 1484–1491 (2011).

86. Shin, C. S., Chaudhari, A. M. & Andriacchi, T. P. The influence of deceleration forces on ACL strain during single-leg landing: a simulation study. *J. Biomech.* **40,** 1145–52 (2007).

87. Dhaher, Y. Y., Kwon, T. & Barry, M. The effect of connective tissue material uncertainties on knee joint mechanics under isolated loading conditions. *J. Biomech.* **43,** 3118–3125 (2010).

88. Guess, T. M., Thiagarajan, G., Kia, M. & Mishra, M. A subject specific multibody model of the knee with menisci. *Med. Eng. Phys.* **32,** 505–15 (2010).

89. Guess, T. M. Forward dynamics simulation using a natural knee with menisci in the multibody framework. *Multibody Syst. Dyn.* **28,** 37–53 (2012).

90. Hast, M. W. & Piazza, S. J. Dual-joint modeling for estimation of total knee replacement contact forces during locomotion. *J. Biomech. Eng.* **135,** 21013 (2013).

91. Stylianou, A. P., Guess, T. M. & Kia, M. Multibody muscle driven model of an instrumented prosthetic knee during squat and toe rise motions. *J. Biomech. Eng.* **135,** 41008 (2013).

92. Lin, Y.-C., Farr, J., Carter, K. & Fregly, B. J. Response surface optimization for joint contact model evaluation. *Journal of applied biomechanics* **22,** 120–30 (2006).

93. Lin, Y.-C., Haftka, R. T., Queipo, N. V & Fregly, B. J. Surrogate articular contact models for computationally efficient multibody dynamic simulations. *Med. Eng. Phys.* **32,** 584–94 (2010).

94. Halloran, J. P., Erdemir, A. & van den Bogert, A. J. Adaptive Surrogate Modeling for Efficient Coupling of Musculoskeletal Control and Tissue Deformation Models. *J. Biomech. Eng.* **131,** 11014 (2009).

95. Smith, C. R., Won Choi, K., Negrut, D. & Thelen, D. G. Efficient computation of cartilage contact pressures within dynamic simulations of movement. *Comput. Methods Biomech. Biomed. Eng. Imaging Vis.* 1–8 (2016). doi:10.1080/21681163.2016.1172346

96. Thelen, D. G. & Anderson, F. C. Using computed muscle control to generate forward dynamic simulations of human walking from experimental data. *J. Biomech.* **39,** 1107–1115 (2006).

97. Anderson, F. C. & Pandy, M. G. A Dynamic Optimization Solution for Vertical Jumping in Three Dimensions. *Comput. Biomech.Biomed.Engin.* **2,** 201–231 (1999).

98. Lee, L. & Umberger, B. R. Generating optimal control simulations of musculoskeletal

movement using OpenSim and MATLAB. *PeerJ* **4,** e1638 (2016).

99. Thelen, D. G., Won Choi, K. & Schmitz, A. M. Co-simulation of neuromuscular dynamics and knee mechanics during human walking. *J. Biomech. Eng.* **136,** 21033 (2014).

100. Andersen, M. S., Damsgaard, M. & Rasmussen, J. Force-dependent Kinematics: A new Analysis Method for Non-conforming Joints. *XIII Int. Symp. Comput. Simul. Biomech. June 30th - July 2nd 2011, Leuven, Belgium* 2 (2011).

101. Leardini, A., Chiari, L., Della, C. U. & Cappozzo, A. Human movement analysis using stereophotogrammetry. Part 3. Soft tissue artifact assessment and compensation. *Gait Posture* **21,** 212–225 (2005).

102. Li, K., Zheng, L., Tashman, S. & Zhang, X. The inaccuracy of surface-measured model-derived tibiofemoral kinematics. *J. Biomech.* **45,** 2719–23 (2012).

103. Marra, M. a *et al.* A Subject-Specific Musculoskeletal Modeling Framework to Predict in Vivo Mechanics of Total Knee Arthroplasty. *J. Biomech. Eng.* **137,** 20904 (2014).

104. Ignasiak, D., Dendorfer, S. & Ferguson, S. J. Thoracolumbar spine model with articulated ribcage for the prediction of dynamic spinal loading. *J. Biomech.* **49,** 959–66 (2016).

105. Sins, L., Tétreault, P., Hagemeister, N. & Nuño, N. Adaptation of the AnyBody™ Musculoskeletal Shoulder Model to the Nonconforming Total Shoulder Arthroplasty Context. *J. Biomech. Eng.* **137,** 101006 (2015).

106. Eschweiler, J. *et al.* Development of a biomechanical model of the wrist joint for patient-specific model guided surgical therapy planning: Part 1. *Proc. Inst. Mech. Eng. Part H J. Eng. Med.* **230,** 310–325 (2016).

107. Zhang, X. *et al.* Prediction of hip joint load and translation using musculoskeletal modelling with force-dependent kinematics and experimental validation. *Proc.Inst.Mech.Eng H.* **229,** 477–490 (2015).

108. Lenhart, R. L. *et al.* Influence of Step Rate and Quadriceps Load Distribution on Patellofemoral Cartilage Contact Pressures during Running. *J. Biomech.* 1–8 (2015). doi:10.1016/j.jbiomech.2015.04.036

109. Lenhart, R. L. *et al.* Influence of patellar position on the knee extensor mechanism in normal and crouched walking. *J. Biomech.* **51,** 1–7 (2017).

110. Smith, C. R., Lenhart, R. L., Kaiser, J., Vignos, M. F. & Thelen, D. G. Influence of Ligament Properties on Tibiofemoral Mechanics in Walking. *J. Knee Surg.* **29,** 99–106 (2016).

Specific Aims

This dissertation had three specific aims involving the creation of a knee model to investigate surgical and conservative treatment of anterior cruciate ligaments (ACL) injuries. The chapters constituting the body of this dissertation are organized as a collection of five manuscripts, three (1, 3, 4) of which have been published and two of which will be submitted shortly (2, 5). Chapter 1 introduces a collision detection algorithm which enables the use of elastic foundation articular contact models within dynamic simulations of movement. Chapter 2 introduces the Concurrent Optimization of Muscle Activations and Kinematics (COMAK) simulation framework to predict muscle forces and internal joint mechanics during movement. Chapter 3 applies COMAK to study the effect of component placement and soft tissue release on knee function in total knee replacement. It also provides validation by comparing predicted joint contact forces to *in vivo* measurements from an instrumented implant. Chapter 4 applies COMAK to study the sensitivity of knee mechanics during walking to ligament stiffness and pretension. Chapter 5 applies COMAK to study the influence of neuromuscular coordination on knee mechanics during walking in the healthy, ACL deficient, and menisci deficient knee.

Aim1: Develop a simulation framework to predict knee mechanics during functional movement

Motivation:

Assessing the influence of treatments for ACL injury on soft tissue loading is complicated by the complexity of the biologic and mechanical systems that interact during functional movements. Computer simulation has potential to provide valuable insight into the sensitivities of cartilage and

ligament loading to gait dynamics, muscle coordination, articular geometries, and soft tissue properties. However, existing simulation frameworks were unable to capture the dynamic coupling between limb dynamics and joint mechanics, or assess the sensitivity of clinically relevant model parameters in a systematic fashion.

Outcome:

This dissertation introduced a probabilistic simulation framework to predict muscle forces, ligament forces, and cartilage loading during walking. The Concurrent Optimization of Muscle Activations and Kinematics (COMAK) simulation routine provides a novel methodology to simulate knee mechanics from motion capture and ground reaction measurements (Chapter 1 & Chapter 2). The application of high throughput computing (HTC) enables probabilistic analyses that enable musculoskeletal simulations to be better leveraged to provide more clinically relevant insight (Chapters 2,3,4&5). The predictive capacity of COMAK was evaluated by comparing predicted joint contact forces against *in vivo* measurements from an instrumented implant (Chapter 3). Through my work and collaborations, we have demonstrated the ability to use the modeling framework to predict tibiofemoral and patellofemoral mechanics during a wide variety of movements including: walking[1,2], running[3], stair-climbing, lunging, and jumping. The framework enables parametric variation of cartilage properties, ligament properties, articular geometries, and neuromuscular coordination strategies. It has been applied to study ACL injury[2], total knee replacement[1], cartilage defect repair and rehabilitation, osteoarthritis, and pediatric orthopedic surgeries for gait disorders[4].

Aim 2: Assess the influence of ACL reconstruction surgical parameters on cartilage loading patterns during walking

Motivation:

Restoration of healthy cartilage loading patterns following ACL reconstruction is important to mitigate the development of osteoarthritis[5]. Current ACL reconstructions do not completely restore knee mechanics during functional movements, however it is not understood how surgical techniques could be altered to provide better outcomes. Computer simulation provides potential to systematically vary surgical parameters such as graft stiffness, pretension, and tunnel location. Additionally, it can provide cause-effect insight to explain correlations found experimentally.

Outcome:

The simulation framework developed in Aim 1 was applied to study the influence of ACL graft stiffness and pretension on knee mechanics during walking (Chapter 4). The framework was also used to study ACL graft tunnel location. Recently, we found a correlation between the sagittal plane angle of the graft in an extend posture and knee kinematics and cartilage contact measured with dynamic MRI. The knee model framework was applied to demonstrate causality in this scenario even in the presence of uncertainty due to graft stiffness and pretension. The COMAK simulation routine was then used to extend this finding to walking. When variability in tunnel placement, graft stiffness and pretension were simulated, the sagittal plane graft angle was the most influential metric in determining the predicted knee mechanics during walking (Appendix A).

Aim 3: Assess the capacity of neuromuscular coordination to restore cartilage loading in ACL deficient knees during walking

Motivation:

Current conservative treatments for ACL injury attempt to restore knee stability through rehabilitative treatment. However, it is unknown whether this treatment can restore cartilage loading to normal patterns during functional movement, which has important implications for the long-term health of the knee. Musculoskeletal computer simulation provides opportunity to establish whether it is mechanically feasible to restore cartilage loading patterns in an ACL deficient knee, and provide insights into the muscles that might be trained to achieve this effect.

Outcome:

The probabilistic simulation framework developed in Aim 1 was applied to assess the effect of variations in muscle coordination strategy on healthy knee mechanics during walking (Chapter 2). A similar approach was then applied to study ACL deficient and menisci deficient knees (Chapter 5). The solution spaces of the muscle redundancy during walking were compared for these three conditions to establish that no neuromuscular coordination strategy exists to restore cartilage loading in an ACL deficient knee if the limb dynamics are unchanged. Furthermore, ACL loading could not be restored to normal in the menisci deficient knee.

Chapter 1

Efficient Computation of Cartilage Contact Pressures within Dynamic Simulations of Movement

Colin R. Smith, Kwang Won Choi, Dan Negrut, Darryl G. Thelen
(Published in Computer Methods in Biomechanics and Biomedical Engineering: Imaging and Visualization)

Abstract

The objective of this study was to assess the use of an advanced collision detection algorithm to simulate cartilage contact pressure patterns within dynamic musculoskeletal simulations of movement. We created a knee model that included articular cartilage contact for the tibiofemoral and patellofemoral joints. Knee mechanics were then predicted within the context of a dynamic gait simulation. At each time step of a simulation, ray-casting was used in conjunction with hierarchical oriented bounding boxes (OBB) to rapidly identify regions of overlap between articulating cartilage surfaces. Local cartilage contact pressure was then computed using an elastic foundation model. Collision detection implemented in parallel on a GPU provided up to a 10x speed increase when using high resolution mesh densities that had >10 triangles/mm2. However, pressure magnitudes converged at considerably lower mesh densities (2.6 triangles/mm2) where CPU and GPU implementations of collision detection exhibited equivalent performance. Simulated tibiofemoral contact locations were comparable to prior experimental measurements, while pressure magnitudes were similar to those predicted by finite element models. We conclude the use of ray-casting with hierarchical OBB for collision detection is a viable method for simulating joint contact mechanics in human movement.

Introduction

The loading of articular cartilage during functional movement is important to consider when investigating cartilage health and pathology. Because cartilage loading cannot be directly measured *in vivo*, computational modelling is a valuable tool to investigate dynamic cartilage loading and provide insight into surgical treatments and rehabilitation protocols. However, the prediction of cartilage loading within multibody movement simulations presents a complex computational problem. While finite element analyses (FEA) are conventionally used to estimate cartilage tissue stress, they remain too computationally expensive to solve within the context of a movement simulation[1,2]. Traditional multibody musculoskeletal models resort to simplified kinematic joints to reduce complexity[3,4], but these intrinsically ignore the load dependent behaviour of the joint and cannot provide estimates of cartilage loading. As a result, elastic foundation models have been introduced to efficiently model joint contact within whole body simulations of movement[5–7].

In elastic foundation models, cartilage is considered an elastic tissue bonded to a rigid bone substrate. The articulating cartilage geometries are represented by surface meshes which can interpenetrate. Pressure on each element in contact is computed independently of neighbouring elements based on the local overlap distance and the thickness of the cartilage tissue. The resulting model of the cartilage tissue layer is mechanically equivalent to a bed of independent nonlinear compressive springs distributed over rigid bones[7]. Elastic foundation approaches have been used to study contact mechanics in various diarthrodial joints including the hip[8], knee[7,9–11], and ankle[9,12].

Although elastic foundation models are substantially faster than FEA, in practice the detection of overlapping faces of high resolution cartilage meshes remains a computational bottleneck. This task becomes remarkably burdensome within a dynamic simulation of movement, where collision detection and penetration depth calculations are repeated a minimum of once per time step[5,13]. A brute

force approach to collision detection evaluates penetration between every pair of elements of two surfaces, resulting in an $O(n^2)$ complexity. Prior biomechanical studies have reduced the computational demand by only searching physically plausible contact regions[7,14]. Meanwhile, the computer graphics community has introduced a number of general purpose algorithms to accelerate collision detection of objects represented by polygon meshes[15]. One approach uses ray-casting in conjunction with hierarchical oriented bounding boxes (OBBs) to efficiently identify overlapping regions of two polygon meshes[16]. The ray-casting OBB algorithm provides local overlap depth estimations making it well suited for joint contact. Additionally, it can be implemented in parallel, and thus in theory made substantially faster when run on a parallelized graphics processor unit (GPU)[17]. However, it remains unclear what mesh resolution is required to obtain reliable cartilage contact pressures and whether the increase in computational speed resulting from a GPU implementation outweighs the memory transfer overhead.

The objective of this study was to assess the feasibility of calculating cartilage contact pressures within a multibody dynamic simulation of movement using ray-casting with OBBs for collision detection. As a test case, knee cartilage contact pressures were simulated during walking using elastic foundation contact models. We investigate the computational efficiency of CPU and GPU implementations of collision detection and also assess the effects of mesh density on pressure magnitudes and contact areas.

Methods

Knee Model

A multibody knee model was developed from magnetic resonance (MR) images of the right knee of a healthy young adult female (age = 23 years, height = 1.65 m, mass=61 kg). Development and validation of the knee model are detailed elsewhere[18]. Briefly, bone and cartilage surface geometries of the tibia, femur and patella were manually segmented from the MR images and converted to triangulated surface meshes (MIMICS, Materialise Group, Leuven, Belgium). The origins, insertions and paths of 14 ligaments were also segmented and represented as bundles of nonlinear springs. The knee model allowed for six degree of freedom (DOF) tibiofemoral and patellofemoral motion. The knee was integrated into a generic lower extremity musculoskeletal model[19], which included 44 muscles acting about the hip, knee and ankle joints (Figure 1). The full model was implemented in SIMM[20] with the Dynamics Pipeline (Musculographics Inc., Santa Rosa, CA) and SD/Fast (Parametric Technology Corp., Needham, MA) used to generate the code describing muscle-tendon dynamics and the multibody equations of motion.

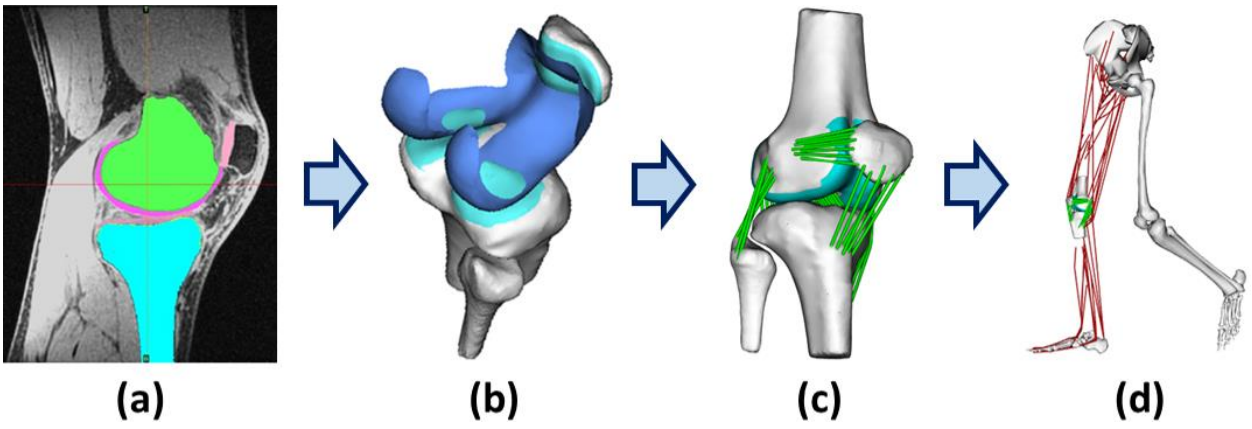

Figure 1 Model development: a) Cartilage, bone and ligament geometries were manually segmented from MR images b) Bone and cartilage geometries were converted to triangulated surface meshes c) Ligaments were represented as bundles of nonlinear springs spanning from origin to insertion d) The knee model was integrated into a generic lower extremity model[19].

Contact Pressure

At each time step of a simulation, cartilage contact pressures were calculated using an elastic foundation model. Cartilage contact was determined by the overlap of cartilage surface meshes fixed to the femur, tibia and patella segments. These segments were positioned in accordance with the current system state. The contacting triangles of cartilage meshes were determined using an OBB collision detection algorithm (Section 2.3).

The contact pressure (p) on an individual triangle in each cartilage mesh was calculated according to elastic foundation theory developed for articular cartilage[7]:

$$p = -\frac{(1-v)E}{(1+v)(1-2v)}\ln(1-\frac{d}{h}) \quad (1)$$

where E is the cartilage elastic modulus, v is the cartilage Poisson's ratio, d is the local overlap depth and h is the local cartilage thickness. E and v were assumed to be 5 MPa and 0.45 respectively[21,22]. The calculation of d is defined in the following section (Eq. 2). Local cartilage thickness (h) was computed by casting a ray from each triangle in the cartilage mesh towards the underlying bone mesh. The ray-triangle intersection was determined using the collision detection algorithm and Eq. 2 determined the local thickness.

Collision Detection

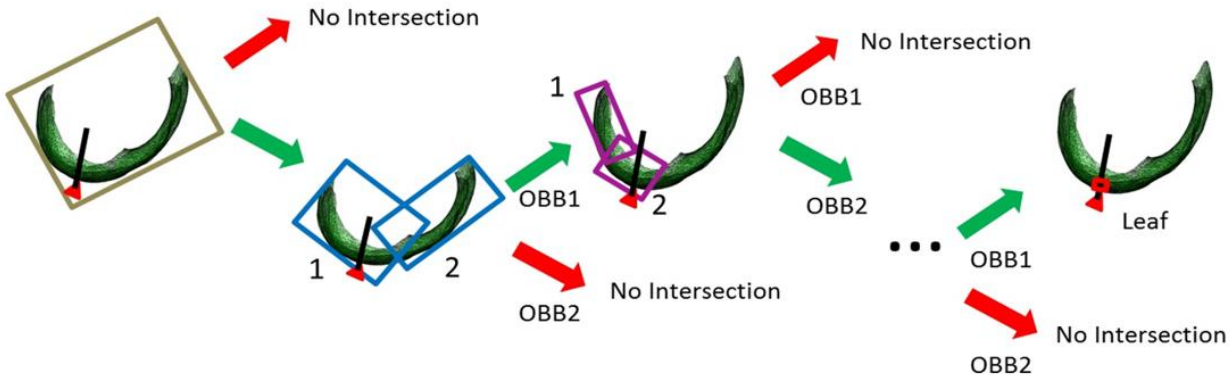

Figure 2 Collision Detection: A ray is cast normal to each triangle in the *contact* mesh. A ray-intersection test is performed for each level in the oriented bounding box (OBB) hierarchy until a leaf node is reached and the contacting triangle in the *target* mesh is determined.

The pressure calculation required local cartilage overlap depth values for each contacting triangle in the surface meshes. Prior to the simulation, an OBB tree was constructed for the femoral cartilage geometry using the Proximity Query Package (PQP) software[23]. The OBB tree was constructed using a top down approach, where the parent box in the hierarchy encloses the entire mesh and is recursively subdivided to generate child OBBs. The lowest level of the OBB tree is a leaf node, which consists of a bounding box fit around a single triangle. The OBBs were oriented to the principal vectors of the covariance matrix calculated from the positions of the enclosed triangle vertices to ensure a tight fit[24].

For each pair of contacting cartilage surfaces, we defined *contact* (tibia/patella) and *target* (femur) surfaces. To check for contact, a normal ray was cast in both directions from the centre of each triangle in the *contact* meshes. A ray-OBB intersection test determined if the ray intersected the parent box of the OBB tree[25]. If no intersection occurred, the triangle was not in contact and the test was terminated. If the ray intersected the parent OBB, then a ray-OBB intersection test was performed for each child OBB in the next sub-hierarchy. This process was repeated recursively until a leaf node was reached, resulting in a pair of potentially contacting triangles (Figure 2).

The depth of penetration (d) for each triangle pair was computed using:

$$d = \frac{(\overrightarrow{P_t} - \overrightarrow{C_c}) \cdot \widehat{n_t}}{\widehat{n_c} \cdot \widehat{n_t}} \quad (2)$$

where $\overrightarrow{P_t}$ is the intersection point on the *target* triangle (femur), $\overrightarrow{C_c}$ is the centre of the ray-casting triangle (*contact* body), $\widehat{n_t}$ is the *target* triangle unit normal vector and $\widehat{n_c}$ is the *contact* triangle unit normal vector (Figure 3). The intersection point on the *target* triangle was used for the distance calculation instead of the triangle centre to insure C0 continuity when the model pose changed and the ray intersected a neighbouring triangle. A positive value of d indicated the triangles were contacting and pressure was computed.

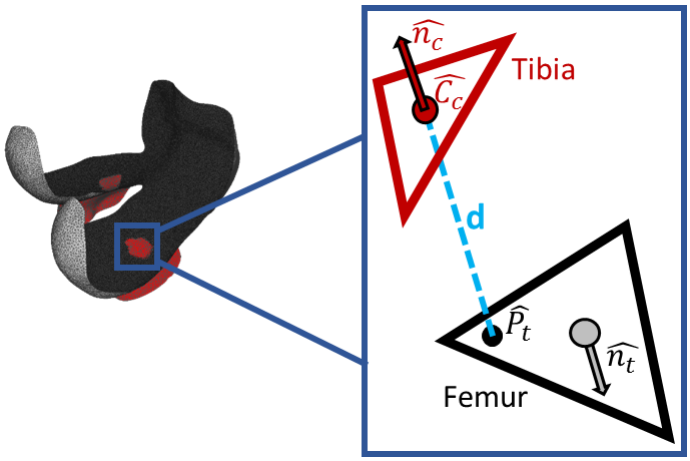

Figure 3 Penetration Depth: The local depth of penetration (d) is defined as the normal distance from the center of a *contact* mesh face to the point of intersection with the *target* mesh.

In practice, we included several constraints on the algorithm which accelerated its computational performance and robustness. A maximum distance threshold was defined to restrict ray intersections to a feasible region. In cases of extreme concavity where multiple OBBs were intersected, each path was traced through the OBB hierarchy. If this resulted in more than one intersected triangle, only the closest was used. Finally, to exploit the small changes in segment poses between time steps, a ray-intersection test was performed with the contacting triangle from the previous time step before progressing through the OBB tree.

GPU Implementation

The collision detection algorithm was implemented both on a Central Processing Unit (CPU: AMD Phenom II X6 1055 T Processor 2.8GHz, with 8GB Main RAM) and a Graphics Processing Unit (GPU: NVIDIA GeForce GTX 560Ti with 1GB Graphics RAM). The OBB tree was constructed on the GPU using the gProximity software[26] which first groups the triangles into hierarchies, then fits OBBs to these groups in parallel using the same principal component definition as the CPU[17]. The GPU implementation of the collision detection relied on Compute Unified Device Architecture (CUDA)[27] to perform all ray-OBB intersection tests of a single hierarchy level in parallel on 384 CUDA cores.

Neuromuscular Simulations of Walking

To assess the performance of the contact algorithm, we used the musculoskeletal model to simulate tibiofemoral cartilage contact pressures during walking. The trajectories of reflective markers placed over bony landmarks, and ground reaction loads were recorded while the subject walked overground at a preferred speed in a motion analysis laboratory[18]. At each frame of the gait cycle, a global optimization inverse kinematics routine determined pelvis translations, pelvis rotations, hip angles, knee flexion angle, and ankle angle that minimized the sum of squared differences between model marker locations and measured marker locations. At this stage, secondary tibiofemoral and all patellofemoral degrees of freedom were assumed to be a constrained function of tibiofemoral flexion, with these functions based on our simulated passive knee behaviour.

A computed muscle control (CMC) algorithm was used to compute the muscle excitations needed to drive the model to track the measured hip, knee and ankle kinematics, while the pelvis motion was prescribed to the measured coordinates[5] (Figure 4). CMC is a feedforward-feedback controller that uses the error between the simulated and measured kinematics at the current time step to compute

muscle excitations required to generate the measured the joint angle trajectories. At each time step, the current pose of the femur, tibia and patella were used to calculate the ligament forces and cartilage contact pressures. Measured ground reactions were applied directly to the feet. The computed muscle excitations were applied to the model and the equations of motion integrated to the next time step where the process was repeated. All tibiofemoral kinematics except flexion and all patellofemoral kinematics were allowed to evolve naturally as a result of the calculated muscle forces, ligament forces and cartilage contact pressures.

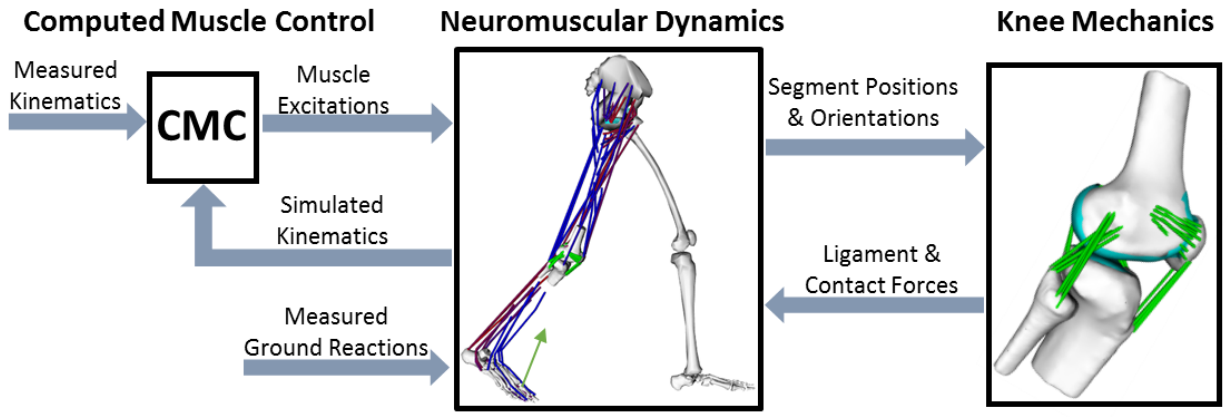

Figure 4 Neuromuscular Simulation: A computed muscle control (CMC) algorithm was used to modulate the lower limb muscle excitations such that the simulation closely tracked the measured hip, knee, and ankle angles. At every time step, the tibia, patella, and femur positions were used to ascertain the tibiofemoral and patellofemoral contact and ligament forces. These forces were then applied within the forward dynamic simulation of the neuromusculoskeletal model.

Performance Tests

We performed a series of tests to assess the influence of the cartilage mesh density and processor implementation on the contact pressure computation time and contact pressure patterns. Computation times needed to calculate the contact pressures were evaluated for the CPU and GPU implementations. These timed computations were performed at a single frame of the walking simulations, with the femur and tibia positions set to correspond to the second peak of the tibiofemoral loading during stance. Computation times were repeated for cartilage surface mesh

resolutions varying from 0.02 triangles/mm^2 to 144 triangles/mm^2. Re-meshing was performed using a proprietary algorithm which ensures uniform tessellation (Geomagic, 3D Systems, Rockhill, SC). Reported GPU times included the transfer time between the main memory in the host and the global memory in the GPU. Additionally, we compared mean pressure, contact area and centre of pressure (COP) to assess the mesh density for which the cartilage surfaces generated converged values.

Results

Neuromuscular Simulation of Walking

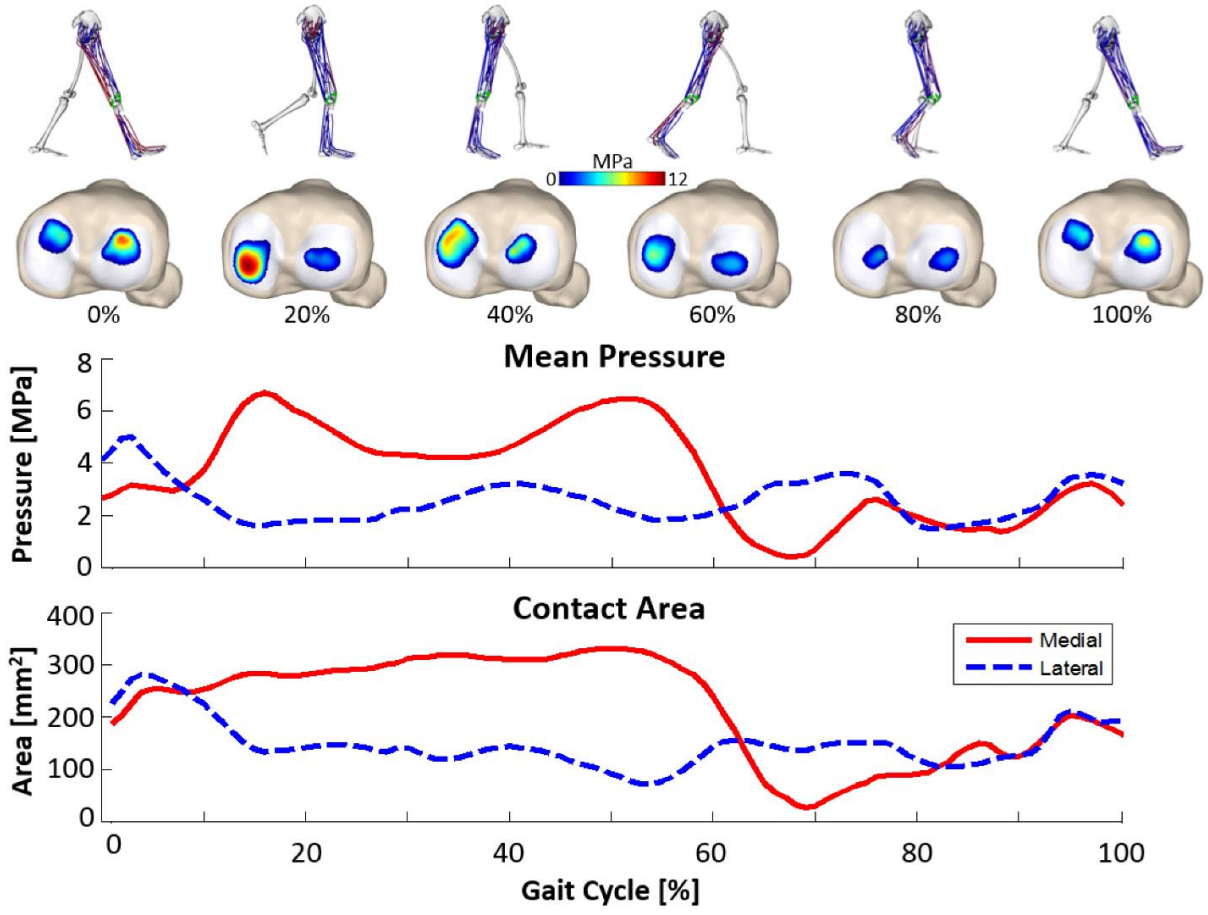

Figure 5 Tibiofemoral Contact: Simulated cartilage contact pressure and area on the medial and lateral compartments of the tibial plateau over a gait cycle.

The nominal muscle-actuated gait simulation closely tracked the measured kinematics (RMS error <1.0^{o} for all joints). Simulation of one gait cycle took 120 minutes to generate using the CPU contact detection implementation and a mesh density of 2.6 triangles/mm^2. Net tibiofemoral contact force patterns exhibited the characteristic double-peak during stance, with the majority of the force passing through the medial compartment. The mean pressure on the medial tibial plateau showed a similar trend with a double peak during stance (1st peak = 6.7 MPa, 2nd peak = 6.5 MPa), and reduced contact pressure during swing. The mean pressure on the lateral tibial plateau peaked at heel strike (5.0 MPa) and then remained relatively constant through the rest of the gait cycle (Figure 5). Contact on the medial compartment moved to the posterior portion of the plateau at the first peak, then to the anterior region of the plateau for the second peak. The medial centre of pressure (COP) translated more than the lateral COP in the anterior-posterior direction over the gait cycle (Range: medial = 14.7 mm, lateral = 10.8mm).

Sensitivity to Mesh Density

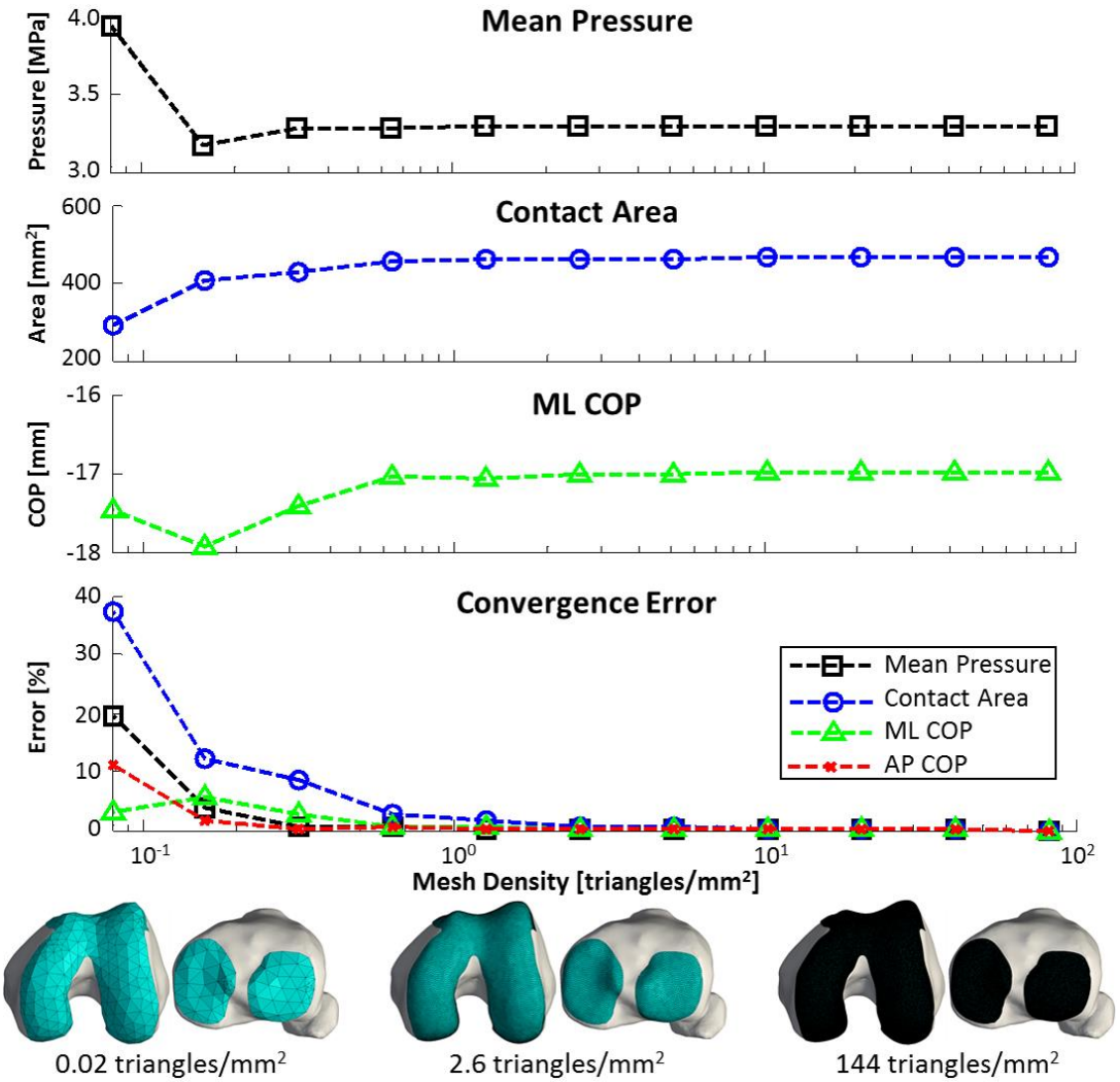

Figure 6 Mesh Convergence: Tibiofemoral pressure calculations were repeated at a single pose with mesh densities varying from 0.02 to 144 triangles/mm^2. Predicted pressure, area and centre of pressure (COP) values were within 1% of the converged value at a mesh density of 2.6 triangles/mm^2.

The mean pressure, contact area and centre of pressure metrics all converged to consistent values as mesh density was increased. A mesh density of at least 2.6 triangles/mm^2 was required for these metrics to fall within 1% of the converged values (Figure 6).

Computation Times

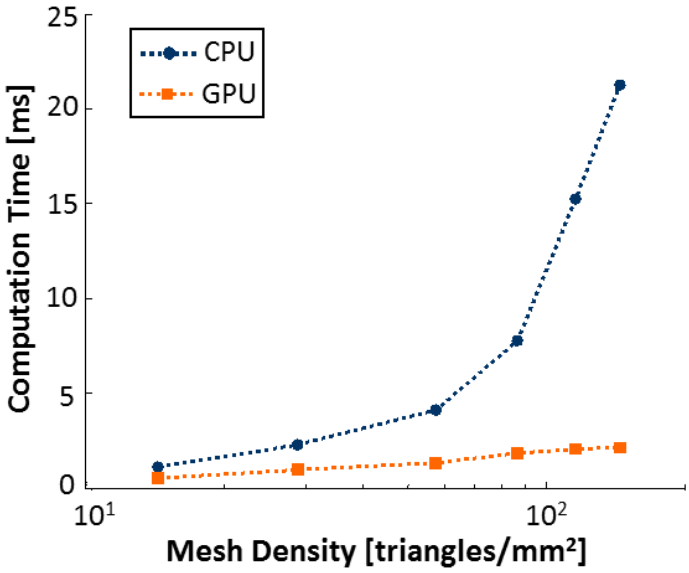

Figure 7 Computation Time: A comparison of computation times for tibiofemoral pressure calculation at a single pose (2nd peak of tibiofemoral loading) for the CPU and GPU implementations of the collision detection algorithm. GPU times include the transfer time between the main memory in the host and the global memory in the GPU. CPU and GPU computation times were similar for cartilage mesh densities lower than ~10 triangles/mm^2.

Solution time for contact detection at a single pose increased with increasing mesh density for both the CPU and GPU implementations. The GPU implementation of the contact detection algorithm resulted in similar computation times to the CPU implementation at mesh densities up to approximately 10 triangles/mm^2. Thereafter, the rate of increase in computation time was greater for the CPU implementation (Figure 7). At the highest tested mesh density of (144 triangles/mm^2), the GPU implementation was 10x faster than the CPU implementation.

Discussion

Computing cartilage contact pressures within a dynamic simulation requires that collision detection is performed at every time step. However, collision detection is computationally demanding when high resolution cartilage surface meshes are used. In this study, we demonstrate that the use of ray casting with oriented bounding boxes can accelerate collision detection, allowing for the simulation of tibiofemoral and patellofemoral cartilage contact pressures within a dynamic simulation of gait. The new computational approach allows for investigations of causal relationships between ligament

properties, contact pressures and muscle coordination to be performed[13], which have great importance to both orthopaedic and rehabilitative medicine.

Our gait simulation predicted the characteristic bimodal loading of the tibiofemoral joint during the stance phase of walking. The medial contact pressures were higher than on the lateral side, and the medial centre of pressure progressed anteriorly from the first peak of tibiofemoral loading to the second peak during stance. *In vivo* tibiofemoral contact pressures during gait have not been measured, thus direct validation is not feasible. However, the simulated pressure patterns agree favourably with image-based measures of tibiofemoral contact patterns during normal gait. Liu et al. measured cartilage deformations of 7 to 23% during the stance phase of gait, with larger anterior-posterior excursions and contact areas on the medial tibial plateau than on the lateral plateau [28]. Our gait simulations show similar trends; our medial contact area estimates area are close to Liu et al.'s measurements, however our lateral contact area tend to be ~50% lower.

Collision detection has been extensively studied in the computer graphics literature, yet the existing algorithms have not been leveraged in biomechanical modelling due in part to their general purpose formulation[14]. We implemented a popular computer graphics approach that combines ray-casting and a hierarchical structure of oriented bounding boxes to identify overlapping faces of two cartilage surfaces. While alternate collision detection algorithms exist that rely on hierarchical structures of various bounding volumes, the OBB is one of the best suited for the joint contact application. Other bounding volumes such as spheres and axis-aligned bounding boxes (AABB) perform fast intersection tests and do well in "rejection tests" when meshes are far apart. However, these algorithms produce looser fitting bounding boxes which result in more "false positives", where a ray intersects the bounding volume, but none of the included triangles. For joint contact applications where congruent meshes are in close proximity, the OBB excels because it fits tightly around the

collection of triangles, yet still allows for fast intersection tests[24,29]. For a mesh density of 2.6 triangles/mm^2, we found the OBB approach was over three orders of magnitude faster than a brute force approach that checks for contact between all face pairs between two surfaces.

Rather than employ general purpose algorithms, prior biomechanical modelling studies have done well to exploit knowledge of the application, such as physically plausible joint behaviour to improve collision detection. Bei and Fregly restricted collision detection to neighbours of previous contact patches, since relatively small changes in pose occur between simulation time steps[7]. Arbabi and colleagues pre-processed cartilage surfaces into spatial bins, which rely on the relative proximity and nature of the movement between cartilage surfaces to reduce the number of computations[14]. We also found that knowledge of small joint motion between time steps could be used to speed up our algorithm. In particular, considerable speedup was achieved by first performing a ray-intersection test with the contacting triangle from the previous time step before repeating the OBB checks. Additionally, although the algorithm could work with closed meshes, we used only the contacting surface of the cartilage to reduce the number of triangles of potential triangle contacts. When implemented in this way, CMC generated gait simulations in ~120 minutes using the minimum mesh density required to achieve converged pressure metrics. While considerably longer than using simplified joints [30], the simulations provide considerably more biomechanical information such as ligament loading, ligament stretch, and cartilage contact pressure patterns[13].

Elastic foundation models treat each face of a cartilage surface mesh independently, which allows them to be easily parallelized on a GPU. We found that a GPU collision detection algorithm[17] was 10x faster than a serial CPU implementation when using very high resolution meshes (144 triangles/mm^2). However, contact pressure and area converged at lower resolution meshes (2.6 triangles/mm^2), where the GPU and CPU implementations exhibited comparable computation times.

The limited computational performance gains at these mesh densities is likely due to the overhead costs associated with data transfer that arises in GPU scientific computing. The GPU implementation may provide benefit for applications which require meshes with large number of faces such as skin-prosthesis interfaces[31,32] or foot-ground contact[33].

There are several limitations to consider in this work. First, we did not include a meniscus in our knee model, which is well recognized to distribute pressure in the tibiofemoral joint. Recent studies have introduced discretized meniscus models[34] that would be well suited to incorporate into our multi-body knee model in the future and will further increase the need for fast contact detection. Additionally, our pressure calculations assumed linearly elastic cartilage tissue behaviour, which clearly ignores viscoelastic effects. The effects of viscoelasticity may be negligible when considered in context of the assumptions required for the elastic foundation model. While the elastic foundation model assumes that the deformation of each element is independent of neighbouring elements, it's predictions of cartilage contact pressures have shown good agreement with FEA models[8,35] and experiments[9]. However, if more complex constitutive representations of cartilage are required, it may be preferable to use gait simulation outputs as boundary conditions on a conventional finite element model.

We conclude that the use of an elastic foundation model with a ray-casting OBB contact detection algorithm is a viable approach for simulating articular contact within the context of dynamic full body movement simulations. The computational speed achieved allows for musculoskeletal simulations involving joint contact to be performed more readily, permitting the use of probabilistic approaches to look at how injury and intervention-induced changes in knee structure may affect *in vivo* knee mechanics and function.

Acknowledgements

The authors gratefully acknowledge the support of National Science Foundation (NSF) Grant 0966535 and National Institutes of Health (NIH) Grant EB015410. Additionally, we thank Rachel Lenhart, Jarred Kaiser and Anne Schmitz for their contributions to the development of the knee model and Radu Serban for his constructive feedback.

References

1. Halloran, J. P., Ackermann, M., Erdemir, A. & van den Bogert, A. J. Concurrent musculoskeletal dynamics and finite element analysis predicts altered gait patterns to reduce foot tissue loading. *J. Biomech.* **43,** 2810–5 (2010).

2. Halloran, J. P., Erdemir, A. & van den Bogert, A. J. Adaptive Surrogate Modeling for Efficient Coupling of Musculoskeletal Control and Tissue Deformation Models. *J. Biomech. Eng.* **131,** 11014 (2009).

3. Delp, S., Loan, J. & Hoy, M. An interactive graphics-based model of the lower extremity to study orthopaedic surgical procedures. *Biomed.* … **37,** 757–767 (1990).

4. Arnold, E. M., Ward, S. R., Lieber, R. L. & Delp, S. L. A Model of the Lower Limb for Analysis of Human Movement. *Ann. Biomed. Eng.* **38,** 269–279 (2010).

5. Thelen, D. G., Choi, K. W. & Schmitz, A. M. Co-Simulation of Neuromuscular Dynamics and Knee Mechanics during Human Walking. *J. Biomech. Eng.* **136,** 1–8 (2014).

6. Guess, T. M., Stylianou, A. P. & Kia, M. Concurrent prediction of muscle and tibiofemoral contact forces during treadmill gait. *J. Biomech. Eng.* **136,** 21032 (2014).

7. Bei, Y. & Fregly, B. J. Multibody dynamic simulation of knee contact mechanics. *Med. Eng.*

Phys. **26,** 777–89 (2004).

8. Abraham, C. L. *et al.* A new discrete element analysis method for predicting hip joint contact stresses. *J. Biomech.* **46,** 1121–7 (2013).

9. Anderson, D. D., Iyer, K. S., Segal, N. A., Lynch, J. A. & Brown, T. D. Implementation of Discrete Element Analysis for Subject-Specific, Population-Wide Investigations of Habitual Contact Stress Exposure. *J. Appl. Biomech.* **26,** 215–223 (2010).

10. Elias, J. J., Wilson, D. R., Adamson, R. & Cosgarea, A. J. Evaluation of a computational model used to predict the patellofemoral contact pressure distribution. *J. Biomech.* **37,** 295–302 (2004).

11. Elias, J. J. & Cosgarea, A. J. Computational modeling: an alternative approach for investigating patellofemoral mechanics. *Sports Med. Arthrosc.* **15,** 89–94 (2007).

12. Haraguchi, N., Armiger, R. S., Myerson, M. S., Campbell, J. T. & Chao, E. Y. S. Prediction of three-dimensional contact stress and ligament tension in the ankle during stance determined from computational modeling. *Foot ankle Int.* **30,** 177–185 (2009).

13. Smith, C. R., Lenhart, R. L., Thelen, D. G., Kaiser, J. & Vignos, M. F. Influence of Ligament Properties on Tibiofemoral Mechanics in Walking. **1,** (2015).

14. Arbabi, E., Boulic, R. & Thalmann, D. Fast collision detection methods for joint surfaces. *J. Biomech.* **42,** 91–99 (2009).

15. Lin, M. & Gottschalk, S. Collision detection between geometric models: A survey. *Proc. IMA Conf. Math. Surfaces* 1–20 (1998). doi:10.1.1.45.3926

16. Arvo, J. & Kirk, D. in *An Introduction to Ray Tracing* 201–262 (1989).

17. Lauterbach, C., Mo, Q. & Manocha, D. in *Computer Graphics Forum* **29,** 419–428 (2010).

18. Lenhart, R. L., Kaiser, J., Smith, C. R. & Thelen, D. G. Prediction and Validation of Load-Dependent Behavior of the Tibiofemoral and Patellofemoral Joints During Movement. *Ann. Biomed. Eng.* (2015). doi:10.1007/s10439-015-1326-3

19. Arnold, E. M., Ward, S. R., Lieber, R. L. & Delp, S. L. A Model of the Lower Limb for Analysis of Human Movement. *Ann. Biomed. Eng.* **38,** 269–279 (2010).

20. Delp, S. & Loan, J. A graphics-based software system to develop and analyze models of musculoskeletal structures. *Comput. Biol. Med.* **25,** 21–34 (1995).

21. Caruntu, D. I. & Hefzy, M. S. 3-D Anatomically Based Dynamic Modeling of the Human Knee to Include Tibio-Femoral and Patello-Femoral Joints. *J. Biomech. Eng.* **126,** 44 (2004).

22. Blankevoort, L. & Huiskes, R. Ligament-Bone Interaction in a Three-Dimensional Model of the Knee. *J. Biomech. Eng.* **113,** 263–269 (1991).

23. Larsen, E., Gottchalk, S., Lin, M. & Manocha, D. PQP - A Proximity Query Package. http://gamma.cs.unc.edu/SSV/ (2014).

24. Gottschalk, S., Lin, M. C. & Manocha, D. OBBTree: A Hierarchical Structure for Rapid Interference Detection. *Proc. 23rd Annu. Conf. Comput. Graph. Interact. Tech.* 171–180 (1996). doi:10.1145/237170.237244

25. Williams, A., Barrus, S., Morley, R. K. & Shirley, P. An Efficient and Robust Ray-Box Intersection Algorithm. *ACM SIGGRAPH 2005 Courses* 9 (2005). doi:10.1080/2151237X.2005.10129188

26. Lauterbach, C., Mo, Q. & Manocha, D. gProximity. http://gamma.cs.unc.edu/GPUCOL/ (2014).

27. Nickolls, J., Buck, I., Garland, M. & Skadron, K. Scalable parallel programming with CUDA. *Queue* **6,** 40 (2008).

28. Liu, F. *et al.* In vivo tibiofemoral cartilage deformation during the stance phase of gait. *J. Biomech.* **43,** 658–65 (2010).

29. Hahn, J. K. Realistic animation of rigid bodies. *ACM SIGGRAPH Comput. Graph.* **22,** 299–308 (1988).

30. Thelen, D. G. & Anderson, F. C. Using computed muscle control to generate forward dynamic simulations of human walking from experimental data. *J. Biomech.* **39,** 1107–15 (2006).

31. Faustini, M. C., Neptune, R. R. & Crawford, R. H. The quasi-static response of compliant prosthetic sockets for transtibial amputees using finite element methods. *Med. Eng. Phys.* **28,** 114–121 (2006).

32. Lee, W. C. C. & Zhang, M. Using computational simulation to aid in the prediction of socket fit: A preliminary study. *Med. Eng. Phys.* **29,** 923–929 (2007).

33. Neptune, R., Wright, I. & van den Bogert, A. J. A method for numerical simulation of single limb ground contact events: application to heel-toe running. *Comput. Methods Biomech. Biomed. Engin.* **3,** 321–334 (2000).

34. Guess, T. M., Thiagarajan, G., Kia, M. & Mishra, M. A subject specific multibody model of the knee with menisci. *Med. Eng. Phys.* **32,** 505–15 (2010).

35. Guess, T. M., Liu, H., Bhashyam, S. & Thiagarajan, G. A multibody knee model with discrete cartilage prediction of tibio-femoral contact mechanics. *Comput. Methods Biomech. Biomed. Engin.* **16,** 256–70 (2013).

Chapter 2

Probabilistic Simulation of Knee Mechanics during Walking using Concurrent Optimization of Muscle Activations and Kinematics (COMAK)

Colin R. Smith, Scott C. E. Brandon, Darryl G. Thelen
(In preparation for PLOS Computational Biology)

Abstract

Concurrent musculoskeletal simulation can provide insight into the roles of individual muscles in determining joint mechanics during functional whole-body movements. We introduce the Concurrent Optimization of Muscle Activations and Kinematics (COMAK) algorithm to predict muscle forces, secondary (unmeasurable) joint kinematics, ligament forces, and articular contact pressures from motion capture and ground reaction data. COMAK optimizes the muscle activations and secondary kinematics to generate the measured accelerations in the primary degrees-of-freedom while minimizing an objective function. To demonstrate the algorithm, we used a subject-specific multibody knee model (femur, tibia, patella, and menisci bodies, 24 degrees-of-freedom) and motion analysis data to predict tibiofemoral and patellofemoral joint mechanics during walking. The COMAK objective function minimized the weighted sum of squared muscle activations, where muscle-specific weights influence the solution of muscle redundancy. Random sampling of these weights in a Monte Carlo analysis generated variable muscle coordination strategies that influenced the predicted knee mechanics. A total of 10,000 simulations were performed using a high throughput computing grid. We found minor variations in predicted kinematics and contact forces during weight acceptance compared to the large variations during push off (Tibiofemoral contact force range: 1st peak 0.15 body-

weight (BW), 2nd peak 1.21 BW). In late stance, the hip, knee, and ankle moments were redistributed between the uniarticular and biarticular muscles, with the rectus femoris, gastrocnemii, and soleus activations exhibiting the strongest correlations with the predicted knee mechanics.

Introduction

The loading experienced by soft tissues within the knee during functional movement has important implications for growth, injury, and pathology[1]. Functional knee mechanics are governed by dynamic interactions across multiple scales involving limb kinetics, muscle loading, ligament loading, and articular contact. Understanding the contributions of these factors to knee function may provide insight into treatments of musculoskeletal pathologies. However, quantification of knee soft tissue loading during movement remains a challenge for both measurement and simulation approaches. Experimental studies are limited by the inability to perform multiple treatments on the same individual and difficulty of obtaining *in vivo* soft tissue loading measurements. Musculoskeletal simulation provides both of these capabilities, but is complicated by muscle redundancy, uncertainty in model parameters, and the complexity of resolving dynamically consistent muscle-driven full-body dynamics and joint mechanics.

Recent advances in musculoskeletal simulation provide improved methods for estimating *in vivo* soft tissue loads and parametric exploration of the multifactorial interactions that govern functional knee mechanics. Novel multibody musculoskeletal simulation algorithms enable limb dynamics and joint mechanics to be resolved simultaneously[2]. This provides dynamic consistency between scales, and better replicates physical reality. However, existing algorithms suffer from long computation times, numerical instability, and simplifying assumptions to compute muscle induced accelerations across six degree-of-freedom (DOF) joints[2]. Analysis techniques for quantifying

uncertainty propagation in musculoskeletal simulations have been introduced, but require extensive computing power or limited sampling of parameter space to accommodate time consuming simulations[3]. In this study, we introduce a novel simulation framework that leverages software and hardware advances to enable the interaction of limb, muscle, and joint mechanics to be investigated over the entire parameter space of a musculoskeletal model during a simulation.

Previous simulation techniques generally follow either a sequential or concurrent approach to predict internal joint mechanics during movement from motion capture and ground reaction measurements. The sequential approach consists of two stages. First, a multibody musculoskeletal simulation is performed with simplified joint representations to predict muscle forces. Second, a finer-scale simulation predicts joint mechanics from the calculated muscle forces. This technique can yield detailed predictions of tissue loading if a finite element analysis is performed[4]. However, the simplified joint representations within the musculoskeletal simulation neglect load dependent joint mechanics, resulting in dynamic inconsistencies between the two stages. Concurrent simulation approaches overcome this limitation by including a detailed joint model within the multibody musculoskeletal simulation. This allows load dependent joint mechanics to be simultaneously predicted with the muscle forces necessary to generate the observed full body movement.

The detailed knee models used in concurrent simulations enable six DOF joints, but must be formulated to enable fast resolution of joint mechanics. Several multibody models of healthy knees[5,6] and total knee replacements (TKR)[7–9] with strand-based ligaments[10] and elastic foundation contact[11–13] have recently been introduced. Another approach incorporates a surrogate representation of a finite element model within the musculoskeletal simulation[14–19]. Recently, state-of-the-art dynamics software engines have introduced novel algorithms to enable finite element joint representations within

multibody simulations[20,21]. Thus, full finite element knee models may be directly included within musculoskeletal simulations in the near future.

We have recently published a review of concurrent simulation techniques that covers previous algorithms in detail[2]. Generally, concurrent simulations require a set of *primary* DOF, which are readily measured using motion capture, and a set of *secondary* DOF, which cannot be measured with confidence. Within the simulation, the multibody model dynamics are used to predict a set of *secondary* kinematics, muscle forces, ligament forces, and articular contact pressures that are dynamically consistent with the measured *primary* kinematics and ground reactions. Several forward and inverse approaches have been used to concurrently simulate knee mechanics during walking[9,22,23], running[24], squatting[25] and landing[26]. We have published applications of a novel simulation routine, Concurrent Optimization of Muscle Activations and Kinematics (COMAK) to study knee mechanics relating to ligament injury[27], total knee replacement[28], and crouch gait[29]. However, we have not yet described the methodology of the simulation routine in detail.

Musculoskeletal simulations have been used to investigate the functional roles of muscles during movement for several decades, but muscle redundancy remains a major challenge[30–33]. Many deterministic approaches using various cost functions and optimization formulations have been proposed to resolve muscle redundancy, however, the correct formulation remains uncertain[34,35]. Stochastic approaches have also been proposed to explore model topology and quantify the sets of feasible activation patterns to perform a task[36]. Beyond muscle redundancy, there have been many metrics proposed to quantify the individual contributions of muscles to generating movements. Induced acceleration analysis has been widely used[31–33], but is difficult to interpret clinically, does not account for neuromuscular compensation, and the results are sensitive to the joint kinematic descriptions[37]. Thus, improved simulation and analysis techniques have potential to provide further

insight into role of individual muscles in functional joint mechanics which could be exploited to understand pathologies and improve treatments.

Variation of the neuromuscular coordination strategy within a concurrent simulation framework can provide insight into the load dependencies of functional knee mechanics. Previously, muscle specific weights were introduced to a static optimization simulation of gait to study the influence of muscle activity on tibiofemoral contact loads[38]. They found tibiofemoral contact forces could be reduced in late stance by selecting a muscle coordination strategy with increased gluteus medius, uniarticular hip flexors, and soleus activity and decreased rectus femoris and gastrocnemii activity. However, the knee model did not capture load dependent effects and their exploration of the muscle weighting parameter space was limited. Nevertheless, these predictions provide a potential mechanical basis to inspire interventions for degenerative knee pathologies such as osteoarthritis.

Probabilistic analyses can quantify uncertainty and parameter sensitivity in musculoskeletal simulations, but require that simulations are repeated with many sets of input parameters[39]. The muscle weights introduced by Demers et al, provide an opportunity to parameterize the neuromuscular coordination strategy and thus resolve muscle redundancy probabilistically. However, the number of required simulations becomes especially burdensome when using concurrent simulation techniques which already introduce additional uncertain ligament and articular contact parameters. High Throughput Computing (HTC) provides a hardware solution to overcome this difficulty and enable large scale Monte Carlo style sensitivity studies. HTC manages pools of computers and schedules simulations to be performed using the next available processor, enabling thousands of simulations to be performed in parallel[40].

This study introduces the methodology behind the concurrent optimization of muscle activations and kinematics (COMAK) simulation framework to probabilistically predict secondary

kinematics, muscle forces, ligament forces, and articular contact pressures during functional movements. The first objective is to formally describe the simulation algorithm and demonstrate its capacity for deterministic prediction of subject-specific joint mechanics. The second objective is to use COMAK and an HTC cluster to quantify the uncertainty in simulation predictions due to an assumed neuromuscular coordination objective, and to access the sensitivity of knee joint contact predictions to neuromuscular coordination.

Methods

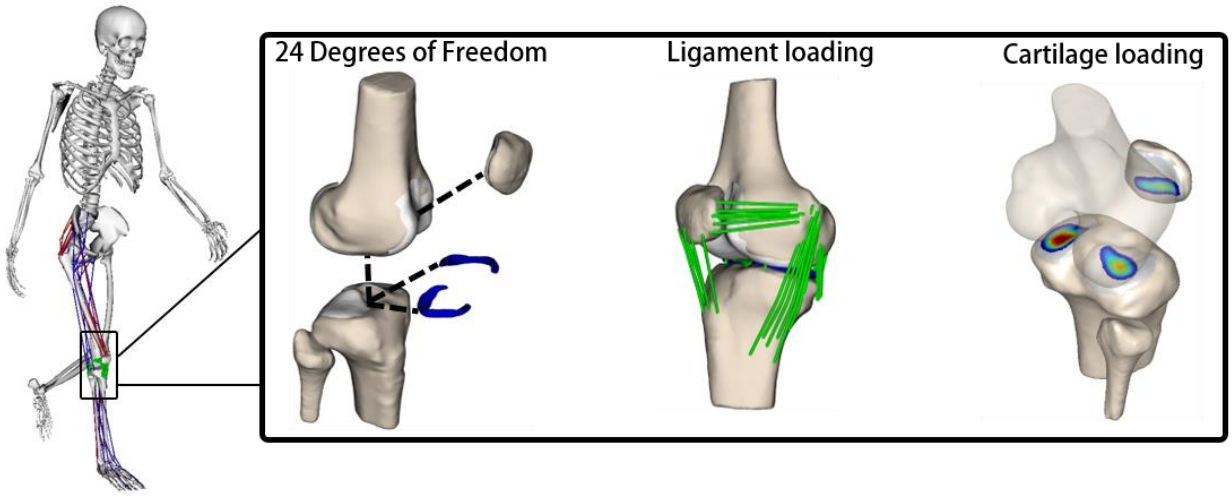

Figure 1 The musculoskeletal model used in this study included a detailed representation of the knee joint[5]. The model included independent femur, tibia, patella and menisci bodies connected by 6 DOF joints. Ligaments were represented by bundles of nonlinear springs, and articular contact between the cartilage and menisci was modeled using an elastic foundation formulation.

Knee Model

We previously developed and validated a multibody knee model which included independent femur, tibia, and patella bodies with six DOF joints, articular contact, and strand-based ligaments[5]. This model included elastic foundation representations of cartilage contact, where the contact pressure is calculated based on the local overlap depth of cartilage meshes[11]. Fourteen passive ligamentous structures of the knee were modeled as bundles of nonlinear springs whose force-strain curve included

a nonlinear toe region at low strains and linear stiffness region at high strains[27]. The knee model was integrated into a generic lower extremity musculoskeletal model which was scaled to our subject based on segment lengths using optical motion capture. The musculoskeletal model included three hip rotations, six DOF tibiofemoral, patellofemoral, and tibiomenisical joints, and a one DOF ankle joint. The model was actuated by 44 muscle-tendon units.

Table 1 Constitutive properties of meniscal ligament attachments

Ligament Name	Linear Stiffness (N/strain)	Reference Strain
Medial Anterior Horn	10000	0.04
Medial Posterior Horn	10000	0.01
Medial Coronary	100	0.08
Lateral Anterior Horn	10000	0.06
Lateral Posterior Horn	10000	0.01
Lateral Coronary	100	0.05
Transverse	300	0.01

For this study, we extended this model to include independent meniscus bodies with six DOF joints (Figure 1). Subject-specific menisci geometries were segmented from the magnetic resonance (MR) images and contact between the menisci and tibial and femoral cartilage was modeled using the elastic foundation formulation (Youngs Modulus = 3 MPa, Poissons Ratio = 0.45). The attachments of the menisci to the tibial plateau were represented by ligament strands representing the anterior and posterior horns, and the coronary ligaments (capsular attachments along the outer circumference of the menisci). The transverse ligament which spans between the anterior regions of the menisci was also represented. The constitutive parameters for these ligaments (Table 1) were selected based on cadaveric studies[41–44] and previous computational models[6,45].

Motion Analysis Data

Motion capture marker trajectories and ground reactions were measured simultaneously while our subject walked overground in a motion analysis laboratory at a self-selected speed. Marker

kinematics were low-pass filtered at 6 Hz. Ground reaction loads were low-pass filtered at 50 Hz. A static upright standing pose was also recorded to scale the musculoskeletal model.

Simulation Framework

We developed the Concurrent Optimization of Muscle Activations and Kinematics (COMAK) algorithm to simultaneously solve for muscle and soft tissue loading during functional movement**.** COMAK integrates motion capture and ground reaction measurements with a musculoskeletal model to resolve soft tissue loading. For COMAK, inverse kinematics is used to compute the coordinates, speeds and accelerations $(q, \dot{q}, \ddot{q})$ of the *primary* model degrees of freedom. Then, numerical optimization is performed to simultaneously solve for the *secondary* kinematics, muscle, ligament, and articular contact forces that generate the measured *primary* joint accelerations while minimizing a cost function that resolves inherent muscle redundancy.

Table 2 Classification of model degrees-of-freedom for COMAK

Prescribed	DOF
pelvis	6
Primary	
hip	3
tibiofemoral flexion	1
ankle	1
Secondary	
tibiofemoral	5
Patellofemoral	6
Meniscal	12

Optical motion capture enables the measurement of full body motion during functional movement, but skin-motion artifact introduces error into the computation of joint kinematics[46,47]. The differentiation between measurable DOFs of high (*primary*) and low (*secondary*) confidence is a key concept in COMAK. The algorithm solves for the muscle and soft tissue loads necessary to generate the measured *primary* kinematics, while simultaneously predicting a

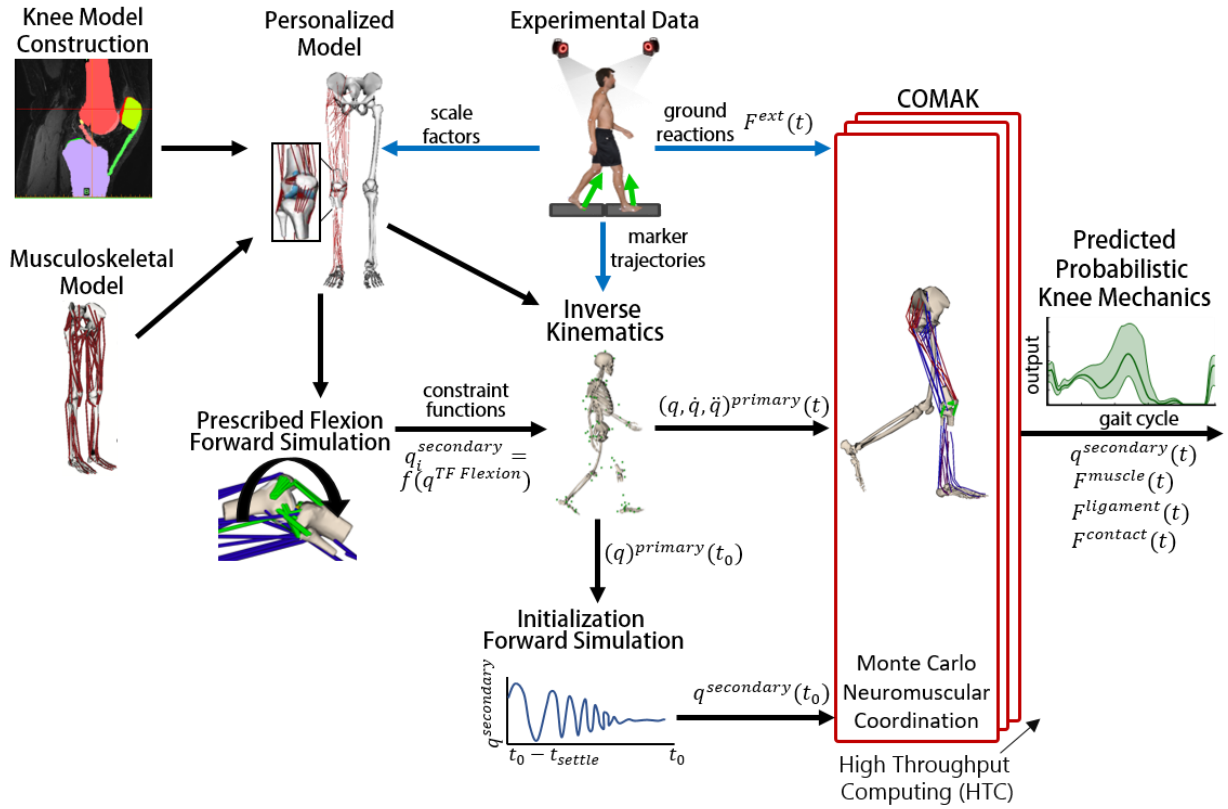

Figure 2 Overview of the Concurrent Optimization of Muscle Activations and Kinematics (COMAK) simulation framework. **Knee Model Construction** Subject-specific bone, cartilage, and ligament geometries are segmented from medical images. Constitutive properties are assumed from cadaver experiments or can be calibrated from experimental data. Alternatively, the knee model can be generated from a statistical shape model. **Personalized Model** A generic musculoskeletal model is scaled based on segment lengths measured in a static pose with motion capture. The knee model is incorporated into the scaled musculoskeletal model to develop a personalized model. **Prescribed Flexion Forward Simulation** A forward dynamic simulation is performed with the personalized model where tibiofemoral flexion is prescribed from 0° to 120°, and the secondary knee kinematics are predicted based on the contact, ligament, and passive muscle forces. These results are used to develop constraint equations that couple the secondary knee kinematics to tibiofemoral flexion during inverse kinematics. **Experimental Data** Motion capture and ground reactions are collected while the subject performs functional movements such as walking. **Inverse Kinematics** A global optimization routine is used to calculate primary kinematics that minimize the differences between measured and modeled marker locations. In this phase, the secondary DOFs are constrained to be functions of tibiofemoral flexion. **Initialization Forward Simulation** The primary model DOFs are fixed at their initial ($\boldsymbol{t_0}$) values from inverse kinematics and the secondary DOFs are allowed to settle into an equilibrium configuration. The resulting posture provides the initial seed to COMAK. **COMAK** The COMAK simulation routine then leverages a high throughput computing grid to perform a Monte Carlo analysis in which neuromuscular coordination strategy is varied to generate probabilistic predictions of secondary knee kinematics, muscle forces, ligament forces, and articular contact pressures.

tibiofemoral flexion and ankle flexion as the *primary* DOFs (Table 2). Tibiofemoral translations, non-sagittal rotations and all patellofemoral and meniscal DOFs cannot be reliably measured with motion capture[48], and thus are designated *secondary* DOFs. Pelvis translations and rotations are also measurable, but classified as *prescribed* DOFs such that their accelerations are prescribed within the multibody model through constraint forces to ensure consistency with observed multi-body dynamics.

A global optimization inverse kinematics routine was used to calculate the joint kinematics of the *primary* and *prescribed* DOFs from the motion capture marker trajectories (Figure 2). This routine determined the generalized coordinates of the *primary* and *prescribed* DOFs that minimized the sum of squared differences between model and measured marker positions at each time step. To enable this calculation, the *secondary* knee DOFs were constrained to be functions of tibiofemoral flexion (*primary*) during the inverse kinematics optimization. These constraints are then removed when later performing the optimization for dynamically-consistent soft tissue loads and *secondary* kinematics (COMAK). This approach assumes that the differences between the constrained *secondary* kinematics and load dependent *secondary* kinematics subsequently predicted by COMAK have negligible influence on the *primary* coordinates calculated by inverse kinematics. To develop *secondary* kinematic constraint functions that are consistent with the articular geometry of the model, we performed passive (muscle activation = 1%) forward simulations where the tibiofemoral flexion is prescribed to travel through its range of motion and the *secondary* kinematics evolve as a result of the contact, ligament and passive muscle forces[5].

Concurrent Optimization

After inverse kinematics, an optimization problem (COMAK) is solved to simultaneously predict the muscle and soft tissue loading and *secondary* kinematics required to generate the measured *primary* accelerations. The optimization is formulated to solve for the muscle activations and *secondary*

coordinates that minimize an objective function while satisfying overall dynamic constraints (Fig. **Error! Reference source not found.**). The dynamic constraints require that the optimized muscle forces and the internal joint loads (ligament and contact forces) resulting from the optimized *secondary* kinematics generate the measured *primary* accelerations, while inducing equilibrium (zero accelerations) in the *secondary* DOFs.

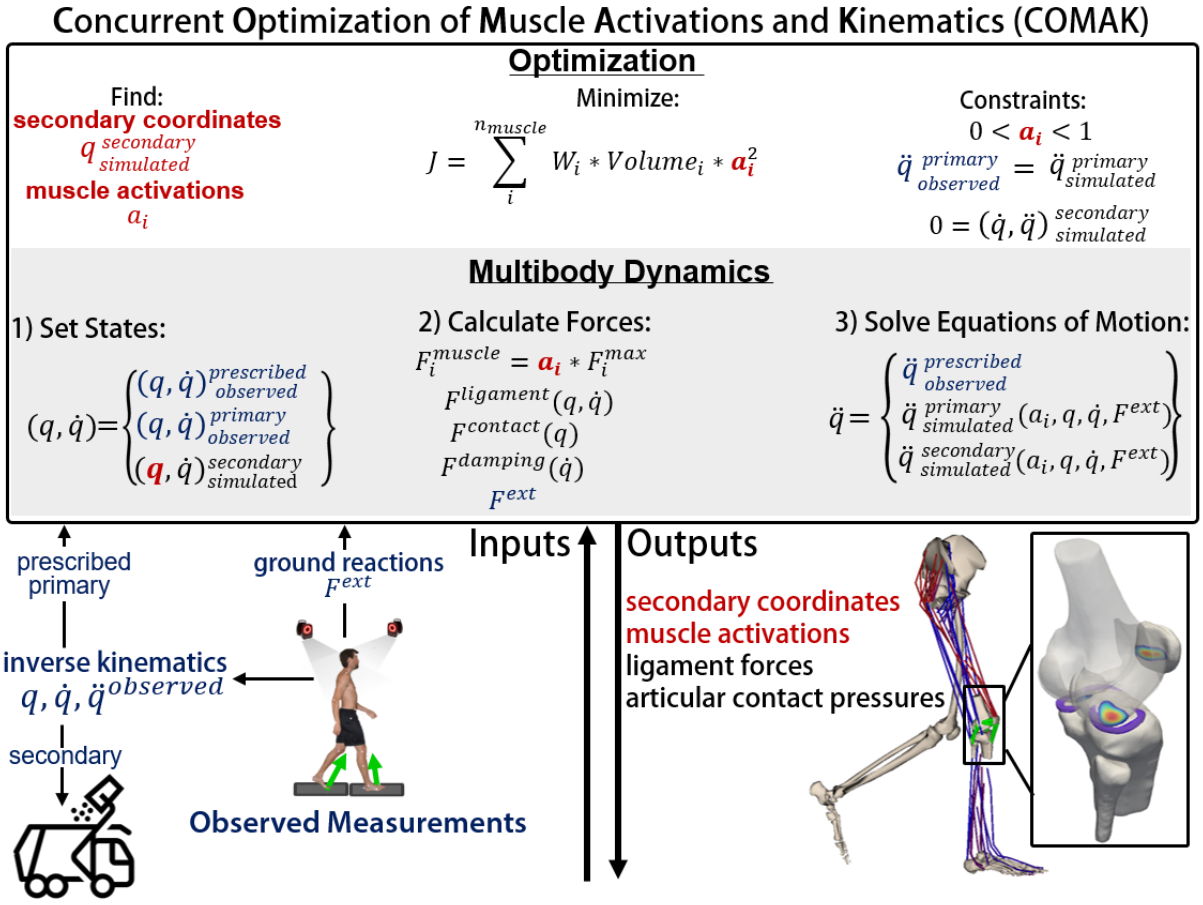

Figure 3 COMAK: Concurrent Optimization of Muscle Activations and Kinematics. The COMAK algorithm is a concurrent simulation method that integrates a multibody musculoskeletal with a detailed knee joint representation and external observations of full body movement to predict soft tissue loading. COMAK is an inverse static optimization method that predicts *secondary* kinematics, muscle forces, ligament forces, and articular contact pressure distributions at each time step. The optimization is formulated to solve for the muscle activations and secondary coordinates that minimize an objective function while satisfying overall dynamic constraints. The dynamic constraints require that optimized muscle forces and internal joint loads (ligament and contact forces) resulting from the optimized *secondary* kinematics generate the measured *primary* accelerations, while inducing equilibrium (zero accelerations) in the *secondary* DOFs. The optimization design variables are denoted in red. Observed quantities are denoted in blue.

At the first time step in COMAK, the *prescribed* coordinates, speeds, and accelerations $(q, \dot{q}, \ddot{q})^{prescribed}$ and *primary* coordinates, and speeds $(q, \dot{q})^{primary}$ are set to their observed values, and a forward simulation is performed with minimal muscle activations (a_i=0.01) to allow the *secondary* coordinates, $q^{secondary}$, to settle into an initial pose. At each subsequent time step, $(q, \dot{q})^{prescribed}$ and $(q, \dot{q})^{primary}$ are set to their observed values, while $q^{secondary}$ and a_i are determined by the optimization. The *secondary* speeds, $\dot{q}^{secondary}$, are determined from the difference between $q^{secondary}$ at the current and previous time steps. After setting the states of the model, the generalized forces are computed and applied. The contact forces are calculated using an elastic foundation model, $F^{contact}(q)$, while the ligament forces are computed using a nonlinear spring model, $F^{ligament}(q, \dot{q})$. Viscous damping forces are applied to each DOF to ensure minimal changes in kinematics between time steps $F^{damping}(\dot{q})$. The muscle forces are computed from the activations $F^{muscle}(a_i)$ and the measured external forces, F^{ext}, are applied to their corresponding segments. The constraint forces to fix the $\ddot{q}^{prescribed}$ to their measured values are applied and the equations of motion are solved for $\ddot{q}^{primary}$ and $\ddot{q}^{secondary}$.

Three constraints are enforced during the optimization for $q^{secondary}$ and a_i. Muscle activations are constrained to vary between 0 and 1, to ensure the resulting muscle forces are physiologically reasonable.

$$0 < a_i < 1 \tag{1}$$

Consistency with measured gait dynamics is ensured by satisfying the constraint that the simulated accelerations of the *primary* degrees of freedom matched the observed values,

$$\ddot{q}_{j}{}_{observed}^{primary} = \sum_{i=1}^{n_{muscles}} a_i F_i^{max} \hat{\ddot{q}}_{j,i}^{muscle}(q) + \ddot{q}_j^{other}(q, \dot{q}) \quad (2)$$

while the accelerations of *secondary* DOFs are constrained to be zero.

$$\ddot{q}_k^{secondary} = 0 = \sum_{i=1}^{n_{muscles}} a_i F_i^{max} \hat{\ddot{q}}_{k,i}^{muscle}(q) + \ddot{q}_k^{other}(q, \dot{q}) \quad (3)$$

In these equations, $\hat{\ddot{q}}_{j,i}^{muscle}$ is the acceleration along coordinate j due to a unit force in muscle i, while $\ddot{q}_j^{other}$ constitutes the accelerations due to all other forces in the multibody system (contact, ligament, damping, external, gravitational, centripetal and Coriolis). The third constraint () assumes that inertial effects due to accelerations in the *secondary* degrees of freedom are negligible. During gait, this assumption is justified given the small mass of the patella and menisci and the small magnitudes of rotational and translational excursion in *secondary* degrees of freedom. The redundancy of the musculoskeletal system allows multiple combinations of $q^{secondary}$ and a_i to fulfill these constraints, thus static optimization must be performed to minimize an objective function and identify a unique solution.

The objective function (J) used by COMAK is generalizable, allowing any user-defined quantity to be minimized. We have found a common cost function proposed for static optimization performs well for COMAK in most applications:

$$J = \sum_{i}^{n_{muscles}} W_i * V_i * a_i^2 \quad (4)$$

Where W_i is a weighting term, V_i is muscle volume and a_i is the muscle activation. The weighting term enables the activation of individual muscles to be penalized within the optimization. Consistent with Demers et al [38], we have found penalizing biarticular muscles (gastrocnemii and rectus femoris)

Table 3 Nominal muscle weights used in the COMAK objective function.

Muscles	Nominial W_i
medial gastrocnemius	4
lateral gastrocnemius	7
hamstrings	2
rectus femoris	3
soleus	0.9
gluteus medius	0.9
gluteus minimus	0.9

necessary to predict tibiofemoral contact forces consistent with measurements from instrumented implants during walking. This redistributes the hip flexor moment and ankle plantarflexor moments to the uniarticular muscles during late stance, reducing the loading in the muscles crossing the knee and thus the compressive contact force. The nominal muscle weight for each muscle was set equal to one ($W_i = 1$), except for those listed in Table 3. Introducing an additional term in the cost function to minimize articular contact energy also produces similar contact force predictions, largely by similarly redistributing the muscle loading to uniarticular muscles [28]. However, the errors in the numerical calculation of the gradient of contact energy with respect to the optimized secondary kinematics can cause convergence issues within the optimization. Thus, we have found the cost function presented above (Equation 4) to be more robust with similar results.

The weighting terms (W_i) also provide a straightforward means to parameterize the muscle coordination objective, enabling probabilistic approaches to resolve muscle redundancy. In this study, we performed a Monte Carlo analysis in which the muscle weights (W_i) were randomly sampled to generate simulations with varying muscle coordination strategies to explore the muscle redundancy solution space. The muscle weights penalize the activation of a muscle if ($W_i > 1$) and encourage the activation if ($W_i < 1$). A high throughput computing (HTC) grid was used to perform 10,000 simulations using the same model and input kinematic and ground reaction data. Muscle weights were parameterized as uniform distributions spanning from 10-10000% of the nominal weight (W_i) value. The bounds on the distributions were determined as the largest range that still enabled all simulations

to converge. The mean values of the predicted kinematics and cartilage loading metrics were less than 1% different when calculated using 9,000 verus 10,000 simulations, ensuring an adequate number of simulations were performed.

The predicted secondary kinematics, muscle activations, ligament loads, and contact metrics were quantified by computing the mean and 5^{th} and 95^{th} percentiles of the probabilistic simulation outputs over the gait cycle. The influence of neuromuscular coordination on predicted joint mechanics was investigated at the instances of the 1^{st} and 2^{nd} peaks in the tibiofemoral contact force. At these time points scatter plots of muscle activation vs kinematics, ligament loads, and contact metrics were generated and the sensitivity was quantified using Spearman's correlation coefficient (R).

Results

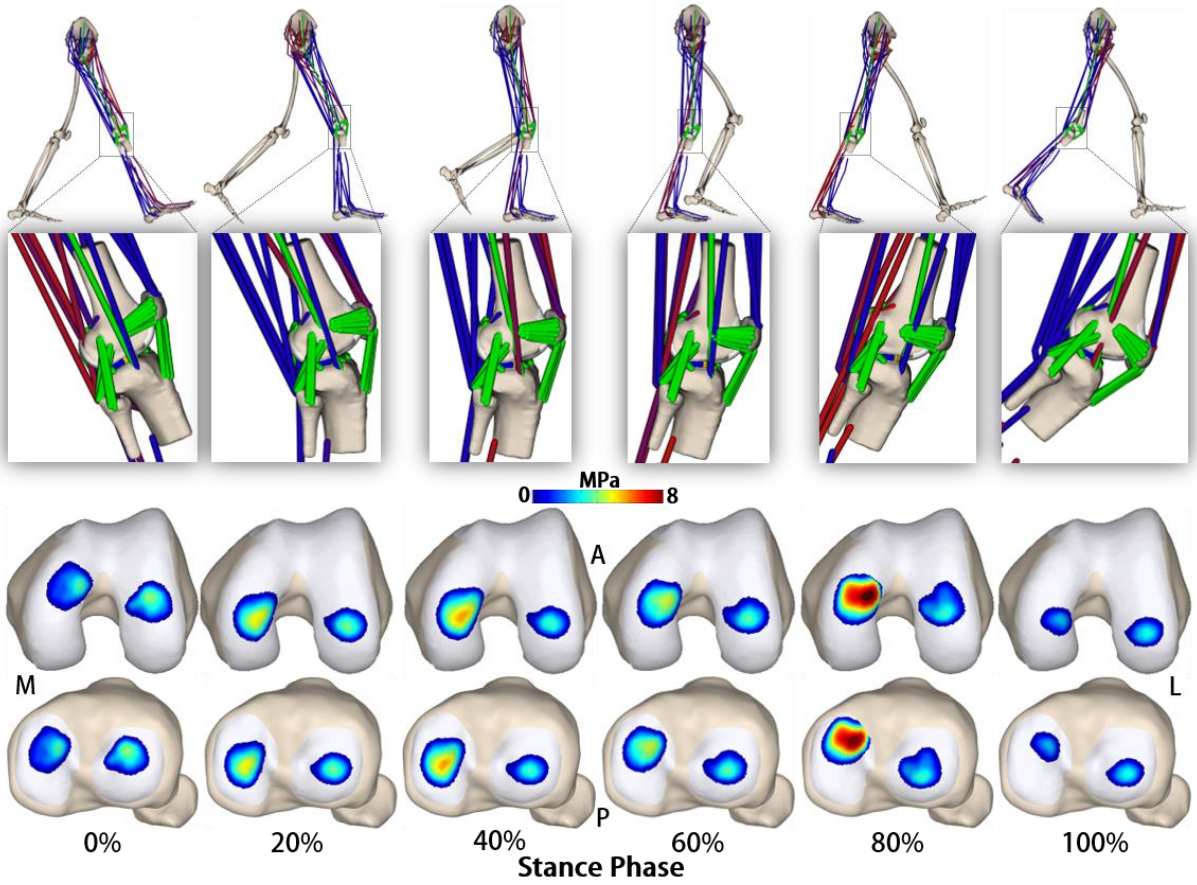

Figure 4 COMAK predictions of muscle activations and knee joint mechanics during the stance phase of walking. The 1st peak of tibiofemoral loading occurred at 28% stance and the second peak occurred at 72% stance. The pressure maps depict cartilage-cartilage contact pressures.

Subject-Specific Simulation

The COMAK simulation algorithm successfully simulated muscle-driven full-body dynamics and knee joint mechanics over the entire measured gait cycle using the MRI based multibody knee model and subject-specific motion capture and ground reaction data (Figure 4). The simulation took 30 minutes on a standard desktop computer, making it well suited for high throughput computing applications. The total knee contact force exhibited the characteristic double peak during stance phase (1st peak: 18% gait cycle, 2nd peak: 48% gait cycle) and majority of the loading was distributed to the

medial plateau (Figure 5). The predicted joint mechanics over the gait cycle are detailed in the context of variable neuromuscular coordination in the following sections.

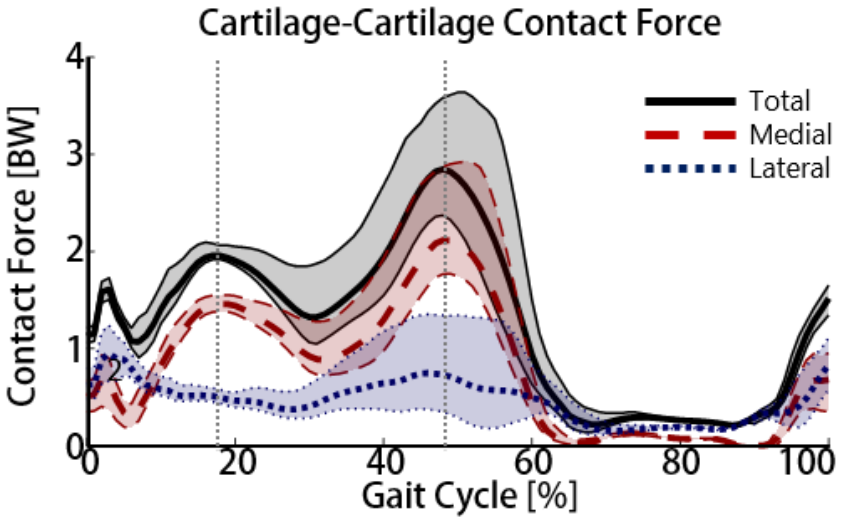

Figure 5 Predicted tibiofemoral contact forces during a simulated gait cycle. The bold centerlines are the mean and shaded regions show the 5th to 95th percentiles of the Monte Carlo analysis of neuromuscular coordination. The vertical dotted lines indicate the instances of 1st and 2nd peak total tibiofemoral contact force.

Variable Neuromuscular Control

Parametrically varying the weighting terms in the COMAK cost function resulted in substantial variation in the predicted neuromuscular control strategies (Figure 6). The largest variations in muscle activity occurred in the second half of stance. At 2nd peak, the parametric muscle weightings redistributed the hip, knee, and ankle moments among the uni- and biarticular muscles. This resulted in substantial variation in psoas, iliacus, biceps femoris short head, gastrocnemii, and soleus muscle

activity.

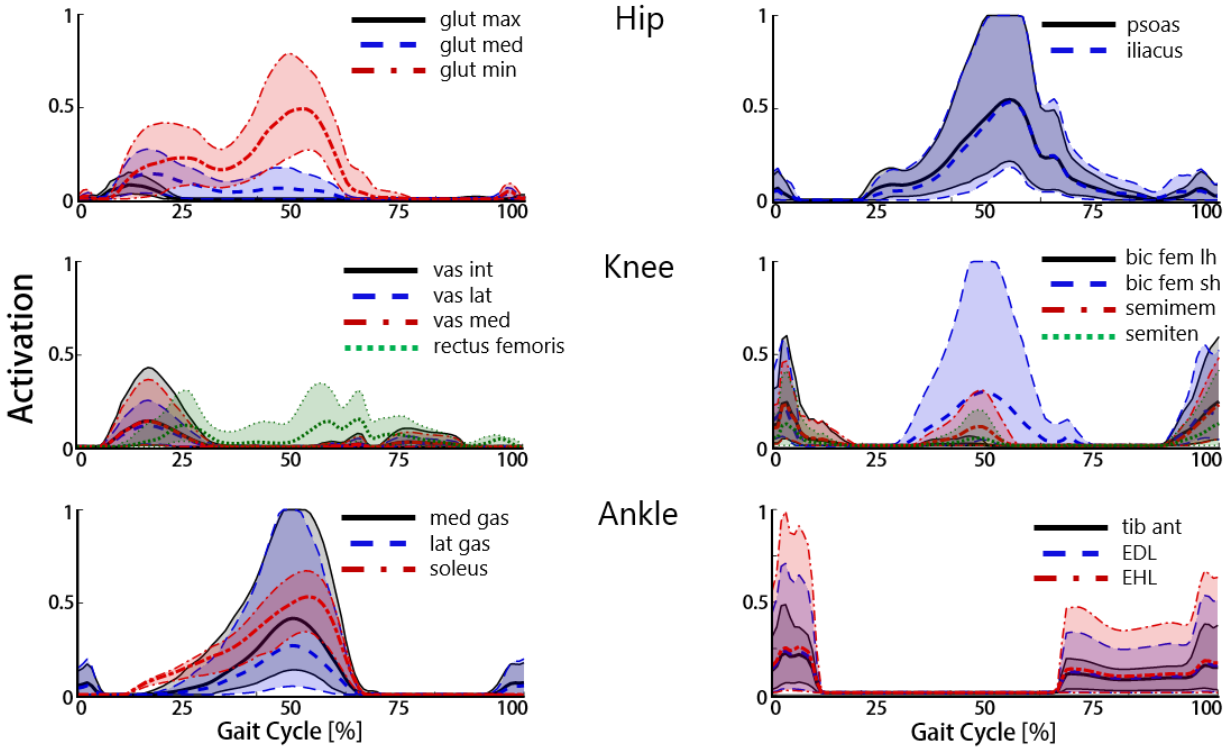

Figure 6 Variations in predicted muscle activations due to the probabilistic nature of the COMAK cost function. The stochastic muscle weightings redistributed the joint torques among the uni and biarticular muscles. EDL extensor digitorum longus, EHL extensor hallucis longus.

The influence of neuromuscular coordination strategy on tibiofemoral contact force (Figure 5) and cartilage-cartilage contact pressures (Figure 7) was highly variable throughout the gait cycle. Only minor variation was present in the total tibiofemoral contact force at 1st peak (5-95th percentile range = 0.15 BW), compared to the significant variation at 2nd peak (5-95th percentile range = 1.21 BW). The effect at 2nd peak was caused by a redistribution of the hip and ankle moments to the biarticular muscles (rectus femoris and gastrocnemii) which induced greater compression forces and higher contact pressures at the knee. Muscle loading induced larger variation in the lateral plateau contact pressure compared to the medial plateau (2nd Peak 5-95th percentile range = 1.69, 0.44 MPa, respectively).

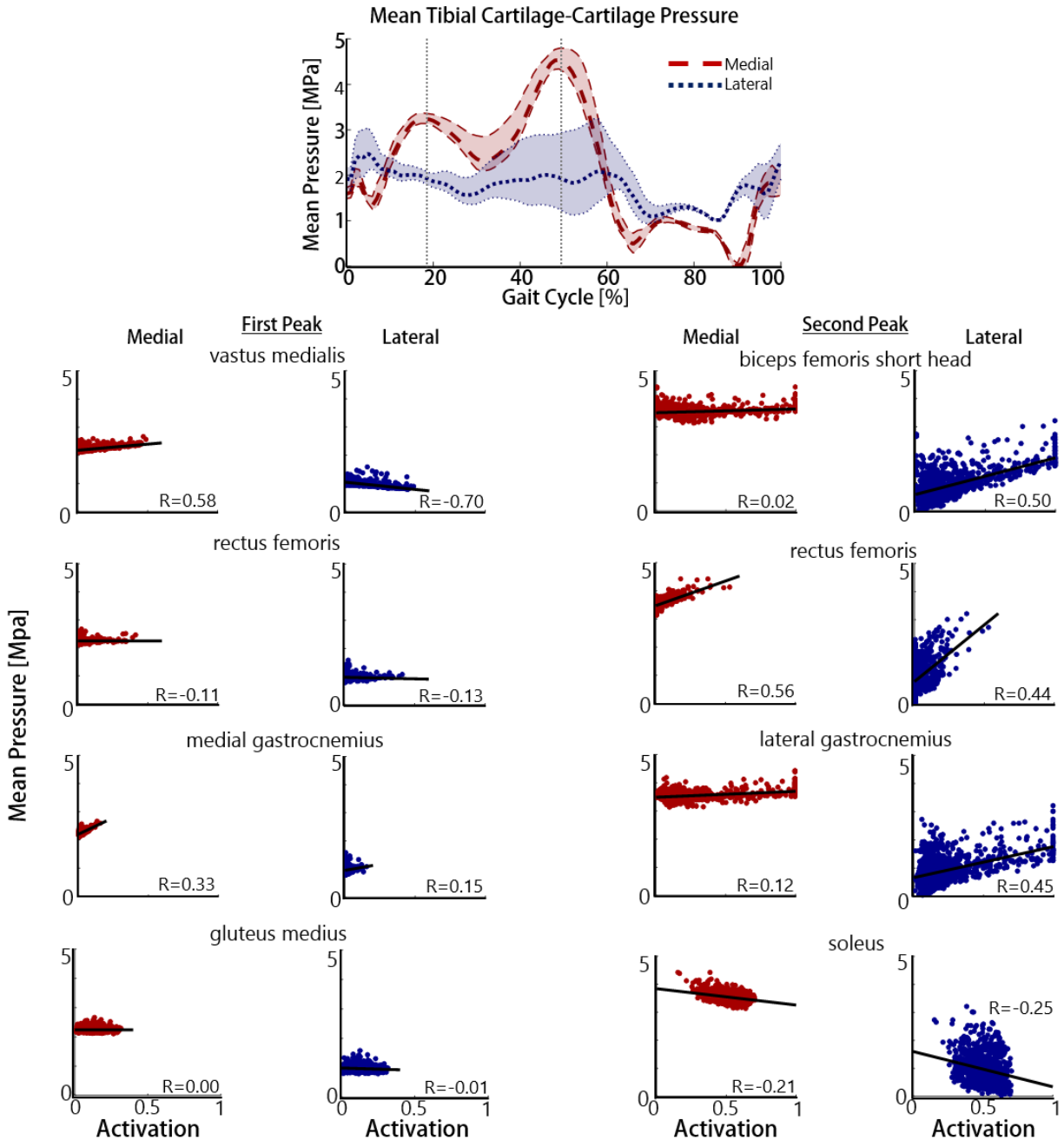

Figure 7 [*Top*] The means (bold centerline) and 5th to 9th percentiles (shaded) of the mean cartilage-cartilage contact pressures on the medial and lateral tibial plateaus. Vertical dotted lines denote the instances of the 1st and 2nd peaks in the tibiofemoral contact force [*Scatter plots*] The sensitivity of mean medial and lateral pressures to muscle activity was quantified using Spearman's correlation coefficient at the instances 1st and 2nd Peak tibiofemoral contact force.

The varied neuromuscular coordination had significant effect on the predicted secondary tibiofemoral kinematics, demonstrating the capability of COMAK to account for the load dependent nature of knee function (Figure 8). The DOFs with the greatest passive laxity: anterior translation and internal rotation, also demonstrated the greatest variability due to muscle loading during walking. These DOFs also demonstrated the greatest excursions over the gait cycle. All secondary tibiofemoral DOFs demonstrated the largest variation during push-off corresponding to the timing the greatest muscle activity variability.

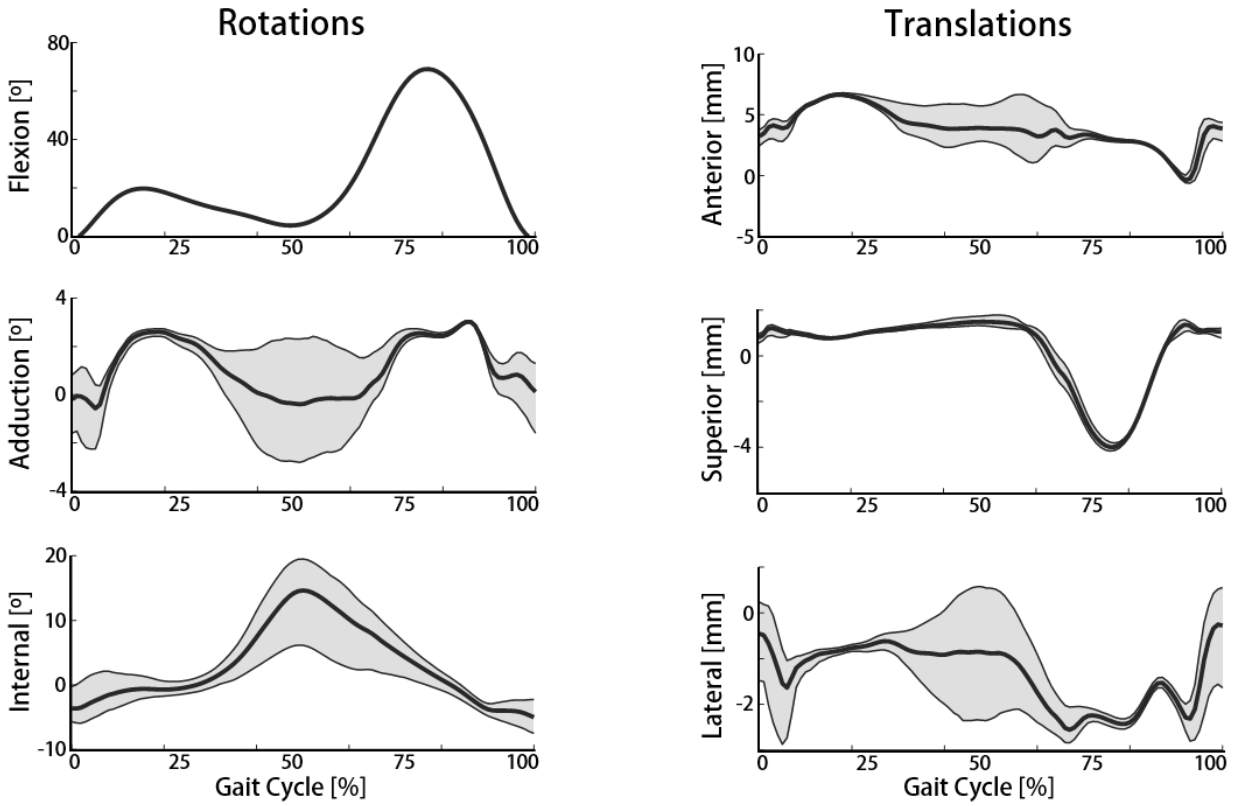

Figure 8 Measured tibiofemoral flexion and predicted *secondary* kinematics over the gait cycle.

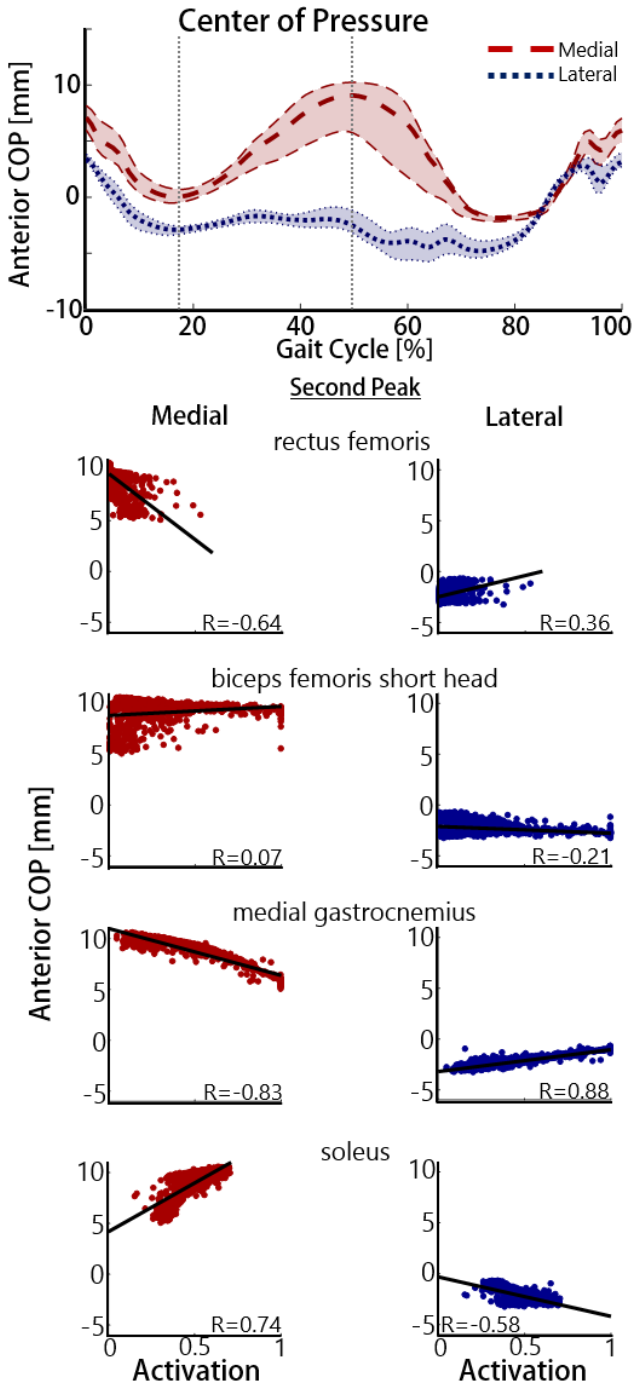

Figure 9 [*Top*] The mean (bold centerline) and 5th-95th percentiles of the anterior location of the center of pressure (COP) on the tibial plateau. [*Scatter plots*] The sensitivity of the anterior COP on the medial and lateral tibial plateaus to muscle activations was quantified at the 2nd peak of tibiofemoral loading.

The predicted locations of cartilage contact on the tibial plateau migrated anteriorly and posteriorly over the gait cycle (Figure 9). The medial contact shifted posteriorly from heel strike to 1st peak, anteriorly from 1st to 2nd peak, posteriorly from 2nd peak through mid-swing, and anteriorly in terminal swing. The lateral contact shifted posteriorly from heel strike to 1st peak, then remained stationary until terminal swing when it progressed back anteriorly.

The neuromuscular coordination induced variations in predicted secondary tibiofemoral kinematics manifested as altered locations of cartilage contact on the tibial plateau throughout the gait cycle. Similar to other metrics, there was limited variability at 1st peak compared to 2nd peak. The medial COP showed greater variability in the anterior-posterior direction, compared to the lateral COP (2nd Peak 5-95th percentile range = 4.3 mm, 1.9 mm, respectively). At the second peak, medial gastrocnemius activation shifted

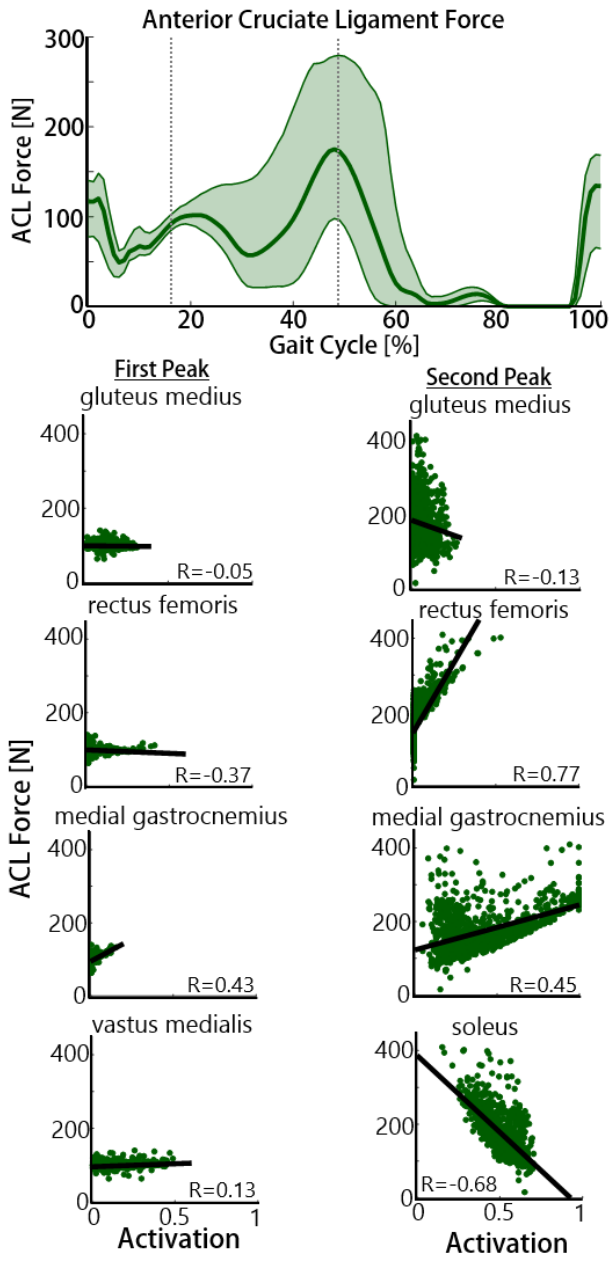

Figure 10 [*Top*] The mean (bold centerline) and 5th-95th percentiles (shaded) of the predicted anterior cruciate ligament (ACL) force over the gait cycle. The dotted vertical lines indicate the 1st and 2nd peaks of tibiofemoral loading. [*Scatter plots*] The sensitivity of the ACL force to muscle activations was quantified at the 1st and 2nd peaks using the Spearman correlation coefficient.

the contact posteriorly on the medial plateau and anteriorly on the lateral plateau. The opposite effect was seen for the lateral gastrocnemius, and soleus.

The predicted loading of the anterior cruciate ligament exhibited three peaks over the gait cycle, at heel strike and at the 1st and 2nd peaks of tibiofemoral loading. At heel strike, the knee is in its most extended posture, at 1st peak the quadriceps are most active, and at 2nd peak the gastrocnemii are most active. The variability increased substantially after 1st peak, and max variability occurred at 2nd peak. At 2nd peak, rectus femoris and gastrocnemius activations increased the loading in the ACL whereas soleus activation decreased ACL loading.

Discussion

In this study, we introduced the methodology behind the Concurrent Optimization of Muscle Activations and Kinematics (COMAK) simulation framework. We used an image-based multibody knee model,

and measured motion capture and ground reaction data to generate subject-specific predictions of *secondary* knee kinematics, muscle forces, ligament forces, and articular contact pressures during walking. A Monte Carlo analysis was performed where muscle weightings in the COMAK objective function were randomly sampled to generate variations in the predicted neuromuscular coordination strategy. The predicted probabilistic knee mechanics showed minimal variability in early stance compared the substantial effects demonstrated in late stance and early swing.

The COMAK simulation routine demonstrated the capability to simulate subject-specific joint mechanics with image-based knee geometries and subject-specific motion analysis data. It should be noted that substantial uncertainty exists in these subject-specific predictions due to difficulty of estimating knee ligament parameters and resolving muscle redundancy. The speed of the simulation algorithm (30 minutes per gait cycle) and minimal memory usage make COMAK well suited for high throughput computing applications. This allows thousands of simulations to be performed in parallel, enabling Monte Carlo style analyses to quantify prediction uncertainty and assess model sensitivities. Here and in previous studies, COMAK has shown robustness to variations in neuromuscular coordination strategy and ligament parameters[8,49]. This trait is especially beneficial for HTC sensitivity studies.

COMAK predictions of knee mechanics during walking largely agreed with the available *in vivo* measurements. Similar to bone-pin measurements, the tibia internally rotated from heel strike to push off and externally rotated through swing (Figure 8)[50]. Combined magnetic resonance and biplane fluoroscopy measurements found greater excursions of the anterior COP on the medial plateau compared to the lateral plateau during stance[51,52]. This finding matches the COMAK simulation predictions (Figure 9). In the future, subject-specific model predictions should be compared against

in vivo subject-specific kinematics measured during functional movement to accurately quantify the true predictive capacity.

Resolving muscle redundancy remains a major challenge for musculoskeletal simulations of movement. Concurrent simulation enables detailed joint models, which add dynamic constraint equations for each additional DOF. However, concurrent simulation also introduces *secondary* DOFs as design variables, resulting in increased model redundancy and uncertainty in predictions. We propose the solution of muscle redundancy should be treated as an uncertain simulation parameter such as segment inertias or muscle model parameters[39]. Thus, in COMAK we probabilistically resolve muscle redundancy using a Monte Carlo analysis where muscle-specific weightings in the optimization cost function are randomly varied to generate a set of feasible neuromuscular coordination solutions. This technique produced variable neuromuscular coordination strategies that generated the same net joint torques to explore the solution space of muscle redundancy. This results in the activation of agonist muscles to compensate for muscles penalized by high weight factors. The scatter plots in Figures 7,9 and 10 demonstrate an effective analysis technique to quantify the sensitivity of predicted knee mechanics to the activation of a given muscle at various time points over the gait cycle. Thus

providing a new simulation based approach to study muscle function which is more intuitive and directly applicable to clinical problems compared to induced acceleration analysis[53].

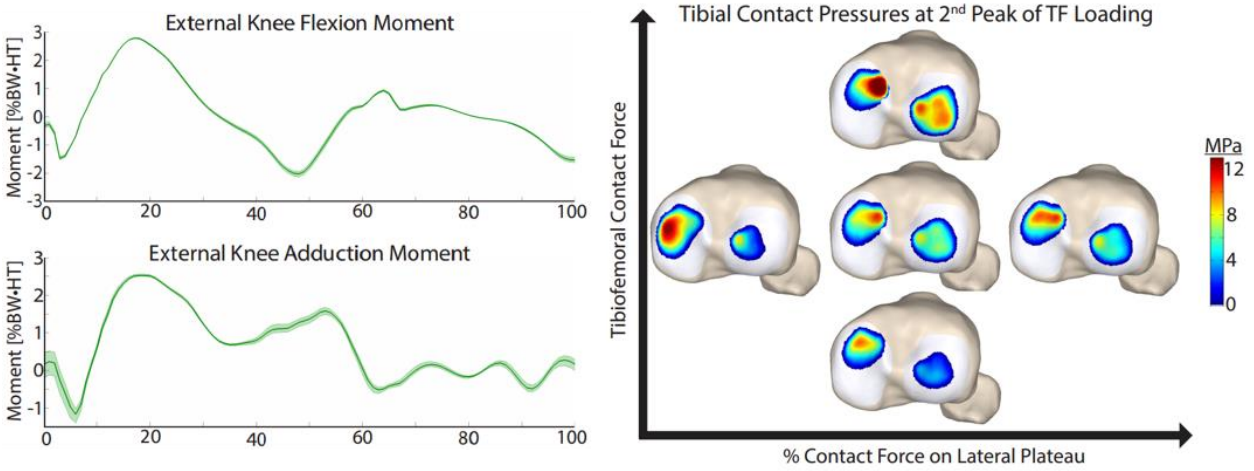

Figure 11 [*Left*] Mean and 5th to 95th percentiles of all simulations for external joint torques over the gait cycle. COMAK constrains all simulations to generate the same accelerations at each DOF, so the small variance is due to differences in predicted *secondary* kinematics. [*Right*] Sample cartilage contact pressure variations due to neuromuscular coordination differences at the 2nd peak of tibiofemoral loading.

The external knee flexion moment and knee adduction moment have been widely used as surrogate measures of cartilage loading[54]. Interestingly, in this study the external joint moments were nearly unchanged across all simulations, yet cartilage pressure patterns exhibited substantial differences at the 2nd peak of tibiofemoral loading (Figure 11). This highlights the importance of looking beyond external measurements of joint torques when considering cartilage loading. Joint moments constrain the solution space to muscle redundancy, but clearly are only one of several factors that contribute to articular contact loading.

Several interesting insights into the influence of neuromuscular coordination on knee mechanics were enabled through the Monte Carlo analysis. For example, while the soleus does not cross the knee, its activation induced an anterior shift in the medial COP and a posterior shift of the lateral COP at the 2nd peak of tibiofemoral loading (Figure 9). These are similar effects to the lateral gastrocnemius, but opposite of the medial gastrocnemius. This phenomenon occurred because

increased soleus activation reduced the needed contribution of the gastrocnemii to the plantar flexor torque, thereby decreasing gastrocnemii activity. Because the medial gastrocnemius has a greater volume than lateral gastrocnemius, it nominally is selected to contribute more to the ankle torque. Thus, if the movement dynamics are unchanged, preferential activation of the soleus leads a greater reduction in medial gastrocnemius contribution to the knee mechanics compared the lateral. This results in opposing sensitivities of the anterior COP on the medial plateau to soleus and medial gastrocnemius activations.

The variability in the predicted knee mechanics due to neuromuscular coordination can provide some insight into the capacity of neuromuscular retraining interventions to affect knee mechanics during walking. At the 1st peak of tibiofemoral loading the variations in muscle activations had minimal effect on the predicted knee mechanics. But at 2nd peak neuromuscular coordination had substantial effect on the knee. Interestingly, there was greater variability induced in the mean pressure on the lateral tibial plateau, but greater variability in the anterior COP on the medial side. This exemplifies the need for musculoskeletal models to capture the complex interactions that govern function knee mechanics.

The COMAK simulation framework has many limitations which must be considered when designing future studies to leverage its capabilities. First and foremost, COMAK is inherently limited by the uncertainty in model parameters and fidelity of the experimental motion analysis measurements. Garbage in, Garbage out. Several modeling assumptions are necessary to COMAK which may have significant effects depending on the application. Dynamic equilibrium is assumed in the *secondary* DOFs, which is only valid if the mass of the affected body is minimal and the accelerations are small. Regardless of the predicted *secondary* kinematics, the external forces are applied in the same location in the global reference frame. This may result in misguided application of the ground reactions to the

foot if substantial differences exist between the assumed *secondary* kinematics in the inverse kinematics phase and the COMAK predictions. Finally, the pelvis coordinates are *prescribed* which may mask dynamic inconsistencies between the motion capture and ground reaction measurements.

The COMAK algorithm provides a powerful simulation routine to concurrently resolve full-body dynamics and joint mechanics. The probabilistic cost function provides a novel approach to account for muscle redundancy and investigate muscle function. While subject-specific predictions of internal joint loading demonstrate the exciting potential for computer simulation, they must be interpreted within the context of model uncertainties and muscle redundancy. The true power of COMAK comes from its ability to leverage concurrent and probabilistic simulation techniques assess the sensitivity of joint mechanics to muscle activity during functional movement.

References

1. Andriacchi, T. P., Koo, S. & Scanlan, S. F. Gait mechanics influence healthy cartilage morphology and osteoarthritis of the knee. *J. Bone Joint Surg. Am.* **91,** 95–101 (2009).

2. Brandon, S. C. E., Smith, C. R. & Thelen, D. G. in *Handbook of Human Motion* 1–34 (2017). doi:10.1007/978-3-319-30808-1_172-1

3. Laz, P. J. & Browne, M. A review of probabilistic analysis in orthopaedic biomechanics. *Proc. Inst. Mech. Eng. Part H J. Eng. Med.* **224,** 927–943 (2010).

4. Besier, T. F., Gold, G. E., Beaupr??, G. S. & Delp, S. L. A Modeling Framework to Estimate Patellofemoral Joint Cartilage Stress In Vivo. *Med. Sci. Sport. Exerc.* **37,** 1924–1930 (2005).

5. Lenhart, R. L., Kaiser, J., Smith, C. R. & Thelen, D. G. Prediction and Validation of Load-Dependent Behavior of the Tibiofemoral and Patellofemoral Joints During Movement. *Ann.*

Biomed. Eng. (2015). doi:10.1007/s10439-015-1326-3

6. Guess, T. M., Thiagarajan, G., Kia, M. & Mishra, M. A subject specific multibody model of the knee with menisci. *Med. Eng. Phys.* **32,** 505–15 (2010).

7. Thelen, D. G., Choi, K. W. & Schmitz, A. M. Co-Simulation of Neuromuscular Dynamics and Knee Mechanics During Human Walking. *J. Biomech. Eng.* **134,** 90202 (2012).

8. Smith, C. R., Vignos, M. F., Lenhart, R. L., Kaiser, J. & Thelen, D. G. The influence of component alignment and ligament properties on tibiofemoral contact forces in total knee replacement. *J. Biomech. Eng.* **138,** (2016).

9. Marra, M. a. *et al.* A Subject-Specific Musculoskeletal Modeling Framework to Predict In Vivo Mechanics of Total Knee Arthroplasty. *J. Biomech. Eng.* **137,** 20904 (2015).

10. Blankevoort, L. & Huiskes, R. Ligament-Bone Interaction in a Three-Dimensional Model of the Knee. *J. Biomech. Eng.* **113,** 263–269 (1991).

11. Smith, R. C., Choi, K. W., Negrut, D. & Thelen, D. G. Efficient Computation of Cartilage Contact Pressures within Dynamic Simulations of Movement. *Comput. Methods Biomech. Biomed. Eng. Imaging Vis.* **1163,** (2016).

12. Bei, Y. & Fregly, B. J. Multibody dynamic simulation of knee contact mechanics. *Med. Eng. Phys.* **26,** 777–89 (2004).

13. Blankevoort, L., Kuiper, J. H., Huiskes, R. & Grootenboer, H. J. ARTICULAR CONTACT IN A THREE-DIMENSIONAL MODEL OF THE KNEE. *J. Biomech.* **24,** 1019–1031 (1991).

14. Halloran, J. P., Erdemir, A. & van den Bogert, A. J. Adaptive Surrogate Modeling for Efficient Coupling of Musculoskeletal Control and Tissue Deformation Models. *J. Biomech. Eng.* **131,**

11014 (2009).

15. Lin, Y.-C., Haftka, R. T., Queipo, N. V & Fregly, B. J. Surrogate articular contact models for computationally efficient multibody dynamic simulations. *Med. Eng. Phys.* **32,** 584–94 (2010).

16. Eskinazi, I. & Fregly, B. An Open-Source Toolbox for Surrogate Modeling of Joint Contact Mechanics. *IEEE Trans. Biomed. Eng.* **9294,** 1–1 (2015).

17. Eskinazi, I. & Fregly, B. J. Surrogate modeling of deformable joint contact using artificial neural networks. *Med. Eng. Phys.* **37,** 885–891 (2015).

18. Walter, J. P. & Pandy, M. G. Dynamic simulation of knee-joint loading during gait using force-feedback control and surrogate contact modelling. *Med. Eng. Phys.* **48,** 196–205 (2017).

19. Marra, M. A. *et al.* Evaluation of a Surrogate Contact Model in Force-Dependent Kinematic Simulations of Total Knee Replacement. *J. Biomech. Eng.* **139,** 81001 (2017).

20. Lloyd, J. E., Stavness, I. & Fels, S. ArtiSynth: A Fast Interactive Biomechanical Modeling Toolkit Combining Multibody and Finite Element Simulation. *Soft Tissue Biomech. Model. Comput. Assist. Surg.* 355–394 (2012). doi:10.1007/8415_2012_126

21. Mazhar, H. *et al.* CHRONO: A parallel multi-physics library for rigid-body, flexible-body, and fluid dynamics. *Mech. Sci.* **4,** 49–64 (2013).

22. Thelen, D. G., Won Choi, K. & Schmitz, A. M. Co-simulation of neuromuscular dynamics and knee mechanics during human walking. *J. Biomech. Eng.* **136,** 21033 (2014).

23. Guess, T. M., Stylianou, A. & Kia, M. A Musculoskeletal Model of Treadmill Gait. *J. Biomech. Eng.* (2014). doi:10.1115/1.4026359

24. Lenhart, R. L. *et al.* Influence of Step Rate and Quadriceps Load Distribution on Patellofemoral

Cartilage Contact Pressures during Running. *J. Biomech.* 1–8 (2015). doi:10.1016/j.jbiomech.2015.04.036

25. Guess, T. M. & Stylianou, A. Simulation of anterior cruciate ligament deficiency in a musculoskeletal model with anatomical knees. *Open Biomed. Eng. J.* **6,** 23–32 (2012).

26. Shin, C. S., Chaudhari, A. M. & Andriacchi, T. P. The influence of deceleration forces on ACL strain during single-leg landing: a simulation study. *J. Biomech.* **40,** 1145–52 (2007).

27. Smith, C., Lenhart, R., Kaiser, J., Vignos, M. & Thelen, D. Influence of Ligament Properties on Tibiofemoral Mechanics in Walking. *J. Knee Surg.* (2015).

28. Smith, C. R., Vignos, M. F., Lenhart, R. L., Kaiser, J. & Thelen, D. G. The Influence of Component Alignment and Ligament Properties on Tibiofemoral Contact Forces in Total Knee Replacement. *J. Biomech. Eng.* **138,** (2016).

29. Smith, C. R., Lenhart, B. S. R. L., Thelen, D. G., Kaiser, J. & Vignos, M. F. Influence of Ligament Properties on Tibiofemoral Mechanics in Walking. **1,** (2015).

30. Seireg, A. & Arvikar, R. J. The Prediction of Musclular Load Sharing and Joint Forces in Lower Extremities during Walking. *JBiomech* **8,** 89–102 (1975).

31. Zajac, F. E. & Gordon, M. E. Determining muscle's force and action in multi-articular movement. *Exerc. Sport Sci. Rev.* **17,** 187–230 (1989).

32. Neptune, R. R., Kautz, S. a & Zajac, F. E. Contributions of the individual ankle plantar flexors to support, forward progression and swing initiation during walking. *J. Biomech.* **34,** 1387–98 (2001).

33. Hamner, S. R., Seth, A. & Delp, S. L. Muscle contributions to propulsion and support during

running. *J. Biomech.* **43,** 2709–16 (2010).

34. Erdemir, A., McLean, S., Herzog, W. & van den Bogert, A. J. Model-based estimation of muscle forces exerted during movements. *Clin. Biomech. (Bristol, Avon)* **22,** 131–54 (2007).

35. Crowninshield, R. D. & Brand, R. a. A physiologically based criterion of muscle force prediction in locomotion. *J. Biomech.* **14,** 793–801 (1981).

36. Valero-Cuevas, F. J., Cohn, B. A., Yngvason, H. F. & Lawrence, E. L. Exploring the high-dimensional structure of muscle redundancy via subject-specific and generic musculoskeletal models. *J. Biomech.* **48,** 2887–2896 (2015).

37. Chen, G. Induced acceleration contributions to locomotion dynamics are not physically well defined. *Gait Posture* **23,** 37–44 (2006).

38. DeMers, M. S., Pal, S. & Delp, S. L. Changes in tibiofemoral forces due to variations in muscle activity during walking. *J. Orthop. Res.* **32,** 769–776 (2014).

39. Myers, C. A., Laz, P. J., Shelburne, K. B. & Davidson, B. S. A Probabilistic Approach to Quantify the Impact of Uncertainty Propagation in Musculoskeletal Simulations. *Ann. Biomed. Eng.* **43,** 1098–1111 (2015).

40. Thain, D., Tannenbaum, T. & Miron, L. Distributed computing in practive: the condor experience. *Concurr. Comput. Pract. Exp.* **17,** 325–356 (2005).

41. Masouros, S. D., McDermott, I. D., Amis, A. A. & Bull, A. M. J. Biomechanics of the meniscus-meniscal ligament construct of the knee. *Knee Surgery, Sport. Traumatol. Arthrosc.* **16,** 1121–1132 (2008).

42. McDermott, I. D., Masouros, S. D. & Amis, A. A. Biomechanics of the menisci of the knee.

Curr. Orthop. **22,** 193–201 (2008).

43. Hauch, K. N., Villegas, D. F. & Haut Donahue, T. L. Geometry, time-dependent and failure properties of human meniscal attachments. *J. Biomech.* **43,** 463–468 (2010).

44. Villegas, D. F., Maes, J. A., Magee, S. D. & Haut Donahue, T. L. Failure properties and strain distribution analysis of meniscal attachments. *J. Biomech.* **40,** 2655–2662 (2007).

45. Haut Donahue, T. L., Rashid, M. M., Hull, M. L. & Jacobs, C. R. A Finite Element Model of the Human Knee Joint for the Study of Tibio-Femoral Contact. *J. Biomech. Eng.* **124,** 273 (2002).

46. Li, K., Zheng, L., Tashman, S. & Zhang, X. The inaccuracy of surface-measured model-derived tibiofemoral kinematics. *J. Biomech.* **45,** 2719–23 (2012).

47. Benoit, D. L. *et al.* Effect of skin movement artifact on knee kinematics during gait and cutting motions measured in vivo. *Gait Posture* **24,** 152–64 (2006).

48. Leardini, A., Chiari, L., Della Croce, U. & Cappozzo, A. Human movement analysis using stereophotogrammetry. Part 3. Soft tissue artifact assessment and compensation. *Gait Posture* **21,** 212–25 (2005).

49. Smith, C. R., Lenhart, R. L., Kaiser, J., Vignos, M. F. & Thelen, D. G. Influence of Ligament Properties on Tibiofemoral Mechanics in Walking. *J. Knee Surg.* (2015). doi:10.1055/s-0035-1558858

50. Lafortune, M. a, Cavanagh, P. R., Sommer, H. J. & Kalenak, A. Three-dimensional kinematics of the human knee during walking. *J. Biomech.* **25,** 347–57 (1992).

51. Liu, F. *et al.* In vivo tibiofemoral cartilage deformation during the stance phase of gait. *J. Biomech.* **43,** 658–65 (2010).

52. Kozanek, M. *et al.* Tibiofemoral kinematics and condylar motion during the stance phase of gait. *J. Biomech.* **42,** 1877–84 (2009).

53. Zajac, F. E., Neptune, R. R. & Kautz, S. a. Biomechanics and muscle coordination of human walking. Part I: introduction to concepts, power transfer, dynamics and simulations. *Gait Posture* **16,** 215–32 (2002).

54. Chehab, E. F., Favre, J., Erhart-Hledik, J. C. & Andriacchi, T. P. Baseline knee adduction and flexion moments during walking are both associated with 5 year cartilage changes in patients with medial knee osteoarthritis. *Osteoarthr. Cartil.* **22,** 1833–1839 (2014).

Chapter 3

The Influence of Component Alignment and Ligament Properties on Tibiofemoral Contact Forces in Total Knee Replacement

Colin R. Smith, Michael F Vignos, Rachel L Lenhart, Jarred Kaiser, Darryl G. Thelen
(Published in the Journal of Biomechanical Engineering)

Abstract

The study objective was to investigate the influence of coronal plane alignment and ligament properties on total knee replacement (TKR) contact loads during walking. We created a subject-specific knee model of an 86 year old male who had an instrumented TKR. The knee model was incorporated into a lower extremity musculoskeletal model, and included deformable contact, ligamentous structures and six degree of freedom tibiofemoral and patellofemoral joints. A novel numerical optimization technique was used to simultaneously predict muscle forces, secondary knee kinematics, ligament forces and joint contact pressures from standard gait analysis data collected on the subject. The nominal knee model predictions of medial, lateral and total contact forces during gait agreed well with TKR measures, with RMS errors of 0.23, 0.22, and 0.33 body weight (BW), respectively. Coronal plane component alignment did not affect total knee contact loads, but did alter the medial-lateral load distribution, with 4° varus and 4° valgus rotations in component alignment inducing +17% and -23% changes in the medial tibiofemoral contact forces at first peak, respectively. A Monte Carlo analysis showed that uncertainties in ligament stiffness and reference strains introduced an approximately ±0.2 BW uncertainty in tibiofemoral force estimates over the gait cycle. Ligament properties had substantial influence on the TKR load distributions, with the medial collateral

ligament and iliotibial band properties having the largest effects on medial and lateral compartment loading during stance phase, respectively. The computational framework provides a viable approach for virtually designing TKR components, considering parametric uncertainty and predicting the effects of joint alignment and soft tissue balancing procedures on TKR function during movement.

Introduction

Component alignment and soft tissue balance can affect the function and longevity of total knee replacements (TKR). Excessive varus and valgus malalignments are associated with substantially higher rates of failure[1]. Further, clinical studies have linked soft tissue imbalances with instability and long-term failures of the joint[2-12]. Soft tissue balance is highly dependent on ligament tensioning achieved surgically, with changes in component thickness and soft tissue releases employed to adjust ligament tension to ensure balance[13-17]. However, despite the clinical significance, it remains challenging to assess the effects of component alignment and ligament stiffness on the *in vivo* behavior of TKR during functional movement. Such information is important to elucidate the underlying mechanical causes of joint failure.

Computational musculoskeletal modeling provides a powerful platform to investigate the sensitivity of TKR behavior during locomotor tasks such as walking. In contrast to cadaveric experiments, computational modeling can be used to comprehensively assess parametric sensitivities of joint mechanics under functional soft tissue and external loads. Thanks in part to the *Grand Challenge Competition to Predict In Vivo Knee Loads* initiated by Fregly and colleagues[18], models used to predict TKR mechanics have seen notable advances in sophistication and veracity in recent years. Entries to the competition have employed various modeling approaches including inverse optimization models[19],

finite element analysis[20], EMG-driven simulations[21] and dynamic simulations that couple movement and joint mechanics[22-24]. However, often modeling studies do not systematically consider the influence that parametric uncertainty[25] can have on predictions of joint contact forces. Such uncertainty analysis is particularly relevant to assessing ligament effects, given that ligament constitutive properties cannot be measured on a subject-specific basis and large variability exists across the population[26-31].

As part of the 2015 "Grand Challenge", the objective of this study was to investigate the influence of joint alignment and uncertain ligament properties on TKR loading during walking. To do this, we created a subject-specific knee model that included deformable contact, ligamentous structures and six degree of freedom tibiofemoral and patellofemoral joints. A novel numerical optimization technique was employed to simultaneously predict muscle forces, secondary knee kinematics, ligament forces and joint contact pressures from experimental gait analysis measures. Model predictions of tibiofemoral contact forces were compared to subject-specific *in vivo* measurements obtained from an instrumented joint replacement. We also used a Monte Carlo approach to assess the effect of uncertainties in ligament stiffness and reference strains on both ligament forces and tibiofemoral contact force predictions.

Methods

Experimental Data

The subject of this study was an 83 year old male with an instrumented right total knee replacement (Mass = 70 kg, Height = 172 cm). The experimental data was provided by the sixth edition of the *Grand Challenge Competition to Predict In Vivo Knee Loads*[32]. Whole body kinematics and ground reaction forces were measured in a standard motion analysis laboratory while the subject

executed two modified styles of overground gait: *smooth* and *bouncy*. The verbal instructions for each walking pattern were to use a "Reduced (Increased) superior-inferior translation of the pelvis during the gait cycle," respectively[18]. Motion capture marker kinematics were collected at 120 Hz and low pass filtered with a cutoff frequency of 6 Hz and ground reaction forces were collected at 1000 Hz and low pass filtered at a cutoff frequency of 50 Hz. Tibial plateau contact loads were measured simultaneously with the other experimental data by an instrumented tibial component. The measured loads were decomposed into medial and lateral components using an empirical regression equation[33].

Knee Model

A three body knee model was developed using the implanted component geometries and subject-specific bone geometries segmented from computed tomography (CT) images (Fig. 1). The tibiofemoral and patellofemoral joints were both modeled as six degrees of freedom (DOF) with deformable contact. An elastic patellar tendon (PT) and eleven elastic ligament bundles were included in the model: anteriolateral and posteriomedial posterior cruciate ligament (aPCL, pPCL), superficial and deep medial collateral ligament (sMCL, dMCL), lateral collateral ligament (LCL), popliteofibular ligament (PFL), posteriomedial capsule (pmCAP), posterior capsule (CAP), iliotibial band (ITB), medial patellofemoral ligament (MPFL), and lateral patellofemoral

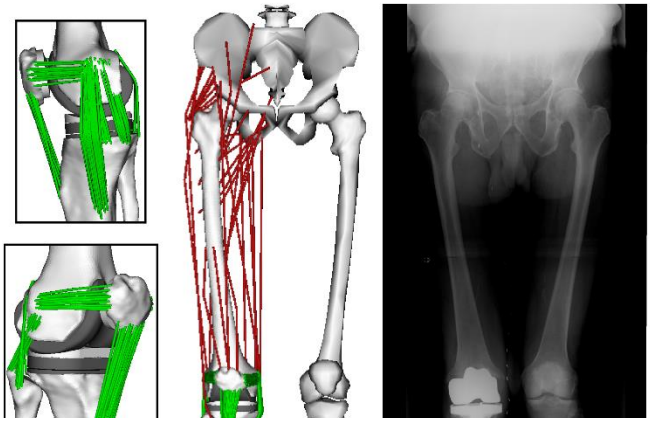

Figure 1 The knee model used subject-specific bone and TKR component geometry and included an extensible patellar tendon (PT) and 11 ligament bundles: anteriolateral and posteriomedial posterior cruciate ligament (aPCL, pPCL), superficial and deep medial collateral ligament (sMCL, dMCL), lateral collateral ligament (LCL), popliteofibular ligament (PFL), posteriomedial capsule (pmCAP), posterior capsule (CAP), iliotibial band (ITB), medial patellofemoral ligament (MPFL), and lateral patellofemoral ligament (LPFL). The knee model was integrated into a generic lower extremity model which included 44 muscle-tendon units acting about the hip, knee and ankle. The coronal plane TKR component alignment in the nominal model was set to match the limb alignment measured for the subject in a standing radiograph.

ligament (LPFL). The anterior cruciate ligament was not included in the model because it was resected during the TKR surgery.

Table 1 Ligament and patellar tendon properties assumed in the unblinded nominal model. For each ligament, the stiffness was evenly divided between the individual strands included in a bundle. Reference strains reflect the strain assumed for the ligament with the knee in a relaxed extended posture.

	Stiffness		Reference Strain		Number of
Name	N/strain	(95% CI)	strain	(95% CI)	**Strands**
aPCL	5700	(2280 - 9120)	0.01	(-0.03 - 0.04)	10
pPCL	2400	(960 - 3840)	-0.06	(-0.10 - -0.02)	10
sMCL	2200	(880 - 3520)	0.03	(-0.01 - 0.07)	20
dMCL	2800	(1120 - 4480)	0.03	(-0.01 - 0.07)	10
LCL	1800	(720 - 2880)	0.06	(0.02 - 0.10)	10
PFL	3000	(1200 - 4800)	-0.01	(-0.05 - 0.03)	10
pmCAP	2000	(800 - 3200)	0.05	(0.01 - 0.09)	10
CAP	4000	(1600 - 6400)	0.08	(0.04 - 0.12)	8
ITB	4000	(1600 - 6400)	0.02	(-0.02 - 0.06)	1
PT	14700	(5880 - 23520)	0.02	(-0.02 - 0.06)	30
mPFL	1000	(400 - 1600)	-0.05	(-0.09 - -0.01)	15
lPFL	800	(320 - 1280)	0.01	(-0.03 - 0.05)	15

Ligaments were modeled as bundles of strands extending between the origin and insertion attachment footprints. Ellipsoidal wrap objects were included for the sMCL, pmCAP and LPFL bundles to prevent penetration of the ligament path into the bone and component geometries. A generic ligament force-strain relationship was used, which assumed the ligament force to be quadratic at low strains and linear at high strains[34,35]. For each ligament bundle, linear stiffness and reference strain parameters were defined to scale the generic force-strain curve (Table 1). The linear stiffness defined the slope of the force-strain curve and the reference strain defined the strain of the ligament in a reference posture (extended knee). Reference strains were then used to compute the ligament slack lengths. Linear stiffness was estimated from ligament cross sectional areas measured from an MRI of a subject of similar stature and an assumed elastic modulus of 125 MPa[26]. Reference strains were adapted from the literature[36-38] . Ligament attachment footprints on the bone mesh geometries were estimated based on

anatomical studies[39-53]. The attachment points of individual line segments were evenly distributed by uniformly sampling B-spline surface representations of the attachment footprints[54].

The articular surface geometries of the tibial, femoral and patellar components were represented as triangulated meshes (10000, 21000, 8000 triangles, respectively). We performed a set of simulations with increasing mesh densities to determine the minimum number of triangles per mesh required to generate converged contact force predictions. Joint contact surface pressures ($\boldsymbol{p}$) were calculated on each triangle based on the local surface penetration depth according to the elastic foundation model[55]:

$$p = \frac{(1-v)E}{(1+v)(1-2v)}\frac{d}{h} \quad (1)$$

where $\boldsymbol{E}$ is the elastic modulus, $\boldsymbol{v}$ is the Poissons ratio, $\boldsymbol{h}$ is the thickness of the tibial insert and $\boldsymbol{d}$ is the penetration depth. The femoral component was assumed to be rigid and the polyethylene tibial insert was assumed to have a uniform thickness of 9 mm and exhibit linearly elastic material properties. The commonly reported value for elastic modulus of polyethylene inserts (E=463 MPa)[56] was reduced by a factor of 10 to improve the numerical stability of contact in the gait simulations. The Poisson's ratio was 0.46[57] . Contacting regions between the articulating surface meshes were determined using ray-casting techniques in conjunction with hierarchical object orientated bounding boxes[38].

Lower Extremity Musculoskeletal Model

The knee model was integrated into a generic lower extremity musculoskeletal model[58] which consisted of pelvis, thigh, shank, and foot segments. The hip was modeled as a 3 DOF ball and socket joint and the ankle as a 1 DOF pin joint. The thigh and shank segments were scaled such that the generic tibia and femur geometries matched the subject-specific bones. All remaining segments were scaled to minimize the differences between anatomical landmarks on the generic model and

anatomical marker positions measured with the subject in a static upright posture. The subject-specific femur and tibia were manually aligned to the scaled generic bones. The femoral and tibial components were placed such that the limb alignment in the coronal plane matched the hip-knee-ankle angle measured from a standing radiograph[59](Fig. 1). The patella was manually positioned relative to the femur such that it matched the CT scans in the reference posture.

The generic model included 44 muscle-tendon units crossing the hip, knee and ankle joints[58]. Individual muscle forces (F) were assumed to linearly scale with activation level (a), i.e. $F=a \cdot F_0$ where F_0 is the maximum isometric force for the muscle. The full model was implemented in SIMM[60] with the Dynamics Pipeline (Musculographics Inc., Santa Rosa, CA) and SD/Fast (Parametric Technology Corp., Needham, MA) used to generate the code describing ligament wrapping and the multibody equations of motion.

Gait Simulations

At each frame of the gait cycles, a global optimization inverse kinematics routine determined pelvis translations, pelvis rotations, hip angles, knee flexion angle and ankle angle that minimized the sum of squares differences between model marker locations and measured marker locations. During inverse kinematics, the secondary tibiofemoral and all patellofemoral kinematics were constrained to be functions of the knee flexion angle. These functions were determined by simulating passive knee flexion (0^o to 70^o) using the subject specific knee model.

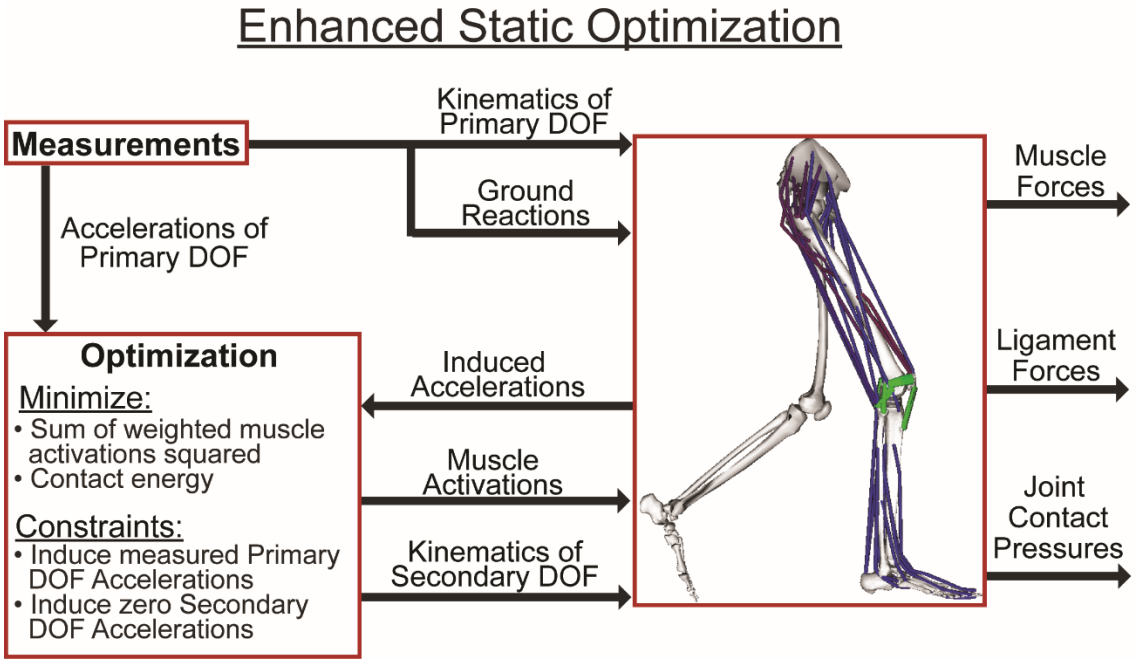

Figure 2 A numerical optimization approach was used to simultaneously predict patellofemoral kinematics, secondary tibiofemoral kinematics and muscle forces that, together with the induced ligament forces and contact pressures, generated the measured hip, knee and ankle accelerations at each time step of a gait cycle. Muscle force distribution was determined by minimizing an objective function that consisted of a sum of volume weighted squared muscle activations and the knee joint contact energy.

An enhanced static optimization (ESO) routine was then used to simultaneously predict the muscle forces, secondary tibiofemoral and patellofemoral kinematics, ligament forces and joint contact pressures at each frame in the gait cycle (Fig. 2). The optimization problem was formulated to solve for muscle activations and secondary knee kinematics which minimized an objective function while satisfying overall dynamic constraints.

$$J = \sum_{i=1}^{n_{muscles}} V_i a_i^2 + w \sum_{j=1}^{n_{faces}} U_j \qquad (2)$$

The objective function (J) minimized the muscle volume (V) weighted sum of squared muscle activations (a)[61] plus the knee joint contact energy. Contact energy (U) associated with each face of a contact mesh was computed as the integral of its force-deformation relationship (Eq 1). The net

contact energy was then obtained by summing energy over all faces of the articulating surface meshes. In a sensitivity study, we found inclusion of the contact energy term reduced tibiofemoral contact loads, particularly at the second loading peak of stance phase. The regularization scale factor w was held constant for all simulations at a value for which further increases had relatively small effects on the predicted peak contact loads. The optimization constraints required that the muscle forces and internal knee loads (contact pressures, ligament forces) produced by the optimized knee kinematics generate the measured hip, knee (flexion), and ankle accelerations while also inducing equilibrium (zero accelerations) in the secondary tibiofemoral and all patellofemoral degrees of freedom. Minor damping effects were included on the knee DOF to ensure the generation of smooth frame-to-frame kinematics (mean damping force and moment magnitudes were less than 10 N and 1 Nm, respectively). Pelvis coordinates were prescribed to reproduce measured values, and measured ground reaction forces and moments were applied directly to the feet. It should be explicitly noted that tibiofemoral and patellofemoral behavior were not pre-assumed in our simulations, but evolved as a result of the interaction of external, joint contact, ligament, and muscle forces. Thus, each gait simulation provided a prediction of the ligament and contact forces over the entire gait cycle which were then analyzed for the purposes of this study.

Grand Challenge Competition

For the blinded phase of the competition, we incorporated the TKR components into a healthy knee model[62], aligning and orienting the components in way that best fit the natural knee cartilage surfaces. For the unblinded phase, we replaced the bone geometries with the subject-specific skeletal geometries provided for the subject. We also repositioned the TKR components to both match the articular surfaces based on the subject's CT scans and coronal alignment based on standing radiographs (Fig. 1). We defined the ligament origins, insertions and wrapping geometries to the subject-specific bone geometries using literature descriptions of normal attachment sites[39-53].

The tibiofemoral medial, lateral and total contact force predictions of the blind and unblinded models were quantitatively evaluated against the measured contact forces for the *smooth* and *bouncy* gait styles by computing the bias (average difference in force predictions), precision (standard deviation of the force prediction errors), R^2 (squared Pearson's correlation coefficient and coefficient of determination) values and root-mean-square (RMS) errors.

Sensitivity to Coronal Plane Alignment

To assess the influence of coronal plane component alignment on the contact force predictions of the model, we performed a series of simulations with the knee alignment modified 2° and 4° varus and valgus from the nominal orientation in a standing posture. This was achieved by rotating the femoral component by 1° and 2° in the coronal plane and counter-rotating the tibial component by an equal amount. Passive forward simulations were performed iteratively with the knee fixed at 0° flexion to settle the tibia and patella and establish a new reference posture. For each reference posture, the unaltered reference strain of each ligament was then used to compute ligament slack lengths. *Smooth* and *bouncy* gaits were then re-simulated using the inverse kinematics and ESO methods described previously.

Probabilistic Simulation

The sensitivity of predicted tibiofemoral contact forces during *smooth* gait to ligament constitutive properties was assessed using the Monte Carlo method. The linear stiffness and reference strains of each ligament bundle were represented by independent Gaussian distributions. The distributions were centered at the nominal model stiffness and reference strain values and the standard deviations were assumed to be 30% of the nominal stiffness and 0.02 strain, respectively[63]. A total of 2,000 simulations were performed on a high throughput computing grid using randomly selected values from the constitutive property distributions. The uncertainty in the predicted medial, lateral

and total tibiofemoral contact forces was quantified by calculating the time varying means and standard deviations of all the simulations. The number of simulations was justified by verifying that the mean of the total tibiofemoral contact force at each frame of the gait cycle varied by less than 1% when the final 10% of the Monte Carlo simulations were removed.

We then performed a sensitivity analysis to determine the relative influence of the properties of each ligament on the predicted tibiofemoral contact forces. At both the first and second peaks of tibiofemoral loading during stance, we computed the Pearson's correlation coefficient (R) to quantify the correlation between the stiffness and reference strain of each ligament to the tibiofemoral contact forces (Fig. 4). The Pearson's correlation coefficients range between -1 and 1, with values of 1 indicating a perfect positive correlation, -1 indicating a perfect negative correlation, and 0 indicating no correlation. The absolute values of the Pearson's correlation coefficients were used to determine the relative influence of the stiffness and reference strain of each ligament on the tibiofemoral contact forces.

Results

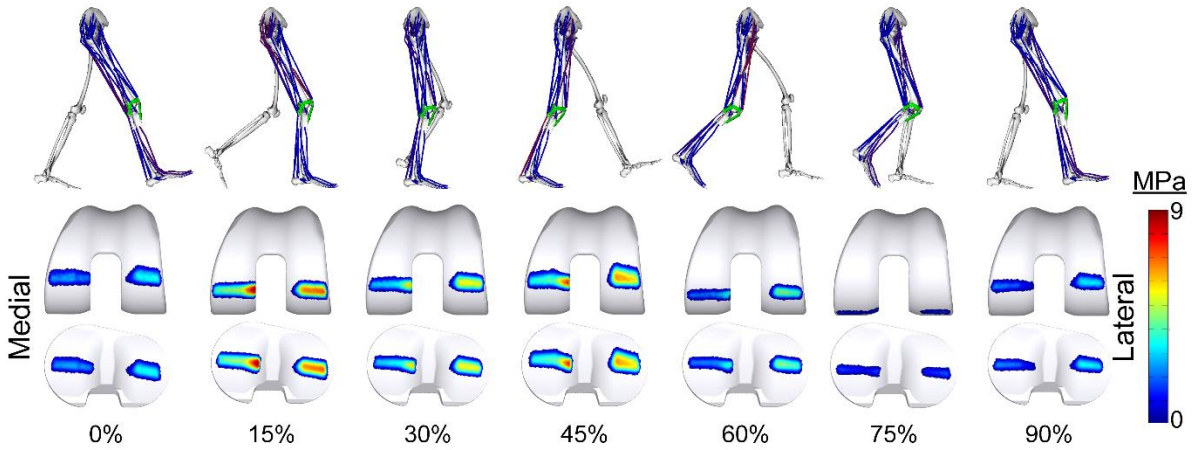

Figure 3 Lower extremity posture, activated muscles (shown in red), and computed contact pressures on the femoral and tibial components throughout the smooth gait cycle.

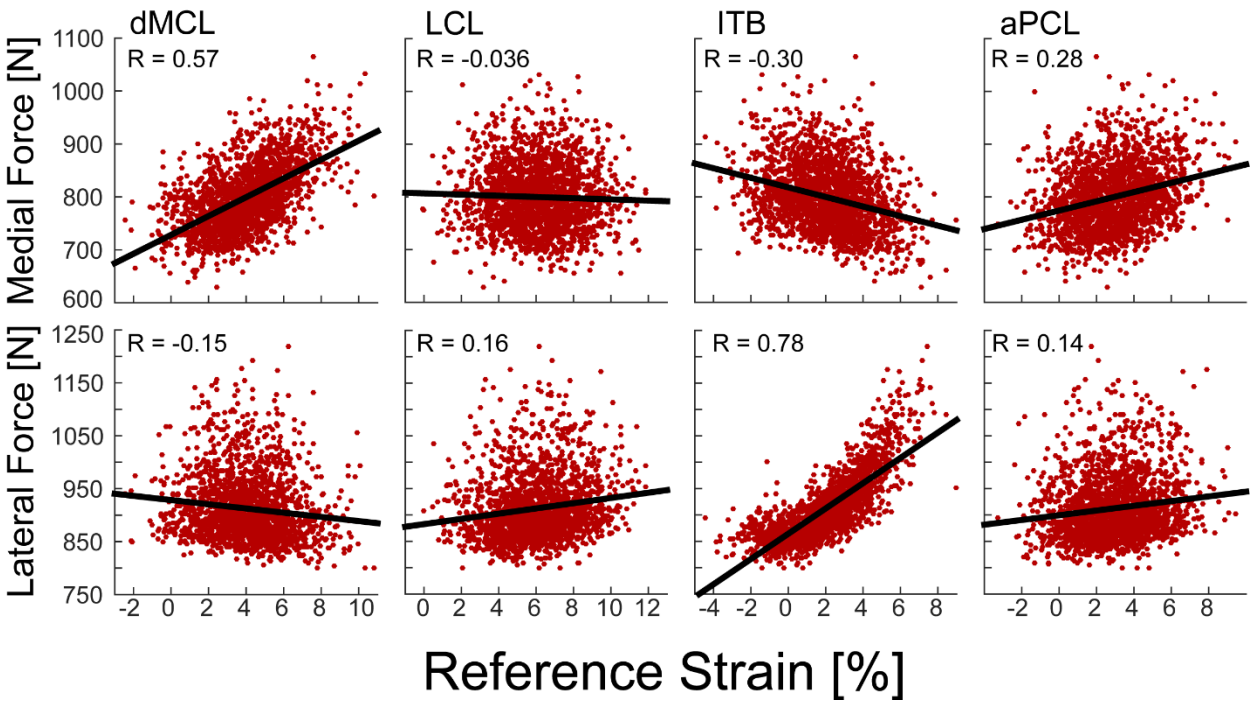

Figure 4 Representative scatter plots showing the correlation between predicted tibiofemoral contact forces at the second peak of tibiofemoral loading during stance and ligament reference strain. Each red point corresponds to 1 of the 2000 simulations ran. The strength of the correlation between the predicted contact forces and the reference strain were evaluated using Pearson's correlation coefficients (R).

The blinded model predictions of total tibiofemoral loading mimicked the overall measured temporal patterns, with Pearson's R^2 values of 0.86 and 0.82 during *smooth* and *bouncy* gait, respectively (Table 2). However, the blinded predictions were biased toward over-predicting the total contact force magnitude (*smooth* = 0.28 BW, *bouncy* = 0.3 BW). Much of the bias arose from over-predicting the loading on the medial compartment throughout the gait cycle, while slightly under-predicting the lateral compartment loading throughout much of stance (Fig. 5). Blinded RMS errors were 0.52 BW and 0.29 BW on the medial and lateral compartments, respectively, in the *smooth* gait trial.

The unblinded model included the subject-specific skeletal geometries and knee joint alignment, as well as ligament attachments determined from the bone geometries. Unblinded total

knee load predictions were substantially more consistent with measurements, with only a slight bias toward over-prediction (*smooth* = 0.10 BW, *bouncy* = 0.18 BW). The temporal patterns of stance phase loading were well predicted on both compartments, while the late swing loading peak on the lateral compartment was predicted to occur slightly later than was measured (Fig. 5). Unblinded RMS errors were reduced to 0.23 BW and 0.22 BW on the medial and lateral compartments, respectively, in the *smooth* gait trial. The corresponding R^2 coefficients of determination were 0.71 and 0.56 for the medial and lateral compartments, respectively.

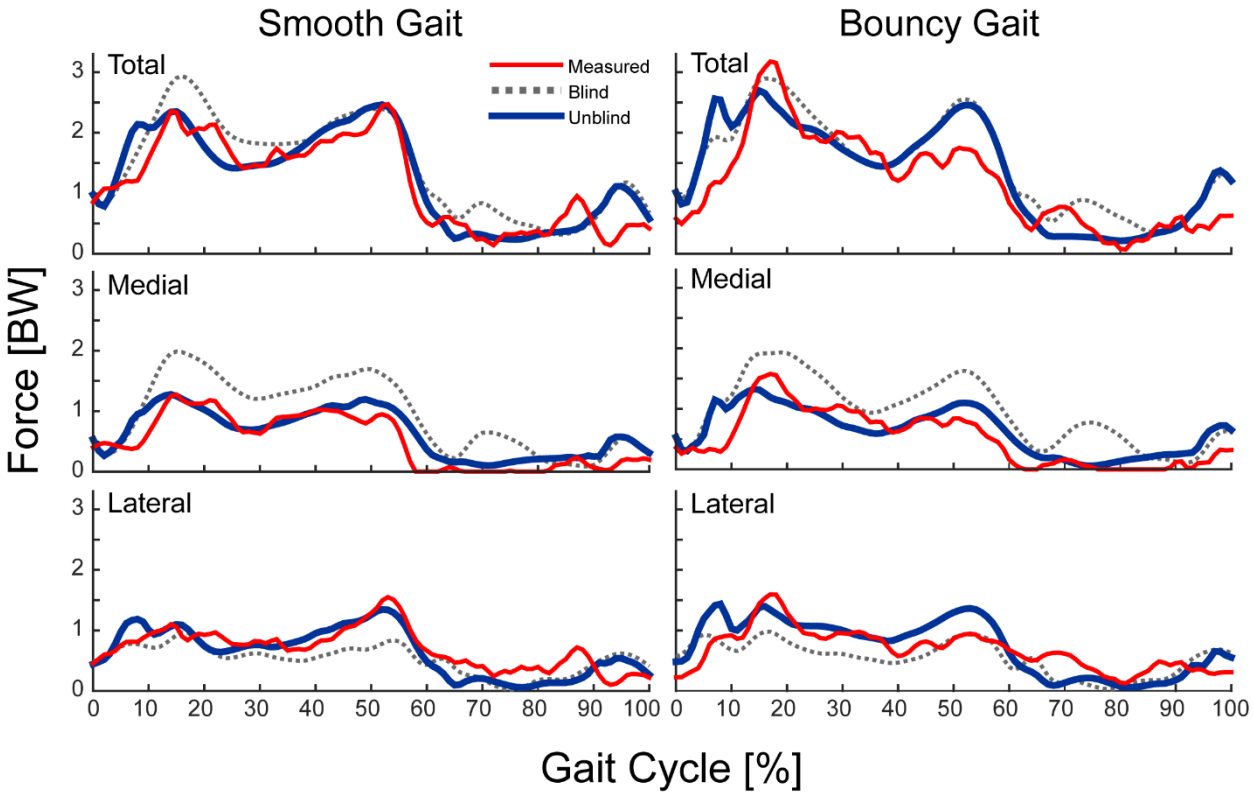

Figure 5 Comparison of blinded and unblinded model predicted tibial component contact forces (in superior direction) to measured contact forces throughout the smooth and bouncy gait cycles. Error metrics are given in Table 2.

Coronal Alignment Effects

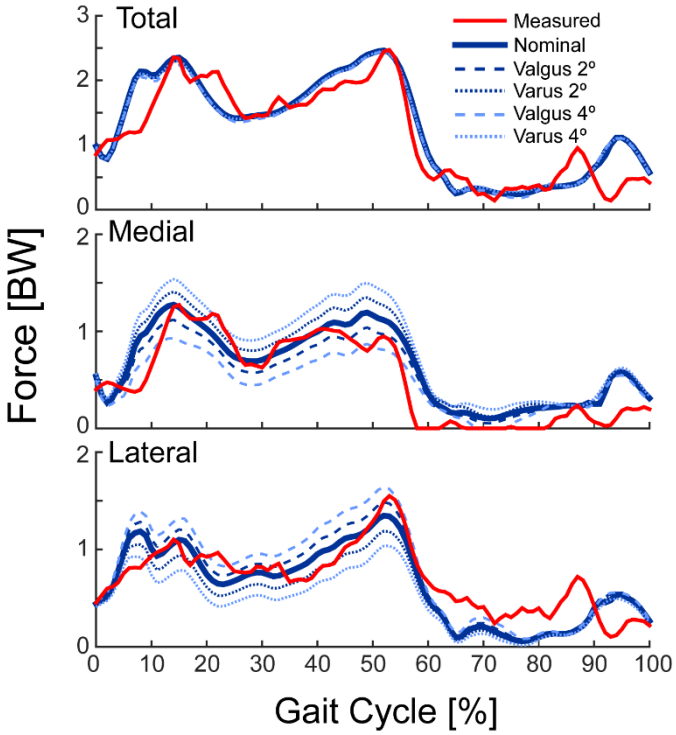

Figure 6 Sensitivity of joint contact forces to variations in coronal plane component alignment for smooth gait. Placing the components in a varus alignment relative to the nominal position shifted more of the force distribution to the medial compartment. The opposite relationship exists when placing the components in a valgus alignment, relative to nominal. Comparable results were found for bouncy gait.

The coronal plane alignment of the TKR components had minimal effect on the net knee contact force over the entire gait cycle, but had a substantial effect on the medial-lateral distribution of the predicted contact forces during stance (Fig. 6). As expected, more varus alignments shifted the contact force distribution to the medial side of the joint, with the medial compartment supporting 42%, 54%, and 67% of the total predicted knee load at the first peak for the 4° valgus, nominal, and 4° varus component alignments, respectively. Similarly, the medial compartment accounted for 33%, 45%, and 58% of the total load at the second peak.

Probabilistic Ligament Simulations

The predicted ligament forces were relatively low with means of <50 N for each of the ligament bundles throughout the gait cycle (Fig 7). The deep MCL, superficial MCL and iliotibial band remained engaged at relatively constant tensions throughout much of stance. The posterior capsule and LCL forces exhibited a distinct peak of ~50 N when the knee was extended in late swing. The PFL and PCL exhibited peak loads just prior to toe-off, and then remained engaged throughout swing.

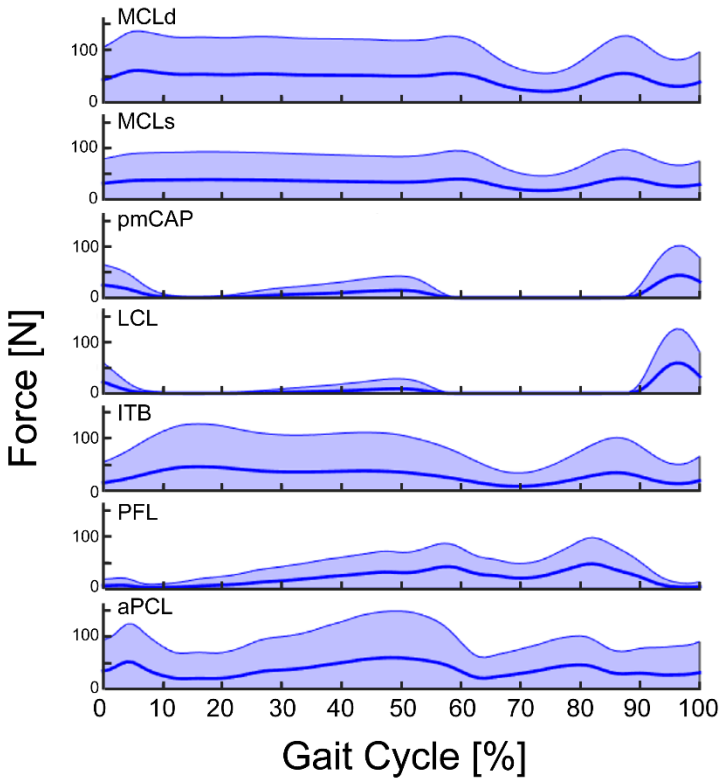

Figure 7 Variability in ligament forces (shaded area represents the range +/- 2 standard deviations) throughout the smooth gait cycle due to uncertainty in ligament stiffness and reference strains. The dark center line is the mean of the Monte Carlo simulations, which is nearly identical to the force predicted by the nominal model.

There was substantial variability in predicted ligament forces due to uncertainty in ligament stiffness and reference strains (Fig. 7). The superficial MCL, deep MCL, PCL and iliotibial band forces were particularly sensitive in stance phase, with the 95% confidence intervals extending from 0 to >100 N for each of these bundles. During swing, posterior capsule and LCL forces were highly sensitive, with magnitudes that could vary from 0 to 100 N in terminal swing.

Ligament properties had similar influence on the predicted medial and lateral contact forces (Fig. 8). The 95% confidence interval (CI) of the predicted medial, lateral and total contact force remained nearly constant (± 0.2 BW) throughout the gait cycle with similar variability seen in the medial and lateral compartments.

For all ligaments, total contact force was positively correlated with ligament stiffness and reference strain (Fig. 9). The properties of the deep and superficial MCL had the primary influence on predicted medial contact force at both first and second peak of tibiofemoral loading in stance. The reference strain of the aPCL was a secondary influence at both peaks and the reference strain of the pmCAP had influence at the second peak. The reference strain of the iliotibial band showed a minor negative correlation throughout stance, acting to shift the load to the lateral compartment. The lateral

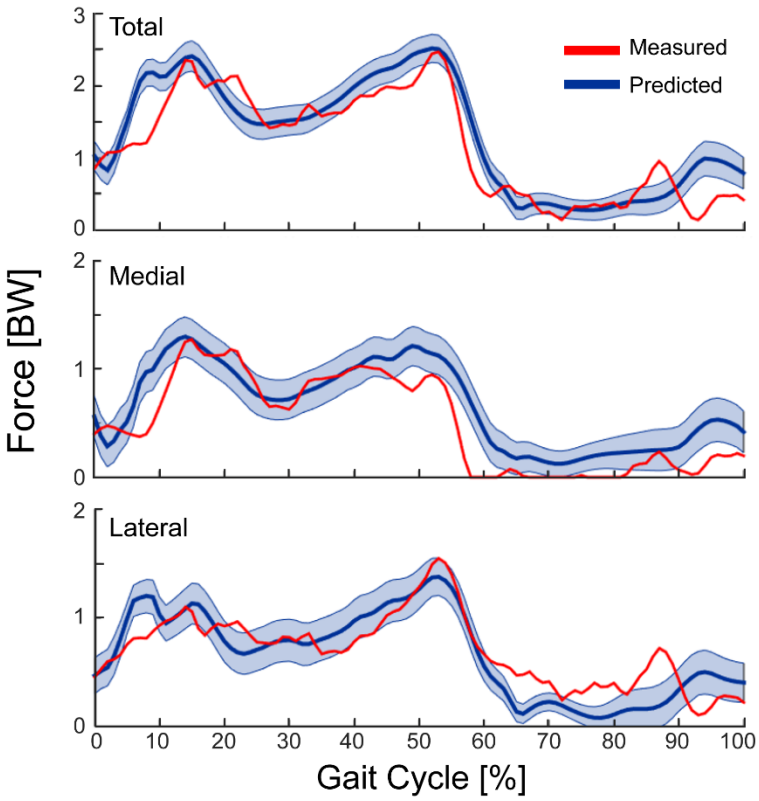

Figure 8 Variability in predicted tibiofemoral joint contact forces (mean +/- 2 standard deviations) throughout smooth gait cycle due to uncertainty in the stiffness and reference strains assumed for ligaments.

contact force was primarily influenced by the properties of the iliotibial band over the entire stance phase. At first peak, the iliotibial band exhibited the highest correlation with load (Stiffness: R = 0.27, Reference Strain: R = 0.81) while the properties of both bundles of the MCL and showed slight negative correlations. At the second peak, the iliotibial band properties were again the primary influence with the PFL, LCL and aPCL acting as secondary positive contributors.

Discussion

Our primary objective was to investigate the effect of TKR component alignment and ligament constitutive properties on tibiofemoral contact forces during gait. To accomplish this, we developed a subject-specific knee model, incorporated it into a lower extremity musculoskeletal model and then used numerical optimization to simultaneously predict muscle, ligament and joint contact loads from motion analysis measures. We found that the incorporation of subject-specific component alignment was critical to achieve predictions of medial-lateral contact force distributions that agreed with measurements from an instrumented TKR. Our sensitivity analysis showed that predicted

Table 2 Agreement between measured and model (blind and unblind) predicted tibiofemoral joint contact forces during the smooth and bouncy gait trials.

***Smooth* Gait**	Medial	Lateral	Total
R^2, Pearson's			
Blinded	0.83	0.48	0.86
Unblinded	0.81	0.70	0.83
R^2, Coefficient of determination			
Blinded	-0.47	0.19	0.68
Unblinded	0.71	0.56	0.79
Bias (BW)			
Blinded	0.44	-0.18	0.28
Unblinded	0.14	-0.06	0.10
Precision (BW)			
Blinded	0.27	0.24	0.30
Unblinded	0.19	0.21	0.32
RMS error (BW)			
Blinded	0.52	0.29	0.40
Unblinded	0.23	0.22	0.33

***Bouncy* Gait**	Medial	Lateral	Total
R^2, Pearson's			
Blinded	0.80	0.42	0.82
Unblinded	0.70	0.61	0.72
R^2, Coefficient of determination			
Blinded	-0.26	0.21	0.66
Unblinded	0.62	0.26	0.62
Bias (BW)			
Blinded	0.44	-0.14	0.30
Unblinded	0.12	0.06	0.18
Precision (BW)			
Blinded	0.25	0.26	0.34
Unblinded	0.25	0.28	0.44
RMS error (BW)			
Blinded	0.50	0.29	0.45
Unblinded	0.28	0.29	0.48

ligament forces and medial-lateral contact force distributions were quite dependent on ligament stiffness and reference strain, with variations of ±0.2 body weight due to uncertainties in these parameters. Ligament properties are often manipulated in TKR procedures, such that our new simulation framework provides a viable approach for predicting the effects of TKR component designs and surgical techniques on post-operative knee function.

Musculoskeletal modeling and simulation techniques have notably advanced in recent years. The "Grand challenge competition to predict in vivo knee loads" has contributed to this advance by providing rich subject-specific data sets of medical images, TKR geometries, motion analysis data and joint contact load measurements, which allow researchers to benchmark various modeling techniques against each other. Prior approaches have included traditional optimization techniques to estimate muscle forces as inputs to finite element models of the knee joint[20], EMG-driven simulations[21] and multi-body dynamic simulations that include joint contact between articulating surfaces[22,24,38]. The 2014 "Grand Challenge" winner introduced a unique optimization approach, termed Force Dependent Kinematics (FDK), that iteratively solved for the muscle forces and secondary

tibiofemoral kinematics that balanced lower extremity dynamics[19]. However, that modeling approach pre-assumed an inextensible patellar tendon, resulting in an artificial kinematic constraint. We have extended the FDK approach by simultaneously solving the muscle forces, secondary tibiofemoral and all patellofemoral kinematics that would induce the measured joint accelerations. Our joint contact load prediction errors (RMS error = 0.33 in *smooth* gait) are comparable to that obtained using FDK (RMS error = 0.26 BW), and slightly better than those that have been obtained using traditional optimization or forward dynamic simulations[18,38].

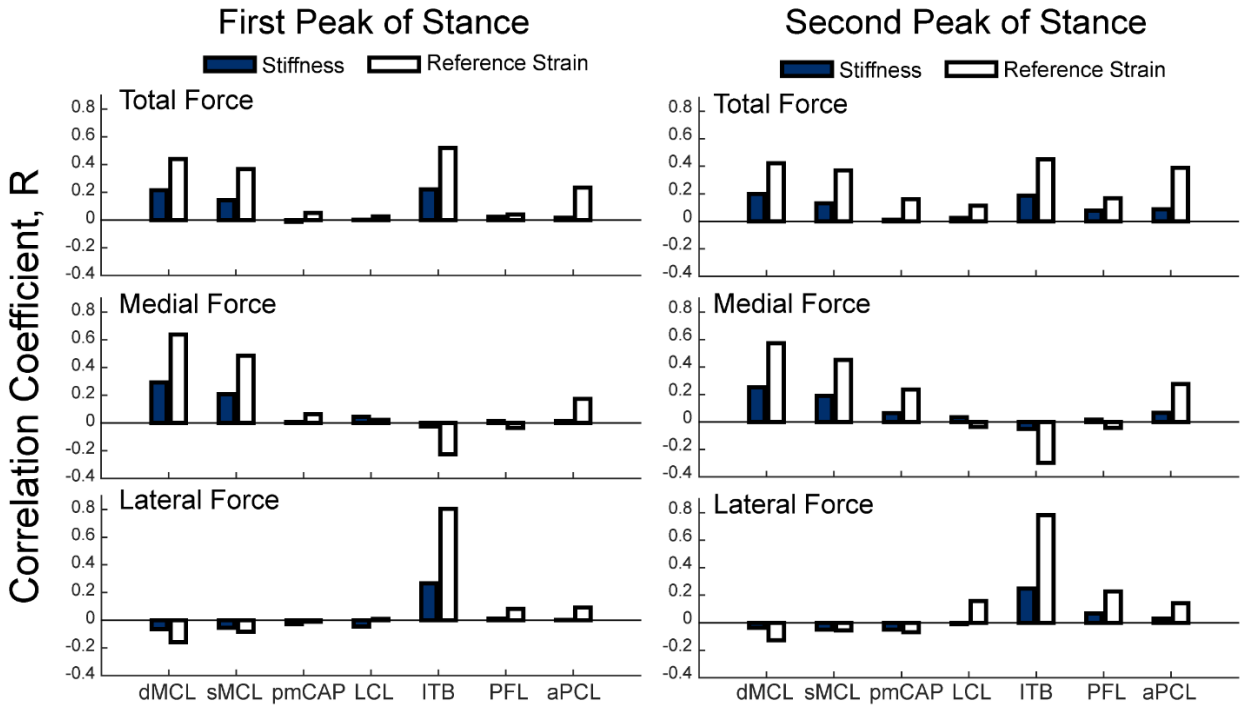

Figure 9 Correlations of tibiofemoral contact forces with ligament stiffness (solid bars) and reference strain (open bars) at the first and second peaks of tibiofemoral loading during stance; dMCL = deep medial collateral ligament; sMCL = superficial medial collateral ligament; pmCAP = posteriomedial capsule; LCL = lateral collateral ligament; ITB = iliotibial band; PFL = popliteofibular ligament; aPCL = anteriolateral posterior cruciate ligament.

Our knee model and simulation technique includes several other notable features. The tibiofemoral and patellofemoral joints are each treated as six DOF. The model represented the ligaments as bundles of strands acting in parallel and included more passive structures of the knee

than prior models. The enhanced static optimization simulation routine provides for simultaneous estimates of muscle forces, ligament forces, joint contact pressures and secondary kinematics at each time step, accounting for the inherent dynamic coupling between them. Of these, the joint contact pressures are particularly relevant in TKR given the links between loading patterns and wear[64-68]. Finally, our simulation times were approximately 20 minutes per gait simulation on a traditional desktop computer (3.10 GHz Intel Xeon Processor, 16 GB RAM). As a result, by deploying simulations in parallel on a high throughput computing grid, 2000 probabilistic simulations can be performed in approximately two hours. This capability allows the use of a Monte Carlo approach to quantitatively assess the influence of uncertain model parameters, such as ligament properties, on knee joint contact.

In agreement with previous modeling studies[38,69,70], the coronal alignment of the femoral and tibial components affected the predicted knee contact loading patterns. While total contact force magnitudes were insensitive to alignment (Fig. 6), each two degree shift in valgus alignment resulted in equal (~0.15 BW) increases and decreases in the lateral and medial loads during stance, respectively. Accordingly, refining the TKR alignment in the model to better match the standing radiograph (Fig. 1) was the single most important factor that improved the agreement between our model predictions and measurements between the blinded and unblinded simulations (Fig. 5). Coronal plane alignment has been linked clinically to TKR component loosening and wear problems[7,71-76], such that our modeling framework could be further used to investigate the interaction of alignment, contact loads and pressure patterns to understand how to better mitigate adverse TKR outcomes.

We systematically considered the influence of ligament properties on our predicted knee contact loading patterns. While prior models in the Grand Challenge Competition have included ligaments[18,19,22,38], our study is the first to consider the dependence of joint loading on uncertain

ligament constitutive properties. The uncertainty analysis is important as there are currently no viable approaches for measuring ligament elasticity *in vivo*. As a result, ligament stiffness and reference strains must be estimated from cadaveric studies[35-38], which contributes to uncertainty in the model. Our results show total knee contact loads varied by ± 0.2 BW 95% confidence intervals given our assumed uncertainty in ligament properties (Fig. 8), and that the total load increased monotonically with stiffness and reference strain for all ligaments (Fig. 9). The latter result arises from the fact that our simulated tibiofemoral kinematics varied minimally with ligament properties, such that an increase in stiffness or reference strain (i.e. shorter slack length) enhanced the ligament tension and thus increased the contact load. The influence of stiffness and reference strain on medial-lateral load distributions was highly variable between ligaments and throughout the gait cycle (Fig. 9). MCL sensitivity was quite interesting with both the deep and superficial bundles exhibiting tensions that varied from 0 to ~100 N during stance (Fig. 7), depending on the properties assumed. Further, increased MCL tension induced an increase in medial compartment loading that exceeded a simultaneous decrease in lateral compartment loading. This is in agreement with a loaded cadaveric study which measured a 46% reduction in medial force and a 9% increase in lateral force at full extension following a major MCL release using an instrumented tibial insert[77]. Of the ligaments considered, lateral compartment loading was most sensitive to the iliotibial band. Given the clinical significance of soft tissue balancing and known effects on long-term TKR function and longevity [67], our modeling framework may aid surgeons in positioning components and in planning soft tissue releases.

The results of this study highlight the clinical and modeling benefits of considering parameter uncertainty and sensitivity when performing musculoskeletal simulations. While previous editions of the Grand Challenge have focused largely on validation, sensitivity studies are also important to establish model credibility[25] . All parameters of musculoskeletal models have experimental errors associated with their values, and even in subject-specific models, many parameters must be estimated

as they cannot be measured. Additionally, musculoskeletal models of the type used in this study can contain thousands of parameters, which makes them subject to redundancy, where multiple parameter combinations could result in agreement with experimental measures. Accordingly, it is important to test the robustness of model predictions to a range of reasonable parameter values, particularly for parameters with large influence or variability[78]. In addition to complementing model validation, sensitivity studies are useful to reveal causal relationships between model parameters and simulated outcomes, making them highly relevant to surgical simulation.

To properly interpret the results of this study, several limitations in methodology must be noted. First, for computational reasons, joint contact pressures were computed using an elastic foundation model[55] rather than a finite element model which could better characterize the component deformation state. The appropriateness of the elastic foundation model for estimating pressure has been previously established for TKR applications[79]. Additionally, the stiffness of polyethylene tibial insert was reduced by an order of magnitude to improve numerical stability of the optimization routine. The decreased stiffness resulted in slightly increased deformation and contact area, but had negligible effects on the secondary knee kinematics and net contact forces. Refined estimates of insert deformation and stress distributions could subsequently be obtained by using the net loads as boundary conditions on a finite element model of the joint replacement.

We assumed muscle geometries based on a published generic musculoskeletal model[58], and assumed that muscle forces scaled linearly with activation. It would be reasonably straight forward to include subject-specific muscle geometry[80-82], if available, and to include more complex models of muscle-tendon dynamics[83,84] if the research application required more information on muscle behavior. We relied on numerical optimization to resolve muscle redundancy, a technique widely studied and used in biomechanics[85]. A traditional objective function based only on muscle activations

[61] resulted in an over-prediction of joint contact loads, as has been observed previously[19,86]. Adding a penalty for high joint contact energy into the objective function (Eq. 2) reduced knee contact forces, largely by redistributing loading among the plantarflexor muscles.

The ligament attachment footprints in the model were determined relative to anatomical landmarks because magnetic resonance images were not available for the subject. However, the locations of ligament attachments in the knee joint relative to bony landmarks have been thoroughly documented in the literature[39-53]. The representation of each ligament bundle by many strands that span the attachment footprints may somewhat mitigate errors associated with single line of action ligament models. The Monte Carlo sampling distributions for the ligament properties were modeled as Gaussian, centered on nominal values derived from population based studies[63] . This assumption was necessitated by the scarcity of experimental data and difficulty of measuring ligament properties *in vivo*. Finally, our sensitivity metrics from the Monte Carlo analysis are first order correlation coefficients, which inherently do not account for nonlinearities or characterize interactions between ligaments. The number of simulations can easily be scaled up using high throughput computing platforms, allowing for more advanced sensitivity analyses[78,87] that consider parametric interactions.

In conclusion, we developed a subject-specific knee model and introduced a novel numerical optimization approach for predicting *in vivo* TKR mechanics during walking. Joint contact force predictions agreed very well with *in vivo* measurements obtained via an instrumented knee replacement. We also used the model to investigate the sensitivity of joint contact loading to component alignment and ligament properties. Thus, the proposed framework provides a viable objective approach for virtually designing TKR components, considering parametric uncertainty and predicting the effects of joint alignment and soft tissue balancing procedures on TKR function in movement.

Acknowledgments

We would like to thank B.J. Fregly, Ph.D., Darryl D'Lima, M.D., Ph.D. and the entire Grand Challenge team for organizing the competition and sharing the experimental data for this study. Additionally, we acknowledge Josh Roth for his contributions on the clinical interpretation of our research. This research was performed using the computing resources and assistance of the UW-Madison Center for High Throughput Computing (www.chtc.cs.wisc.edu).

Funding

We gratefully acknowledge the support of NIH grants AR062733, EB015410 and HD084213, and a NSF graduate research fellowship (MV).

References

1 Fang, D. M., Ritter, M. A. & Davis, K. E. Coronal alignment in total knee arthroplasty: just how important is it? *J Arthroplasty* **24**, 39-43, doi:10.1016/j.arth.2009.04.034 (2009).

2 Insall, J. Correction of arthritic deformities of the knee. *Arthritis and allied conditions: a textbook of rheumatology. Tenth ed. Philadelphia: Lea and Febiger*, 771-784 (1985).

3 Sambatakakis, A., Wilton, T. & Newton, G. Radiographic sign of persistent soft-tissue imbalance after knee replacement. *Journal of Bone & Joint Surgery, British Volume* **73**, 751-756 (1991).

4 Freeman, M., Todd, R., Bamert, P. & Day, W. ICLH arthroplasty of the knee: 1968--1977. *Journal of Bone & Joint Surgery, British Volume* **60**, 339-344 (1978).

5 Insall, J. N., Binazzi, R., Soudry, M. & Mestriner, L. A. Total knee arthroplasty. *Clinical orthopaedics and related research* **192**, 13-22 (1985).

6 Wasielewski, R. C., Galante, J. O., Leighty, R. M., Natarajan, R. N. & Rosenberg, A. G. Wear patterns on retrieved polyethylene tibial inserts and their relationship to technical considerations during total knee arthroplasty. *Clinical orthopaedics and related research* **299**, 31-43 (1994).

7 WINDSOR, R. E., SCUDERI, G. R., MORAN, M. C. & INSALL, J. N. Mechanisms of failure of the femoral and tibial components in total knee arthroplasty. *Clinical orthopaedics and related research* **248**, 15-20 (1989).

8 Lotke, P. A. & Ecker, M. L. Influence of positioning of prosthesis in total knee replacement. *The Journal of Bone & Joint Surgery* **59**, 77-79 (1977).

9 Karachalios, T., Sarangi, P. & Newman, J. Severe varus and valgus deformities treated by total knee arthroplasty. *Journal of Bone & Joint Surgery, British Volume* **76**, 938-942 (1994).

10 Teeny, S. M., Krackow, K. A., Hungerford, D. S. & Jones, M. Primary Total Knee Arthroplasty in Patients With Severe Varus Deformity A Comparative Study. *Clinical orthopaedics and related research* **273**, 19-31 (1991).

11 Dorr, L. D. & Boiardo, R. A. Technical considerations in total knee arthroplasty. *Clinical orthopaedics and related research* **205**, 5-11 (1986).

12 Matsuda, S. *et al.* Changes in knee alignment after total knee arthroplasty. *The Journal of arthroplasty* **14**, 566-570 (1999).

13 Krackow, K. A. & Mihalko, W. M. The effect of medial release on flexion and extension gaps in cadaveric knees: implications for soft-tissue balancing in total knee arthroplasty. *The American journal of knee surgery* **12**, 222-228 (1998).

14 Whiteside, L. A., Saeki, K. & Mihalko, W. M. Functional Medial Ligament Balancing in Total Knee Arthroplasty. *Clinical orthopaedics and related research* **380**, 45-57 (2000).

15 Yagishita, K., Muneta, T. & Ikeda, H. Step-by-step measurements of soft tissue balancing during total knee arthroplasty for patients with varus knees. *The Journal of arthroplasty* **18**, 313-320 (2003).

16 Scott, W. N. *Insall & Scott surgery of the knee*. (Elsevier Health Sciences, 2011).

17 Mihalko, W. M., Saleh, K. J., Krackow, K. A. & Whiteside, L. A. Soft-tissue balancing during total knee arthroplasty in the varus knee. *Journal of the American Academy of Orthopaedic Surgeons* **17**, 766-774 (2009).

18 Kinney, A. L., Besier, T. F., D'Lima, D. D. & Fregly, B. J. Update on grand challenge competition to predict in vivo knee loads. *J Biomech Eng* **135**, 021012, doi:10.1115/1.4023255 (2013).

19 Marra, M. A. *et al.* A subject-specific musculoskeletal modeling framework to predict in vivo mechanics of total knee arthroplasty. *J Biomech Eng* **137**, 020904, doi:10.1115/1.4029258 (2015).

20 Kim, Y.-H., Park, W.-M. & Phuong, B. T. T. in *ASME 2010 Summer Bioengineering Conference*. 267-268 (American Society of Mechanical Engineers).

21 Manal, K. & Buchanan, T. S. An electromyogram-driven musculoskeletal model of the knee to predict in vivo joint contact forces during normal and novel gait patterns. *J Biomech Eng* **135**, 021014, doi:10.1115/1.4023457 (2013).

22 Guess, T. M., Stylianou, A. P. & Kia, M. Concurrent prediction of muscle and tibiofemoral contact forces during treadmill gait. *J Biomech Eng* **136**, 021032, doi:10.1115/1.4026359 (2014).

23 Thelen, D. G., Choi, K. W. & Schmitz, A. M. Co-Simulation of Neuromuscular Dynamics and Knee Mechanics during Human Walking. *J Biomech Eng*, doi:10.1115/1.4026358 (2014).

24 Hast, M. W. & Piazza, S. J. Dual-joint modeling for estimation of total knee replacement contact forces during locomotion. *J Biomech Eng* **135**, 021013 (2013).

25 Anderson, A. E., Ellis, B. J. & Weiss, J. A. Verification, validation and sensitivity studies in computational biomechanics. *Computer methods in biomechanics and biomedical engineering* **10**, 171-184 (2007).

26 Chandrashekar, N., Mansouri, H., Slauterbeck, J. & Hashemi, J. Sex-based differences in the tensile properties of the human anterior cruciate ligament. *Journal of biomechanics* **39**, 2943-2950, doi:http://dx.doi.org/10.1016/j.jbiomech.2005.10.031 (2006).

27 Claes, L., Beyer, A., Krischke, W. & Schmid, R. in *Biomechanics of Human Knee Ligaments, Proc. European Society of Biomechanics* 22 (1987).

28 Noyes, F. R. & Grood, E. S. The strength of the anterior cruciate ligament in humans and Rhesus monkeys. *The Journal of Bone & Joint Surgery* **58**, 1074-1082 (1976).

29 Prietto, M., Bain, J., Stonebrook, S. & Settlage, R. Tensile strength of the human posterior cruciate ligament (PCL). *Trans Orthop Res Soc* **13**, 736-745 (1988).

30 Trent, P. S., Walker, P. S. & Wolf, B. Ligament length patterns, strength, and rotational axes of the knee joint. *Clinical orthopaedics and related research* **117**, 263-270 (1976).

31 Woo, S. L.-Y., Hollis, J. M., Adams, D. J., Lyon, R. M. & Takai, S. Tensile properties of the human femur-anterior cruciate ligament-tibia complex The effects of specimen age and orientation. *The American journal of sports medicine* **19**, 217-225 (1991).

32 Fregly, B. J. *et al.* Grand challenge competition to predict in vivo knee loads. *Journal of Orthopaedic Research* **30**, 503-513 (2012).

33 Meyer, A. J. *et al.* in *ASME 2011 Summer Bioengineering Conference*. 389-390 (American Society of Mechanical Engineers).

34 Smith, C. R., Lenhart, R. L., Kaiser, J., Vignos, M. F. & Thelen, D. G. Influence of Ligament Properties on Tibiofemoral Mechanics in Walking. *The journal of knee surgery* (2015).

35 Blankevoort, L. & Huiskes, R. Ligament-bone interaction in a three-dimensional model of the knee. *J Biomech Eng* **113**, 263-269 (1991).

36 Shelburne, K. B., Pandy, M. G., Anderson, F. C. & Torry, M. R. Pattern of anterior cruciate ligament force in normal walking. *Journal of biomechanics* **37**, 797-805 (2004).

37 Shin, C. S., Chaudhari, A. M. & Andriacchi, T. P. The influence of deceleration forces on ACL strain during single-leg landing: a simulation study. *Journal of biomechanics* **40**, 1145-1152 (2007).

38 Thelen, D. G., Choi, K. W. & Schmitz, A. M. Co-simulation of neuromuscular dynamics and knee mechanics during human walking. *J Biomech Eng* **136**, 021033 (2014).

39 Amis, A., Firer, P., Mountney, J., Senavongse, W. & Thomas, N. Anatomy and biomechanics of the medial patellofemoral ligament. *The Knee* **10**, 215-220 (2003).

40 Amis, A., Gupte, C., Bull, A. & Edwards, A. Anatomy of the posterior cruciate ligament and the meniscofemoral ligaments. *Knee Surgery, Sports Traumatology, Arthroscopy* **14**, 257-263 (2006).

41 Basso, O., Johnson, D. & Amis, A. The anatomy of the patellar tendon. *Knee Surgery, Sports Traumatology, Arthroscopy* **9**, 2-5 (2001).

42 Edwards, A., Bull, A. M. & Amis, A. A. The attachments of the fiber bundles of the posterior cruciate ligament: an anatomic study. *Arthroscopy: The Journal of Arthroscopic & Related Surgery* **23**, 284-290 (2007).

43 Ferretti, M., Ekdahl, M., Shen, W. & Fu, F. H. Osseous landmarks of the femoral attachment of the anterior cruciate ligament: an anatomic study. *Arthroscopy: The Journal of Arthroscopic & Related Surgery* **23**, 1218-1225 (2007).

44 Giron, F., Cuomo, P., Aglietti, P., Bull, A. M. & Amis, A. A. Femoral attachment of the anterior cruciate ligament. *Knee Surgery, Sports Traumatology, Arthroscopy* **14**, 250-256 (2006).

45 Kopf, S. *et al.* A systematic review of the femoral origin and tibial insertion morphology of the ACL. *Knee Surgery, Sports Traumatology, Arthroscopy* **17**, 213-219 (2009).

46 LaPrade, R. F., Ly, T. V., Wentorf, F. A. & Engebretsen, L. The Posterolateral Attachments of the Knee A Qualitative and Quantitative Morphologic Analysis of the Fibular Collateral Ligament, Popliteus Tendon, Popliteofibular Ligament, and Lateral Gastrocnemius Tendon*. *The American Journal of Sports Medicine* **31**, 854-860 (2003).

47 Liu, F. *et al.* Morphology of the medial collateral ligament of the knee. *Journal of orthopaedic surgery and research* **5**, 1-8 (2010).

48 Meister, B. R., Michael, S. P., Moyer, R. A., Kelly, J. D. & Schneck, C. D. Anatomy and kinematics of the lateral collateral ligament of the knee. *The American Journal of Sports Medicine* **28**, 869-878 (2000).

49 Nomura, E., Inoue, M. & Osada, N. Anatomical analysis of the medial patellofemoral ligament of the knee, especially the femoral attachment. *Knee Surgery, Sports Traumatology, Arthroscopy* **13**, 510-515 (2005).

50 Rachmat, H. *et al.* Generating finite element models of the knee: How accurately can we determine ligament attachment sites from MRI scans? *Medical engineering & physics* **36**, 701-707 (2014).

51 Robinson, J., Sanchez-Ballester, J., Bull, A., de WM Thomas, R. & Amis, A. The posteromedial corner revisited AN ANATOMICAL DESCRIPTION OF THE PASSIVE RESTRAINING STRUCTURES OF THE MEDIAL ASPECT OF THE HUMAN KNEE. *Journal of Bone & Joint Surgery, British Volume* **86**, 674-681 (2004).

52 Sugita, T. & Amis, A. A. Anatomic and biomechanical study of the lateral collateral and popliteofibular ligaments. *The American Journal of Sports Medicine* **29**, 466-472 (2001).

53 Wijdicks, C. A. *et al.* Radiographic identification of the primary medial knee structures. *The Journal of Bone & Joint Surgery* **91**, 521-529 (2009).

54 Vignos, M. F., Smith, C. R. & Thelen, D. G. in *13th International Symposium on Computer Methods in Biomechanics and Biomedical Engineering* (Montreal, Quebec, CA, 2015).

55 Bei, Y. & Fregly, B. J. Multibody dynamic simulation of knee contact mechanics. *Medical engineering & physics* **26**, 777-789 (2004).

56 Kurtz, S., Jewett, C., Bergström, J., Foulds, J. & Edidin, A. Miniature specimen shear punch test for UHMWPE used in total joint replacements. *Biomaterials* **23**, 1907-1919 (2002).

57 Bartel, D., Rawlinson, J., Burstein, A., Ranawat, C. & Flynn Jr, W. Stresses in polyethylene components of contemporary total knee replacements. *Clinical orthopaedics and related research* **317**, 76-82 (1995).

58 Arnold, E. M., Ward, S. R., Lieber, R. L. & Delp, S. L. A model of the lower limb for analysis of human movement. *Annals of biomedical engineering* **38**, 269-279 (2010).

59 Jeffery, R. S., Morris, R. W. & Denham, R. A. Coronal alignment after total knee replacement. *Journal of Bone & Joint Surgery, British Volume* **73**, 709-714 (1991).

60 Delp, S. L. & Loan, J. P. A computational framework for simulating and analyzing human and animal movement. *Computing in Science & Engineering* **2**, 46-55 (2000).

61 Happee, R. Inverse dynamic optimization including muscular dynamics, a new simulation method applied to goal directed movements. *J Biomech* **27**, 953-960 (1994).

62 Lenhart, R. L., Kaiser, J., Smith, C. R. & Thelen, D. G. Prediction and Validation of Load-Dependent Behavior of the Tibiofemoral and Patellofemoral Joints During Movement. *Annals of biomedical engineering*, 1-11 (2015).

63 Baldwin, M. A., Laz, P. J., Stowe, J. Q. & Rullkoetter, P. J. Efficient probabilistic representation of tibiofemoral soft tissue constraint. *Comput Methods Biomech Biomed Engin* **12**, 651-659 (2009).

64 Reinders, J. *et al.* Wear testing of moderate activities of daily living using in vivo measured knee joint loading. *PloS one* **10** (2015).

65 Wimmer, M., Knowlton, C., Pourzal, R., McEwen, P. & Andriacchi, T. Clinical TKA Wear Rates and Their Association With Gait Parameters. *Bone & Joint Journal Orthopaedic Proceedings Supplement* **95**, 587-587 (2013).

66 Abdel-Jaber, S., Belvedere, C., Leardini, A. & Affatato, S. Wear simulation of total knee prostheses using load and kinematics waveforms from stair climbing. *Journal of biomechanics* (2015).

67 Babazadeh, S., Stoney, J. D., Lim, K. & Choong, P. F. The relevance of ligament balancing in total knee arthroplasty: how important is it? A systematic review of the literature. *Orthopedic reviews* **1** (2009).

68 Fregly, B. J., Sawyer, W. G., Harman, M. K. & Banks, S. A. Computational wear prediction of a total knee replacement from in vivo kinematics. *Journal of biomechanics* **38**, 305-314 (2005).

69 Lerner, Z. F., DeMers, M. S., Delp, S. L. & Browning, R. C. How tibiofemoral alignment and contact locations affect predictions of medial and lateral tibiofemoral contact forces. *Journal of biomechanics* **48**, 644-650 (2015).

70 Chen, Z. *et al.* Effect of component mal-rotation on knee loading in total knee arthroplasty using multi-body dynamics modeling under a simulated walking gait. *J Orthop Res* **33**, 1287-1296, doi:10.1002/jor.22908 (2015).

71 Srivastava, A. *et al.* Effect of tibial component varus on wear in total knee arthroplasty. *The Knee* **19**, 560-563, doi:http://dx.doi.org/10.1016/j.knee.2011.11.003 (2012).

72 Ritter, M. A., Faris, P. M., Keating, E. M. & Meding, J. B. Postoperative Alignment of Total Knee Replacement Its Effect on Survival. *Clinical orthopaedics and related research* **299**, 153-156 (1994).

73 Feng, E. L., Stulberg, S. D. & Wixson, R. L. Progressive subluxation and polyethylene wear in total knee replacements with flat articular surfaces. *Clinical orthopaedics and related research* **299**, 60-71 (1994).

74 D'Lima, D. D., Hermida, J. C., Chen, P. C. & Colwell Jr, C. W. Polyethylene wear and variations in knee kinematics. *Clinical orthopaedics and related research* **392**, 124-130 (2001).

75 Hernigou, P. & Deschamps, G. Alignment influences wear in the knee after medial unicompartmental arthroplasty. *Clinical orthopaedics and related research* **423**, 161-165 (2004).

76 Werner, F. W., Ayers, D. C., Maletsky, L. P. & Rullkoetter, P. J. The effect of valgus/varus malalignment on load distribution in total knee replacements. *Journal of biomechanics* **38**, 349-355 (2005).

77 Crottet, D. *et al.* Ligament balancing in TKA: evaluation of a force-sensing device and the influence of patellar eversion and ligament release. *Journal of biomechanics* **40**, 1709-1715 (2007).

78 Hicks, J. L., Uchida, T. K., Seth, A., Rajagopal, A. & Delp, S. L. Is My Model Good Enough? Best Practices for Verification and Validation of Musculoskeletal Models and Simulations of Movement. *J Biomech Eng* **137**, 020905 (2015).

79 Halloran, J. P., Easley, S. K., Petrella, A. J. & Rullkoetter, P. J. Comparison of deformable and elastic foundation finite element simulations for predicting knee replacement mechanics. *J Biomech Eng* **127**, 813-818 (2005).

80 Scheys, L., Loeckx, D., Spaepen, A., Suetens, P. & Jonkers, I. Atlas-based non-rigid image registration to automatically define line-of-action muscle models: a validation study. *Journal of biomechanics* **42**, 565-572 (2009).

81 Blemker, S. S., Asakawa, D. S., Gold, G. E. & Delp, S. L. Image-based musculoskeletal modeling: Applications, advances, and future opportunities. *Journal of magnetic resonance imaging* **25**, 441-451 (2007).

82 Valente, G. *et al.* Are subject-specific musculoskeletal models robust to the uncertainties in parameter identification? (2014).

83 Thelen, D. G. Adjustment of muscle mechanics model parameters to simulate dynamic contractions in older adults. *J Biomech Eng* **125**, 70-77 (2003).

84 Millard, M., Uchida, T., Seth, A. & Delp, S. L. Flexing computational muscle: modeling and simulation of musculotendon dynamics. *J Biomech Eng* **135**, 021005 (2013).

85 Erdemir, A., McLean, S., Herzog, W. & van den Bogert, A. J. Model-based estimation of muscle forces exerted during movements. *Clin Biomech (Bristol, Avon)* **22**, 131-154 (2007).

86 Gerus, P. *et al.* Subject-specific knee joint geometry improves predictions of medial tibiofemoral contact forces. *J Biomech* **46**, 2778-2786, doi:10.1016/j.jbiomech.2013.09.005 (2013).

87 Laz, P. & Browne, M. A review of probabilistic analysis in orthopaedic biomechanics. *Proceedings of the Institution of Mechanical Engineers, Part H: Journal of Engineering in Medicine* **224**, 927-943 (2010).

Chapter 4

Influence of Ligament Properties on Tibiofemoral Mechanics in Walking

Colin R. Smith, Rachel L Lenhart, Jarred Kaiser, Michael F Vignos, Darryl G. Thelen
(Published in the Journal of Biomechanical Engineering)

Abstract

Computational knee models provide a powerful platform to investigate the effects of injury and surgery on functional knee behavior. The objective of this study was to use a multibody knee model to investigate the influence of ligament properties on tibiofemoral kinematics and cartilage contact pressures in the stance phase of walking. The knee model included 14 ligament bundles and articular cartilage contact acting across the tibiofemoral and patellofemoral joints. The knee was incorporated into a lower extremity musculoskeletal model and was used to simulate knee mechanics during the stance phase of normal walking. A Monte Carlo approach was employed to assess the influence of ligament stiffness and reference strain on knee mechanics. The anterior cruciate ligament (ACL), medial collateral ligament (MCL), and posterior capsule properties exhibited significant influence on anterior tibial translation at heel strike, with the ACL acting as the primary restraint to anterior tibial translation in mid-stance. The MCL and lateral collateral ligament (LCL) exhibited the greatest influence on tibial rotation from heel strike through mid-stance. Simulated tibial plateau contact location was dependent on the ACL, MCL, and LCL properties, while pressure magnitudes were most dependent on the ACL. A decrease in ACL stiffness or reference strain significantly increased the average contact pressure in mid-stance, with the pressure migrating posteriorly on the medial tibial plateau. These ligament-dependent shifts in tibiofemoral cartilage contact during walking

are potentially relevant to consider when investigating the causes of early-onset osteoarthritis following knee ligament injury and surgical treatment.

Introduction

Computational knee models are useful for investigating joint mechanics in both injured and surgically repaired states. For example, prior studies have used knee models to study the influence of ACL tears, ligament reconstruction, and tendon transfers on knee kinematics and cartilage loading patterns[1,2]. Accurate descriptions of soft tissue anatomy and mechanics are needed for these applications, which can make the models computationally demanding to solve[3,4]. As a result, knee models often are only used to simulate simple loading scenarios, such as laxity tests and isolated quadriceps loading[5-7]. However, it is often important clinically to understand knee mechanics during functional multi-joint tasks such as walking.

Physics-based musculoskeletal modeling approaches have evolved with recent advancements in computational and medical imaging technologies and provide a consistent framework to simulate the muscular coordination of whole body movement. For example, simulations of subject-specific gait dynamics are now readily performed[8]. However, the musculoskeletal models used in most current gait simulations have simplified representations of the knee[9], which lack the anatomical detail needed to simulate soft tissue injuries or surgical procedures. To address this limitation, advanced multibody knee models have been introduced that include detailed representations of anatomical structures[10-13], but are less computationally demanding than finite element approaches[5,14]. Multibody knee models are hence suitable for simulations of movement, and thus can be used to investigate the influence of soft tissue procedures on functional knee mechanics.

Subject-specific knee models can be created from high resolution MR images. A series of image slices is segmented to create 3D geometric representations of articular cartilage surfaces and ligament attachment sites, which are then used to characterize cartilage contact and ligamentous constraints acting about the tibiofemoral and patellofemoral joints[15]. In multibody knee models, the ligaments are typically represented as bundles of nonlinear springs acting between origin and insertion footprints[16]. Constitutive properties of the soft tissues are then needed to compute the internal tissue loads that arise with movement. However, these constitutive properties cannot currently be measured *in vivo* on a subject-specific basis. As a result, parametric uncertainty exists in the model which should be considered when simulating functional knee mechanics.

The objective of this study was to use a probabilistic approach to investigate the propagation of uncertain ligament constitutive properties onto knee mechanics in gait. Specifically, we assessed the effect of variations in ligament stiffness and reference strain on tibiofemoral kinematics and tibial contact when the quadriceps are loaded in the first half of stance. Additionally, we used a sensitivity analysis to determine the ligament constitutive properties that had significant effects on the tibiofemoral kinematics and tibial contact.

Methods

Knee model: We segmented the bone and cartilage surface geometries of the femur, tibia, and patella from MR images collected on a young adult female (age 23 yrs, height 1.65 m, mass 61 kg). Cartilage surfaces were represented by high resolution triangulated meshes and regions of contact between articulating cartilage surfaces were determined using ray-casting techniques together with hierarchical bounding boxes[17]. The combined thickness of the articulating cartilage was assumed to be

6 mm for both the tibiofemoral and patellofemoral joints. A nonlinear elastic foundation formulation[18] was used to compute pressure acting on each triangle face in contact based on the depth of penetration, the cartilage thickness, and assumed material properties (elastic modulus of 5 MPa, Poisson's ratio of 0.45[19]) (Fig. 1). The tibiofemoral and patellofemoral joints were both modeled as 6 DOF, allowing the cartilage contact, ligament, and muscle forces to determine their kinematics.

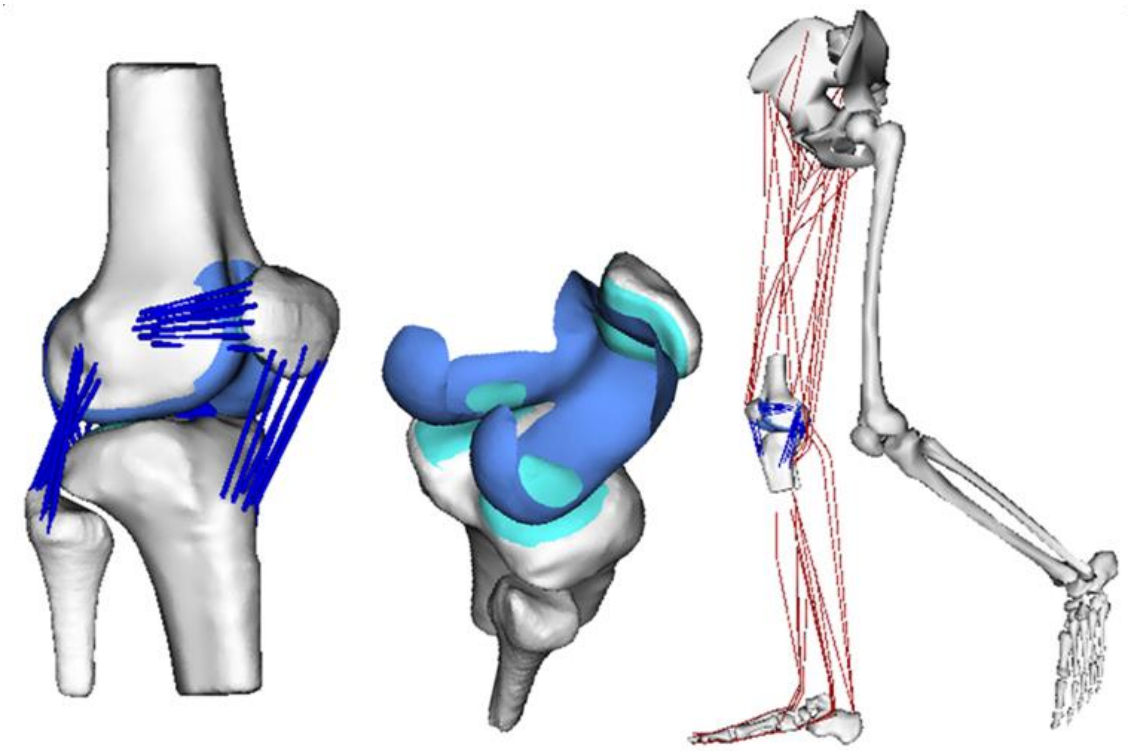

Figure 1 A multibody knee model was created that included six degree of freedom tibiofemoral and patellofemoral joints. Tibiofemoral and patellofemoral contact pressures were computed using an elastic foundation model, with local pressure calculated as a nonlinear function of the depth of penetration between articulating surfaces. To simulate walking, the knee was incorporated into a lower extremity musculoskeletal model with 44 muscles acting about the hip, knee and ankle.

The origins, insertions, and paths of the major knee ligaments were segmented from the MR images which included the: superficial and deep medial collateral ligament (sMCL, dMCL), lateral collateral ligament (LCL), anteriomedial and posteriolateral anterior cruciate ligament (aACL, pACL),

anteriolateral and posteriomedial posterior cruciate ligament (aPCL, pPCL), patellar tendon (PT), medial and lateral patellofemoral ligaments (MPFL, LPFL), popliteofibular ligament (PFL), posteriomedial capsule (pmCAP), the posterior capsule (CAP), and the iliotibial band (ITB). Each ligament was represented by bundles of nonlinear springs spanning from origin to insertion. Ligament paths were reconstructed by using ellipsoidal and cylindrical wrap objects to model wrapping of the ligaments over bony geometries. The ligament force-strain relationship was assumed to be quadratic at low strains and linear at higher strains (Fig. 2)[20]. Linear stiffness was estimated from the ligament cross-sectional areas as measured from the MRI. Reference strains were adapted from the literature[21,22].

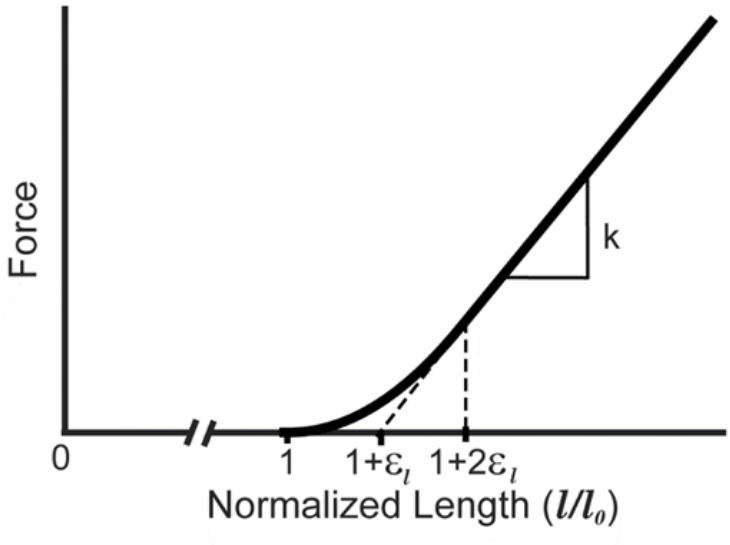

Figure 2 The generic ligament force-strain curve was scaled by the ligament-specific stiffness (k) and slack length (l_0). Slack length was computed from reference strain ($\boldsymbol{\varepsilon_{ref}}$) by scaling the ligament length in an extended knee reference configuration (l_{ref}) through the relationship $l_0 = l_{ref}/(\mathbf{1} + \boldsymbol{\varepsilon_{ref}})$. The strain that defined the transition from nonlinear behavior to linear behavior was assumed to be εl=0.03.

The knee was integrated into an existing lower extremity musculoskeletal model[9], which included 44 muscles acting about the hip, knee, and ankle joints. The full model was implemented in SIMM[23] with the Dynamics Pipeline (Musculographics Inc., Santa Rosa, CA) and SD/Fast (Parametric Technology Corp., Needham, MA) used to generate code describing muscle-tendon dynamics and the multibody equations of motion. The predictive capacity of the model was previously validated by comparing simulated passive and active knee kinematics with subject-specific *in vivo* 3D knee kinematics measured with dynamic MRI[26].

Whole body kinematics and ground reactions were recorded while the subject walked overground in a motion analysis laboratory. The lower extremity model was scaled to the subject based on segment lengths determined in a standing upright posture. During walking, marker kinematics were collected at 100 Hz and then low-pass filtered at 12 Hz. Ground reaction forces were simultaneously collected at 2000 Hz (force plate model BP400600, AMTI, Watertown, MA) and then low-pass filtered at 50 Hz. A global optimization inverse kinematics routine determined pelvis translations, pelvis rotations, hip angles, knee flexion, and ankle dorsiflexion that best agreed with marker positions measured during gait [24]. At this stage, secondary tibiofemoral and all patellofemoral degrees of freedom (DOF) were assumed to be a constrained function of knee flexion, with these functions based on our simulated passive knee behavior[25].

At each frame of a gait cycle, an enhanced static optimization (ESO) routine was then used to calculate muscle forces, patellofemoral kinematics, and secondary tibiofemoral kinematics that minimized an objective function while satisfying overall dynamic constraints[26]. The objective function was a weighted sum of squared muscle activations, with a regularization term added to minimize frame-to-frame variations in secondary kinematics. The optimization constraints required that the muscle forces and internal knee loads (contact pressures, ligament forces) produced by the optimized knee kinematics generate the measured hip, knee (flexion), and ankle accelerations. The pelvis coordinates were prescribed to reproduce measured values, and measured ground reaction forces were applied directly to the feet. It should be explicitly noted that only knee flexion was prescribed in the gait simulation, with all other tibiofemoral and patellofemoral DOFs being allowed to evolve as a result of cartilage contact, ligament, and muscle forces. Each gait simulation provided a prediction of the tibiofemoral and patellofemoral kinematics and contact from heel strike through the mid-stance phase of walking (Fig. 3)

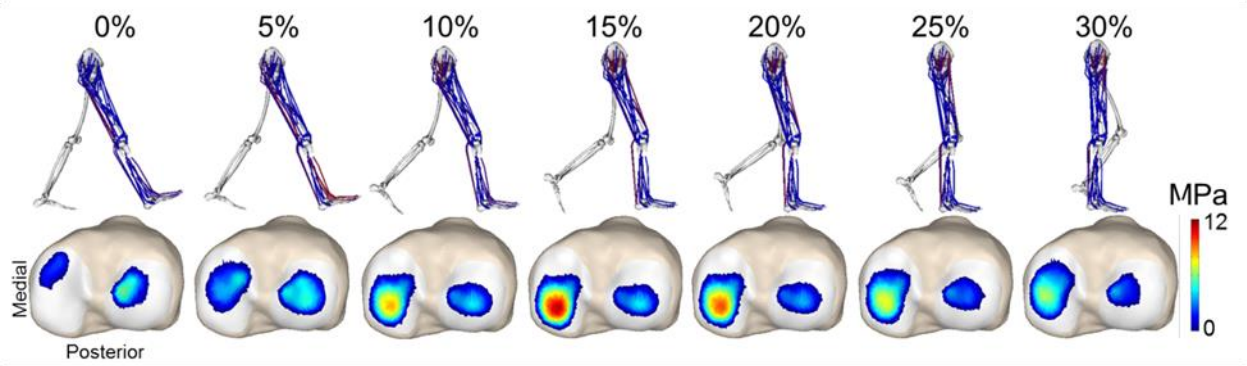

Figure 3 Simulation of tibial plateau contact pressures from heel strike (0%) through mid-stance phase of gait. The first loading peak (~15%) preferentially loads the medial tibial plateau.

We used the Monte Carlo method to assess the propagation of uncertainties in ligament constitutive properties onto simulated tibiofemoral mechanics. The linear stiffness and reference strains of each of the ligament bundles was represented by independent Gaussian distributions centered at the nominal model values with standard deviations of 30% of the mean stiffness and 0.02 strain, respectively[16]. A total of 2000 simulations were performed on a high throughput computing grid using randomly selected values from the constitutive property distributions. The uncertainty in the predicted secondary tibiofemoral kinematics and tibial contact metrics (average pressure, contact area, center of pressure) was quantified by calculating the time varying means and standard deviations of all the simulations for each output (Fig. 4).

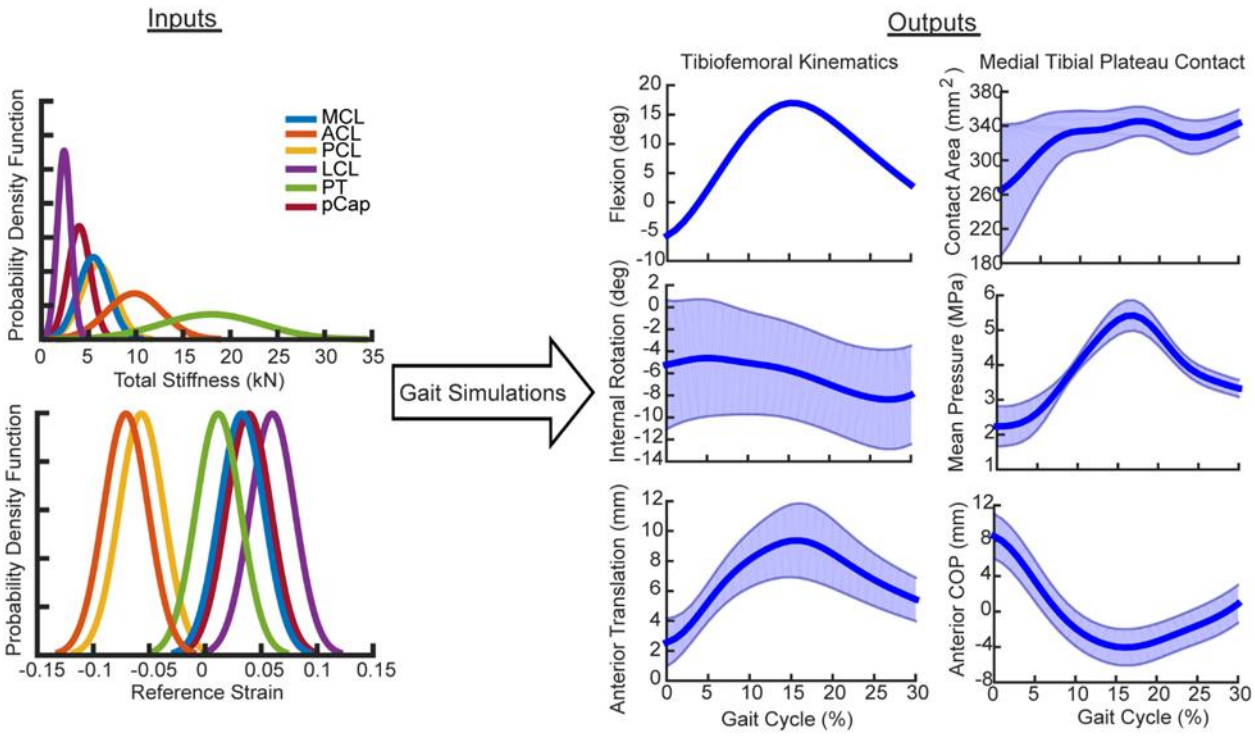

Figure 4 The Monte Carlo analysis was performed by varying the linear stiffness and reference strain of the ligaments using independent Gaussian distributions, and repeating the gait simulations to determine the effect on tibiofemoral kinematics and tibial contact metrics. The output plots show the mean (solid line) ± 2 standard deviations (shaded region).

We performed a sensitivity analysis to determine the relative importance of the stiffness and reference strain of each ligament on simulated tibiofemoral kinematics and contact metrics. At heel strike and the first peak of tibiofemoral loading, we computed the Pearson's correlation coefficient (R) and corresponding p-value to quantify the correlation between the stiffness and reference strain of each ligament to both kinematics and contact metrics (Fig. 5). Correlations were considered statistically significant if $p<0.05$. The Pearson's correlation coefficients varied between -1 and 1, with values of 1 indicating a strong positive correlation, -1 indicating a strong negative correlation and 0 indicating no correlation. The absolute value of the Pearson's correlation coefficients was used to determine the relative influence of the stiffness and reference strain of each ligament on the output metrics.

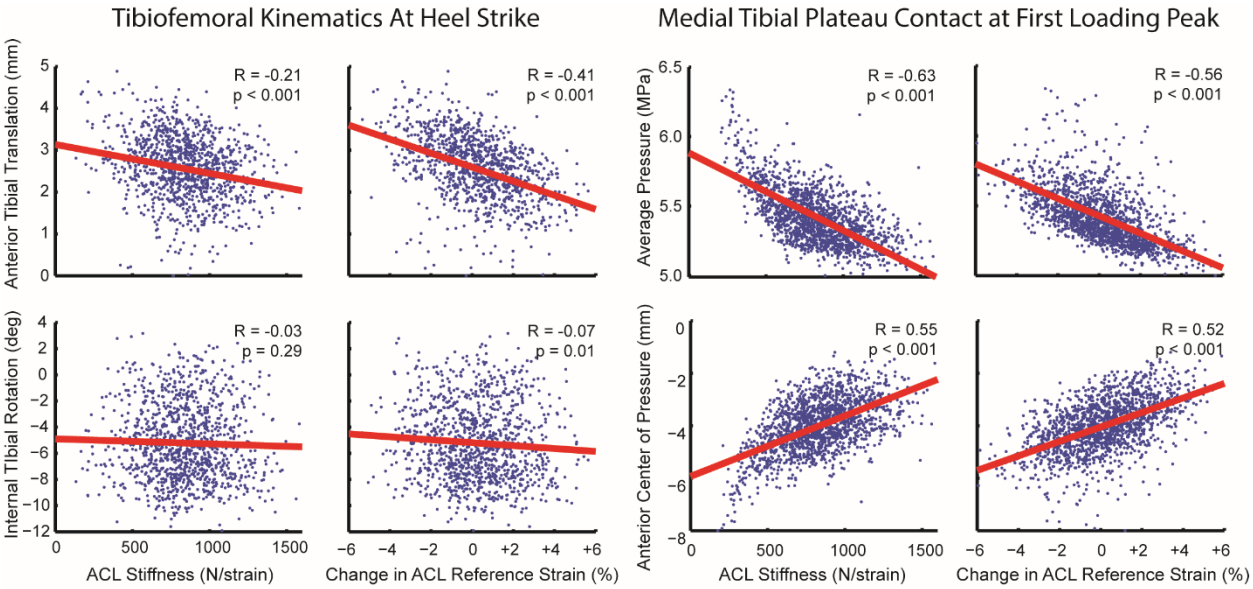

Figure 5 Sample scatter plots illustrating the sensitivity of tibiofemoral kinematics and tibial contact metrics to variations in ACL stiffness and reference strain. ACL properties exhibited significant influence on anterior tibial translation at heel strike. Medial tibial plateau contact pressures increased and migrated posteriorly in response to either a reduction in ACL stiffness or reference strain. ACL reference strain had a small, but significant, influence on tibial rotation at heel strike, with greater slack length (smaller reference strain) associated with internal tibial rotation.

Results

Variability in knee mechanics: Anterior tibial translation and internal tibial rotation exhibited marked variability when uncertainties in ligament parameters were considered. Tibial translation variability was posture dependent with a 95% confidence interval of ±1.5 mm at heel strike and ±3 mm at mid-stance (Fig. 4). The 95% confidence interval for tibial rotation was ±5 deg at heel strike and decreased slightly at mid-stance. The average tibial plateau contact pressure 95% confidence interval ranged from 5-6 MPa at the first peak of loading. The center of medial contact pressure exhibited a 95% confidence interval of ±2 mm in the anterior-posterior direction.

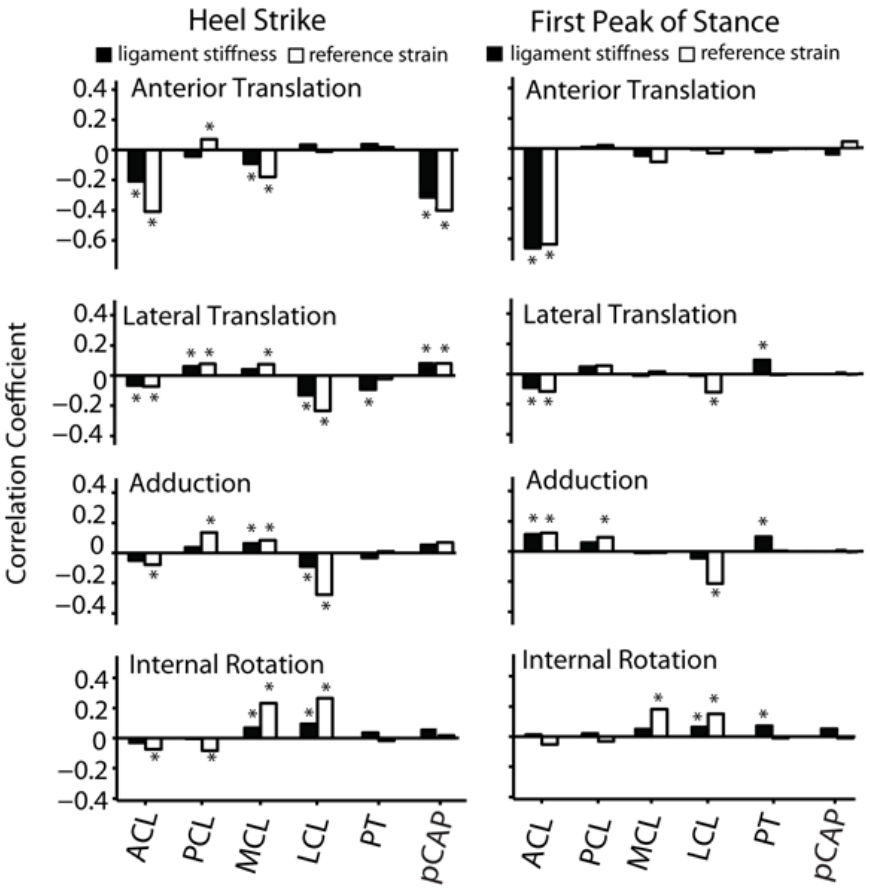

Figure 6 Correlations between tibiofemoral kinematics and ligament stiffness (solid bars) and reference strains (open bars) at heel strike and first tibiofemoral loading peak of stance. Notation: ACL – anterior cruciate ligament, PCL – anterolateral bundle of posterior cruciate ligament, MCL – medial collateral ligament, LCL – lateral collateral ligament, PT – patellar tendon, pCAP – posterior capsule. Significance denoted by * ($p<0.05$).

Kinematic Correlations (Fig. 6): At heel strike, the ACL, MCL, and posterior capsule exhibited the greatest influence on anterior tibial translation. However, by the time of first peak loading, anterior tibial translation was only significantly influenced by the ACL. Internal rotation at heel strike was primarily guided by the MCL and LCL, with the reference strains of these ligaments being more influential than the stiffness. ACL reference strains had secondary influence, being negatively correlated with internal rotation. At the time of first peak loading, tibial rotation remained significantly influenced by the MCL and LCL. The LCL, ACL and patellar tendon all exerted significant influence on lateral translation and adduction in mid-stance, with increased patellar tendon stiffness acting to

adduct the knee. Both adduction and lateral tibial translation were most influenced by the LCL, with the ACL, PCL, MCL and PT also exhibiting significant influence.

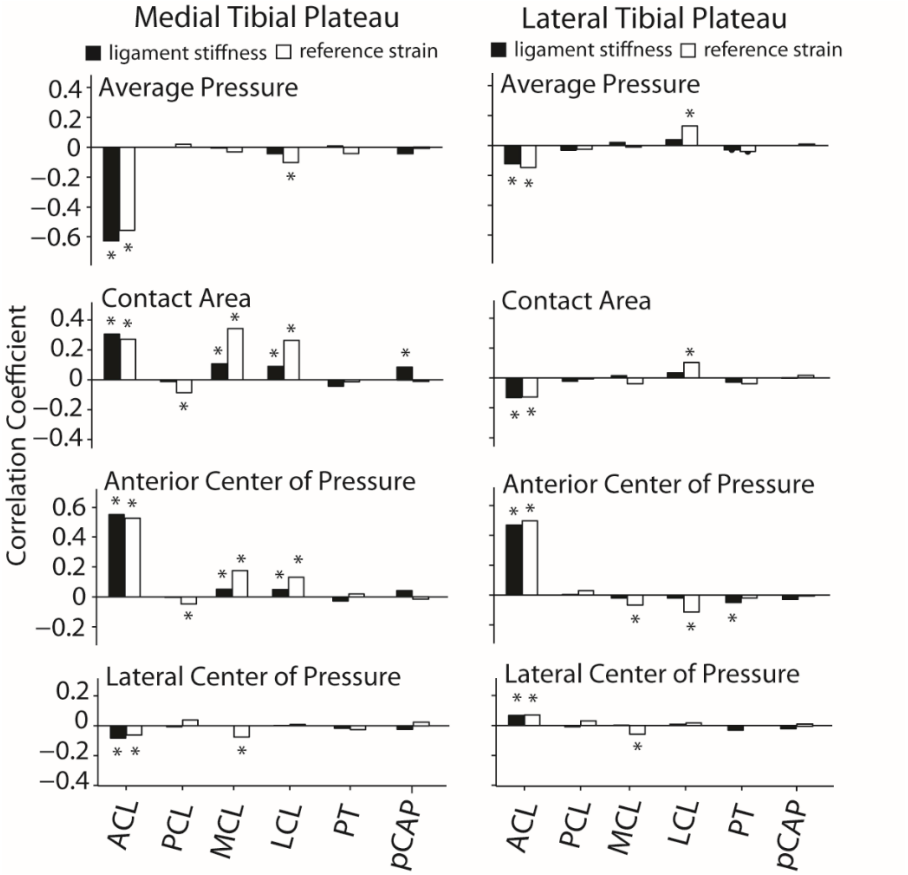

Figure 7 Correlations between tibial plateau contact metrics and ligament stiffness (solid bars) and reference strains (open bars) at first loading peak of stance. Abbreviations given in Fig. 6. Significance denoted by *p<0.05.

Tibial Contact Correlations (Fig. 7): At mid-stance, an increase in ACL stiffness or reference strain was highly correlated with a decrease in contact pressure, with the effect being greater on the medial tibial plateau. Medial contact area was positively correlated with increased ACL, MCL, and LCL stiffness and reference strains. However, an increase in ACL stiffness or reference strain reduced contact area on the lateral side. The anterior-posterior location of center of pressure was highly correlated with ACL stiffness and reference strain on both the medial and lateral sides. MCL and LCL also exhibited influence on the anterior-posterior center of pressure location, with the reference strains again being more influential than the stiffness. The lateral center of pressure location was negatively

correlated with ACL properties on the medial side, but positively correlated on the lateral side. The MCL reference strain also exerted a minor influence on medial-lateral center of pressure location.

Discussion

The objective of this study was to examine the sensitivity of tibiofemoral kinematics and contact metrics to variations in ligament constitutive properties. Previously, the influence of individual ligaments has been evaluated under isolated loading conditions using cadaveric experimentation[27-30] and computational models[6,7,31,32]. We extended these prior studies by considering ligament influence during a functional task, walking, that involves time varying posture, muscle forces, and external loading. We found that ACL properties had the primary influence on average tibial cartilage contact pressure in mid-stance. The medial and lateral collateral ligament properties modulated tibial rotation at heel strike and exhibited secondary influence on cartilage contact location in mid-stance. Given the inherent uncertainty that exists in ligament properties, these sensitivities are important to consider when using computational models to investigate the surgical treatment of knee injuries and disease.

Anterior tibial translation and rotation were the most sensitive degrees of freedom to variations in ligament constitutive properties (Fig. 4). Cadaveric studies have previously demonstrated the importance of the ACL in restraining anterior translation[6,7,27]. Similarly, we found both the ACL stiffness and reference strain to have the greatest effect on anterior translation from heel strike through mid-stance. The influence of other ligaments on anterior translation were posture dependent, with the posterior capsule and MCL acting as secondary constraints to anterior translation at heel strike. Variations in MCL and LCL constitutive properties were more highly correlated with tibial rotation than the ACL. This finding is in agreement with experimental studies which have examined the

combined effect of the ACL, MCL, and LCL[29-31]. For example, Markolf et al. found that while the ACL does provide rotational stability in an extended knee, its contribution was less than the MCL. Additionally, the contribution of the ACL decreased greatly in flexed postures[30], which is consistent with our sensitivity results suggesting the ACL influence on rotation diminishes as the knee is flexed in mid-stance.

Cartilage pressure, contact area, and contact location were most sensitive to the stiffness and reference strain of the ACL. An increase in ACL stiffness non-intuitively induced a reduction in cartilage contact pressure in mid-stance, particularly on the medial tibial plateau (Fig. 8). This result likely arises from the high degree of conformity between the curvatures of the medial femoral and tibial cartilage geometry, which makes contact pressure sensitive to small kinematic variations[33]. Specifically, a stiffer ACL provides a restraint to anterior tibial translation when the quadriceps are loaded in mid-stance, thereby maintaining contact in an area of high geometric conformity. In contrast, a compliant or longer ACL allows anterior tibial translation, such that contact pressure on the concave posterior aspect of the tibial plateau serves as a secondary restraint to anterior tibial translation. As a result, simulating gait with a reduced ACL stiffness or smaller reference strain induced an increase in contact pressure, particularly on the posterior aspect of the medial tibial plateau (Fig. 8).

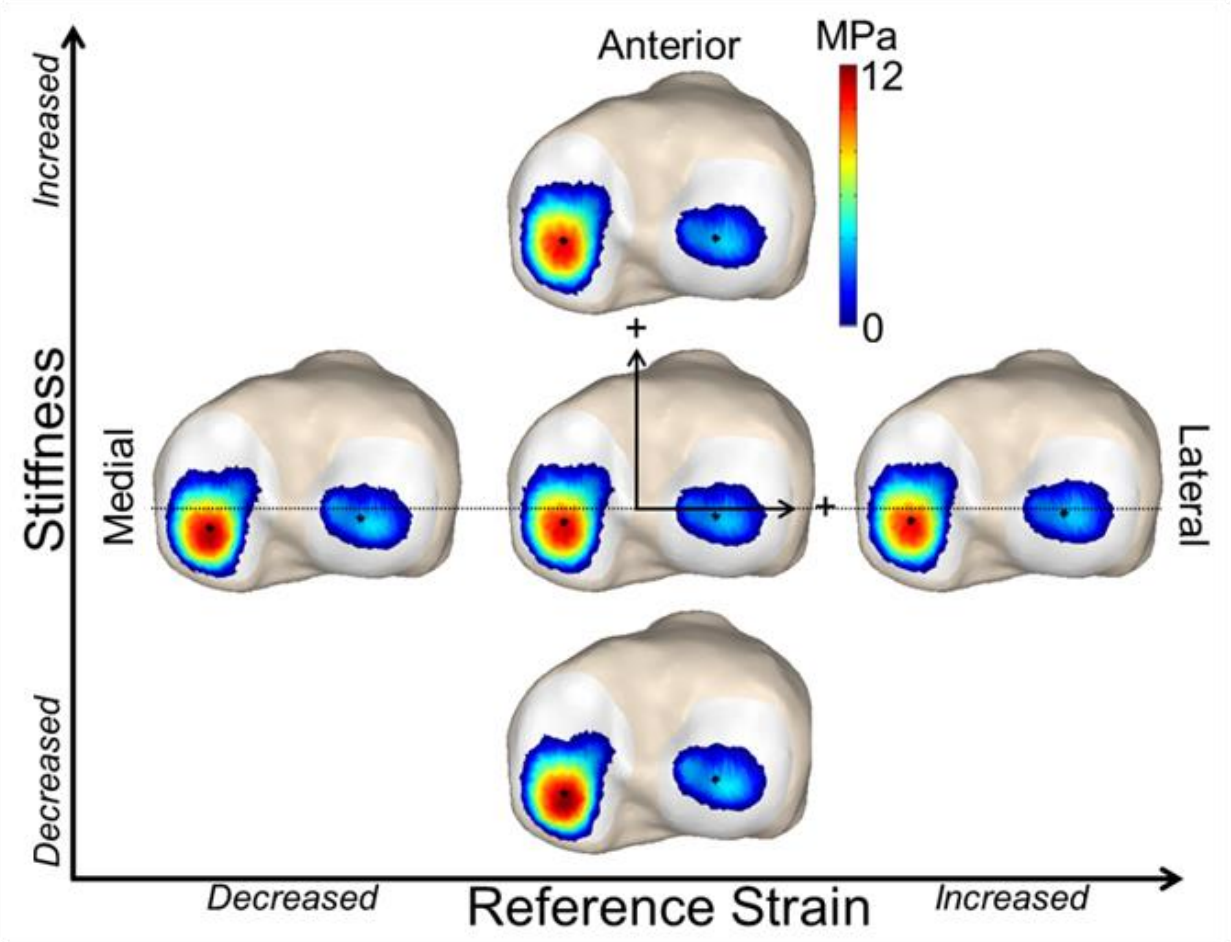

Figure 8 . Illustration of the influence of ACL stiffness and reference strain on tibial plateau contact pressures. Tibial contact pressure patterns resulting from gait simulations with · 45% change in stiffness, or a · 0.03 shift in reference stiffness are shown. Note that a decrease in either ACL stiffness or reference strain results in both an increase in peak contact pressure and a posterior migration of the contact on the medial tibial plateau.

The sensitivity to the properties of the ACL is of particular interest due to the prevalence of ACL injuries and associated long-term risk for osteoarthritis following ACL reconstruction[34,35]. Surgical factors such as graft type, pretension, and fixation method can affect ligament stiffness and reference strains. Thus, a graft stiffness that is reduced compared to the native ACL could induce anterior tibial translation and elevated contact pressure during walking. It has been speculated that such altered cartilage loading mechanics could contribute to the initiation and progression of osteoarthritis[36].

A few limitations of the model and sensitivity analysis must be noted in order to properly interpret the results. The articular surface and ligament geometries were based on a single, healthy female subject. A more thorough exploration of multiple knee geometries is warranted to determine if the ligament sensitivities are geometry dependent. While we were not able to validate our simulations of knee mechanics in gait, we previously showed the nominal knee model predicted passive and active tibiofemoral and patellofemoral kinematics that were consistent with subject-specific dynamic MRI measures[12]. However, the nominal knee model relies on ligament properties derived from population based studies[37], which makes it critical to consider the propagation of this uncertainty when used in subject-specific models[38]. The sparsity and large range of experimental measures of ligament properties prevents a thorough analysis of their distribution within the population. An assumption of independent Gaussian distributions was therefore used, with previously assumed variances in ligament stiffness and reference strain[39]. Finally, our sensitivity metrics are first order correlation coefficients, which inherently do not account for nonlinearities or characterize interactions between ligaments. More advanced sensitivity analysis techniques exist[37], and are becoming suitable for use as knee modeling and computational approaches needed to facilitate large scale explorations improve.

We conclude that probabilistic analysis of a multibody knee model is a powerful approach for exploring knee kinematic and cartilage contact sensitivities to knee ligament constitutive properties during functional movement. Our results highlight the strong influence that ligament stiffness and reference length have on cartilage contact loading patterns during walking. The method and findings are important to consider when using models to explore surgical treatments used to treat knee injury and disease.

References

1. Li, G., J. Suggs, and T. Gill, *The effect of anterior cruciate ligament injury on knee joint function under a simulated muscle load: a three-dimensional computational simulation.* Annals of biomedical engineering, 2002. **30**(5): p. 713-20.

2. Barry, M.J., T.H. Kwon, and Y.Y. Dhaher, *Probabilistic musculoskeletal modeling of the knee: A preliminary examination of an ACL-reconstruction.* Conference proceedings : ... Annual International Conference of the IEEE Engineering in Medicine and Biology Society. IEEE Engineering in Medicine and Biology Society. Conference, 2010. **2010**: p. 5440-3.

3. Gerus, P., et al., *Subject-specific knee joint geometry improves predictions of medial tibiofemoral contact forces.* Journal of biomechanics, 2013. **46**(16): p. 2778-2786.

4. Valente, G., et al., *Muscle discretization affects the loading transferred to bones in lower-limb musculoskeletal models.* Proceedings of the Institution of Mechanical Engineers, Part H: Journal of Engineering in Medicine, 2011: p. 0954411911425863.

5. Dhaher, Y.Y., T.H. Kwon, and M. Barry, *The effect of connective tissue material uncertainties on knee joint mechanics under isolated loading conditions.* Journal of biomechanics, 2010. **43**(16): p. 3118-25.

6. Li, G., J. Suggs, and T. Gill, *The effect of anterior cruciate ligament injury on knee joint function under a simulated muscle load: a three-dimensional computational simulation.* Annals of Biomedical Engineering, 2002. **30**(5): p. 713-720.

7. Suggs, J., C. Wang, and G. Li, *The effect of graft stiffness on knee joint biomechanics after ACL reconstruction—a 3D computational simulation.* Clinical biomechanics, 2003. **18**(1): p. 35-43.

8. Delp, S.L., et al., *OpenSim: open-source software to create and analyze dynamic simulations of movement.* IEEE Trans Biomed Eng, 2007. **54**(11): p. 1940-50.

9. Arnold, E.M., et al., *A model of the lower limb for analysis of human movement.* Annals of biomedical engineering, 2010. **38**(2): p. 269-79.

10. Guess, T.M., et al., *A multibody knee model with discrete cartilage prediction of tibio-femoral contact mechanics.* Computer methods in biomechanics and biomedical engineering, 2013. **16**(3): p. 256-70.

11. Lin, Y.C., et al., *Simultaneous prediction of muscle and contact forces in the knee during gait.* Journal of biomechanics, 2010. **43**(5): p. 945-52.

12. Lenhart, R.L., et al., *Prediction and validation of load-dependent behavior of the tibiofemoral and patellofemoral joints during movement.* Annals of biomedical engineering, 2015: p. conditionally accepted.

13. Guess, T.M., et al., *A subject specific multibody model of the knee with menisci.* Medical engineering & physics, 2010. **32**(5): p. 505-15.

14. Erdemir, A., *Open Knee: A Pathway to Community Driven Modeling and Simulation in Joint Biomechanics.* Journal of medical devices, 2013. **7**(4): p. 0409101-409101.

15. Weimer, K., et al. *Development and validation of a subject-specific computational human knee model in a dynamic knee simulator.* in *Summer Bioengineering Conference, Keystone, CO*. 2007.

16. Baldwin, M.A., et al., *Efficient probabilistic representation of tibiofemoral soft tissue constraint.* Computer methods in biomechanics and biomedical engineering, 2009. **12**(6): p. 651-9.

17. Thelen, D.G., K.W. Choi, and A.M. Schmitz, *Co-Simulation of Neuromuscular Dynamics and Knee Mechanics During Human Walking.* Journal of biomechanical engineering, 2014. **136**(2): p. 021033.

18. Bei, Y. and B.J. Fregly, *Multibody dynamic simulation of knee contact mechanics.* Medical engineering & physics, 2004. **26**(9): p. 777-789.

19. Askew, M. and V. Mow, *The biomechanical function of the collagen fibril ultrastructure of articular cartilage.* Journal of biomechanical engineering, 1978. **100**(3): p. 105-115.

20. Blankevoort, L., et al., *Articular contact in a three-dimensional model of the knee.* Journal of Biomechanics, 1991. **24**(11): p. 1019-1031.

21. Shelburne, K.B., M.R. Torry, and M.G. Pandy, *Contributions of muscles, ligaments, and the ground-reaction force to tibiofemoral joint loading during normal gait.* Journal of Orthopaedic Research, 2006. **24**(10): p. 1983-1990.

22. Shin, C.S., A.M. Chaudhari, and T.P. Andriacchi, *The influence of deceleration forces on ACL strain during single-leg landing: a simulation study.* Journal of Biomechanics, 2007. **40**(5): p. 1145-1152.

23. Delp, S.L. and J.P. Loan, *A computational framework for simulating and analyzing human and animal movement.* Comput. Sci. Eng., 2000. **2**(5): p. 46-55.

24. Lu, T.W. and J.J. O'connor, *Bone position estimation from skin marker co-ordinates using global optimisation with joint constraints.* J. Biomech, 1999. **32**(2): p. 129-134.

25. Arnold, E.M., et al., *A model of the lower limb for analysis of human movement.* Ann. Biomed. Eng, 2010. **38**(2): p. 269-279.

26. Lenhart, R.L., et al., *Influence of step rate and quadriceps load distribution on patellofemoral cartilage contact pressures during running.* Journal of Biomechanics, 2015. **in review**.

27. Melby, A., et al., *The effects of graft tensioning on the laxity and kinematics of the anterior cruciate ligament reconstructed knee.* Arthroscopy: The Journal of Arthroscopic & Related Surgery, 1991. **7**(3): p. 257-266.

28. Fukubayashi, T., et al., *An in vitro biomechanical evaluation of anterior-posterior motion of the knee. Tibial displacement, rotation, and torque.* The Journal of Bone & Joint Surgery, 1982. **64**(2): p. 258-264.

29. Shoemaker, S.C. and K.L. Markolf, *Effects of joint load on the stiffness and laxity of ligament-deficient knees. An in vitro study of the anterior cruciate and medial collateral ligaments.* The Journal of Bone & Joint Surgery, 1985. **67**(1): p. 136-146.

30. Markolf, K.L., J. Mensch, and H. Amstutz, *Stiffness and laxity of the knee--the contributions of the supporting structures. A quantitative in vitro study.* The Journal of Bone & Joint Surgery, 1976. **58**(5): p. 583-594.

31. Li, G., et al., *A validated three-dimensional computational model of a human knee joint.* Journal of biomechanical engineering, 1999. **121**(6): p. 657-662.

32. Dhaher, Y.Y., T.-H. Kwon, and M. Barry, *The effect of connective tissue material uncertainties on knee joint mechanics under isolated loading conditions.* Journal of biomechanics, 2010. **43**(16): p. 3118-3125.

33. Andriacchi, T.P., et al., *Rotational changes at the knee after ACL injury cause cartilage thinning.* Clinical orthopaedics and related research, 2006. **442**: p. 39-44.

34. Struewer, J., et al., *Knee function and prevalence of osteoarthritis after isolated anterior cruciate ligament reconstruction using bone-patellar tendon-bone graft: long-term follow-up.* International orthopaedics, 2012. **36**(1): p. 171-177.

35. Streich, N.A., et al., *Long-term outcome of anterior cruciate ligament reconstruction with an autologous four-strand semitendinosus tendon autograft.* International orthopaedics, 2013. **37**(2): p. 279-284.

36. Andriacchi, T.P., et al., *A framework for the in vivo pathomechanics of osteoarthritis at the knee.* Ann Biomed Eng, 2004. **32**(3): p. 447-57.

37. Laz, P.J. and M. Browne, *A review of probabilistic analysis in orthopaedic biomechanics.* Proceedings of the Institution of Mechanical Engineers. Part H, Journal of engineering in medicine, 2010. **224**(8): p. 927-43.

38. Anderson, A.E., B.J. Ellis, and J.A. Weiss, *Verification, validation and sensitivity studies in computational biomechanics.* Computer methods in biomechanics and biomedical engineering, 2007. **10**(3): p. 171-84.

39. Baldwin, M.A., et al., *Efficient probabilistic representation of tibiofemoral soft tissue constraint.* Computer methods in biomechanics and biomedical engineering, 2009. **12**(6): p. 651-659.

Chapter 5

Can Altered Neuromuscular Coordination Restore Soft Tissue Loading Patterns in ACL and Meniscal Deficient Knees during Walking?

Colin R. Smith, Scott C.E. Brandon, Darryl Thelen
(In preparation for the Journal of Biomechanics for the American Society of Biomechanics Young Scientist Pre-doctoral Award)

Introduction

A subset of patients with anterior cruciate ligament (ACL) and meniscal injuries can achieve knee stability during functional movement through altered neuromuscular coordination, enabling them to forgo surgery[1]. However, it is uncertain whether these patients can also restore knee loading to pre-injury patterns, which has important consequences for the long-term health of the joint. Injuries to the ACL, and particularly the menisci, increase the incidence of early onset osteoarthritis (OA)[2]. Damage to these structures may alter loading patterns and disrupt cartilage tissue homeostasis, which leads to degeneration[3]. Accordingly, modern ACL reconstruction surgical techniques are evaluated by their ability to restore healthy knee kinematic patterns during functional movements[4,5]. Meanwhile, conservative treatment for ACL and meniscal injury is largely focused on restoring knee function, and it remains uncertain whether the mechanical constraints allow an altered neuromuscular coordination to achieve pre-injury cartilage and ligament loading patterns[6].

A neuromuscular coordination strategy that restores cartilage loading in an ACL deficient knee must provide muscular restraint to accommodate the increased knee laxity. *In vivo* and *in vitro* experiments indicate an increase in passive anterior and internal-external rotation laxity in ACL deficient knees[7]. Under simple loading conditions, it appears some individuals can compensate for this

passive laxity through active muscle control. During open-chain knee flexion-extension measured by dynamic MRI, the majority of ACL deficient patients showed altered kinematics, however, select patients exhibited healthy tibiofemoral kinematic patterns[8]. It is not known whether this ability extends to functional movements. During walking, lunging, and stair climbing, increased tibial anterior translation, medial translation and internal rotation have been observed in ACL deficient patients[9–12]. However, it was not reported if any individual subjects were able to achieve healthy knee kinematics, and thus it remains unknown whether conservative treatment for ACL injury has potential to restore healthy cartilage loading patterns and preserve the long-term health of the knee.

The meniscus distributes loading across the cartilage surface and provides secondary restraint to the tibiofemoral joint[13]. Damage to the meniscus changes the articular geometry, resulting in altered cartilage loading and high rates of OA[2]. Meniscal injury is initially treated conservatively because of the difficulty of meniscal repair and poor outcomes following meniscectomy[14]. An altered neuromuscular coordination strategy cannot restore loading patterns following meniscal damage because of the altered articular contact geometry. However, active muscle forces could potentially supplement the diminished joint restraint of a damaged meniscus to prevent overloading of other structures such as the ACL. Meniscectomy increases the strain in the ACL[15], predisposes the native ACL to injury[16] and increases the potential for failure of ACL grafts[17]. Thus, a possible goal for conservative treatment of meniscal damage would focus neuromuscular training to develop a coordination strategy that prevents overloading the ACL. Currently, it is unknown whether this goal is mechanically achievable.

Musculoskeletal simulation enables systematic investigation of the dynamic coupling between neuromuscular coordination and joint mechanics in healthy and injured knees. In open-chain knee extension tasks, simplified sagittal plane knee models predicted that hamstrings co-contraction reduces

ACL loading[18] and can restore anterior translation patterns in an ACL deficient knee[19]. Simulation studies on the ability of muscle forces to restore anterior translation during walking are less conclusive. A sagittal plane analysis of an ACL deficient knee at heel strike found that a 56% hamstring activation could restore tibial anterior translation to healthy magnitudes[20]. By applying muscle forces calculated in a forward dynamic simulation of walking to a multibody knee model, Shelburne et al predicted ACL deficiency increased anterior translation throughout stance and early swing[21]. They also found increased hamstrings activation and decreased quadriceps activation could restore tibial anterior translation in the ACL deficient knee[22]. An EMG driven model also predicted increased anterior translation in the ACL deficient knee during walking, but found that while co-activation of the knee flexors reduced anterior translation, it could not fully restore it to healthy patterns. These studies provide the current mechanistic basis for understanding of the role of muscles in compensating for ACL deficiency, but are limited by modeling simplifications including two dimensional analyses, dynamic decoupling of limb movements and joint mechanics, neglect of the meniscus, and the inability to explicitly study cartilage loading patterns.

This study leverages a novel musculoskeletal simulation framework to identify the differences in soft tissue loading patterns caused by ACL and menisci deficiency and investigates whether these differences could be mitigated through an altered neuromuscular coordination strategy. The first objective was to identify the differences in cartilage and ligament loading patterns during walking for healthy, ACL deficient, menisci deficient, and ACL-menisci deficient knees. The second objective was to investigate potential neuromuscular coordination strategies to restore cartilage loading in ACL deficient knees and ACL loading in meniscal deficient knees to healthy patterns.

Methods

A multibody knee model of a healthy female subject (Age = 23, Height = 1.65m, Mass = 61kg) was previously constructed and validated against dynamic magnetic resonance images (MRI)[23]. The original model, which included femur, tibia, and patella bodies, was extended in this study to include independent menisci bodies. Each of the joints in the knee model allowed six degrees-of-freedom (DOF) of relative motion. Articular contact (cartilage-cartilage (E=5 Mpa, v=0.45) and (cartilage-meniscus (E=3MPa, v=0.45)) was modeled using an elastic foundation formulation[24,25]. Ligament and capsular structures were represented by bundles of nonlinear springs[26]. In addition to the 14 structures previously included in the model, we added representations of the anterior and posterior meniscal horns, transverse ligament, and circumferential attachment of the menisci to the tibial plateau. The knee was integrated into a scaled generic lower extremity model that included 44 muscles spanning the hip, knee and ankle joints.

Skin mounted marker kinematics and ground reactions were measured for the subject during overground walking in a motion analysis laboratory. A global optimization inverse kinematics routine was used to calculate the trajectories of the *prescribed* (6-pelvis) and *primary* (3-hip, 1-tibiofemoral flexion, 1-ankle) DOFs. During this procedure, the *secondary* DOFs (5-tibiofemoral, 6-patellofemoral and 12-meniscal) were constrained to be functions of tibiofemoral flexion. These functions were determined from a forward simulation in which the muscles were minimally activated (a=0.02) and tibiofemoral flexion was prescribed from 0^o to 120^o while the *secondary* kinematics were unconstrained.

The Concurrent Optimization of Muscle Activations and Kinematics (COMAK) algorithm was then used to predict the muscle forces, *secondary* knee kinematics, ligament forces and articular contact pressures necessary to reproduce the measured accelerations of the *primary* kinematics during walking[27] (Figure 1). At each time step, the muscle activations and *secondary* kinematics were optimized to

generate the measured accelerations for the *primary* DOFs and equilibrium (zero accelerations) in the *secondary* DOFs while minimizing a cost function. The cost function was the volume-weighted sum of squared muscle activations and included muscle specific weighting terms (W_i). The muscle weights penalize the activation of a muscle if ($W_i > 1$) and encourage the activation if ($W_i < 1$). The nominal muscle weight for each muscle was set equal to one ($W_i = 1$), except for the medial gastrocnemius ($W_i = 4$), lateral gastrocnemius ($W_i = 7$), hamstrings ($W_i = 2$), rectus femoris ($W_i = 3$), soleus ($W_i = 0.9$), gluteus minimus ($W_i = 0.9$), and gluteus medius ($W_i = 0.9$). These weightings were selected to reduce the knee contact force to physiologic magnitudes[28,29].

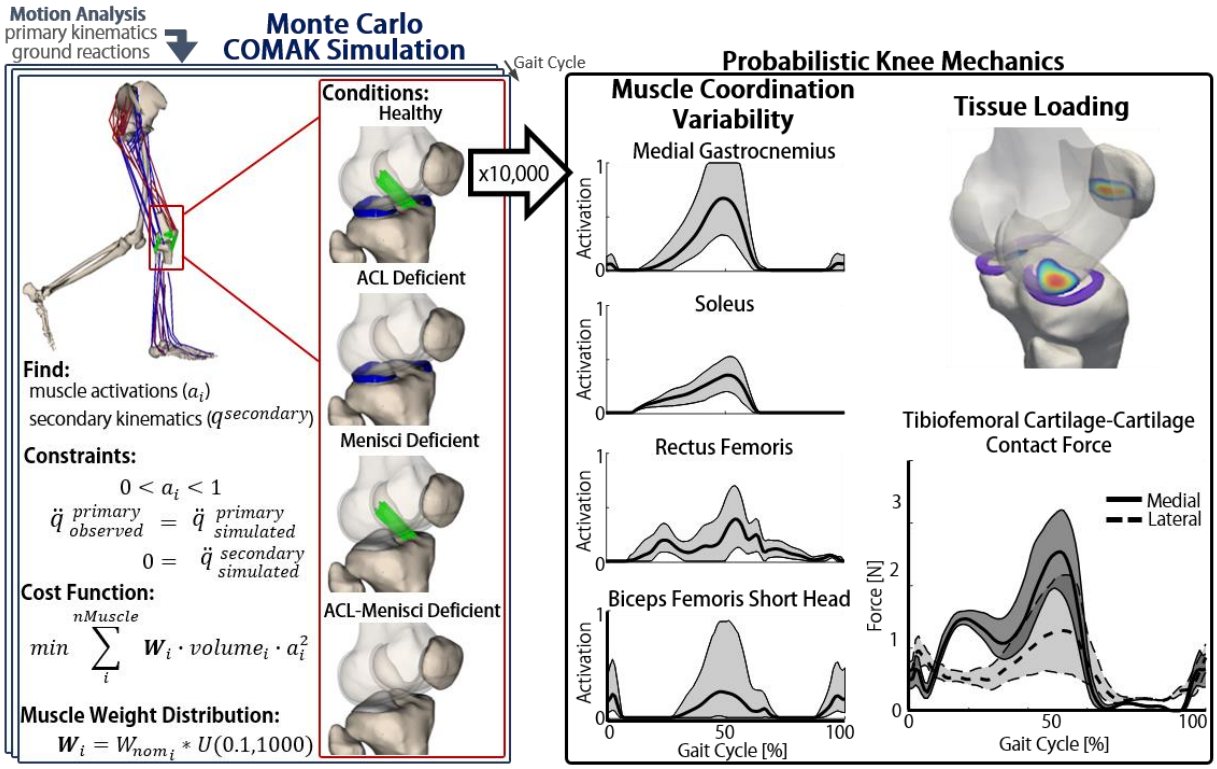

Figure 1 The COMAK simulation framework was used to predict the secondary knee kinematics, muscle forces, ligament forces, and articular contact pressures necessary to generate the measured motion. Simulations were performed using the same input gait measurements for four knee conditions: healthy, ACL deficient, menisci deficient and ACL-Menisci deficient. For the healthy, ACL deficient and menisci deficient conditions, a Monte Carlo analysis (10,000 simulations) was performed in which the weightings on each muscle in the COMAK cost function were varied to generate neuromuscular coordination patterns to explore the solution space of muscle redundancy.

The COMAK simulations were repeated using intact, ACL deficient, menisci deficient, and ACL-menisci deficient conditions in the knee model. For the intact, ACL deficient, and menisci deficient conditions, a Monte Carlo analysis was performed in which the muscle weights (W_i) were randomly sampled to generate simulations with varying muscle coordination strategies to explore the muscle redundancy solution space. Muscle weights were parameterized as uniform distributions spanning from 10-10000% of the nominal weight (W_i) value. The bounds on the distributions were determined as the largest range that still enabled all simulations to converge. A high throughput computing grid was used to perform 10,000 simulations for each condition. The mean values of the predicted kinematics and cartilage loading metrics were less than 1% different when calculated using 9,000 vs 10,000 simulations, ensuring an adequate number of simulations were performed.

For each condition, the predicted anterior translation, internal rotation, cartilage contact pressures and ACL loading were compared. The variability in joint mechanics induced by different neuromuscular coordination strategies was quantified by calculating the mean, and 5^{th} and 95^{th} percentiles of each metric. The sensitivity of each metric to the activation of each muscle was determined by calculating the Spearman correlation coefficient at the instances of the first and second peaks in the tibiofemoral loading.

Results

The predicted tibiofemoral contact forces of each condition demonstrated the characteristic double peak (1^{st} peak: 17%, 2^{nd} peak: 48% of the gait cycle), with a greater proportion of the loading directed through the medial compartment (Figure 1) during stance. In the nominal simulation for each condition, anterior tibial translation and ACL loading (when present) were greatest at nearly the same instance as 1^{st} Peak, which coincides with peak quadriceps activation. The predicted internal rotation increased throughout stance, with peak internal rotation occurring slightly before toe-off.

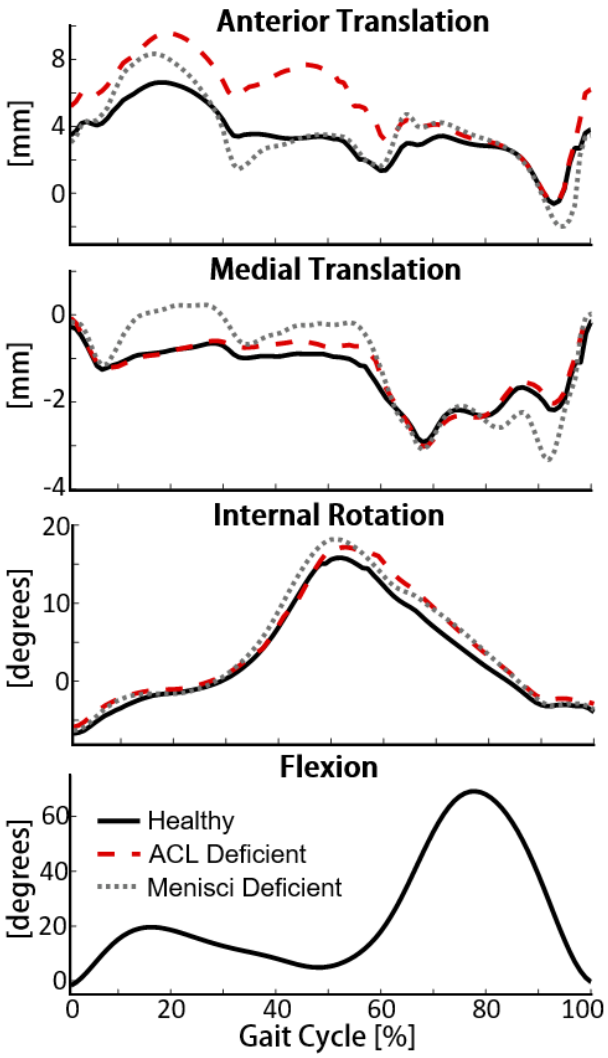

Figure 2 For each knee condition, the flexion angle was set to the measured value, while the secondary knee kinematics were predicted by the COMAK algorithm.

ACL Deficient

The introduction of ACL deficiency resulted in substantial alterations in the predicted knee mechanics compared to the healthy knee. The tibia shifted anteriorly in terminal swing. This anterior shift persisted throughout stance and early swing, before converging back to the healthy pattern at mid-swing (Figure 2). The greatest difference in anterior translation (3 mm) occurred in early stance when the quadriceps activation was greatest. The ACL deficient knee also exhibited increased internal rotation at push off, which persisted throughout the swing phase, and increased medial translation during the second half of stance.

These altered kinematics manifested as substantially different cartilage loading patterns compared to the healthy knee (Figure 3). At the 1st and 2nd peaks of tibiofemoral loading, the anterior location of the center of pressure (COP) on the medial tibial plateau was 1.7 mm and 2.3 mm posterior to the healthy COP, respectively. On the lateral side, the COP was 1.8 mm and 0.35 mm posterior to healthy at 1st and 2nd peaks. The mean cartilage-cartilage contact pressure was slightly lower on both plateaus at 1st and 2nd peaks in the ACL deficient knee compared to healthy because a greater portion of the contact was shifted on to the meniscus (Figure 6).

Menisci Deficient

The menisci deficient knee experienced considerably higher cartilage contact pressures and increased loading in the remaining passive knee structures. Meniscal deficiency resulted an anterior shift of the tibia in early stance, and a posterior shift in late stance (Figure 2), demonstrating the ability of the menisci to provide both anterior and posterior restraint to the knee. There was also an increase in the internal rotation and medial translation during stance. The medial tibial COP was shifted 1.5 mm posteriorly at 1st peak and 0.6 mm anteriorly at 2nd peak. The lateral COP was 0.5 mm anterior and 0.6 mm anterior at the 2nd peak. The loading in the ACL was 2.4x higher in the meniscus deficient knee compared to the healthy knee at peak quadriceps loading.

ACL-Mensici Deficient

The ACL and menisci deficient knee lacked passive restraint to anterior loads, resulting in substantially greater anterior translation at 1st peak when the quadriceps were active. At this instance, the contact shifted to the posterior edge of the tibial plateau resulting in excessive contact pressures. The knee was not stable enough for the stochastic variation of muscle coordination patterns to be performed for this condition.

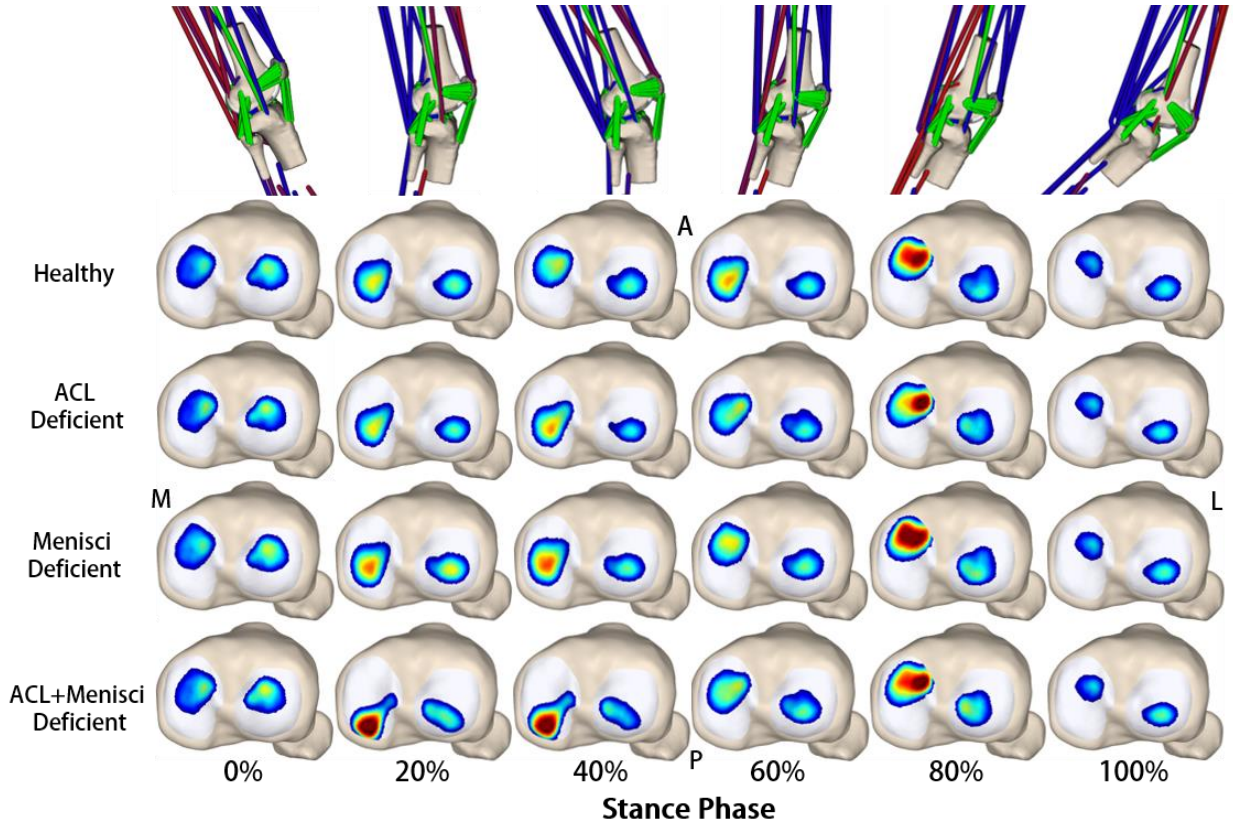

Figure 3 A comparison of tibial cartilage-cartilage contact pressure patterns for each condition over the stance phase of walking. Pressure maps at the 1st peak of tibiofemoral loading (17% gait cycle, 28% stance) are shown in Figure 8. The 2nd peak of tibiofemoral loading (48% gait cycle, 72% stance) demonstrates similar pressure patterns to the 80% column. The muscle activations and knee kinematics for the nominal simulation of the intact condition are visualized at the top of the figure.

Altered Neuromuscular Coordination

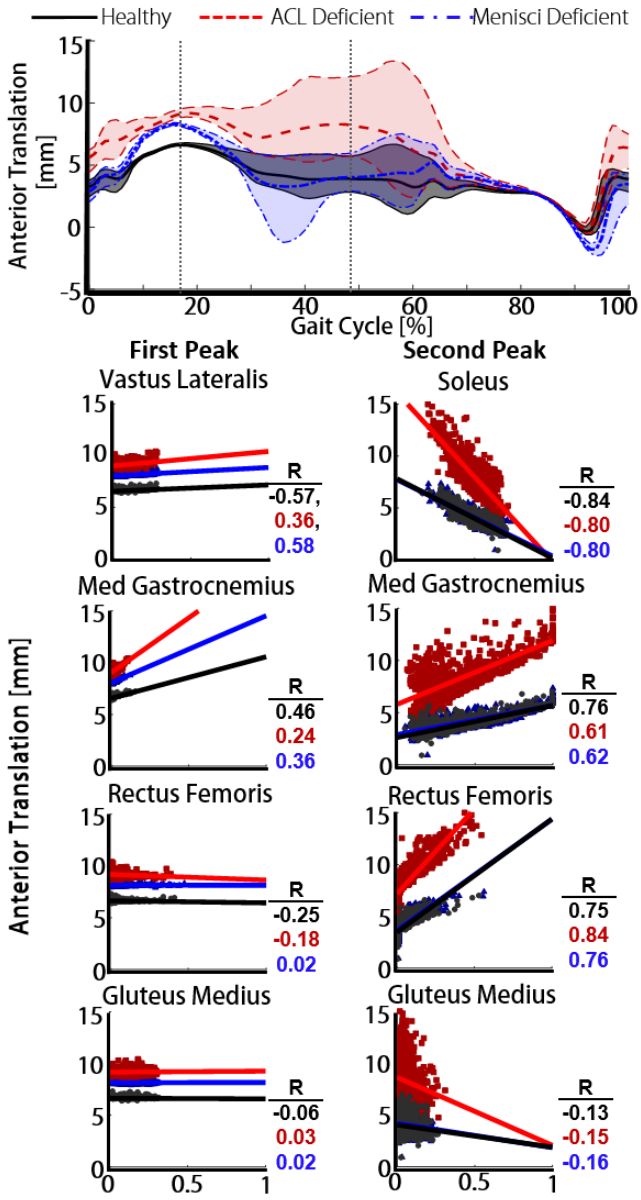

Figure 4 – [*Top Plot*] The results of each batch of 10,000 simulations is summarized by the mean (bold centerline) and 5th-95th percentiles (shaded region) of anterior tibial translation over the gait cycle is for each condition. The dotted vertical lines depict the instances of the 1st and 2nd peaks of tibiofemoral loading. *[Scatter Plots*] The scatter plots reveal the sensitivity of anterior translation to activation of each muscle at the 1st and 2nd peaks in tibiofemoral loading. The best fit line and Spearman correlation coefficient were calculated for the healthy (black), ACL deficient (red) and menisci deficient (blue) conditions.

The stochastic muscle weightings within the COMAK cost function introduced variability in the predicted muscle activations (Figure 1), knee kinematics (Figures 4 & 5), cartilage contact pressures (Figure 6) and ACL forces (Figure 7) during walking for the healthy, ACL deficient, and menisci deficient knees. At the first peak of tibiofemoral loading, there was minimal variability in the predicted knee mechanics for all three conditions. Contrarily, substantial variability was present from the second peak of tibiofemoral loading through toe off and early swing. Mean cartilage-cartilage contact pressure showed greater variability on the lateral side compared to the medial. This late stance variability was caused by a redistribution of the hip, knee, and ankle torques between uni-articular and biarticular muscles. For example, if the ankle plantarflexion torque was generated by the gastrocnemii rather than the soleus, increased

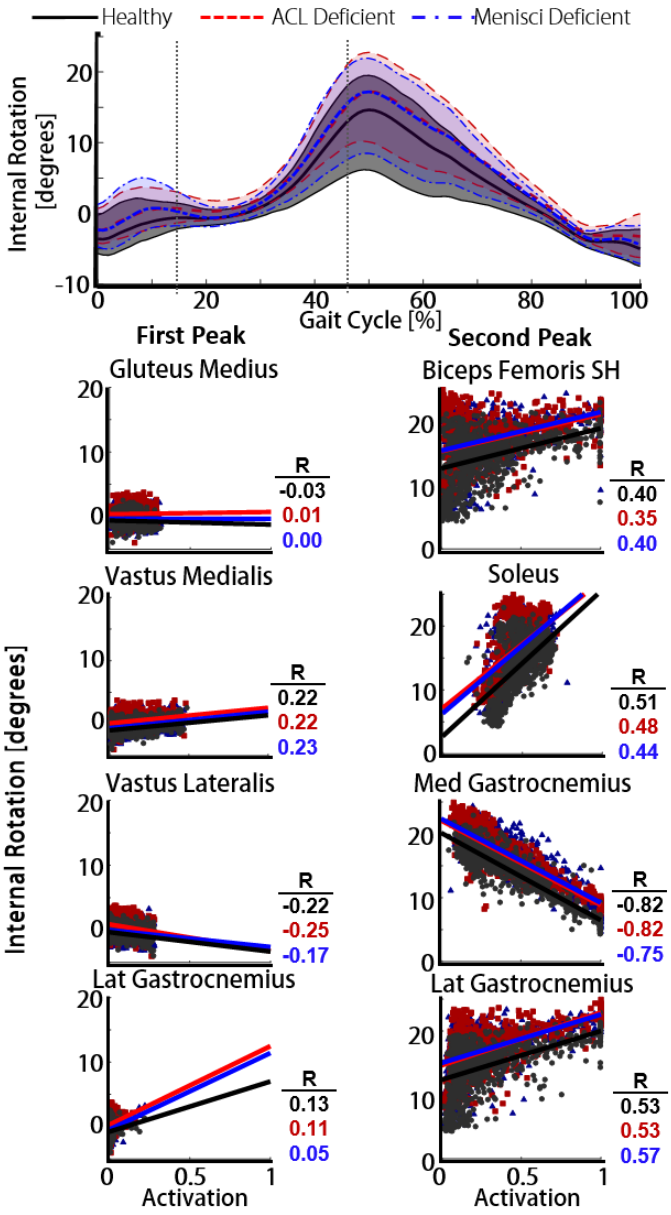

Figure 5 – [*Top Plot]* The mean (bold center line) and 5th-95th percentiles of the internal rotation for the variable neuromuscular coordination simulations are plotted over the gait cycle. The dotted vertical lines coincide with the 1st and 2nd peaks of tibiofemoral loading. [*Scatter plots*] The sensitivity of predicted internal rotation at the 1st and 2nd peaks to the activation of each muscle was quantified using Spearman's correlation coefficient for the healthy (black), ACL deficient (red), and menisci deficient (blue) conditions.

contact force and anterior translation occured at the knee. If the hip flexion torque was generated by the rectus femoris, an extension torque was applied to the knee which had to be overcome by the gastrocnemii, leading to increased knee contact force and anterior translation.

In the ACL deficient knee, the cartilage loading was not restored to healthy patterns by any of the 10,000 muscle coordination strategies tested. The missing restraint provided by the ACL resulted in increased anterior tibial translation for all coordination patterns, particularly during stance (Figure 4). In late stance, preferential activation of the soleus compared to the gastrocnemii reduced the anterior translation, but this effect did not fully restore healthy anterior translation patterns. However, the internal rotation could be restored to healthy patterns (Figure 5) by preferentially activating the lateral vastus compared to medial vastus during load acceptance, and the medial

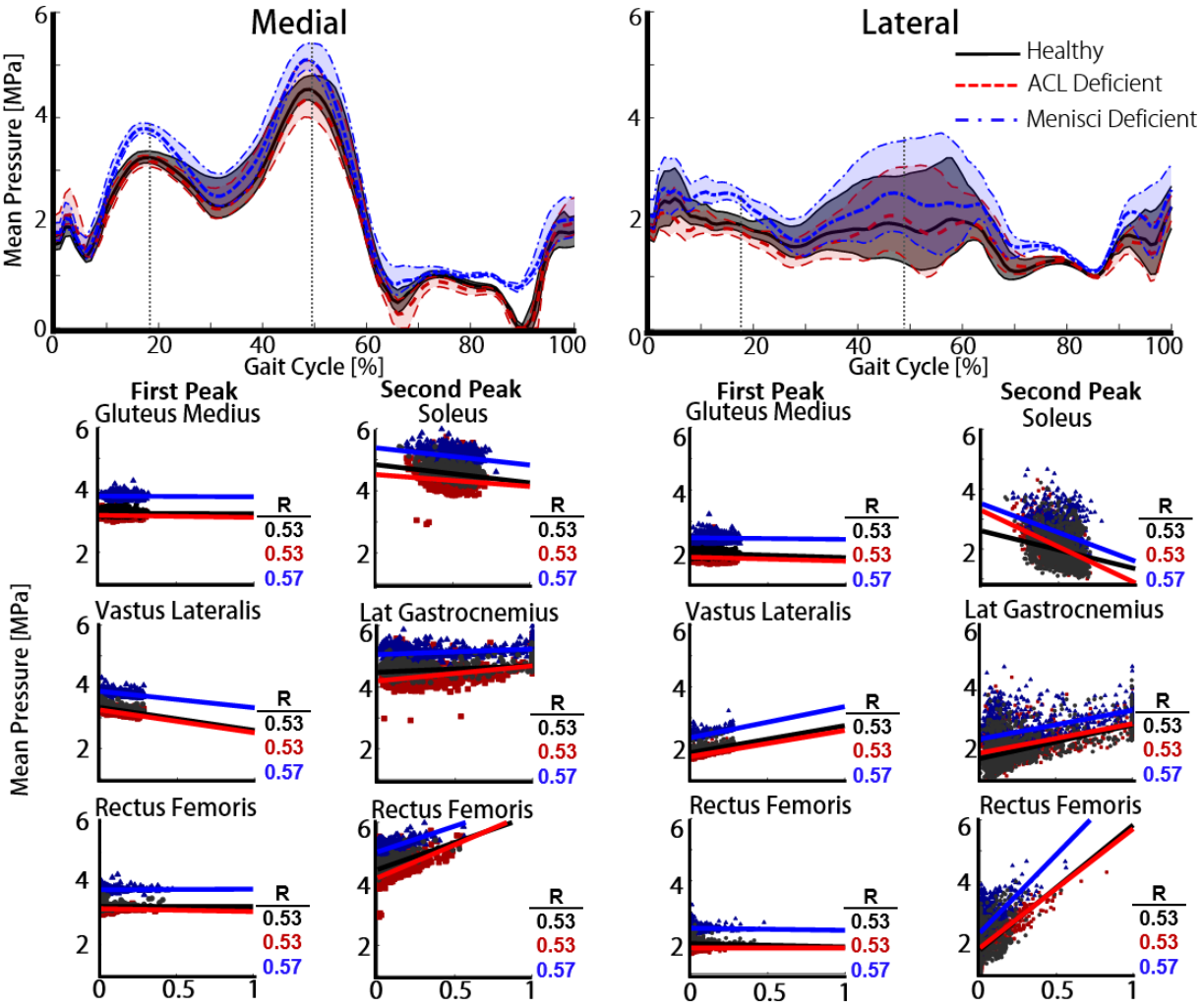

Figure 6 – [*Top Plot*] The mean (bold centerline) and 5th-95th percentiles (shaded) of the cartilage-cartilage contact pressures on the medial and lateral tibial plateaus are shown for variable neuromuscular coordination simulations for each condition. The vertical dotted lines indicate the 1st and 2nd peaks of tibiofemoral loading. [*Scatter plots*] The sensitivity of the mean cartilage-cartilage contact pressures was accessed at the 1st and 2nd peaks of tibiofemoral loading using the Spearman correlation coefficient (R).

gastrocnemius over the lateral gastrocnemius during push off. The mean cartilage-cartilage contact pressures were generally similar to the healthy knee (Figure 6). The mean pressures were reduced on the medial plateau in late stance and mid-swing and the lateral plateau during early stance when the contact was shifted onto the meniscus in the ACL deficient knee.

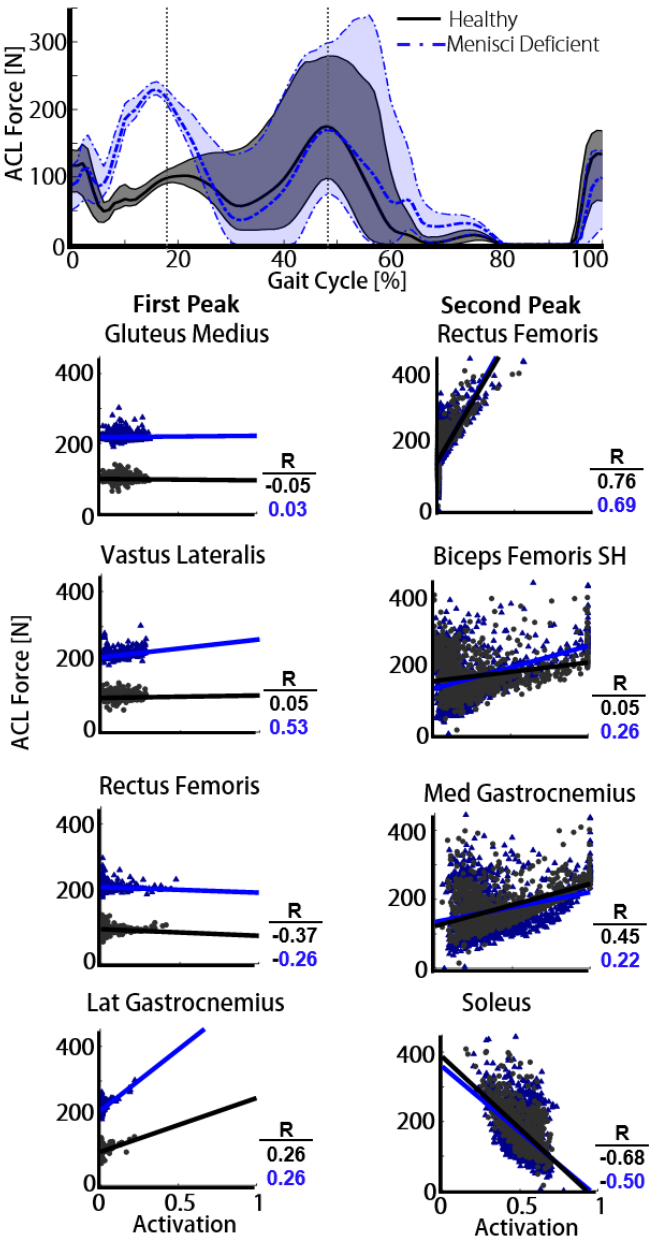

Figure 7- [*Top Plot*] The mean (bold centerline) and 5th to 95th percentiles (shaded) of ACL force for the variable neuromuscular coordination simulations of the intact (black) and menisci deficient (blue) knees. The vertical dotted lines indicate the instances of 1st and 2nd peaks of tibiofemoral loading. [Scatter Plots] The sensitivity of ACL force to muscle activations at 1st and 2nd peaks is assessed through the Spearman correlation coefficient (R).

In the meniscal deficient knee, the mean cartilage-cartilage contact pressures were generally higher than the healthy and ACL deficient knees regardless of the muscle coordination pattern (Figure 6). This was especially true at the first peak of tibiofemoral loading where there was no overlap between the 5-95th percentiles of the mean medial and lateral pressures for the healthy and menisci deficient conditions. In the first half of stance phase when the quadriceps were active, the altered neuromuscular coordination strategies could not restore ACL loading to healthy magnitudes in the menisci deficient knee.

Discussion

In this study, we used musculoskeletal simulation to investigate the differences in cartilage loading patterns during walking in healthy, ACL deficient, menisci deficient, and ACL-menisci deficient knees. We then tested whether altered neuromuscular coordination could restore healthy soft tissue loading patterns in the pathologic knees. In the ACL deficient

knee, we found a posterior shift in the medial contact and a minor increase in contact pressure. In the menisci deficient knee, we found a minor posterior shift in the medial contact and a substantial increase in contact pressure. In the ACL-menisci deficient knee, we found the cartilage contact shifted to the extreme posterior boundary of the tibial cartilage, resulting in excessive contact pressures and subluxation of the joint. Altered neuromuscular coordination was unable to restore the cartilage contact locations in the ACL deficient knee nor the contact pressure magnitudes nor ACL loading in the menisci deficient case.

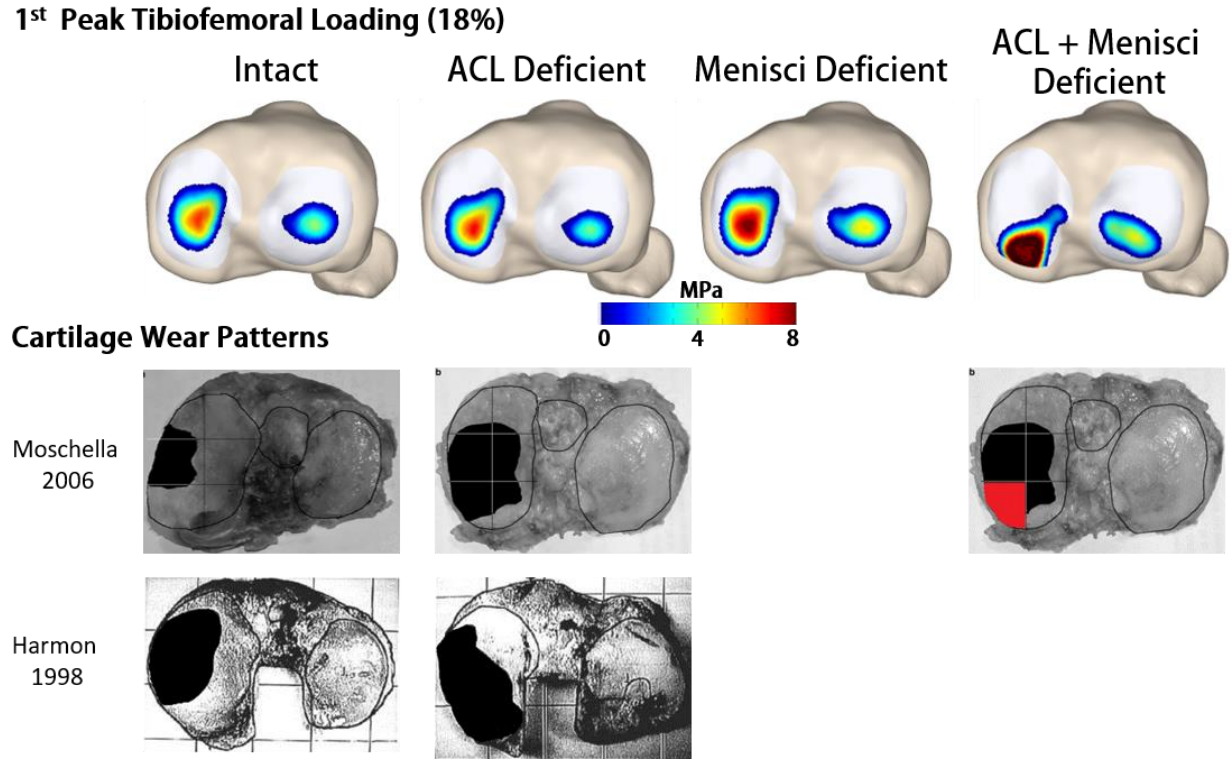

Figure 8 Predicted cartilage contact pressures at the instance of 1st peak tibiofemoral loading compared against wear patterns found on tibial resections from total knee replacement surgeries[30,31]. The black regions indicate representative wear patterns for each knee condition. The red coloring indicates a region where 20% of ACL deficient knees and 46% of ACL-menisci deficient knees showed severe cartilage wear.

The regions of altered cartilage contact pressure patterns in the injured conditions at the first peak of tibiofemoral loading (also peak ACL loading in the healthy knee, 18% of gait cycle) corresponded well with reported regions of cartilage wear (Figure 8). Two studies examining tibial

plateau resections from total knee replacements found a posterior shift and increased area in wear patterns on the medial plateau in ACL deficient knees compared to ACL intact knees. We found increased pressure and a posterior shift in the medial tibial COP in the ACL deficient knee compared to healthy at first peak. Harmon et al found menisci deficiency shifted medial plateau wear patterns medially towards the tibial spine[30]. Moschella reported that severe cartilage wear was found on the posterior lateral corner of the medial plateau in 20% of ACL deficient knees and 46% of ACL-menisci deficient knees[31]. We found the contact pressures increased substantially in this region with the removal of the meniscus in the ACL-deficient knee. These comparisons support the notion that shifts in cartilage loading patterns due to soft tissue injury are an important contributor to the initiation of osteoarthritis (OA).

We found muscle coordination had significant effect on the predicted knee mechanics in both the healthy and injured conditions, particularly during the second half of stance phase. However, the minimal overlap of the muscle redundancy solution space between the healthy and ACL deficient knee in anterior translation suggests that cartilage loading patterns could not be restored through altered neuromuscular coordination. The meniscal deficient knee showed increased contact pressures and ACL loads that could not be restored through neuromuscular coordination. The interactions between the rectus femoris, biceps femoris, gastrocnemii, and soleus activations in late stance played a particularly significant role in governing the predicted knee mechanics. At this point in the gait cycle, hip flexion, knee flexion and ankle plantar flexion moments must be generated by the muscles. The distribution of the hip flexion moment between the uniarticular muscles and the rectus femoris, and the distribution of the ankle flexion moment between the soleus and gastrocnemii had significant ramifications at the knee. Coordination strategies that favored the rectus femoris to generate the hip flexion torque and gastrocnemii to generate the knee flexion and ankle plantar flexion resulted in the largest anterior translations, cartilage contact pressures, and ACL loads (when present).

Muscle electromyograms have been extensively studied in ACL deficient patients with widely variable results. One common theme among these studies is the use of co-contraction to "stiffen" or "stabilize" the knee. Our simulations demonstrate that the quadriceps and gastrocnemii are antagonists and the hamstrings are agonists to the ACL. Thus, a quadriceps and hamstrings co-contraction will offset in anterior translation, whereas a quadriceps-gastrocnemii co-contraction will substantially increase the anterior translation. This prediction is consistent with *in vivo* measurements of ACL strain during transcutaneous electrical muscle stimulation of these muscle groups[32]. Over the range of neuromuscular coordination strategies we simulated, the variable co-contraction led to ranges in mean pressure of 0.44 MPa on the medial plateau, and 1.69 MPa at second peak. This reinforces the hypothesis that co-contraction leads to higher contact loads which may be detrimental to the long-term health of the joint.

Our simulations are likely most representative of a subset of ACL deficient patients characterized as "copers". Copers achieve knee stability during functional movement through adapted neuromuscular coordination[1]. Similar to our simulations where the primary kinematics and ground reactions are unchanged between each knee condition, copers do not have significantly different marker-measured kinematics nor ground reactions from the healthy population[33]. Copers are characterized as having superior neuromuscular control, which allows them to finely adjust their activation patterns to achieve stability. In the highest achieving copers, minimal changes in muscle activation patterns from healthy controls are found[33]. Our simulations suggest that the mechanical difference between the healthy and ACL deficient knee would require either a significant change in the joint moments or muscle activations to restore anterior translation in the ACL deficient knee.

Our application of the COMAK simulation framework to study muscle coordination in ACL injury has several limitations. The experimental gait data and knee model are from a single healthy

subject, and both knee geometry[6] and limb dynamics are known to influence the joint mechanics in ACL deficient knees. Furthermore, we performed our analyses using a single set of ligament stiffness and slack lengths, however, there is substantial uncertainty in these parameters[34], they vary widely among the population[35], and they have a significant effect on predicted knee joint mechanics[36]. Additionally, the stochastic muscle weightings in the COMAK objective function may not have induced enough variability to explore the entire muscle redundancy solution space.

With current techniques, surgical reconstruction and conservative treatment of ACL injury have similar rates of OA[2]. Our model predicts that conservative treatment will not be able to restore cartilage loading in an ACL deficient knee. Thus, with continued improvements towards replicating the function of the native ACL, reconstruction will likely prove superior in restoring tissue loading. However, for many patients, conservative treatment will remain a viable treatment option. The fact that not all ACL deficient patients exhibit signs of osteoarthritis suggests that cartilage loading is not the sole factor in initiating pathogenesis.

Supplemental Figures

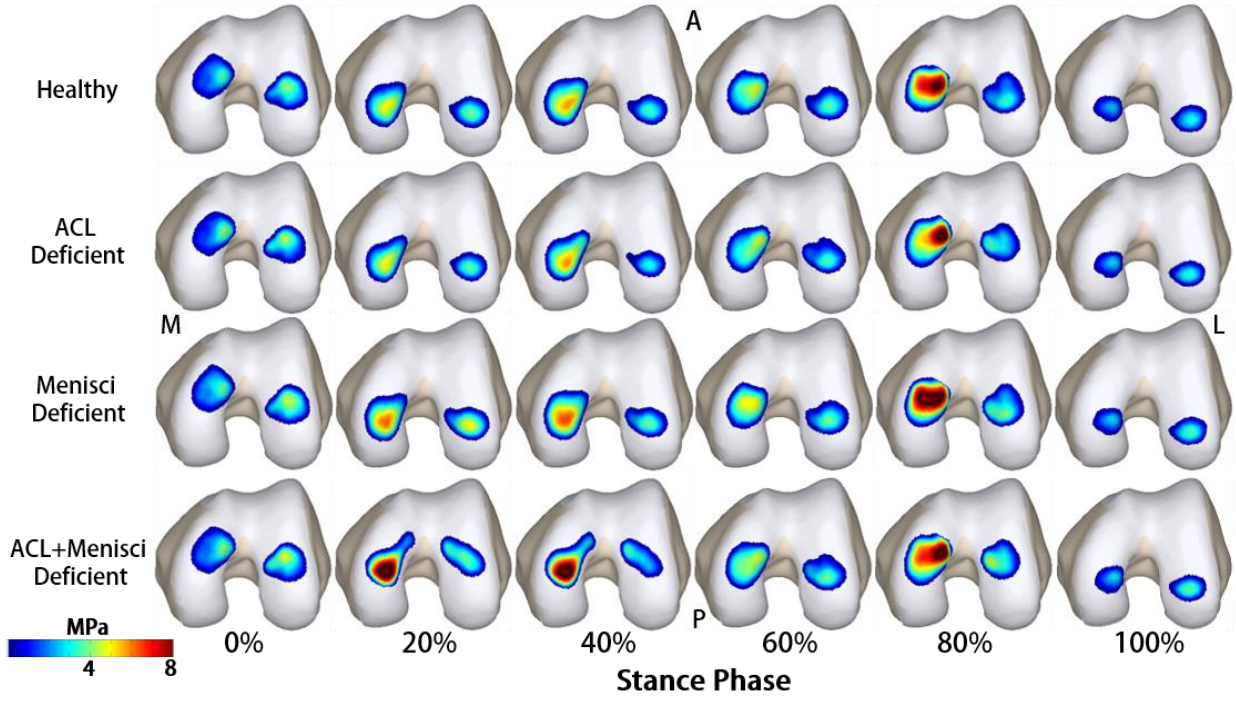

Figure 9 Femoral cartilage-cartilage contact pressure for each condition over the stance phase of walking.

References

1. Kaplan, Y. Identifying Individuals With an Anterior Cruciate Ligament-Deficient Knee as Copers and Noncopers: A Narrative Literature Review. *J. Orthop. Sports Phys. Ther.* **41,** 758–766 (2011).

2. Lohmander, L. S., Englund, P. M., Dahl, L. L. & Roos, E. M. The Long-term Consequence of Anterior Cruciate Ligament and Meniscus Injuries: Osteoarthritis. *Am. J. Sports Med.* **35,** 1756–1769 (2007).

3. Griffin, T. M. & Guilak, F. The Role of Mechanical Loading in the Onset and Progression of Osteoarthritis. *Exerc. Sport Sci. Rev.* **33,** 195–200 (2005).

4. Tashman, S., Collon, D., Anderson, K., Kolowich, P. & Anderst, W. Abnormal Rotational Knee Motion During Running After Anterior Cruciate Ligament Reconstruction. *Am. J. Sports Med.* **32,** 975–983 (2004).

5. Hoshino, Y., Fu, F. H., Irrgang, J. J. & Tashman, S. Can joint contact dynamics be restored by anterior cruciate ligament reconstruction? *Clin. Orthop. Relat. Res.* **471,** 2924–2931 (2013).

6. Shao, Q., MacLeod, T. D., Manal, K. & Buchanan, T. S. Estimation of ligament loading and anterior tibial translation in healthy and ACL-deficient knees during gait and the influence of increasing tibial slope using EMG-driven approach. *Ann. Biomed. Eng.* **39,** 110–121 (2011).

7. Moewis, P. *et al.* The restoration of passive rotational tibio-femoral laxity after anterior cruciate ligament reconstruction. *PLoS One* **11,** 1–14 (2016).

8. Barrance, P., Williams, G., Snyder-Mackler, L. & Buchanan, T. Do ACL-injured copers exhibit differences in knee kinematics?: An MRI study. *Clin. Orthop. Relat. Res.* **454,** 74–80 (2007).

9. Stergiou, N., Ristanis, S., Moraiti, C. & Georgoulis, A. D. Tibial Rotation in Anterior Cruciate Ligament (ACL) - Deficient and ACL-Reconstructed Knees. *Sport. Med* **37,** 601–613 (2007).

10. DeFrate, L. E. *et al.* The 6 Degrees of Freedom Kinematics of the Knee After Anterior Cruciate Ligament Deficiency. *Am. J. Sports Med.* **34,** 1240–1246 (2006).

11. Isaac, D. L. *et al.* In-vivo sagittal plane knee kinematics: ACL intact, deficient and reconstructed knees. *Knee* **12,** 25–31 (2005).

12. Waite, J. C., Beard, D. J., Dodd, C. A. F., Murray, D. W. & Gill, H. S. In vivo kinematics of the ACL-deficient limb during running and cutting. *Knee Surgery, Sport. Traumatol. Arthrosc.* **13,** 377–384 (2005).

13. McDermott, I. D., Masouros, S. D. & Amis, A. A. Biomechanics of the menisci of the knee. *Curr. Orthop.* **22,** 193–201 (2008).

14. Englund, M., Roemer, F. W., Hayashi, D., Crema, M. D. & Guermazi, A. Meniscus pathology, osteoarthritis and the treatment controversy. *Nat. Rev. Rheumatol.* **8,** 412–419 (2012).

15. Spang, J. T. *et al.* The Effect of Medial Meniscectomy and Meniscal Allograft Transplantation on Knee and Anterior Cruciate Ligament Biomechanics. *Arthrosc. - J. Arthrosc. Relat. Surg.* **26,** 192–201 (2010).

16. Papageorgiou, C. D. *et al.* The biomechanical interdependence between the anterior cruciate ligament replacement graft and the medial meniscus. *Am. J. Sports Med.* **29,** 226–231 (2001).

17. Trojani, C. *et al.* Causes for failure of ACL reconstruction and influence of meniscectomies after revision. *Knee Surgery, Sport. Traumatol. Arthrosc.* **19,** 196–201 (2011).

18. O'Connor, J. J. Can muscle co-contraction protect knee ligaments after injury or repair? *J. bone Jt. Surg. Br. Vol.* **75,** 41–48 (1993).

19. Yanagawa, T., Shelburne, K., Serpas, F. & Pandy, M. Effect of hamstrings muscle action on stability of the ACL-deficient knee in isokinetic extension exercise. *Clin. Biomech.* **17,** 705–712 (2002).

20. Liu, W. & Maitland, M. E. The effect of hamstring muscle compensation for anterior laxity in the ACL-deficient knee during gait. *J. Biomech.* **33,** 871–879 (2000).

21. Shelburne, K. B., Pandy, M. G. & Torry, M. R. Comparison of shear forces and ligament loading in the healthy and ACL-deficient knee during gait. *J. Biomech.* **37,** 313–319 (2004).

22. Shelburne, K. B., Torry, M. R. & Pandy, M. G. Effect of muscle compensation on knee

instability during ACL-deficient gait. *Med. Sci. Sports Exerc.* **37,** 642–648 (2005).

23. Lenhart, R. L., Kaiser, J., Smith, C. R. & Thelen, D. G. Prediction and Validation of Load-Dependent Behavior of the Tibiofemoral and Patellofemoral Joints During Movement. *Ann. Biomed. Eng.* (2015). doi:10.1007/s10439-015-1326-3

24. Smith, R. C., Choi, K. W., Negrut, D. & Thelen, D. G. Efficient Computation of Cartilage Contact Pressures within Dynamic Simulations of Movement. *Comput. Methods Biomech. Biomed. Eng. Imaging Vis.* **1163,** (2016).

25. Bei, Y. & Fregly, B. J. Multibody dynamic simulation of knee contact mechanics. *Med. Eng. Phys.* **26,** 777–89 (2004).

26. Blankevoort, L. & Huiskes, R. Ligament-Bone Interaction in a Three-Dimensional Model of the Knee. *J. Biomech. Eng.* **113,** 263–269 (1991).

27. Brandon, S. C. E., Smith, C. R. & Thelen, D. G. in *Handbook of Human Motion* 1–34 (2017). doi:10.1007/978-3-319-30808-1_172-1

28. DeMers, M. S., Pal, S. & Delp, S. L. Changes in tibiofemoral forces due to variations in muscle activity during walking. *J. Orthop. Res.* **32,** 769–776 (2014).

29. Steele, K. M., DeMers, M. S., Schwartz, M. H. & Delp, S. L. Compressive tibiofemoral force during crouch gait. *Gait Posture* **35,** 556–560 (2012).

30. Harmon, M. & Markovich, G. Wear patterns on tibial plateaus from varus and valgus osteoarthritic knees. *Clin. Orthop. Relat. Res.* **352,** 149–158 (1998).

31. Moschella, D., Blasi, a, Leardini, a, Ensini, a & Catani, F. Wear patterns on tibial plateau from varus osteoarthritic knees. *Clin. Biomech. (Bristol, Avon)* **21,** 152–8 (2006).

32. Fleming, B. C. *et al.* The gastrocnemius muscle is an antagonist of the anterior cruciate ligament. *J. Orthop. Res.* **19,** 1178–84 (2001).

33. Rudolph, K. S., Axe, M. J., Buchanan, T. S., Scholz, J. P. & Snyder-Mackler, L. Dynamic stability in the anterior cruciate ligament deficient knee. *Knee Surgery, Sport. Traumatol. Arthrosc.* **9,** 62–71 (2001).

34. Laz, P. J., Stowe, J. Q., Baldwin, M. a, Petrella, A. J. & Rullkoetter, P. J. Incorporating uncertainty in mechanical properties for finite element-based evaluation of bone mechanics. *J. Biomech.* **40,** 2831–6 (2007).

35. Chandrashekar, N., Mansouri, H., Slauterbeck, J. & Hashemi, J. Sex-based differences in the tensile properties of the human anterior cruciate ligament. *J. Biomech.* **39,** 2943–50 (2006).

36. Smith, C. R., Lenhart, R. L., Kaiser, J., Vignos, M. F. & Thelen, D. G. Influence of Ligament Properties on Tibiofemoral Mechanics in Walking. *J. Knee Surg.* (2015). doi:10.1055/s-0035-1558858

Conclusion

Contributions and perspectives towards advancing musculoskeletal simulation and ACL injury treatments

This dissertation provided four major contributions to musculoskeletal simulation and its application to the treatment of anterior cruciate ligament injury. A new simulation framework was developed to predict internal knee joint loading during functional movement. The framework was then leveraged to gain insight into both conservative rehabilitation and surgical reconstruction treatments for ACL rupture.

Musculoskeletal Simulation

Simulation continues to demonstrate its potential to provide insight into the fundamentals of musculoskeletal biomechanics and improve clinical treatments. This dissertation developed simulation and analysis techniques to study ACL injury treatments in a novel multiscale and multifactorial manner.

COMAK Simulation Framework

The first contribution of this dissertation was the development of the concurrent optimization of muscle activations and kinematics (COMAK) simulation framework. COMAK provides a general-purpose simulation algorithm to concurrently resolve full-body and joint mechanics during functional movement. This enabled an investigation of the influence of neuromuscular coordination and ACL graft parameters on tibiofemoral cartilage loading during walking. In future work, this capability could provide insights beyond ACL injuries to other pathologies and joints.

Several improvements could be made to the simulation framework and analyses methods in future work. The probabalistic sensitivity analyses performed in the previous chapters can be extended to study multi-parameter interactions. The parametric nature of the model can be extended with a statistical shape model to study the influence of articular geometry on knee mechanics. Additionally, gait dynamics of a population could be parameterized to study their effect on joint loading. The parametric framework introduced in this dissertation will enable straight forward integration of these advancements for future studies of muscle driven joint mechanics.

The treatment of muscle redundancy as a modeling uncertainty in this dissertation provides a new perspective on a problem that remains unsolved in biomechanics. Chapter 2 provides a detailed description of this methodology and its application to study the influence of neuromuscular coordination on healthy knee mechanics during walking. Here, quantifying the sensitivity of predicted joint mechanics to muscle activity provides a simple interpretation of a single muscle's influence on the knee function. Chapter 5 provides a demonstration where establishing the mechanical bounds on the muscle redundancy solution space provided the novel insight that soft tissue loading could not be restored in an ACL deficient knee.

High Throughput Computing

The second important contribution of this dissertation was the introduction of high throughput computing (HTC) resources to the musculoskeletal simulation field, which enables a new category of computational methods to be leveraged. The brute computational strength of HTC resources now enable 'relatively' simplistic approaches to answer difficult research questions. An example of this exists in Chapter 5. Here the feasible muscle redundancy solution spaces of the healthy, ACL deficient, and menisci deficient knees were compared using 30,000 unique simulations. This showed that no altered neuromuscular coordination strategy exists that could restore soft tissue

loading in the injured knees. We had previously failed to solve this problem using optimization based methods to search for a coordination strategy to restore cartilage loading in an ACL deficient knee.

ACL Injury Treatments

Conservative Treatment

Conservative rehabilitation of ACL injuries is an important treatment option for copers, and patients willing to adapt their functional activities to avoid instances of knee instability. A better fundamental understanding of the influence of muscles on knee joint mechanics will likely provide important insights to improve rehabilitation protocols. The recent introduction of concurrent simulation techniques will enable a new generation of computational studies of muscle driven joint mechanics.

The third contribution of this dissertation was the application of the COMAK simulation framework to study muscle coordination strategies in ACL deficient knees. This demonstrated the inability of neuromuscular coordination to restore cartilage and soft tissue loading patterns in injured knees, providing valuable insight for clinicians and patients considering treatment options. Despite this finding, conservative treatment remains a viable option for many patients and there are numerous examples of individuals who cope with ACL deficiency and do not exhibit signs of early osteoarthritis. In future, the COMAK simulation framework could be adapted to study the capacity of altered limb dynamics and neuromuscular coordination patterns to influence joint stability. These methods could provide the sensitivity of joint stability to individual muscle activations throughout the gait cycle and may provide insight to physical therapists.

ACL Reconstruction

The ACL reconstruction procedure has undergone several iterations towards replicating the anatomy and function of the native ACL with minimally invasive techniques. The evolution from extra-articular to intra-articular reconstruction, introduction of arthroscopic technologies, and improvement in techniques for tunnel positioning and graft fixation have led to better short clinical outcomes. However, risk for post-traumatic osteoarthritis remains high in this population resulting in considerable opportunity to this improve treatment of ACL injuries.

The fourth contribution of this dissertation was to demonstrate the importance of replicating the geometry of the intact contralateral ACL when performing the ACL reconstruction surgery. Our recent work using dynamic imaging and computer simulation suggests that replicating the patient-specific ACL anatomy is critical to restore pre-injury soft tissue loading patterns. The sagittal plane angle of the ACL was correlated with tibiofemoral kinematics measured with dynamic MRI during a loaded flexion-extension task (Appendix). This cause-effect relationship was then demonstrated using forward dynamic musculoskeletal simulations of the open-chain task. The COMAK simulation framework extended these findings to walking. A more vertical sagittal plane graft angle was shown to increase anterior translation and internal rotation, and shift the center of pressure on the medial tibial cartilage posteriorly during stance. Thus, improvements in surgical techniques should be focused on better replicating the geometry of the native ACL. Enabling high surgical precision through advanced imaging, surgical planning, and robotic and patient-specific surgical tools may provide the next break through to further improving this treatment.

Conclusion

This dissertation developed a multiscale musculoskeletal simulation framework to study cartilage and ligament loading during muscle driven movements. The framework leveraged high

throughput computing to perform probabilistic analyses that revealed the influence of neuromuscular coordination and ACL graft parameters on functional knee mechanics. The application of the framework to study knee joint mechanics provided several insights into conservative and surgical treatments of ACL injury. In the future, this framework will hopefully provide insights into additional joint pathologies and where muscle driven joint mechanics contribute to treatment outcomes.

Appendix – Conference Abstracts

Title:

The Effect of Cartilage Thickness on Tibiofemoral Contact Pressure During Gait

Introduction:

Articular cartilage loading is often linked with tissue health, with sufficient loading needed to enable tissue homeostasis but excessive loading potentially leading to tissue degeneration and osteoarthritis (OA) [1]. However, the complexity of measuring or calculating cartilage loads during movement has hindered quantitative research on the topic. Cartilage contact pressure estimates have recently gained clinical relevance as high tibiofemoral cartilage pressures calculated from standing radiographs, were shown to predict the development of pain and OA [2,3]. However, the underlying morphological factors that can lead to high cartilage contact pressure are not well understood. One theory is that cartilage thinning leads to increasingly higher pressures resulting in a "downward spiral" of cartilage tissue degeneration [1]. To assess the link between cartilage thinning and articular contact pressures, we developed a novel musculoskeletal simulation framework capable of calculating tibiofemoral cartilage pressures during gait. The objective of this study was to investigate the effect of cartilage tissue thickness on the magnitude and distribution of tibiofemoral cartilage contact pressures during the stance phase of gait.

Methods:

We developed a three-body dynamic knee model from segmented MR images of a healthy young female (age = 22, height = 179 cm, mass =79 kg).The model included six degree-of-freedom (dof) tibiofemoral (TF) and patellofemoral (PF) joints, nine ligaments and triangulated high resolution meshes of cartilage surface geometries. The ligaments were modeled as bundles of nonlinear springs which spanned from the footprint of the origin to the insertion, with wrapping included about bony structures. Cartilage contact pressure was calculated using an elastic foundation model, in which the pressure is a nonlinear function of the depth of penetration of two articulating cartilage meshes. Cartilage penetration depth was computed using a ray casting technique to find the closest point between a triangle in the distal segment (e.g. tibia plateau) and the proximal cartilage surface (e.g. femoral condyles) [4]. Note that cartilage thickness at a point represents the sum of the cartilage thicknesses of the two articular surfaces at the point of contact. The full knee model was shown to replicate the *in vivo* kinematic behavior of the knee as measured by dynamic MRI.

A musculoskeletal model was used to simulate tibiofemoral and patellofemoral mechanics during gait. The subject-specific knee model was integrated with a generic lower extremity musculoskeletal model that included 44 Hill-type muscle-tendon units acting about the hip, knee and ankle joints [5]. The lower extremity model was first scaled to match the subject's anthropometrics, and then the subject-specific bones were aligned to the generic femur, tibia and patella. Whole body kinematics and ground reaction forces were measured from the subject during overground walking at a preferred speed. A Computed Muscle Control (CMC) co-simulation framework was then used to modulate the lower extremity muscle excitations to match hip, knee flexion and ankle angular trajectories throughout a full gait cycle (Fig. 1) [6]. Note that the CMC algorithm only tracks knee flexion, such that the other 5 TF dof and all 6 PF dof evolved naturally as a result of external loads, muscle forces, ligament tension and articular contact pressures. We first simulated gait using the variable cartilage thickness measured over the cartilage surfaces in the MR images. The gait simulations were then re-generated with assumed constant TF cartilage thicknesses of 2, 4, 6, 8 and 10mm. The surface geometry of the cartilage surfaces was unaltered between simulations.

Results:

Both the tibia plateau pressure magnitude and contact area were greater on the medial side relative to the lateral side at the first peak of tibiofemoral loading during the stance phase of gait. Overall, the peak and average contact pressures increased nonlinearly as the cartilage thickness decreased (Fig. 2), with pressure rising substantially as cartilage thickness dropped below 4 mm. In the medial compartment, the peak pressure increased from 8.3 MPa to 18.9 MPa (127%) and the average pressure increased from 1.5 MPa to 3.8 MPa (151 %) between the simulations with cartilage thicknesses of 10mm and 2mm. Correspondingly, the medial tibial plateau contact area decreased by 63% and lateral contact area decreased by 45% between the 10mm and 2mm thicknesses. The distribution of the pressure over the contact area also was greatly affected by cartilage thickness, with the thinner cartilage showing a greater percentage of the contact area experiencing high pressures (Fig. 3). Similar effects of cartilage thickness on pressure and contact area were obtained at the time of the second peak in the stance phase TF loading.

Discussion:

The relationship between cartilage morphology and tissue loading is important for understanding the causes and treatment of OA. Our simulations suggest that cartilage tissue thickness has a highly

nonlinear effect on contact pressures during the stance phase of gait. In particular, combined cartilage tissue thicknesses below 4 mm were found to lead to substantially higher peak and average cartilage contact pressures. This change was the result of thin cartilage producing a substantially smaller articulation contact area, necessitating higher pressures to generate the same net joint contact load. Use of a variable thickness cartilage as measured from MR images produced average and peak contact pressure estimates that were between values obtained with constant 4 and 6 mm thickness tissues. Thus, it would appear that the healthy tissue morphology is adapted to be in a range that makes the tissue pressure less sensitive to the thickness. The computational framework is formulated in a way that allows future study on the influence of other morphological features (e.g. curvature) and walking mechanics on cartilage pressures. Such information could prove beneficial for rigorously assessing OA risk and investigating clinical interventions that can mitigate that risk.

Significance:

This study suggests that tibiofemoral cartilage pressure during gait varies nonlinearly with cartilage tissue thickness, with a threshold minimal thickness below which one sees substantially decreased contact area and increased localized pressure. This morphologically altered mechanical loading could contribute to the downward spiral of cartilage degeneration seen in OA.

References

1. Andriacchi, T. P., Koo, S. & Scanlan, S. F. Gait mechanics influence healthy cartilage morphology and osteoarthritis of the knee. *J. Bone Joint Surg. Am.* **91,** 95–101 (2009).

2. Segal, N. a *et al.* Baseline articular contact stress levels predict incident symptomatic knee osteoarthritis development in the MOST cohort. *J. Orthop. Res.* **27,** 1562–8 (2009).

3. Segal, N. a *et al.* Elevated tibiofemoral articular contact stress predicts risk for bone marrow lesions and cartilage damage at 30 months. *Osteoarthritis Cartilage* **20,** 1120–6 (2012).

4. Arnold, E. M., Ward, S. R., Lieber, R. L. & Delp, S. L. A Model of the Lower Limb for Analysis of Human Movement. *Ann. Biomed. Eng.* **38,** 269–279 (2010).

5. Bei, Y. & Fregly, B. J. Multibody dynamic simulation of knee contact mechanics. *Med. Eng. Phys.* **26,** 777–89 (2004).

6. Thelen, D. G., Choi, K. W. & Schmitz, A. M. Co-Simulation of Neuromuscular Dynamics and Knee Mechanics during Human Walking. *J. Biomech. Eng.* **136,** 1–8 (2014).

Figures:

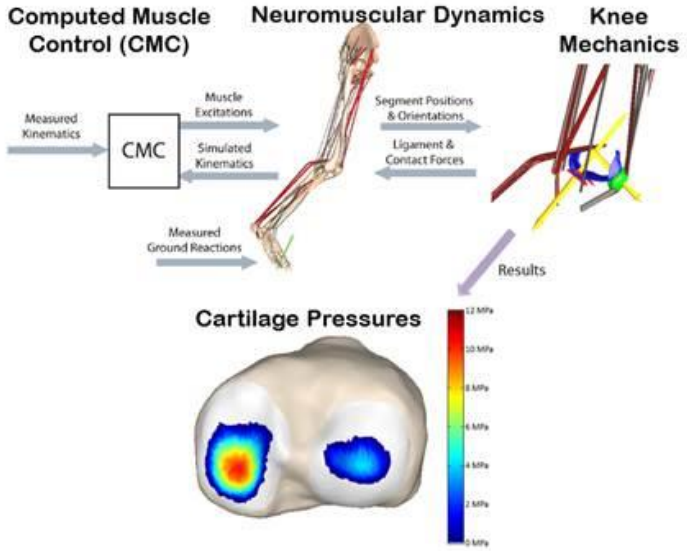

Figure 1: Musculoskeletal simulation framework

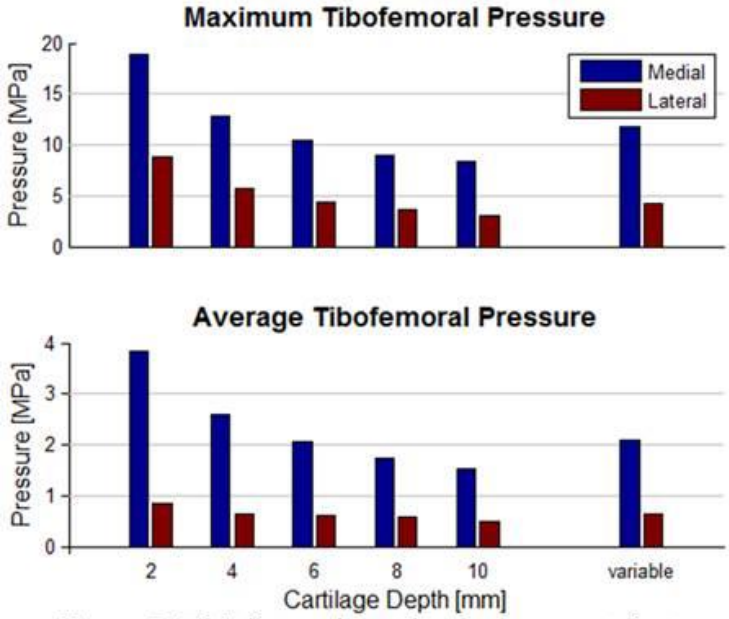

Figure 2: Tibiofemoral cartilage pressure at first peak of TF loading during stance

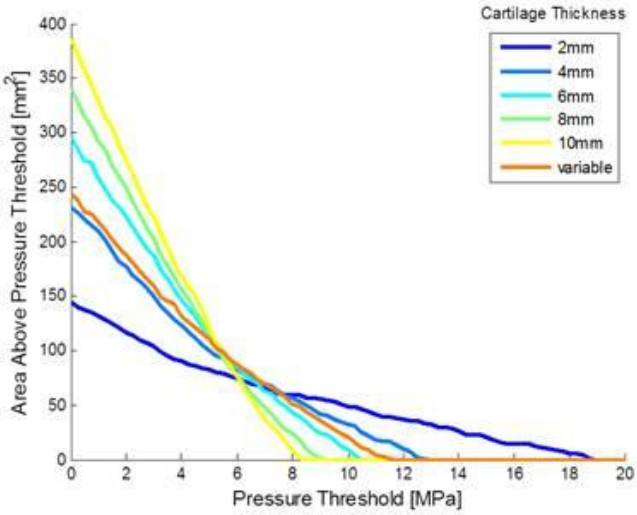

Figure 3: Medial tibiofemoral contact area above pressure threshold at first peak of TF loading during stance

SB³C2015
Summer Biomechanics, Bioengineering and BIotransport Conference
June 17-20, 2015,Snowbird Resort, Utah, USA

THE INFLUENCE OF CARTILAGE MORPHOLOGY AND ELASTICITY ON TIBIOFEMORAL CONTACT PRESSURES DURING WALKING

Colin R. Smith (1), Rachel L. Lenhart (2), Jarred Kaiser (1), Michael F. Vignos (1), Darryl G. Thelen (1,2,3)

(1) Department of Mechanical Engineering
University of Wisconsin-Madison
Madison, WI, USA

(2) Department of Biomedical Engineering
University of Wisconsin-Madison
Madison, WI, USA

(3) Department of Orthopedics and Rehabilitation
University of Wisconsin-Madison
Madison, WI, USA

INTRODUCTION

Articular cartilage overloading during gait is recognized as a factor affecting the development and progression of knee osteoarthritis (OA). Accordingly, the external Knee Adduction Moment (KAM) is often used as a surrogate measure of contact force on the medial compartment of the tibiofemoral joint, where OA often develops (1). However, the KAM may not be an indicator of localized tissue stress and strain which can induce damage over multiple loading cycles. Thus, it may be more relevant to estimate cartilage contact pressure and tissue deformation during gait. However, current gait models employ a highly simplified knee joint model that only allows for estimates of net joint contact loads (2). To overcome this limitation, we developed a multi-body dynamic knee model that includes representations of the major ligaments and articular surfaces of the tibiofemoral and patellofemoral joints (3). The increased degrees of freedom included in this model allow for prediction of cartilage pressures in the context of full-body walking simulations.

There are three objectives of this study. First, to introduce an Enhanced Static Optimization (ESO) simulation routine to simultaneously calculate muscle forces, cartilage pressures, ligament forces, and secondary knee kinematics from subject-specific gait measures. Second, to evaluate whether the KAM is predictive of medial cartilage contact pressures during gait. Finally, to investigate how variations in cartilage morphology and material properties can alter cartilage contact pressures and deformations.

METHODS

A 3 body, 12 DOF knee model was developed from MR images of a healthy adult female (1.65 m, 61 kg). Fourteen ligament bundles were represented by nonlinear elastic springs, with wrapping surfaces used to prevent penetration of bony geometries. Articular cartilage surfaces were segmented from the images and represented by high resolution meshes. Given the bone segment positions in space, cartilage contact pressures were computed by detecting overlap between articulating surfaces, and using an elastic foundation model to compute pressure based on the depth of penetration and an assumed elastic modulus for cartilage tissue. The predictive capacity of the model was validated by comparing simulated passive and active knee motion with *in vivo* 3D knee kinematics measured with dynamic MRI (3). The knee model was integrated into an existing lower extremity musculoskeletal model (2), which included 43 muscles acting about the hip, knee and ankle joints.

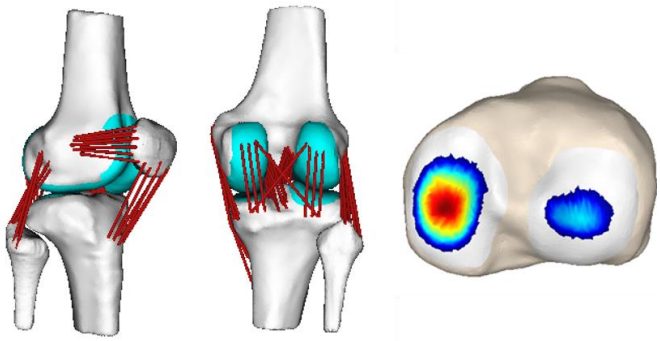

Figure 1 – Multibody 12 degree of freedom knee model and representative pressure map

To estimate tissue loading and knee kinematics during gait, we developed the ESO routine. Similar to standard static optimization, ESO uses numerical optimization to calculate active muscle forces needed to satisfy whole body equations of motion. However, ESO also

simultaneously calculates the secondary joint kinematics (5 tibiofemoral and 6 patellofemoral DOF) which induce ligament forces and cartilage contact pressures that, along with the estimated muscle forces, generate the measured primary joint accelerations and zero accelerations in the secondary knee DOF. The formal cost function of the optimization minimizes the sum of the squared muscle activations, weighted by muscle volume. A regularization term, the sum of squared changes in secondary kinematics from the previous time step, is used to constrain the solution over time.

We used the model and ESO routine to estimate internal tissue loads from measured gait kinematics and ground reaction forces collected on the same subject for which we constructed the knee model. These analyses were repeated for 5 values of tibiofemoral cartilage thicknesses (combined tibial and femoral thickness ranging from 2mm-10mm) and 6 values of cartilage modulus of elasticity (5 MPa – 25 MPa). For each solution, we computed the mean contact pressure and mean percent deformation for the contacting cartilage on both the medial and lateral tibial plateau.

RESULTS

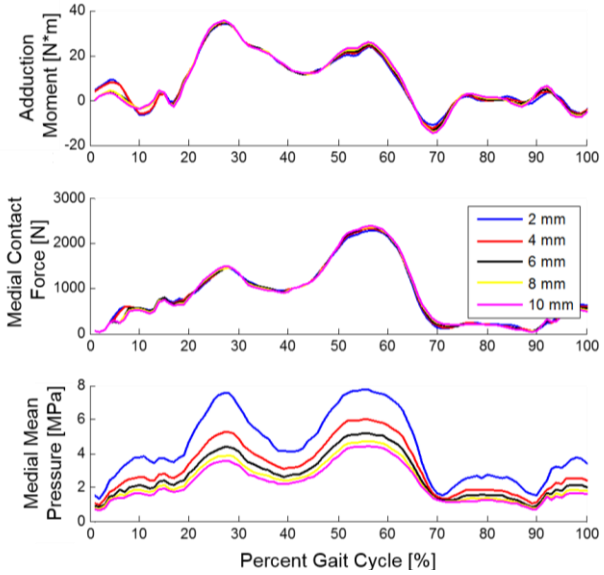

Figure 2 - Knee adduction moment, medial contact force and medial mean contact pressure over a simulated gait cycle for various cartilage thicknesses

The nominal simulation results indicate that the KAM shows a similar temporal trend over the gait cycle to the medial contact force and the mean medial cartilage pressure. However, as the thickness of the cartilage is varied from 2 mm to 10 mm the mean cartilage pressure varies by a factor of 2 while the knee adduction moment remains virtually unchanged (Figure 2). The medial contact force also shows nearly no change. The same results were seen for variations in the cartilage elastic modulus, where the mean pressures showed substantial changes over the gait cycle between elastic modulus values, but the KAM and medial contact force remained unchanged (not shown).

Solving the ESO routine with different cartilage thicknesses and elastic moduli had a relatively small effect on the frontal plane knee alignment, inducing only subtle changes in the KAM. However, cartilage properties substantially altered both the mean contact pressure and percent cartilage deformation (Figure 3).

Decreasing cartilage elastic modulus from 25 to 5 MPa reduced the mean contact pressure from 8 to 5 MPa, but increased the cartilage deformation from 9% to 22%. In contrast, decreasing the combined cartilage thickness from 10 to 2 mm resulted in increases in both the mean contact pressure (4.2 to 7.6 MPa) and the mean cartilage deformation (20% to 30%).

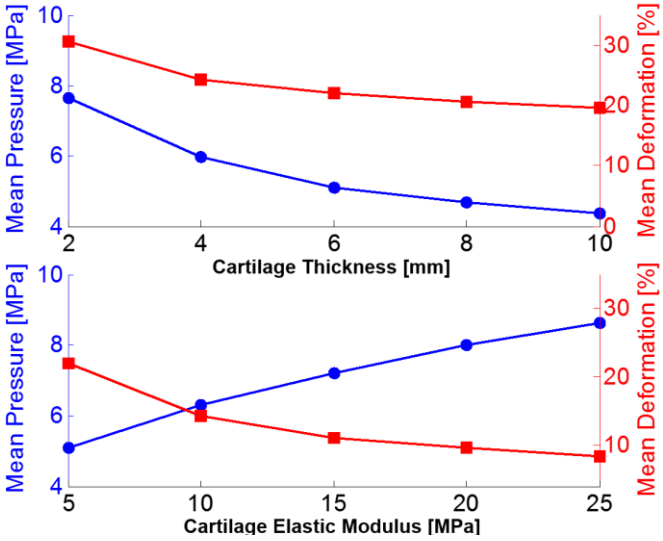

Figure 3 – The effect of cartilage thickness and elastic modulus on medial tibial cartilage mean pressures and mean deformations (depth of cartilage overlap/cartilage thickness*100%) at the second peak of tibiofemoral force during gait

DISCUSSION

We demonstrated the capability of our 12 DOF knee model and EOS simulation routine to predict cartilage contact pressures during movement. This novel approach allows calculation of localized cartilage pressures in the knee joint and has great promise for better predicting the development of OA.

Our simulation results indicate that the KAM does show the same temporal trends as the medial contact force and mean pressure over a gait cycle. However, the KAM and medial contact force are not able to predict changes in pressure that arise from changes in material properties of the cartilage. These results are similar to studies of loads measured from instrumented knee implants which showed the trend of the KAM correlates well to the medial knee contact force [4], however the KAM was less able to predict changes in the medial knee contact force associated with gait modifications [5].

The sensitivity of cartilage contact pressure and deformation to cartilage properties is relevant to consider in the context of OA. As OA progresses, cartilage becomes thinner and the collagen network is damaged leading to a decrease in elastic modulus [6]. Our results suggest these changes can alter both the localized cartilage tissue stresses and strains, potentially leading to further cartilage damage and degeneration. Further study is needed to assess how these observations vary with alternative gait patterns and different cartilage surfaces.

ACKNOWLEDGEMENTS NIH EB015410

REFERENCES

[1] Sharma, L et al., *Arthritis & Rheum.*, 41:1233-40, 1998.
[2] Arnold EM et al., *Ann of Biomed Eng*, 38:269-79.
[3] Lenhart RL et al., *WCB*, 2014.
[4] Zhao, D. et al., *J. Orthop. Res.*, 25:789-797, 2007.
[5] Walter, JP et al., *J. Orthop. Res.*, 28:1348-54, 2010.
[6] Silver, FH et al., *Matrix Biol.*, 21:129-137, 2002

XV International Symposium on Computer Simulation in Biomechanics
July 9th – 11th 2015, Edinburgh, UK

A Variable Cartilage Property Formulation of the Elastic Foundation Model to Predict Contact Pressures during Walking

Colin Smith[1], Rachel Lenhart[2], and Darryl Thelen[1,2,3]

[1] Department of Mechanical Engineering, [2] Department of Biomedical Engineering, [3] Department of Orthopedics and Rehabilitation, University of Wisconsin-Madison, United States of America
Email: dgthelen@wisc.edu, Web: http://uwnmbl.engr.wisc.edu/

INTRODUCTION

Cartilage loading patterns are an important aspect to understand the pathogenesis of knee osteoarthritis (OA). Since there is no viable method to measure joint loads *in vivo*, contact patterns must be estimated from computational models. Knee models often use an elastic foundation representation to estimate contact pressure [1,2,3]. However, the common formulation of the elastic foundation model for cartilage [3] assumes the two articulating cartilage surfaces have the same elasticity and thickness. This assumption does not account for spatially varying changes in cartilage thickness or elasticity between surfaces. In this study, we present an improved formulation of the elastic foundation model which allows for spatially varying thickness and material properties of the contacting surfaces. We demonstrate the importance of this improved formulation by simulating gait with variable cartilage thickness maps measured from magnetic resonance (MR) images.

METHODS

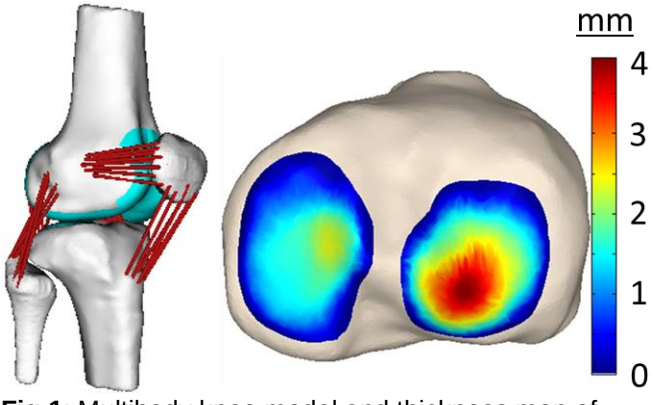

Fig 1: Multibody knee model and thickness map of tibial cartilage. The maximum thickness on the medial and lateral surfaces are 2.4 and 4.0 mm, respectively

We developed a multi-body knee model that included six DOF representations of the tibiofemoral and patellofemoral joints. Bone segments, cartilage surfaces and ligament attachments points were segmented from static MR images of a healthy young female (age=23) knee. The knee model was incorporated into a generic multibody musculoskeletal model [4] that included 44 muscle-tendon units acting about the hip, knee and ankle. We validated the knee model by comparing simulated knee kinematics with direct *in vivo* measures obtained using dynamic MRI [5].

Whole body kinematics and ground reactions were recorded while the subject walked overground in a motion analysis laboratory. At each frame of a gait cycle, we then used an enhanced static optimization (ESO) routine [6] to calculate muscle forces, patellofemoral kinematics and secondary tibiofemoral kinematics that minimized a weighted sum of muscle activations squared while satisfying overall dynamic constraints. The constraints required that the patellofemoral kinematics and secondary tibiofemoral kinematics produce ligament loads and cartilage contact pressures that, together with the muscle forces, generate the measured hip, knee and ankle accelerations.

Tibiofemoral and patellofemoral cartilage contact pressures were computed from the knee kinematics based on the depth of rigid body penetration of the contacting cartilage meshes. Depth of penetration for each triangle in a mesh was computed using a ray casting technique [3]. Contact pressure was then derived according to plane-strain elasticity theory, which assumes each cartilage surface represents an elastic layer of finite thickness bonded to a rigid subsurface. Previous applications computed contact pressure, p, via [3]:

$$p = -\frac{(1-v)E}{(1+v)(1-2v)}\ln\left[1-\frac{d}{h}\right] \qquad \text{(Eq. 1)}$$

where E is elastic modulus, v is poissons ratio, d is the penetration depth and h is the combined thickness of the two cartilage surfaces. To allow each cartilage surface to have unique definitions of E, v and h, we defined separate elastic foundation models for each surface:

$$p_1 = -\frac{(1-v_1)E_1}{(1+v_1)(1-2v_1)}\ln\left[1-\frac{d_1}{h_1}\right] \quad \text{(Eq. 2)}$$

$$p_2 = -\frac{(1-v_2)E_2}{(1+v_2)(1-2v_2)}\ln\left[1-\frac{d_2}{h_2}\right] \quad \text{(Eq. 3)}$$

We introduced two additional equations resulting from the equilibrium of pressures in pairs of contacting triangles, and the equivalence of the sum of the individual surface penetration depths to the total penetration depth.

$$p_1 = p_2 \quad \text{(Eq. 4)}$$

$$d_1 + d_2 = d \quad \text{(Eq. 5)}$$

Simultaneous solution of Eq. (2-5) results in the pressure and unique deformation for every triangle on each of the cartilage surfaces.

We simulated gait with both elastic foundation formulations (Eq. 1, and Eq. 2-5). Cartilage pressures computed using constant cartilage thicknesses of 2, 4, 6 and 8 mm and the lumped parameter model were compared against the improved formulation using variable cartilage thickness measured directly from the MRI images.

RESULTS AND DISCUSSION

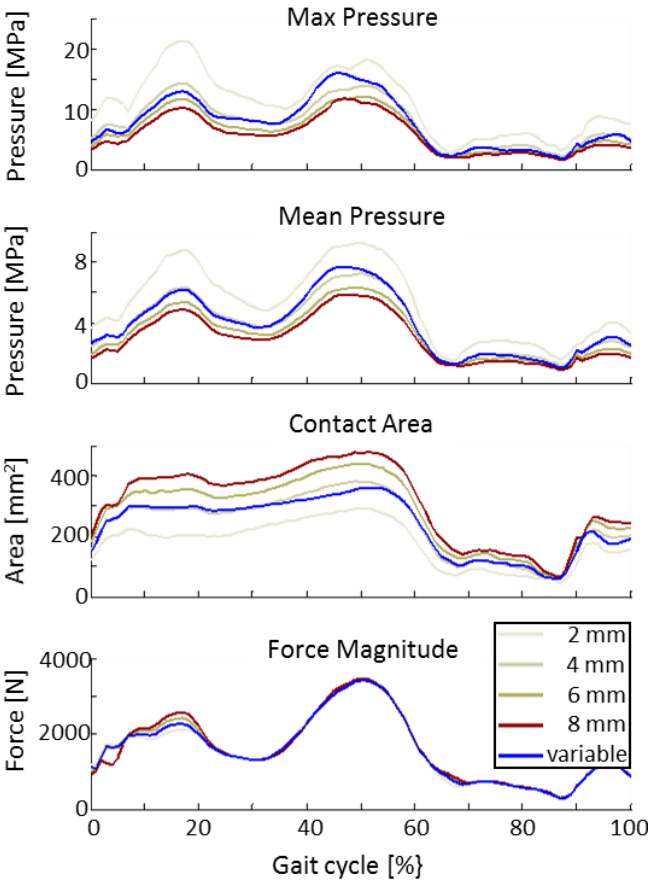

Fig 2: Contact metrics of the medial tibial plateau

The gait simulations indicate that the previous formulation of the elastic foundation model using constant thicknesses of 2, 4, 6, and 8 mm result in 23.4, -4.3, -16.7, -22.9% differences in the mean medial tibial contact pressures respectively at the second peak of tibiofemoral contact force during stance (Fig. 2).

The spatial distribution of cartilage pressure showed substantial change as well, demonstrated by the cartilage pressure maps shown in Fig. 3.

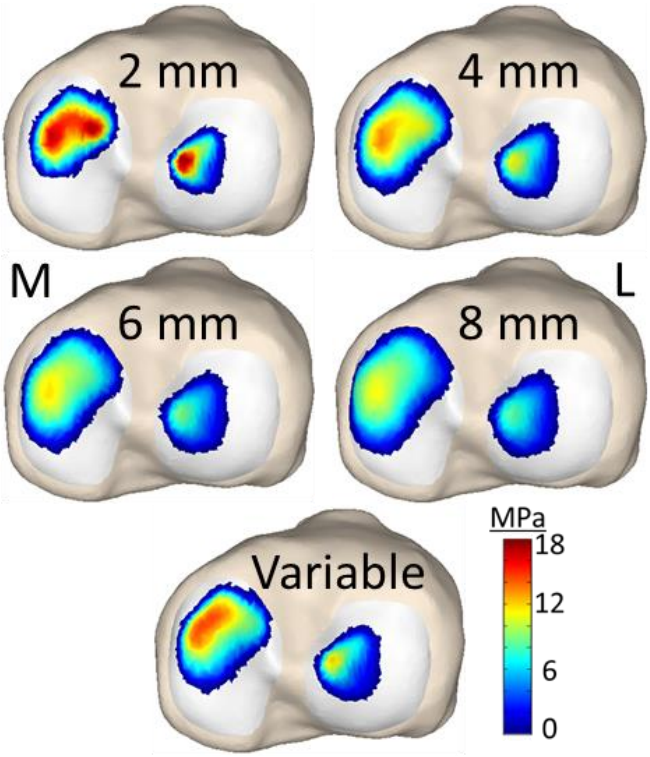

Fig 3: Tibial cartilage pressure at second peak of TF force for constant and variable cartilage thickness

CONCLUSIONS

We introduced an improved formulation of the elastic foundation model for use in gait simulations which allows for cartilage thickness and elastic properties to vary between contacting surfaces. The inclusion of variable cartilage thickness in gait simulations resulted in substantial differences in contact pressures compared to simulations using constant cartilage thickness. Additionally, the improved contact model formulation allows for future research on cartilage defects and disease progression where altered cartilage thickness and elastic properties are present.

REFERENCES

1. Blankevoort L, et al. *J Biomech* **24**: 1019-1031, 1991.
2. Pandy M, et al. *Comput Method Biomec* **1**: 87-108, 1997.

3. Bei Y, et al. *Med Eng Phys* **26**: 777-789, 2004.
4. Arnold E, et al. *Ann Biomed Eng* **38**: 269-279, 2010.
5. Lenhart R, et al. *Ann Biomed Eng.* submitted, 2014.
6. Lenhart R, et al. *J Biomech*. submitted, 2014.

ACKNOWLEDGEMENTS
NIH EB015410

The Sensitivity of Predicted Knee Contact Mechanics during Gait to Variations in Ligament Properties

[1] Colin Smith, [1]Rachel Lenhart and [1]Darryl Thelen

[1] University of Wisconsin-Madison, Madison WI, USA
email: dgthelen@wisc.edu, web: http://uwnmbl.engr.wisc.edu/

INTRODUCTION

Subject-specific multibody models of the knee joint provide valuable insight into the mechanics of the healthy and pathologic knee during movement. However, the quality of the predictions of these models is directly dependent on the accuracy of the model parameters. While knee model geometries can be segmented from magnetic resonance (MR) images, other parameters such as ligament stiffness and reference strains must be estimated. As a result, the uncertainty in these ligament parameters can propagate into the predicted knee mechanics. The objective of this study was to use a probabilistic approach to evaluate the propagation of variations in ligament properties onto knee kinematics and cartilage contact pressures.

METHODS

A three body, 12 DOF knee model was developed from MR images of a healthy adult female (1.65 m, 61 kg). Fourteen ligaments were represented by bundles of nonlinear elastic springs, with wrapping surfaces included to prevent penetration of bony geometries. Articular cartilage surfaces were segmented from the MR images and represented by high resolution meshes. Cartilage contact pressures were calculated by detecting overlap between the articulating surfaces and using an elastic foundation model to determine pressure based on the depth of penetration. The knee model was integrated into an existing lower extremity musculoskeletal model [1], which included 43 muscles acting about the hip, knee and ankle joints. The predictive capacity of the model was validated by comparing simulated passive and active knee kinematics with *in vivo* 3D knee kinematics measured with dynamic MRI [2].

Whole body kinematics and ground reactions were recorded while the subject walked overground in a motion analysis laboratory. At each frame of a gait cycle, an enhanced static optimization (ESO) routine [3] was used to calculate muscle forces, patellofemoral kinematics and secondary tibiofemoral kinematics that minimized a weighted sum of squared muscle activations while satisfying overall dynamic constraints. The constraints required that the muscle forces and internal knee loads (contact pressures, ligament forces) produced by the optimized knee kinematics generate the measured hip, knee (flexion) and ankle accelerations.

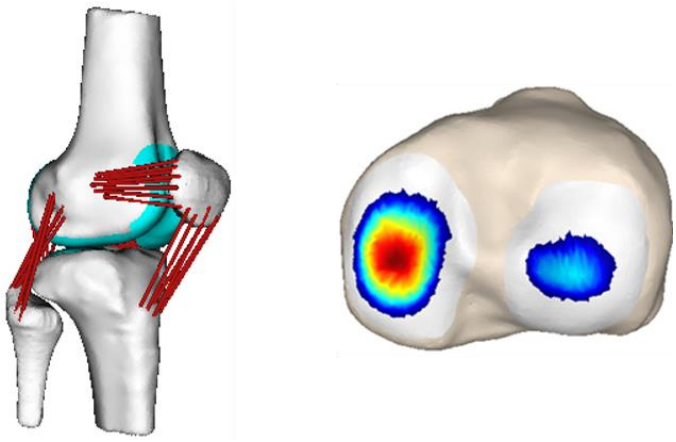

Figure 1: Multibody 12 degree of freedom knee model and representative pressure map

We performed a monte carlo analysis to evaluate the propagation of uncertainty in ligament stiffness and reference strain values into predicted joint mechanics. Nominal values were determined from previous models [4] and tuned to ensure predicted passive kinematics reproduced measured passive kinematics. In the probabilistic analysis, ligament stiffness and reference strains were represented by normal distributions centered at the nominal values with standard deviations of 30% of the mean and 0.2, respectively [5]. A total of 2000 simulations were performed using a high throughput computing grid using randomly selected values from the parameter distributions.

RESULTS AND DISCUSSION

The predicted tibiofemoral kinematics showed variability in each of the degrees of freedom. Internal-external rotation showed the most variability with the maximum standard deviation (5.6^o) occurring during swing phase. The superior-inferior translation and medial-lateral translations showed similar variability to the anterior-posterior translation.

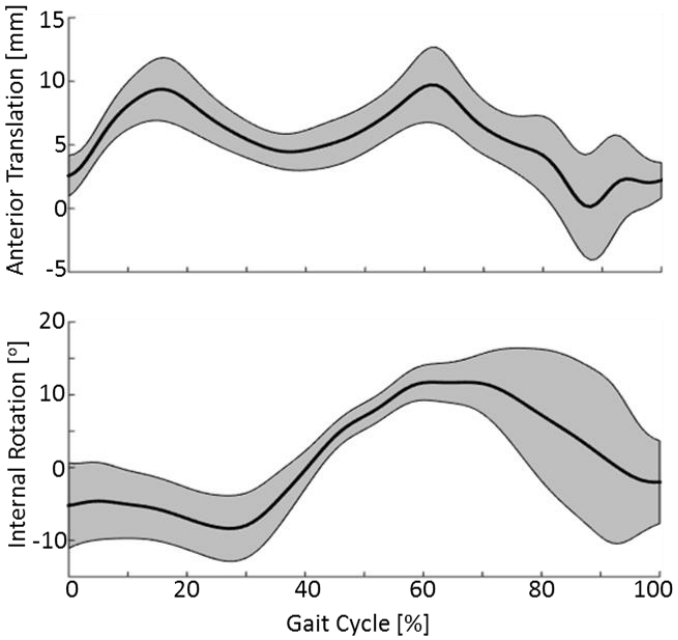

Figure 2: Anterior translation and internal rotation of the tibiofemoral joint during gait. The black line and shaded area represent the mean ± 2 standard deviatons of the monte carlo simulations.

Metrics of articular contact such as mean pressure and contact area also showed substantial variability. The mean pressure on the medial and lateral tibial plateaus had a maximum standard deviation of 0.52 MPa and 0.86 MPa, respectively. The medial and lateral contact areas showed maximum standard deviations of 45.9 mm^2 and 48.0 mm^2.

Further analysis will reveal the individual ligaments which contribute the most to the variability in the predicted results. This will provide valuable insight into the function of specific ligaments during walking.

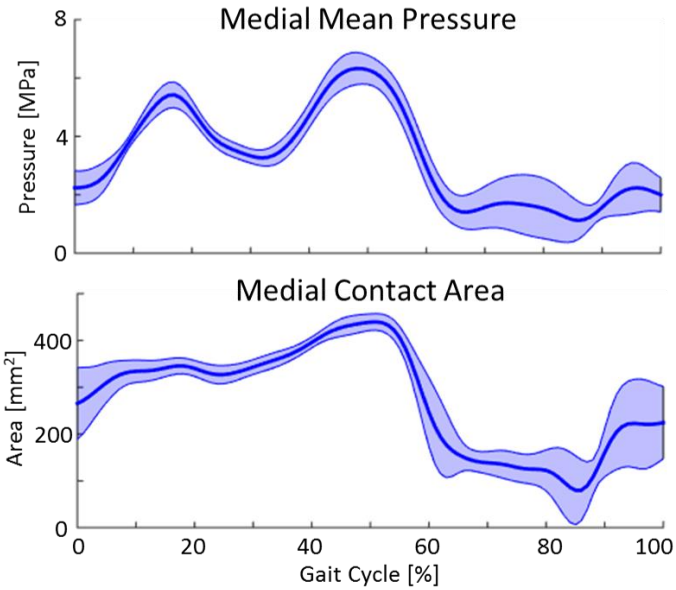

Figure 3: Mean pressure and contact area of the medial tibial plateau over a gait cycle. The blue line and shaded area represent the mean ± 2 standard deviatons of the monte carlo simulations.

CONCLUSIONS

The probabilistic analysis showed that variations in ligament stiffness and reference strains produce substantial variability in the predicted tibiofemoral kinematics and contact mechanics. This indicates that future work is required to accurately determine the values of the ligament parameters.

REFERENCES

1. Arnold, EM, et al. *Ann of Biomed Eng* **38**, 269-79, 2010.
2. Lenhart, RL, et al. *Ann of Biomed Eng* submitted, 2014.
3. Lenhart, RL, et al. *J Biomech* submitted, 2014
4. Blankevoort, L, et al. *J Biomech Eng* **113**, 263-269, 1991
5. Baldwin, MA, et al. *Comput Methods Biomech Biomed Engin* **12**, 651-659, 2009

ACKNOWLEDGEMENTS

NIH EB015410

The Effect of Ligament Properties on Tibiofemoral Kinematics and Contact Pressure during Gait

Colin R Smith, Rachel L Lenhart, Jarred Kaiser, Michael F Vignos, Darryl G Thelen
University of Wisconsin-Madison, Madison WI, USA

Introduction

Computational multibody dynamic models provide an efficient means to study the influence of soft tissue injury on functional knee mechanics. We recently introduced a novel validated multibody knee model that can predict 6 DOF tibiofemoral (TF) and patellofemoral (PF) kinematics during walking [1]. In this study, we used a Monte Carlo analysis to assess how injury-induced changes in ligament properties can affect tibiofemoral kinematics and cartilage contact pressure during the stance phase of gait.

Methods

A subject-specific knee model was created from MR images. Fourteen ligaments were represented by bundles of nonlinear elastic springs [2], with wrapping surfaces included to prevent penetration of bony geometries. TF and PF cartilage contact pressures were calculated using an elastic foundation model. The knee was integrated into a lower extremity musculoskeletal model [3] (Fig. 1a), and has been validated against *in vivo* kinematics measured via dynamic MRI [1].

Whole body kinematics and ground reactions were measured during overground, preferred-speed walking. At each time step in gait, an Enhanced Static Optimization (ESO) routine [4] simultaneously calculated muscle forces, patellofemoral and secondary tibiofemoral kinematics, ligament forces and cartilage contact pressures. This routine minimized a weighted sum of squared muscle activations while satisfying the constraint that the muscle forces, and internal knee loads generate the measured hip, knee (flexion) and ankle accelerations.

A Monte Carlo analysis was performed in which the ligament stiffness and reference strains were randomly varied. Each ligament's stiffness and reference strain were represented as Gaussian variables with standard deviations of 30% of the nominal stiffness and 0.02, respectively [5]. A total of 2000 gait simulations were performed on a high-throughput computing cluster. We assessed the correlation (Pearson's correlation coefficient R) of individual ligament parameters to kinematics and contact metrics at the first peak of tibiofemoral loading

Results

The anterior cruciate ligament (ACL) acted as the primary restraint to anterior translation in mid-stance. The medial (MCL) and lateral collateral ligaments (LCL) had the greatest influence on tibial rotation from heel strike through mid-stance. Tibial plateau contact location was dependent on the ACL, MCL and LCL properties, while pressure magnitudes were most dependent on the ACL (Fig. 1b). A decrease in ACL stiffness increased average contact pressure in mid-stance, with the pressure migrating posteriorly on the medial tibial plateau (Fig. 1c).

Conclusions

Our results illustrates the strong effect that injury or surgically changed ACL properties can have on cartilage contact pressure patterns. These altered mechanics could serve as a precursor to the early onset of osteoarthritis often seen in ACL injured individuals (REF).

References

[1] Lenhart et al. *Ann of Biomed Eng*, in press, 2015.
[2] Blankevoort L et al. *J Biomech Eng*, 13, 263-69, 1991.
[3] Arnold, EM et al. *Ann of Biomed Eng*, 38, 269-79, 2010.
[4] Lenhart et al. *J Biomech*, in press, 2015.
[5] Baldwin, MA et al. *Comput Methods Biomech Biomed Engin*, 12, 651-659, 2009.

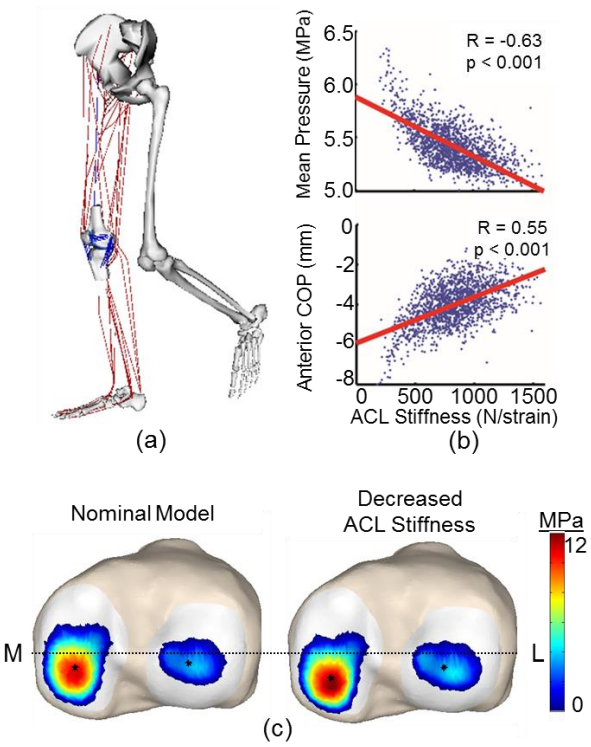

Figure 1 (a) Lower extremity model (b) ACL stiffness effects at mid-stance (c) Tibial pressure maps at mid-stance

Workshop on Biomechanical and Parametric Modeling of Human Anatomy 2015

Enhanced Static Optimization: A Simulation Framework for Prediction of Knee Mechanics during Movement

Colin R Smith, Darryl G Thelen

University of Wisconsin-Madison, Madison WI, USA
web: http://uwnmbl.engr.wisc.edu, *email*: dgthelen@wisc.edu

Introduction

Knowledge of *in vivo* knee mechanics such as cartilage contact pressures and ligament forces during functional movements is valuable for the design of surgical treatments and rehabilitation protocols for soft tissue injury. However, as these quantities cannot be measured *in vivo*, it is compelling to predict them through computational simulation. Accordingly, we have developed a multibody knee model and Enhanced Static Optimization (ESO) simulation framework to predict knee mechanics during movement. The objective of this study is to give an overview of ESO and demonstrate its ability to predict knee mechanics during a variety of functional tasks including walking, running, jumping and lunging.

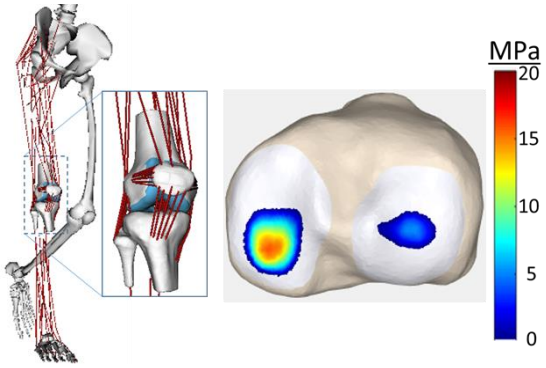

Figure 1: Lower limb musculoskeletal model with multibody 12 degree of freedom knee model and ESO predicted pressure map at first peak of tibiofemoral loading during walking

Methods

The multibody knee model was constructed from MR images of a healthy adult female (1.65 m, 61 kg, age: 23). It consists of three bodies (femur, patella, tibia), with 6 degree of freedom tibiofemoral and patellofemoral joints. The model includes the major ligaments and posterior capsule of the knee represented as 14 bundles of nonlinear springs [1]. Articular cartilage surfaces are represented by high resolution triangular meshes segmented from the MR images. Cartilage contact pressures are calculated by detecting overlap between the articulating surfaces and using an elastic foundation model to determine pressure based on the depth of penetration [2]. The knee model was integrated into an existing lower extremity musculoskeletal model [3], which included 43 muscles acting about the hip, knee and ankle joints. The predictive capacity of the model was validated by comparing simulated passive and active knee kinematics with *in vivo* 3D knee kinematics measured with dynamic MRI [4].

The ESO simulation framework is formulated similarly to standard static optimization in that it is posed as an optimization problem to solve for a set of muscle forces which generate the measured primary joint accelerations while minimizing the weighted sum of muscle activations squared and satisfying the overall dynamic constraints. However, in ESO, the patellofemoral and secondary tibiofemoral kinematics are included in the optimization as design variables. Additionally, the accelerations in these degrees of freedom are constrained to be zero. As a result, at every time point in a simulation, ESO simultaneously predicts muscles forces, patellofemoral and secondary tibiofemoral kinematics, ligament forces and cartilage contact pressures. The overall dynamic constraints require that the muscle forces and internal knee loads (contact pressures, ligament forces) produced by the optimized knee kinematics generate the measured hip, knee (flexion) and ankle accelerations.

Results and Discussion

To evaluate the robustness of our model and ESO, we applied the simulation framework to submaximal exertion, maximal exertion and high impact movements. Whole body kinematics and ground reaction forces were recorded in a motion analysis laboratory while a subject performed a variety of common and rehabilitation exercises. The ESO framework was then used to simulate the knee mechanics and the predicted cartilage pressure maps of the activities were compared. For each of the exercises, the simulations converged and produced contact forces similar to those measured using an instrumented implant [5]. As a result, the ESO framework proved capable to simulate a variety of human movements including athletic movements and those with extreme joint angles.

References

[1] Blankevoort, L, et al. *J Biomech Eng*, 1991
[2] Bei, Y, Fregly, BJ. Med Eng Phys, 2004
[3] Arnold, EM, et al. *Ann of Biomed Eng* 2010.
[4] Lenhart, RL, et al. *Ann of Biomed Eng*, 2015
[5]Bergmann, G, et al. PLOS One, 2014

The Influence of the ACL Femoral Attachment on Knee Mechanics during Gait: A Simulation Study

Colin R. Smith[1], Michael F. Vignos[1], Darryl G. Thelen[1]
[1]University of Wisconsin-Madison, Madison, WI

Disclosures: Colin R. Smith (N), Michael F. Vignos (N), Darryl G. Thelen (N)

INTRODUCTION:

Understanding influence of the orientation of the anterior cruciate ligament (ACL) on knee mechanics is important for improving ACL reconstruction surgeries and their long term outcomes. Previous approaches to study effects of ACL orientation have included cadaveric experiments [1] and retrospective motion capture studies of gait following ACL reconstructions [2]. These studies have provided an understanding of ACL geometry effects on knee laxity under simple loading conditions and its statistical relationship with joint torques during gait. However, such experimental studies are limited in terms of the metrics which can be directly measured, and difficulties in isolating the causal influence of the ACL geometry in isolation of other confounding variables. Multibody computational models can provide complimentary insight to experimental studies, by directly simulating the effects of ACL geometry on tibiofemoral kinematics, cartilage contact pressures, and ligament loading during gait.

METHODS:

A three body, 12 DOF knee model was developed from MR images of a healthy adult female (1.65 m, 61 kg). Fourteen ligaments were represented by bundles of nonlinear elastic springs, with wrapping surfaces included to prevent penetration of bony geometries. Articular cartilage surfaces were segmented from the MR images and represented by high resolution meshes. Cartilage contact pressures were calculated by detecting overlap between the articulating surfaces and using an elastic foundation model to determine localized pressure based on the degree of cartilage overlap. The knee model was integrated into an existing lower extremity musculoskeletal model [3], which included 43 muscles acting about the hip, knee and ankle joints. The predictive capacity of the model was previously validated by comparing simulated passive and active knee kinematics with *in vivo* measurements obtained with dynamic MRI [4].

Whole body kinematics and ground reactions were recorded while the subject walked overground in a motion analysis laboratory. At each frame of a gait cycle, an enhanced static optimization (ESO) routine [5] was used to calculate muscle forces, secondary tibiofemoral and patellofemoral kinematics that minimized a weighted sum of squared muscle activations while satisfying overall dynamic constraints. The constraints required that the muscle forces and internal knee loads (contact pressures, ligament forces) produced by the optimized knee kinematics generate the measured hip, knee (flexion) and ankle accelerations. An initial simulation was performed with the nominal knee model, followed by two sets of simulations in which the ACL femoral attachments were varied by +10, +5, -5 and –10 mm in the anterior-posterior and medial lateral directions respectively. The predicted tibiofemoral kinematics, tibial cartilage contact and ACL loads were compared for all simulations.

RESULTS:

The orientation of the ACL in both the sagittal and coronal planes had substantial effects on knee mechanics. As the ACL became more vertical in the sagittal plane, the maximum tibiofemoral anterior translation and external rotation increased during stance phase by 2.9 mm and 2.2^{o} respectively, from the most posterior to the most anterior femoral ACL attachments. Medial translation and adduction varied by less than 1 mm and 1^{o} respectively. As the ACL became more vertical in the coronal plane, the maximum anterior (3.0 mm) and medial (2.1 mm) translations and adduction (1.5^{o}) and external rotations (5.1 ^{o}) showed considerable change during stance.

Coronal plane orientation showed a stronger effect on the tibial contact mechanics than the sagittal plane orientation. A more horizontal ACL in the coronal plane led to a posterior migration of the center of pressure COP (4.4 mm) and an increase of 30% of the ratio of mean medial and lateral plateau pressures at the first peak of stance. A more vertical ACL in the sagittal plane showed a similar posterior migration of the COP (1.2 mm) and increase of medial lateral pressure ratio (12 %), but of smaller magnitude (Figure 2). Conversely, the loading of the ACL during stance phase was more strongly affected by the sagittal plane orientation. The peak ACL loading during stance increased by 40% as the ACL became more vertical in the sagittal plane, and increased by 23% across all coronal plane angles.

DISCUSSION:

The results of this study indicate that the orientations of the ACL in both the sagittal and coronal planes have substantial effects on knee mechanics. The coronal plane orientation shows a greater influence on the tibial plateau contact pressures, while the sagittal plane orientation showed a larger effect on the loading of the ACL. The effect of the ACL orientation on kinematics, contact pressures and ACL loadings have not been reported previously for a functional movement such as gait.

SIGNIFICANCE:

This study reinforces the importance of considering the geometry of the ACL graft during reconstruction surgeries as even small variations can lead to substantial differences in tibiofemoral mechanics during gait.

REFERENCES:

[1] Zavras, T.D. et al. *Knee Surg Sports Traumatol Arthrosc*. 13, 92-100 (2005). [2] Scanlan, SF et al. Am J Sports Med. 37, 2173-2178 (2009). [3] Arnold, EM et al. Ann Biomed Eng. 38, 289-79 (2010). [4] Lenhart, RL et al. Ann Biomed Eng. Epub (2015). [5] Lenhart, RL et al. J Biomech. Epub (2015).

ACKNOWLEDGEMENTS: NIH EB015410

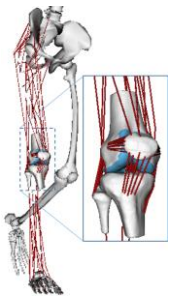

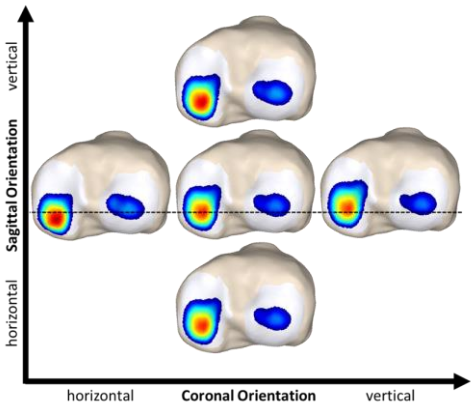

Effects of Muscle Strength Variations on Simulated Muscle Loads and Knee Mechanics during Walking

[1] Colin R Smith and [1]Darryl G Thelen

[1] University of Wisconsin-Madison, Madison, WI, USA
email: crsmith25@wisc.edu, web: http://uwnmbl.engr.wisc.edu/

INTRODUCTION

Neuromuscular coordination and internal knee tissue mechanics are inherently coupled. This coupling is especially apparent in the pathologic knee, where ligament and cartilage loads are highly dependent on muscle forces, and neuromuscular coordination is often altered to accommodate the pathologic joint. A better fundamental understanding of this coupling during locomotion could improve neuromuscular retraining approaches for pathologies such as anterior cruciate ligament injury and osteoarthritis.

The complex coupling of muscle and soft tissue loading about the knee creates potential for computational modeling to provide valuable insight. While musculoskeletal models have long been used to study neuromuscular coordination in movement, existing models often assume a highly simplified representation of the knee. At the other extreme, complex knee models predict the interaction of muscle, ligament and cartilage tissue loads without considering neuromuscular coordination. We have recently introduced a novel multibody knee model and probabilistic simulation framework to study the interaction of neuromuscular coordination and internal knee mechanics during movement [1]. This study considers the influence of individual muscles on internal knee mechanics during walking by stochastically varying the isometric muscle strengths in the model.

METHODS

A three body, 12 DOF knee model was developed from MR images of a healthy adult female (1.65 m, 61 kg). Fourteen ligaments were represented by bundles of nonlinear elastic springs, with wrapping surfaces included to prevent penetration of bony geometries. Articular cartilage surfaces were segmented from the MR images and represented by high resolution meshes. Cartilage contact pressures were calculated based on the overlap depth between the articulating surfaces using an elastic foundation model. The knee model was integrated into an existing lower extremity musculoskeletal model [2], which included 43 muscles acting about the hip, knee and ankle joints. The predictive capacity of the model was validated by comparing simulated passive and active knee kinematics with *in vivo* 3D knee kinematics measured with dynamic MRI [3].

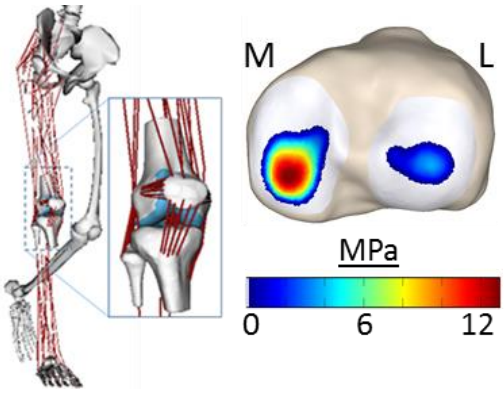

Figure 1: Knee model and predicted tibial contact pressure map at first peak of tibiofemoral loading

Whole body kinematics and ground reactions were recorded while the subject walked overground in a motion analysis laboratory. At each frame of a gait cycle, an optimization routine termed COMAK (concurrent optimization of muscle activations and kinematics) calculated the muscle forces, patellofemoral kinematics and secondary tibiofemoral kinematics that minimized a weighted sum of squared muscle activations cost function while satisfying overall dynamic constraints. The constraints required that the muscle forces and internal knee loads (contact pressures, ligament forces) produced by the optimized knee kinematics

generate the measured hip, knee (flexion) and ankle accelerations.

To investigate the influence of neuromuscular coordination on knee mechanics, we used a high throughput computing grid to perform a parametric Monte Carlo analysis. We performed 2000 simulations in which the maximum isometric muscle strengths were randomly sampled from a Gaussian distribution centered at the nominal model value with a standard deviation of 20% of the mean. By varying the strengths of the muscles, the probabilistic simulations result in differing neuromuscular coordination strategies. To compare the influence of muscle force variability on the variability in the resulting knee mechanics, we compared the coefficient of variation (CV) of the gastrocnemius, vastii and hamstrings forces at their peak to the CV of tibiofemoral kinematics and cartilage loading metrics at the same time points.

RESULTS AND DISCUSSION

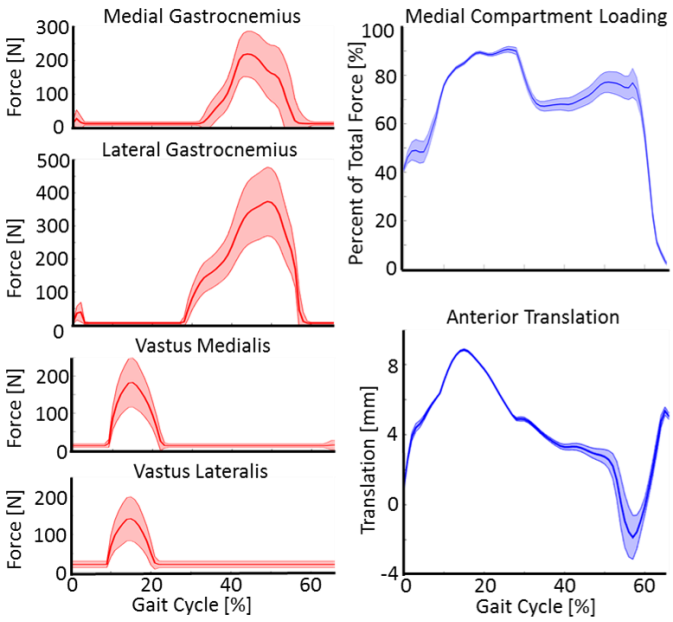

Figure 2 Mean and 95% confidence intervals for predicted muscle forces and knee mechanics for 2000 simulations.

Generally, we found that large variations in muscle forces did not lead to large alterations in knee joint mechanics. This was especially true during the first half of the stance phase when the quadriceps were active. The CV of the vastus medialis and vastus lateralis were 0.16 and 0.20 respectively, while the CV of anterior translation and total tibiofemoral contact force were an order of magnitude smaller (0.003 and 0.004) at the same time point.
Variations in the gastrocnemii and hamstring forces resulted in slightly larger effects on the knee joint mechanics. The CV of the medial and lateral gastrocnemii were 0.18 and 0.14, while the CV of the anterior translation, internal rotation and percentage of the contact force acting through the medial compartment were 0.05, 0.18 and 0.02, respectively. The CVs of the semimembranosus, semitendinosus, biceps femoris short head and long head were 0.19, 0.20, 0.20 and 0.01, respectively, and the corresponding CVs of the anterior translation, internal rotation and percentage of the contact force through the medial compartment were 0.03, 0.08 and 0.04, respectively.

The increased influence of the variations in the gastrocnemii and hamstrings forces compared to the quadriceps is likely due to their biarticular function. While the CVs of each of these muscle groups were similar, the variations in the gastrocnemii and hamstrings forces occurred due to redistribution of the ankle moment to the soleus and hip moment to the gluteus maximus. The variation in the vastii muscle forces was largely due to a redistribution of the knee moment between the vastii muscles.

In future work, we plan to investigate alternative optimization cost functions which will induce varying amounts co-contraction to better understand how joint stiffening can alter the magnitudes and locations of cartilage contact stresses. We expect this will result in larger variability in the predicted knee joint mechanics and may reveal muscle coordination strategies that are beneficial to restore healthy knee behavior in pathologic populations.

REFERENCES

1. Smith CR, et al. *J Knee Surg* **29**, *99-106*, 2016.
2. Arnold EM, et al. *Ann Biomed Eng* **38**, 269-279, 2010.
3. Lenhart RL, et al. *Ann Biomed Eng* **43**, 2675-2685, 2015.

ACKNOWLEDGEMENTS

NIH EB015410 and HD084213

Interaction of Muscle Coordination and Internal Knee Mechanics during Movement

[1]Colin R Smith (crsmith25@wisc.edu) and [1]Darryl G Thelen
[1] University of Wisconsin-Madison, Madison, WI, USA

Neuromuscular coordination and internal knee tissue mechanics are inherently coupled. This coupling is especially apparent in the pathologic knee, where ligament and cartilage loads are highly dependent on muscle loading, and neuromuscular coordination is often altered to accommodate pathologic joint behavior. A better fundamental understanding of this coupling during locomotion could improve both orthopedic and neuromuscular retraining treatments for pathologies such as anterior cruciate ligament injury and osteoarthritis. The complex coupling of muscle and soft tissue loading about the knee creates potential for computational modeling to provide valuable insight. Musculoskeletal models have been created to study neuromuscular coordination in movement, but often use a highly simplified representation of the knee joint. At the other extreme, complex knee models predict the interaction of muscle, ligament and cartilage tissue loads without considering neuromuscular coordination. We have developed a novel multibody knee model and probabilistic simulation framework to study the interaction of neuromuscular coordination and internal knee mechanics during movement.

We constructed a three body knee model that included 6 degree of freedom tibiofemoral and patellofemoral joints. Cartilage surfaces and ligament attachments were segmented from MR images of a healthy adult female. Fourteen ligaments were represented by bundles of nonlinear elastic springs. Cartilage contact pressures were calculated using an elastic foundation model. The knee model was integrated into a generic musculoskeletal model and validated by comparing simulated knee kinematics with *in vivo* kinematics measured by dynamic MRI [1].

Our simulation routine predicts internal knee tissue loads from kinetic and kinematic measurements of gait. At each time step, an optimization routine termed COMAK (concurrent optimization of muscle activations and kinematics) calculates the muscle forces, patellofemoral kinematics and secondary tibiofemoral kinematics that minimize a weighted sum of squared muscle activations while satisfying overall dynamic constraints. The constraints require that the muscle forces and internal knee loads (contact pressures, ligament forces) generate the measured hip, knee (flexion) and ankle accelerations [2].

To investigate the influence of neuromuscular coordination on knee behavior, we performed a parametric Monte Carlo analysis of 2000 simulations that randomly varied isometric muscle strengths by up to ±60% of the values in the nominal model. By varying the muscle strengths, the COMAK algorithm produces variable neuromuscular coordination strategies. Our simulations show that predicted muscle forces exhibit greater variability than net cartilage tissue loads. We are now investigating alternative optimization cost functions that induce co-contraction to better understand how joint stiffening can alter the magnitudes and locations of cartilage contact stresses.

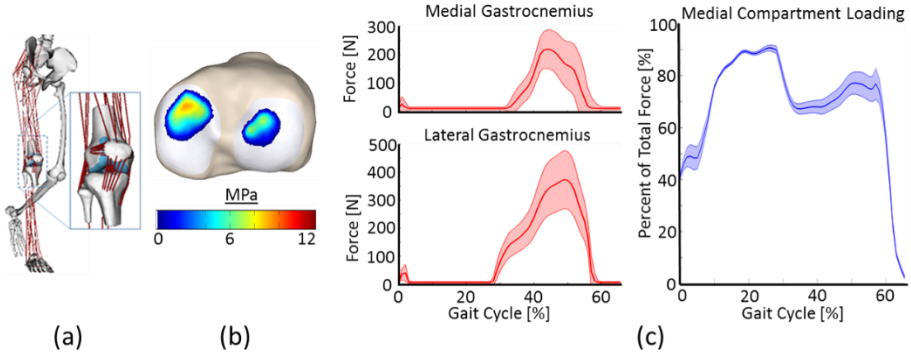

Figure 1:
a) Multibody knee model.
b) Tibial cartilage contact pressure at peak gastrocnemius loading.
c) Mean and 95% CI of muscle and knee joint loading during the stance phase of gait.

References

1. Lenhart RL (2015) Prediction and Validation of Load-Dependent. Ann Biomed Eng 43(11):2675–85.
2. Smith CR (2016) Influence of Ligament Properties on Tibiofemoral Mechanics. J Knee Surg 29(2):99–106.

Acknowledgments NIH EB015410 and HD084213

Simulation of Coupled Neuromuscular Coordination and Knee Joint Mechanics during Movement

Colin R Smith[1], Darryl G Thelen[1,2,3]
[1]Department of Mechanical Engineering, [2]Department of Biomedical Engineering, [3]Department of Orthopedics and Rehabilitation
University of Wisconsin-Madison, Madison, WI, USA

Abstract:

Knee joint behavior during locomotion results from interactions of neuromuscular coordination, passive joint structures, and articular contact mechanics. Because of the complexity of this dynamic system, these variables are often studied in isolation. Musculoskeletal models with simplified knee joint representations are used to investigate neuromuscular coordination during movement. Detailed finite element models predict the interaction of muscle, ligament and cartilage tissue loads at the joint level, without considering coordination and whole body movement dynamics. A mechanistic model that incorporates the functional interaction between neuromuscular coordination, knee joint structure and whole body movement is important to understand the causes of knee pathologies and to improve surgical treatments.

We recently introduced a novel multibody knee model that includes six degree of freedom tibiofemoral and patellofemoral joints. Cartilage surfaces and ligament attachments were segmented from MR images of a healthy adult female. Fourteen ligaments were represented by bundles of nonlinear elastic springs. Cartilage contact pressures are calculated using an elastic foundation model. The knee model was integrated into a generic musculoskeletal model and validated by comparing simulated knee kinematics with *in vivo* kinematics measured by dynamic MRI [1]. We also introduced a novel simulation routine, termed COMAK (concurrent optimization of muscle activations and kinematics), that predicts internal knee tissue loads from kinematic and kinetic measurements of movement. At each time step, COMAK calculates the muscle forces, secondary knee kinematics, ligament forces and cartilage contact pressures that minimize the weighted sum of squared muscle activations while satisfying overall dynamic constraints. The constraints require that the muscle forces and internal knee loads generate the measured hip, knee (flexion) and ankle accelerations [2]. The model and simulation routine are being implemented in OpenSim and will be made publically available through simtk.org.

To investigate the influence of neuromuscular coordination and structural joint properties on knee behavior during walking, we used a high throughput computing cluster to perform probabilistic analyses. By treating model and simulation parameters as stochastic variables, we have assessed the sensitivity of predicted knee mechanics to neuromuscular coordination strategies and model geometric and constitutive properties. Recently, we have begun evaluating the use of statistical shape modeling to rapidly generate subject-specific knee models, as well as to study the influence of articular surface geometry and ligament attachment location on knee mechanics during movement. We envision our novel approach will enable the next generation of motion analysis tools, in which subject-specific joint behavior can be simulated, and the effects of interventions can be predicted and considered for clinical treatment planning.

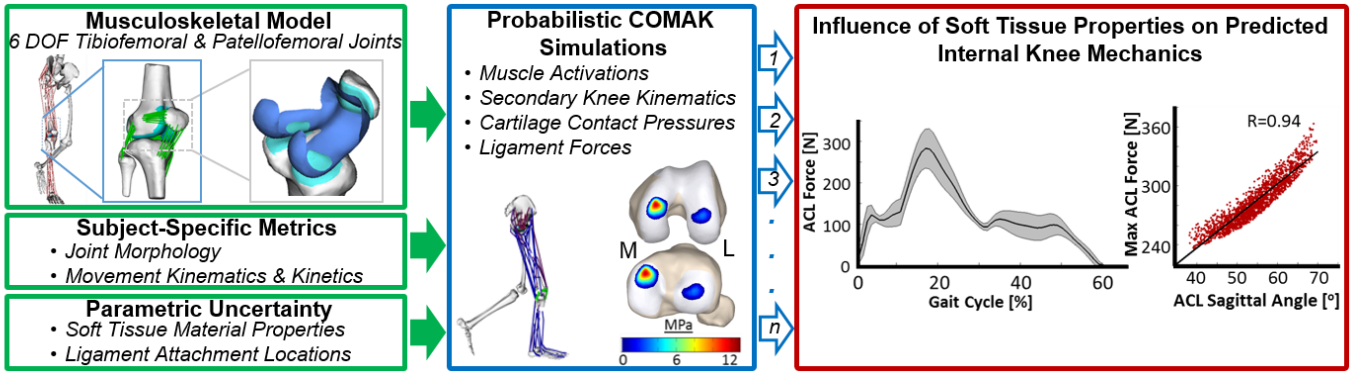

Figure Caption: Probabilistic analyses of model and simulation parameters allow for sensitivity studies of knee mechanics to neuromuscular coordination strategies, model geometries and material properties.

Acknowledgments: NIH EB015410 and HD084213, NCSRR Visiting Scholars Program

References:

[1] Lenhart RL, et al. (2015) “Prediction and Validation of Load Dependent Behavior of the Tibiofemoral and Patellofemoral Joints during Movement.” Annals of Biomedical Engineering, 43(11): 2675-85.
[2] Smith, CR, et al (2016). “Influence of Ligament Properties on Tibiofemoral Mechanics in Walking”. J Knee Surg 29(2): 99-106

A High Throughput Computing Approach to Stochastic Simulation of Cartilage Loading during Walking

Colin R Smith
U Wisconsin-Madison
1513 University Ave
Madison, WI, 53706
crsmith25@wisc.edu

Allison Clouthier
Queen's University
130 Stuart St
Kingston, ON, K7L3N6
5alc1@queensu.ca

Michael F Vignos
U Wisconsin-Madison
1513 University Ave
Madison, WI, 53706
mvignos@wisc.edu

Scott C Brandon
U Wisconsin-Madison
1513 University Ave
Madison, WI, 53706
sbrandon2@wisc.edu

Darryl G Thelen
U Wisconsin-Madison
1513 University Ave
Madison, WI, 53706
dgthelen@wisc.edu

1. Introduction

Knee cartilage loading during walking is determined by complex interactions of gait dynamics, muscle coordination, and passive joint structures. A better understanding of the influence of these factors on cartilage loading will provide insight into the etiology of osteoarthritis (OA) and improve treatments. Joint loading during locomotion is commonly studied using musculoskeletal modeling, with most studies relying on deterministic models based on population average geometries and parameters [1]. Alternatively, if the factors contributing to cartilage loading are modeled parametrically, this enables extensive uncertainty and sensitivity analyses, structure-function investigations and population modeling. We present a simulation framework that leverages statistical shape modeling, a novel solution algorithm and high throughput computing (HTC) to stochastically investigate functional knee mechanics.

2. Methods

We previously developed and validated a multibody knee model with 6 degree of freedom tibiofemoral and patellofemoral joints [2]. The knee model was integrated into a lower extremity musculoskeletal model [1] and the COMAK (Concurrent Optimization of Muscle Activations and Kinematics) simulation framework was introduced to predict muscle forces, secondary knee kinematics, ligament forces and cartilage contact pressures during movement from motion capture and ground reaction data [3].

We extended this model and simulation framework to enable parametric variation of knee geometry, cartilage and ligament constitutive properties, neuromuscular coordination, and gait dynamics to investigate the contributions of these factors to cartilage loading. Ligament and cartilage constitutive properties were modeled as

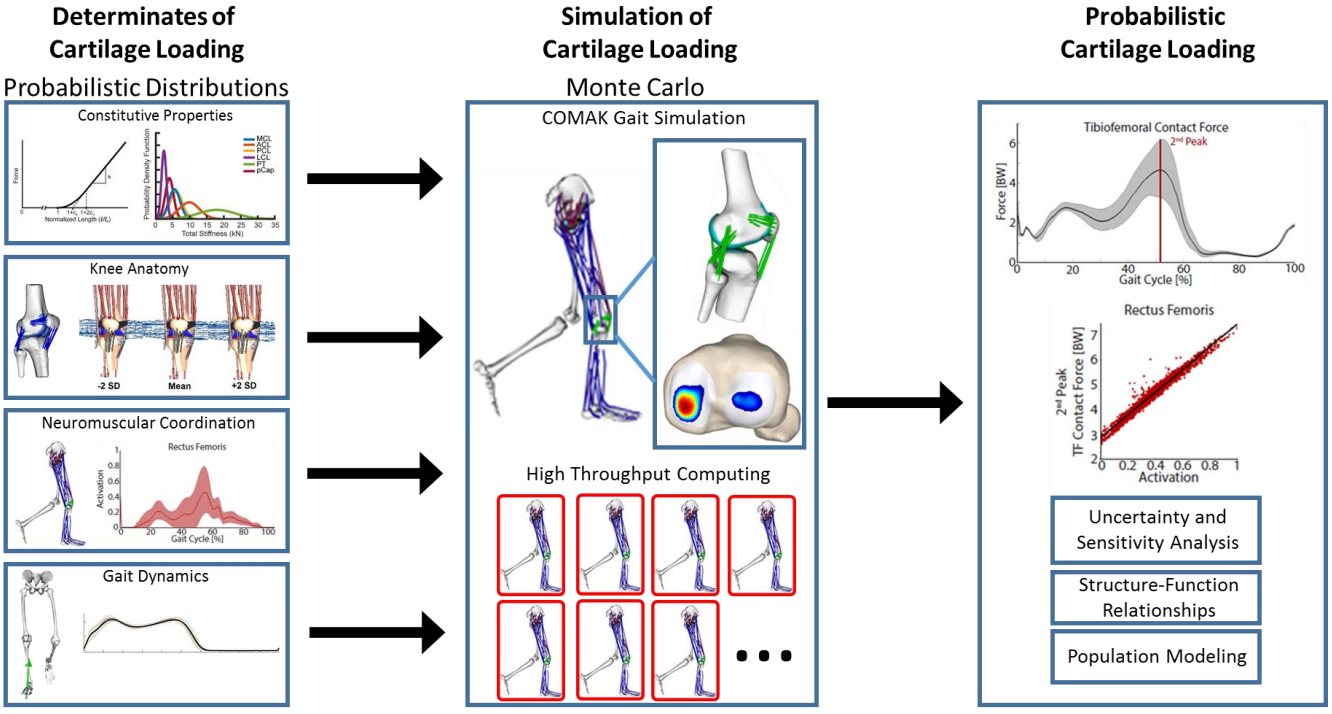

Figure 1. Framework for stochastic simulation of cartilage loading. High throughput computing and Monte Carlo sampling of parametric inputs enables uncertainty and sensitivity analyses, structure-function relationships and population modeling.

Gaussian distributions parameterized based on population data from cadaveric specimens. Knee geometries were parameterized using a statistical shape model. The model was developed based on segmented MR images of 14 young healthy subjects and included the bones and cartilage of the femur, tibia and patella. Ligament attachments and path wrap objects were placed on the mean shape model and linked to mesh nodes such that they morphed with the shape model.

Parameterizing locomotor factors to generate distributions of neuromuscular coordination and gait dynamics proved more challenging. Neuromuscular coordination was varied by introducing individual muscle weighting terms into the COMAK cost function. The weight factors are sampled from probabilistic distributions and penalize or encourage activation of their respective muscle within the optimized solution to muscle redundancy. Parameterization of gait dynamics requires a sample is generated with dynamic consistency between the joint kinematics and ground reactions. We are currently investigating methods to combine statistical representations of the kinematics and ground reactions [4] with residual elimination algorithms [5] to meet this requirement.

To stochastically simulate cartilage loading, we used Monte Carlo sampling of the parametric inputs and leveraged a HTC grid to perform thousands of simulations spanning the population variation. The correlation between each input parameter and the resulting cartilage loading metrics were then calculated to establish the relative influence of each input at specific instances in the gait cycle (Figure 1).

3. Results

In our work to date, we have used the stochastic simulation framework to perform uncertainty and sensitivity analyses, and investigate structure-function relationships. In a validation study comparing predicted knee contact forces to measured forces from an instrumented knee replacement, we used the stochastic framework to evaluate the propagation of uncertainty in ligament constitutive properties to contact force predictions [3]. Additionally, we used the stochastic framework to study the structure-function relationship of the anterior cruciate ligament (ACL) and knee mechanics to inform the placement and properties of the graft in ACL reconstruction surgery [6]. The relationship between neuromuscular coordination and knee mechanics during walking was also investigated to provide insight to neuromuscular retraining following knee injury. Recently, we have applied the framework to investigate the influence of knee geometry on cartilage loading using the statistical shape model.

4. Discussion

With the emergence of parametric models of human anatomy and locomotor function, the feasibility and capabilities of stochastic simulation have improved substantially. We introduced a powerful yet computationally tractable stochastic simulation framework that leverages parametric modeling and high throughput computing to investigate cartilage loading during walking. We applied the framework to study model uncertainty and sensitivity as well as clinically relevant structure-function relationships. An important benefit of the framework is that it does not require all inputs to be parameterized from the same data set, allowing the combination of existing incomplete databases.

In future work we intend to parameterize both healthy and clinical populations to construct population based models. This will allow predictions of subject specific cartilage loading to be analyzed within the context of a population. Additionally, it will allow comparisons of input distributions and simulated knee mechanics between healthy and clinical populations to reveal the consequences of pathologic symptoms on cartilage loading.

5. Acknowledgments

NIH EB015410 and HD084213

References

[1] E. Arnold et al., “A Model of the Lower Limb for Analysis of Human Movement,” *Ann Biomed Eng*, vol. 38, no. 2, pp. 269-279, 2010.

[2] R. L. Lenhart et al., “Prediction and Validation of Load-Dependent Behavior of the Tibiofemoral and Patellofemoral Joints During Movement,” *Ann Biomed Eng*, vol. 43, no. 11, pp. 2675-2685, 2015.

[3] C. R. Smith et al., “The Influence of Component Alignment and Ligament Properties on Tibiofemoral Contact Forces in Total Knee Replacement,” *J Biomech Eng*, vol. 138, no. 2, 2016.

[4] Y. Yun et al., “Statistical method for prediction of gait kinematics with Gaussian process regression,” *J Biomech*, vol. 41, no. 1, pp. 186-192, 2014.

[5] C. D. Remy, and D.G. Thelen, “Optimal estimation of dynamically consistent kinematics and kinetics for forward dynamic simulation of gait,” J Biomech Eng, vol. 131, no. 3, 2009

[6] C. R. Smith et al, “Influence of Ligament Properties on Tibiofemoral Mechanics in Walking,” *J Knee Surg*, vol 1, no. 212, 2015.

Stochastic Simulation of Functional Knee Mechanics Enabled via Statistical Shape Modeling and High Throughput Computing

[1] Colin R Smith, [2]Yasin Dhaher, [1]Darryl G Thelen
[1] Department of Mechanical Engineering, University of Wisconsin-Madison, Madison, WI, USA
[2] Rehabilitation Institute of Chicago, Chicago, IL, USA

Articular cartilage loading is determined by complex mechanics across multiple scales resulting from interactions between cartilage contact, ligament tension, limb dynamics, and neuromuscular coordination. Simulating the contributions of these factors to knee behavior can enhance our understanding of knee pathologies, e.g. osteoarthritis, and enable improvements in clinical treatments. In this abstract, we present a multiscale knee model and simulation framework that leverage recent advancements in musculoskeletal simulation, statistical shape modeling, and high throughput computing (HTC). The framework is used to stochastically simulate muscle, ligament and cartilage loading during complex movements such as gait.

A multibody knee model with six degree-of-freedom tibiofemoral and patellofemoral joints was integrated into a lower extremity musculoskeletal model. Fourteen ligaments are represented by bundles of nonlinear springs. An elastic foundation model is used to compute cartilage contact pressure. The ligament attachment and articular geometries can be constructed from medical images [1] or generated from a statistical shape model to investigate population variability. A novel simulation routine, Concurrent Optimization of Muscle Activations and Kinematics (COMAK), simultaneously predicts muscle forces, ligament loads and cartilage contact pressures that are consistent with measured movement dynamics [1]. We have performed Monte Carlo analyses to assess the influence of parametric uncertainty on simulated knee mechanics by representing the constitutive properties, neuromuscular coordination patterns, and knee geometries as population distributions and leveraging HTC to run thousands of simulations in parallel.

COMAK can simulate internal knee mechanics over a gait cycle in under 30 minutes on a standard desktop computer. When deployed in parallel on a HTC grid, several thousand stochastic gait simulations can be performed in a few hours [1]. The framework has been used to investigate the influence of ligament properties on cartilage contact pressures during walking [1]. Furthermore, we are using the framework to simulate the influence of surgical factors on knee behavior following anterior cruciate ligament (ACL) reconstruction and patellar tendon advancement (PTA) procedures. The knee model and COMAK simulation routine are now being implemented into OpenSim 4.0. A webinar demonstrating the use of OpenSim with the freely available HTC resources of the Open Science Grid is available online [2].

We aim to improve the fidelity of the articular cartilage model to investigate the subtle alterations in internal cartilage loading that likely are an important factor in the initiation of osteoarthritis. We developed a finite element model of the knee that incorporates the structural hierarchies of the cartilage tissue enabling detailed investigation of the microstructure mechanics [3]. In the future, we intend to apply the COMAK predicted joint mechanics as boundary conditions to this finite element model to investigate the influence of macroscale interventions such as gait retraining and orthopedic surgeries on the loading of the cartilage microstructure.

Funded by NIH EB015410, HD084213, HD065690.

1. Smith CR, et al., *J Knee Surg* **29**(02):99-106, 2016.
2. Smith CR, et al., https://web.stanford.edu/group/opensim/support/event_details.html?id=169
3. Adouni A, et al., J Biomech 49:2891-2898, 2016

Stochastic Simulation of Knee Mechanics Enabled via Novel Solution Techniques and High Throughput Computing

[1] **Colin R Smith**, [1]Darryl G Thelen
[1]University of Wisconsin-Madison
Corresponding author email: crsmith25@wisc.edu

INTRODUCTION

Internal knee mechanics result from complex interactions between passive ligamentous structures, articular contact, limb dynamics, and neuromuscular coordination. Understanding the contributions of each of these factors to knee behavior can enable improvements in surgical treatments for knee pathologies. Dynamic musculoskeletal simulation is a potentially powerful approach to gain insight into these interactions. However, conventional musculoskeletal models rely on a simplified representation of the knee [1], which doesn't include ligaments or contact. Further, musculoskeletal models often presume mean parameter estimates, thereby ignoring the inherent uncertainties in model predictions. In this abstract, we describe a multibody knee model and simulation framework which leverage recent advancements in musculoskeletal simulation, statistical shape modeling, and high throughput computing (HTC). The framework is used to stochastically simulate muscle, ligament and cartilage loading during complex movements such as gait.

METHODS

The three-body knee model has six degree-of-freedom tibiofemoral and patellofemoral joints (Figure 1). Fourteen ligaments are represented by bundles of nonlinear springs. An elastic foundation model is used to compute contact pressure between articular cartilage surfaces [2]. The ligament attachment and articular geometries are constructed from subject-specific MR images [3] or generated from a statistical shape model to investigate population variability [4]. A novel simulation routine, Concurrent Optimization of Muscle Activations and Kinematics (COMAK), simultaneously predicts muscle forces, ligament loads and cartilage contact pressures that are consistent with overall movement dynamics [3]. We leverage HTC to perform thousands of independent simulations in parallel, allowing us to perform extensive sensitivity studies. By parameterizing the constitutive properties, neuromuscular coordination patterns, and knee geometries as population distributions, we are also able to use HTC to perform Monte Carlo simulations to assess the influence of parametric uncertainty on simulated knee mechanics.

RESULTS AND DISCUSSION

COMAK is able to simulate internal knee mechanics over a gait cycle in less than 30 minutes on a standard desktop computer. When deployed in parallel on a HTC grid, several thousand stochastic gait simulations can completed in a few hours [3]. The framework has been used to investigate the influence of ligament properties on cartilage contact pressures during walking [3]. We have also simulated the effects of patella height on the behavior of the knee extensor mechanism in normal and crouch gait [5].

The COMAK solution technique and HTC enable increasingly complex simulations of internal joint mechanics to be performed. In our own lab, we are using the framework to simulate the influence of surgical factors on knee behavior following anterior cruciate ligament (ACL) reconstruction and patellar tendon advancement (PTA) procedures. The knee model and COMAK simulation routine were initially implemented in custom code, but are now being ported into OpenSim 4.0. Model predictions, e.g. cartilage contact pressures, can be visualized in FEBio (Figure 1). A webinar demonstrating the use of OpenSim with the freely available HTC resources of the Open Science Grid is available online [6].

CONCLUSIONS

Advances in imaging, shape modeling, solution algorithms and computing resources enable the simulation of detailed joint mechanics during movement. These advances provide a powerful platform to simulate complex orthopedic procedures and predict the effect of surgical factors on joint behavior during functional movement.

ACKNOWLEDGEMENTS

NIH EB015410, HD084213, HD065690

REFERENCES

1. Arnold E, et al., *Ann Biomed Eng*. **38**(2):269-279, 2010
2. Smith CR, et al., *CMBBE I&V*. online, 2016.
3. Smith CR, et al., *J Knee Surg* **29**(02):99-106, 2016.
4. Clouthier A, et al., *ORS*, San Diego, 2017.
5. Lenhart RL, et al., *J Biomech*. **51**:1-7,2017.
6. Smith CR, et al., https://web.stanford.edu/group/opensim/support/event_details.html?id=169

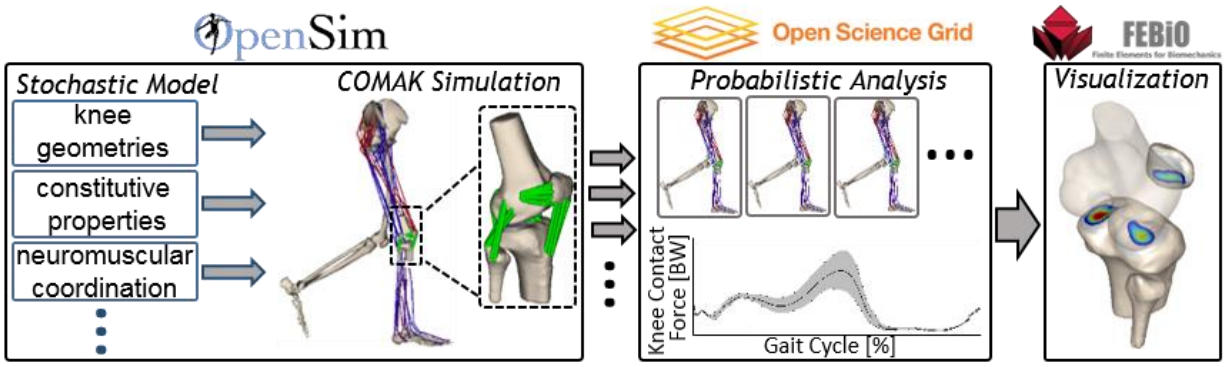

Figure 1: The simulation framework uses the following freely available resources: OpenSim (http://opensim.stanford.edu) for musculoskeletal simulation, the Open Science Grid (https://www.opensciencegrid.org) for high throughput computing, and FEBio (https://febio.org) for visualization of predicted cartilage contact pressures.

SIMULATED ACL AND MENISCI DEFICENCY PREDICTS ALTERED KNEE MECHANICS DURING WALKING

[1]Colin R Smith, [1]Scott CE Brandon, [1]Darryl G Thelen

[1]University of Wisconsin-Madison, Madison, WI, USA
email: crsmith25@wisc.edu, web: http:// uwnmbl.engr.wisc.edu/

INTRODUCTION

Rupture of the anterior cruciate ligament (ACL) leads to an increased risk of early onset osteoarthritis (OA), especially in cases of a concomitant meniscal injury [1]. It has been hypothesized that altered knee mechanics resulting from such injuries contribute to the initiation of OA [2]. However, it is challenging to assess how soft tissue injuries will affect knee mechanics during functional movement. *In vivo* cartilage loading results from the interaction of movement dynamics, neuromuscular coordination, passive ligamentous structures, and cartilage properties and morphology, all of which are known to change following soft tissue injury [3]. We have developed an integrated multibody knee model and movement simulation framework to investigate the influence of these factors on cartilage loading. In this study, we performed virtual resections of the ACL and menisci to study their influence on cartilage loading and functional knee mechanics during walking.

METHODS

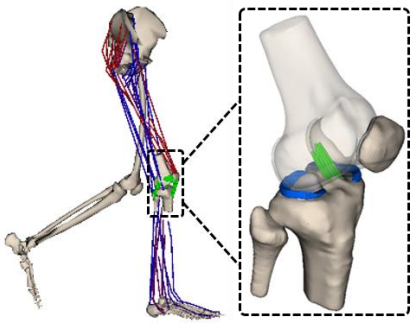

Figure 1: Multibody knee model with 6 DOF joints, ligaments, and cartilage and meniscal contact.

A multibody knee model with independent femur, tibia, patella, and medial and lateral menisci bodies was constructed from magnetic resonance images and integrated into a generic musculoskeletal model [2] (Fig. 1). The bodies were connected by six degree of freedom (DOF) joints and constrained by ligaments and articular contact. Fourteen ligaments and the meniscal horns were represented as bundles of nonlinear springs. An elastic foundation model was used to compute contact pressure for cartilage-cartilage and meniscal-cartilage interactions.

Full body kinematics and ground reaction forces were measured in a motion analysis lab during overground walking (1.2 m/s). A novel simulation routine, Concurrent Optimization of Muscle Activations and Kinematics (COMAK), was used to predict muscle forces, ligament loads, and cartilage and meniscal contact pressures during walking [2]. COMAK simultaneously optimizes muscle activations and secondary knee kinematics (5 tibiofemoral DOF, 6 patellofemoral DOF, and 12 menisci DOF) to satisfy both whole-body and joint-level movement dynamics, while minimizing a weighted squared muscle activation objective function. The simulation was repeated for four cases: intact, ACL deficient (ACLd), menisci deficient and combined ACLd and menisci deficient.

RESULTS AND DISCUSSION

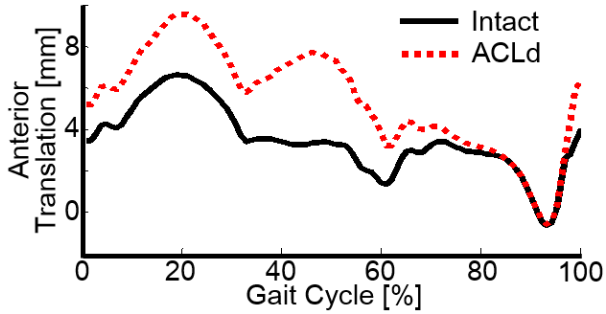

Figure 2: Predicted anterior tibial translation in the healthy and ACL deficient knee during walking.

Compared to the intact simulation, the ACLd knee demonstrated increased anterior translation (Fig. 2) and internal rotation throughout stance (max: 4.4 mm, 3°). In early and mid-swing, these kinematics converged towards the intact pattern, but diverged

again in terminal swing. A similar trend was predicted for the menisci deficient knee. The combined ACLd and menisci deficient knee induced substantially larger anterior translation throughout stance, with instances of posterior tibial subluxation in swing.

Both ACL deficiency and menisci deficiency substantially altered cartilage loading on the tibial plateau throughout the gait cycle (Fig 3). At the instant of peak ACL force in the intact simulation, the primary change in the ACLd knee was a posterior shift in the medial (2.4 mm) and lateral (2 mm) center of pressure (COP). In the menisci deficient case, there was an increase in peak pressure (+1.3 MPa) and a posterior shift in the medial COP (1.5 mm). The combined ACLd and menisci deficient knee experienced a dramatic increase in peak contact pressure (+6.2 MPa) and posterior shifts in the medial (9.7 mm) and lateral COP (3.3 mm).

The medial meniscus provided the primary restraint to anterior tibial translation in the ACLd case, along with secondary contributions from the lateral meniscus, MCL, LCL and IT band (Fig. 4). In the menisci deficient knee, the peak loading in the ACL increased by 1.9x to provide anterior restraint. In the combined ACL and meniscus deficient knee, the loading in the MCL increased by 6.6x at the instant of peak ACL loading in the intact knee. In the ACLd and menisci deficient cases, the anterior shift of the tibia oriented the patellar tendon more vertically in the sagittal plane, and thus reduced the anterior restraint required of the passive knee structures. In the combined ACLd and menisci deficient case, the magnitude of the anterior tibial translation resulted in a brief portion of stance where the patellar tendon applied a posterior force to the tibia.

Our simulation predictions corroborate experimental studies of the ACL deficient knee. Using dual fluoroscopy and MRI, Li et al. found a posterior shift of tibial contact on the medial plateau in ACL deficient knees during lunging [3]. Similar to our simulation predictions, Andriacchi et al found alterations in anterior translation and internal rotation during the terminal portion of swing, which persisted throughout stance [4].

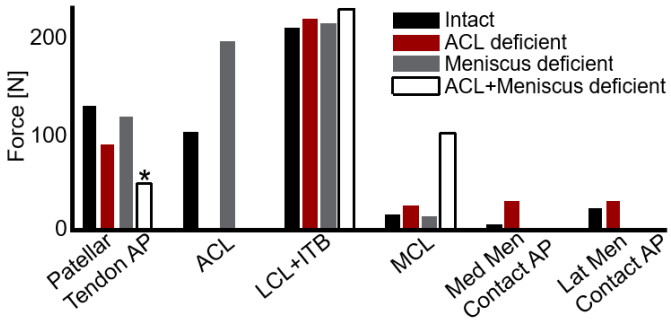

Figure 4: Loading in the passive knee structures at the instant of peak ACL force during gait in the intact knee. AP: Anterior force component. (*) Denotes the patellar tendon applied a posterior force to the tibia.

CONCLUSIONS

Our simulation predictions suggest that injury to the ACL and/or meniscus leads to altered cartilage contact locations and pressure magnitudes during walking. In the future, we intend to use this simulation framework to investigate muscle coordination and movement strategies that can restore normative cartilage loading patterns in knees with ACL deficiency and/or meniscal damage.

REFERENCES

1. Oiestad BE. *Amer J Sports Med* **37**, 1434, 2009.
2. Griffin T. *Exerc Sport Sci Rev* **33**, 195-200, 2005.
3. Chaudhari A. *Med Sci Sports Exerc* **40**, 215, 2008.
4. Smith CR, et al. *J Knee Surg* **29**, 99-106, 2016.
5. Li G, et al. *JBJS* **88**, 1826-34, 2006.
6. Andriacchi T, et al. *J Biomech* **38**, 293-98, 2005.

ACKNOWLEDGMENTS

NIH EB015410, HD084213

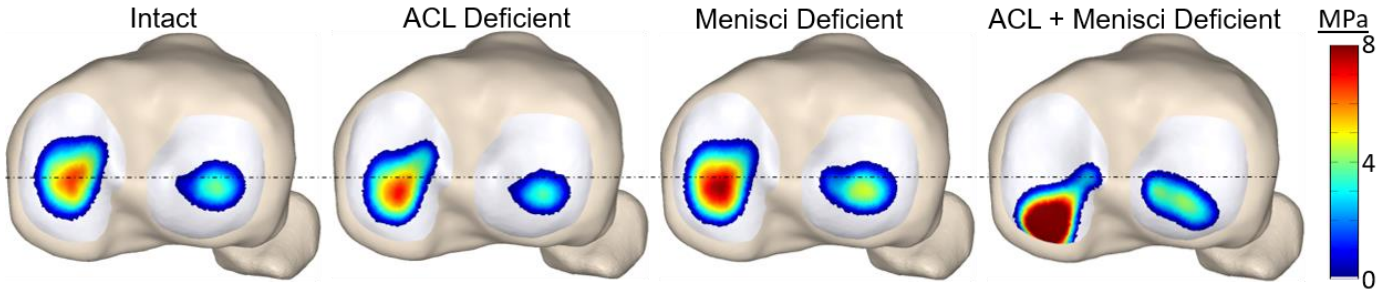

Figure 3: Tibial cartilage pressure patterns due to cartilage-cartilage contact at the instant of peak ACL loading in the intact knee for intact, ACL deficient, menisci deficient and combined ACLd and menisci deficient cases.

Tunnel Position in ACL Reconstruction has Substantial Influence on Cartilage Loading During Walking

Colin R. Smith[1], Michael F. Vignos[1], Darryl G. Thelen[1]
[1]University of Wisconsin-Madison, Madison, WI
crsmith25@wisc.edu

Disclosures: Colin R. Smith (N), Michael F. Vignos (N), Darryl G. Thelen (N)

INTRODUCTION: Dynamic imaging experiments have revealed that anterior cruciate ligament (ACL) reconstruction often fails to restore normative tibiofemoral kinematics during functional movement. These kinematic abnormalities alter cartilage loading and contribute to early-onset osteoarthritis (OA) [1]. We recently found that bilateral differences in the sagittal plane angles of a patient's intact and reconstructed ACL are correlated with asymmetric tibiofemoral kinematics measured by dynamic MRI during an open-chain knee flexion-extension task [2]. However, it is unknown whether these relationships extend to walking, and the direct cause-effect relationship between controllable surgical factors and altered joint mechanics has not been established. The purpose of this study was to use surgical simulations to determine the cause-effect relationships between ACL graft geometry, stiffness, and pretension on knee mechanics during walking. The model provides an objective basis for interpreting empirical observations on ACL reconstructed knees and could be used to inform adjustments to surgical procedures to better restore healthy knee mechanics.

METHODS: We developed a multibody knee model with femur, tibia, patella, and menisci bodies connected by 6 degree of freedom joints from MRI of a healthy female (23 years). The knee was integrated into a full body musculoskeletal model [3]. Articular contact pressures (cartilage-cartilage and cartilage-meniscus) were computed using an elastic foundation formulation and ligaments were represented as bundles of nonlinear springs. The predictive capacity of the model was validated by comparing simulated knee kinematics against *in vivo* measures made by dynamic MRI during a loaded flexion-extension task. Whole body kinematics and ground reactions were collected during overground walking. The COMAK simulation algorithm was then used to predict the secondary knee kinematics, muscle and ligament forces, and articular contact pressures necessary to replicate the overall measured motion (Figure 1a) [4].

A Monte Carlo analysis (10,000 surgical simulations) was performed to quantify the effect of graft tunnel placement, stiffness, and pretension on knee mechanics during walking. The ACL attachment footprint was varied in a uniform distribution ± 5 mm anterior-posteriorly and medial-laterally on the tibial plateau, and ± 5 mm anterior-posteriorly and superior-inferiorly on the femoral condyle. The ACL stiffness and reference strain were varied in uniform distributions ranging from ±50% of the nominal stiffness and ± 0.03 of the nominal reference strain. To quantify the relative importance of the surgical factors and determine their influence on knee mechanics, the predicted secondary tibiofemoral kinematics and cartilage loading patterns were correlated to the ACL graft geometry, stiffness and reference strain using Spearman's correlation coefficient (R) (Figure 1b).

RESULTS: Simulated surgical variability had substantial influence on tibiofemoral mechanics during walking. In particular, there was substantial variation in predicted anterior translation (max range = 8.6 mm), internal rotational (max range = 4.2º), and the anterior location of the center of pressure (COP) on the medial plateau (max range = 5.9 mm) during stance. Of the surgical parameters considered, the ACL graft geometry measures had the greatest effect on the predicted knee mechanics. At the instance of peak ACL loading (15% of gait cycle), anterior translation and internal rotation were most correlated with the ACL sagittal plane angle (R=0.63, -0.36, respectively). The anterior location of the center of pressure (COP) on both the medial and lateral tibial plateaus was most correlated to the sagittal plane angle, while the lateral location of the COP for both plateaus was most correlated to the coronal angle, axial angle and lateral tibial attachment location (Figure 1c).

DISCUSSION: This study suggests ACL graft orientation angles are the surgical factors most strongly associated with knee mechanics during walking. ACL graft stiffness and pretension had some influence on cartilage contact locations, but had minimal effect on loading magnitudes. Our results provide mechanistic insights into prior empirical observations. In our model, a more vertical sagittal plane graft orientation reduced the anterior-posterior contribution of the ACL force. This resulted in increased anterior translation during walking and provides a mechanism to explain the correlation found empirically between sagittal graft angle and anterior translation in an open-chain knee flexion-extension task [2]. Similar to our model predictions, a positive correlation between internal tibial rotation and both ACL sagittal and axial plane angles has also been found previously during walking using the point cluster technique [5].

SIGNIFICANCE/CLINICAL RELEVANCE: This study indicates that anatomic placement of the bone tunnels during ACL reconstruction is important to restore normative knee mechanics during walking and mitigate the risk of OA. In particular, positioning the tunnels to replicate the native sagittal plane angle of the ACL appears especially important to restore the location of cartilage loading on the medial tibial plateau.

REFERENCES: [1] Tashman, *Am J Sports Med*, 32(4), 2004. [2] Vignos, ASB, 2017. [3] Lenhart, *Ann Biomed Eng*, 43(11), 2015. [4] Smith, *J Knee Surg*, 29(2), 2016. [5] Scanlan, *J Exp Clin Med*, 3(5), 2011.

ACKNOWLEDGEMENTS: NIH EB015410, HD084213